The regulation of cell volume-dependent mitochondrial DNA homeostasis in budding yeast and the consequences on cell physiology

Dissertation der Fakultät für Biologie
der Ludwig-Maximilians-Universität München

Alissa Alexandrine Benedikt

München, Juni 2025

Diese Dissertation wurde angefertigt
unter der Leitung von Dr. Kurt Schmoller
im Bereich des Institute of Functional Epigenetics
des Helmholtz Zentrum München.

Erstgutachter/in:	Prof. Dr. Christof Osman
Zweitgutachter/in:	Prof. Dr. Pascal Falter-Braun
Tag der Abgabe:	06. Juni 2025
Tag der mündlichen Prüfung:	05. Februar 2026

ERKLÄRUNG

Ich versichere hiermit an Eides statt, dass meine Dissertation selbständig und ohne unerlaubte Hilfsmittel angefertigt worden ist.
Die vorliegende Dissertation wurde weder ganz, noch teilweise bei einer anderen Prüfungskommission vorgelegt.
Ich habe noch zu keinem früheren Zeitpunkt versucht, eine Dissertation einzureichen oder an einer Doktorprüfung teilzunehmen.

München, den 18. Februar 2026

Alissa Alexandrine Benedikt

Affidavit

Herewith I certify under oath that I wrote the accompanying Dissertation myself.

Title: 'The regulation of cell volume-dependent mitochondrial DNA homeostasis in budding yeast and the consequences on cell physiology'

In the thesis no other sources and aids have been used than those indicated. The passages of the thesis that are taken in wording or meaning from other sources have been marked with an indication of the sources (including the World Wide Web and other electronic text and data collections). Furthermore, all parts of the thesis that were de novo generated with the help of artificial intelligence tools were identified by footnotes/annotations at the appropriate places and the artificial intelligence tools used were listed. The prompts used were listed in the appendix. This statement applies to all text, graphics, drawings, sketch maps, and pictorial representations contained in the Work.

Munich, 18.02.2026

(Location/date)

Alissa Alexandrine Benedikt A.Benedikt

(First and last name in block letters) (Signature)

Declaration

Hereby I declare that this work, complete or in parts, has not yet been submitted to another examination institution and that I did not undergo another doctoral examination without success.

Munich, 18.02.2026 A.Benedikt

(Location/date) (Signature)

Parts of this work were published in:

Seel, A., Padovani, F., Mayer, M. *et al.* Regulation with cell size ensures mitochondrial DNA homeostasis during cell growth. *Nat Struct Mol Biol* **30**, 1549–1560 (2023). https://doi.org/10.1038/s41594-023-01091-8

Table of contents

List of Figures

List of Tables

List of Abbreviations

General abbreviations	Description
ADP	Adenosine diphosphate
AmpR	Ampicillin resistance
ATP	Adenosine triphosphate
BCA	Bicinchoninic acid
C. glabrata	*Candida glabrata*
cDNA	Complementary DNA
CIP	Calf intestinal alkaline phosphatase
Cq	Quantification cycle
ddH_2O	Double-distilled water
DNA	Deoxyribonucleic acid
DTT	Dithiothreitol
E.Coli	*Escherichia coli*
EDTA	Ethylenediaminetetraacetic acid
EdU	5'-ethynyl-2'-deoxyuridine
ERMD	ER-associated mitochondrial division
ERMES	ER-mitochondria encounter structure
ETC	Electron transport chain
$FAD/FADH_2$	Flavin adenine dinucleotide
GA	Gibson Assembly
H^+	Proton
H_2O_2	Hydrogen peroxide
HCl	Hydrochloric acid
HU	Hydroxyurea
hdhMX	Hygromycine
K. lactis	*Kluyveromyces lactis*
MAT	Mating type
MICOS	Mitochondrial contract sites complexes
MMD	mtDNA maintenance disorders
mRNA	Messenger RNA
mtDNA	Mitochondrial DNA
mtNetwork	Mitochondrial network
NaCl	Sodium chloride
NAD/NADH	Nicotinamide adenine dinucleotide
NaOH	Sodium hydroxide
nDNA	Nuclear DNA
$O_2^{\bullet-}$	superoxide anion radical
OD	Optical density
OXPHOS	Oxidative phosphorylation
PCA	Principal component analysis
PCI	Phenol-chloroform-isamyl alcohol
PCR	Polymerase Chain Reaction
PMD	Primary mitochondrial disease
PMSF	Phenylmethylsulfonyl Fluoride

qPCR	Quantitative PCR
R^2	Coefficient of determination
RCR	Rolling-circle replication
RE	Restriction enzyme
rep	Replicate
RNA	Ribonucleic acid
ROS	Reactive oxygen species
rRNA	Ribosomal RNA
RT-qPCR	Reverse transcription qPCR
S. cerevisiae	*Saccharomyces cerevisiae*
SDS	Sodium dodecyl sulfate
SLSD	Single large-scale deletions
SMD	Secondary mitochondrial disease
ssDNA	Single-strand DNA
TAE	Tris-acetate-EDTA buffer
TCA	Citric acid cycle
TE	Tris-EDTA buffer
TFA	Trifluoroacetic acid
T-PMT	Transmitted light detector
tRNA	Transfer RNA
UTR	Untranslated region
UV	Ultraviolet
WT	Wild type
ΔΨ	Mitochondrial membrane potential
ρ^-	Rho minus; petite yeast cell with fractioned mtDNA
ρ^+	Rho plus; yeast cell with functional mtDNA
ρ^0	Rho zero; petite yeast cell without mtDNA

Abbreviations of Units	Description
%	Percent
°C	Degree celsius
Arb.u.	Arbitrary unit
bp	Base pairs
Da	Dalton
fL	Femtolitre
g	Gram
h	Hours
k	Kilo
L	Litre
m	Meter
mA	Milliampere
M	Molar
min	Minutes
V	Volt
v/v	Volume per volume
w/v	Weight per volume
x g	Times gravity

Abstract

Mitochondria are important cellular organelles that contain their own genome. They are of great importance for the cell, particularly due to their role in providing energy for the cell. Accordingly, numerous diseases are linked to mitochondrial misregulation and mutations in mitochondrial DNA (mtDNA). Unlike the cell cycle-dependent replication of nuclear DNA, the mechanism of mtDNA homeostasis is not well understood. Developing a better understanding of how mtDNA is regulated would thus be a crucial step towards combating mitochondrial-related disorders. A well-known model organism, which is highly suitable due to its numerous advantages, such as the possibility to manipulate its mtDNA, is *Saccharomyces cerevisiae.* A recent study in budding yeast has shown that mtDNA copy number increases with cell volume, keeping mtDNA concentrations stable during cell growth. Additionally, it is proposed that the coupling of mtDNA to cell volume is governed by nuclear-encoded limiting factors for mtDNA replication and maintenance, which increase in amount as cell volume grows, resulting in a corresponding increase in mtDNA copy number. Furthermore, the two main components of this limiting machinery for mtDNA maintenance were identified as the mitochondrial DNA polymerase Mip1 and the packaging factor Abf2. However, the results indicate the involvement of additional limiting factors.

This thesis aimed to identify the mechanism of how mtDNA copy number is regulated with cell volume and the implications of misregulated mtDNA concentrations for cell function. By constructing and analyzing over 40 different strains, the mitochondrial single-strand DNA-binding protein Rim1 was identified as a third factor of the limiting machinery. The model proposed in this thesis considers the cell volume-dependent amount of the limiting machinery (Abf2, Mip1, Rim1) as a determinant of mtDNA copy number. To test whether cell volume does indeed not influence mtDNA copy number independently of the amount of this limiting machinery, this thesis also aims to create strains with constant amounts of the mtDNA-limiting factors with increasing cell volumes by driving the three genes under a histone promoter.

Along this line of understanding the mtDNA-regulation through the mtDNA-limiting machinery, being able to manipulate the concentration of its three factors, provides a unique opportunity to study the impact of physiologically misregulated mtDNA copy number in budding yeast. The findings of this thesis revealed a surprising robustness of the yeast with changing mtDNA concentrations in both fermentable and non-fermentable media. Altered mtDNA concentrations did not lead to any changes in cell volume, measured by Coulter counter and microscopy, nor in nDNA copy number, assessed by bud counts. A slightly faster cell growth for strains with higher mtDNA copy numbers was observed in non-fermentable media but not in fermentable media, when analyzing measurements of optical density, competition assays, and microscopy data. Moreover, the petite frequency of the strains decreases as mtDNA copy number increases. Additionally, with increasing mtDNA copy numbers, a delayed response to low glucose stress was identified by performing a microscopy media-switch experiment.

Using RNA sequencing and mass spectrometry, the expression rates at RNA and protein levels were determined for selected strains with misregulated mtDNA copy numbers. This identified an increase of mitochondrial transcripts largely proportional to the mtDNA copy number, while the corresponding proteins are regulated individually. The relative concentration of some mitochondrial-encoded proteins increased with increasing mtDNA concentrations, whereas others stayed constant.

To analyze the dependency of the mitochondrial network length and number of nucleoids on mtDNA copy number, live-cell microscopy using a LacI-LacO system to visualize mitochondria was used in strains with increasing mtDNA copy numbers. The strains with higher genomic copies of the limiting machinery resulted in increased mtDNA copy numbers but did not show any differences regarding the length of the network or number of nucleoids compared to wild type.

The fact that the amount of most mitochondrial-encoded proteins, as well as the network length and nucleoid number, is maintained constant despite increasing mtDNA concentrations, hints towards a potentially constant maintenance of mitochondrial respiration. This could be the reason for the observed robustness of the cells against the mtDNA copy number alterations. Also, this might be a potential way for budding yeast to cope with moderate mtDNA copy number changes in nature. Additionally, this thesis provides evidence that the possible underlying regulator mechanism may be related to mitochondrial protein dosage compensation and/or mitophagy. However, the exact mechanism of how the cells maintain a healthy state with changing mtDNA copy number requires further studies in the future.

Graphical abstract

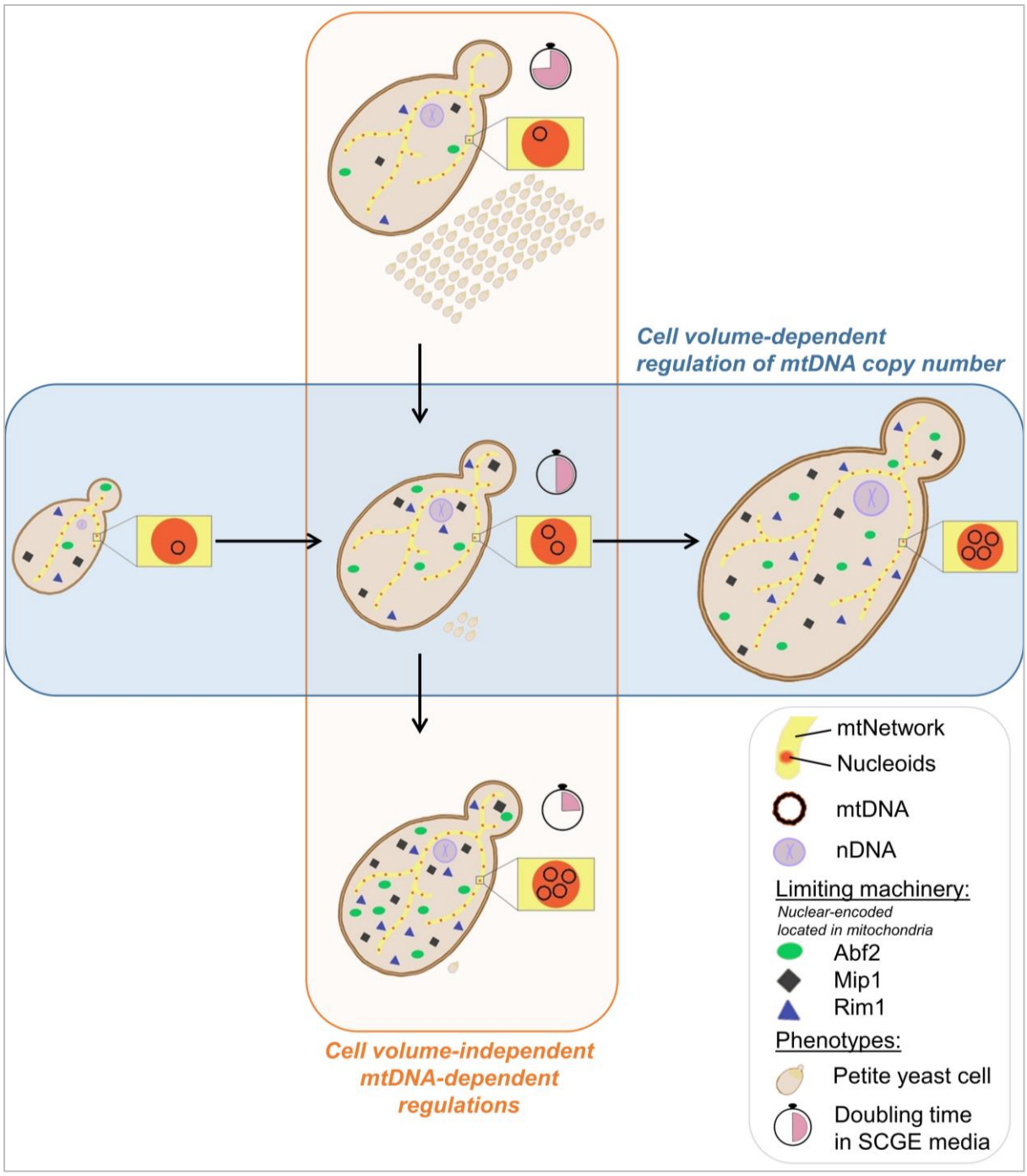

Zusammenfassung

Mitochondrien sind wichtige Organellen einer Zelle, welche ihr eigenes Genom enthalten. Insbesondere aufgrund ihrer Rolle bei der Bereitstellung von Energie sind sie von großer Bedeutung für die Zelle. Deshalb sind zahlreiche Krankheiten mit einer mitochondrialen Fehlregulation verbunden und weisen Mutationen in der mitochondrialen DNA (mtDNA) auf. Im Gegensatz zur zellzyklusabhängigen Replikation der nuklearen DNA ist der Mechanismus der mtDNA-Homöostase noch nicht gut verstanden. Die Entwicklung eines besseren Verständnisses der Regulierung der mtDNA wäre daher ein entscheidender Schritt zur Bekämpfung mitochondrienbedingter Krankheiten. Ein bekannter Modellorganismus, der sich aufgrund seiner zahlreichen Vorteile wie der Möglichkeit, die mtDNA genetisch zu manipulieren, hervorragend eignet, ist *Saccharomyces cerevisiae*. Eine kürzlich durchgeführte Studie hat gezeigt, dass die mtDNA-Kopienzahl in Hefe mit dem Zellvolumen zunimmt und die mtDNA-Konzentration während des Zellwachstums stabil bleibt. Darüber hinaus wird davon ausgegangen, dass die Kopplung der mtDNA an das Zellvolumen durch nukleär kodierte limitierende Faktoren für die mtDNA-Replikation und -Stabilisation reguliert wird. Deren Menge nimmt mit wachsendem Zellvolumen zu, was zu einem entsprechenden Anstieg der mtDNA-Kopienzahl führt. Als die beiden Hauptkomponenten dieser limitierenden Maschinerie für die mtDNA-Homöostase wurden die mitochondriale DNA-Polymerase Mip1 und der Verpackungsfaktor Abf2 identifiziert. Die Ergebnisse deuten jedoch auf die Beteiligung weiterer limitierender Faktoren hin.

Ziel dieser Arbeit war es, den Mechanismus zu ermitteln, wie die mtDNA-Kopienzahl mit dem Zellvolumen reguliert wird, und die Auswirkungen einer fehlregulierten mtDNA-Konzentration auf die Zellfunktion zu untersuchen. Durch die Konstruktion und Analyse von über 40 verschiedenen Hefestämmen wurde das mitochondriale Einzelstrang DNA-bindende Protein Rim1 als ein dritter Faktor der limitierenden Maschinerie identifiziert. Das in dieser Arbeit vorgeschlagene Modell betrachtet die vom Zellvolumen abhängige Menge der limitierenden Faktoren (Abf2, Mip1, Rim1) als eine Determinante der mtDNA-Kopienzahl. Um zu testen, ob das Zellvolumen tatsächlich keinen Einfluss auf die mtDNA-Kopienzahl unabhängig von der Menge dieser limitierenden Maschinerie hat, zielt diese Arbeit auch darauf ab, Stämme mit konstanten Mengen der mtDNA-limitierenden Faktoren mit zunehmendem Zellvolumen zu erzeugen, indem die drei Gene von einem Histonpromotor exprimiert werden.

Das Verständnis der mtDNA-Regulierung durch die limitierende Maschinerie bietet die einzigartige Gelegenheit, durch die Möglichkeit von veränderten Konzentrationen der drei Faktoren, die Auswirkungen einer physiologisch fehlregulierten mtDNA-Kopienzahl in Hefen zu untersuchen. Die Ergebnisse dieser Arbeit zeigten eine überraschende Robustheit der Hefe bei veränderten mtDNA-Konzentrationen sowohl in fermentierbaren als auch in nicht fermentierbaren Medien. Veränderte mtDNA-Konzentrationen führten weder zu einer Veränderung des Zellvolumens, das mit einem Coulter-Zähler und durch Mikroskopie gemessen wurde, noch zu einer Veränderung der nDNA-Kopienzahl, die durch Knospenzählung ermittelt wurde. In nicht fermentierbarem Medium, nicht jedoch in fermentierbarem Medium, wurde ein etwas schnelleres Zellwachstum für Stämme mit höheren mtDNA-Kopienzahlen beobachtet. Dies wurde mittels OD-Messungen, Konkurrenz-Assays und Mikroskopiedaten analysiert. Außerdem nimmt die Petitfrequenz der Stämme mit steigender mtDNA-Kopienzahl ab. Darüber hinaus wurde während eines Medienwechsel-

Mikroskopie-Experiments mit zunehmender mtDNA-Kopienzahl eine verzögerte Reaktion auf niedrigen Glukosestress festgestellt.

Mittels RNA-Sequenzierung und Massenspektrometrie wurden die Expressionsraten auf RNA- und Proteinebene für ausgewählte Stämme mit fehlregulierten mtDNA-Kopienzahlen bestimmt. Dabei wurde ein Anstieg der mitochondrialen Transkripte festgestellt, der weitgehend proportional zur mtDNA-Kopienzahl ist, während die entsprechenden Proteine individuell reguliert wurden. Die relative Konzentration einiger mitochondrial kodierter Proteine steigt mit zunehmender mtDNA-Konzentration, während andere konstant bleiben.

Um die Abhängigkeit der Länge des mitochondrialen Netzwerks und der Anzahl der Nukleoide von der mtDNA-Kopienzahl zu analysieren, wurden Stämme mit steigender mtDNA-Kopienzahl Lebendzellmikroskopie unter Verwendung eines LacI-LacO-Systems zur Visualisierung von Mitochondrien eingesetzt. Die Stämme mit höheren genomischen Kopien der limitierenden Maschinerie führten zu einer erhöhten mtDNA-Kopienzahl, zeigten aber keine Unterschiede hinsichtlich der Länge des Netzwerks oder der Anzahl der Nukleoide im Vergleich zum Wildtyp.

Die Tatsache, dass die Menge der meisten mitochondrial kodierten Proteine sowie die Länge des Netzwerks und die Anzahl der Nukleoide trotz steigender mtDNA-Konzentrationen konstant bleiben, deutet auf eine potenziell konstante mitochondriale Zellatmung hin. Dies könnte der Grund für die beobachtete Robustheit der Zellen gegenüber Veränderungen der mtDNA-Kopienzahl sein. Ebenso könnte dies auch ein möglicher Weg für die Hefe sein, mit moderaten Veränderungen der mtDNA-Kopienzahl in der Natur fertig zu werden. Darüber hinaus liefert diese Arbeit Hinweise darauf, dass der zugrundeliegende Regulierungsmechanismus mit dem Ausgleich der mitochondrialen Proteindosierung und/oder Mitophagie zusammenhängen könnte. Der genaue Mechanismus, wie die Zellen einen gesunden Zustand bei veränderter mtDNA-Kopienzahl aufrechterhalten, erfordert in Zukunft jedoch weitere Experimente.

1. Introduction

Human diseases can be caused by many factors, one of which is the disruption of mitochondrial homeostasis (Niyazov *et al.*, 2016). A large number of diseases are documented to be related to mitochondria, including diabetes and Alzheimer's (Poulton *et al.*, 1989; Rötig *et al.*, 1992; Dunbar *et al.*, 1993; Keogh and Chinnery, 2015). In this context, an important role is played by mitochondrial DNA (mtDNA), whose mutation is documented in around 80% of mitochondrial diseases in adults (Wen *et al.*, 2025). The evolutionary background of mitochondria explains the importance of this organelle and the existence of mtDNA: As the endosymbiosis theory describes, mitochondria developed by incorporation and evolution of an alphaproteobacterium into a host cell (Wang and Wu, 2015). The establishment of this new organelle can be based on various advantages for the cell, such as the ability to produce energy via fermentation (Margulis, 1970). Although mitochondria are composed of two membranes (Lemasters, 2007), illustrating their incorporation in the past, they have lost their full autonomy by becoming a part of all eukaryotic cells (Alberts *et al.*, 2025). During evolution, parts of their genome were transferred into the nuclear host DNA (Alberts *et al.*, 2025). Nevertheless, they still contain their own restricted DNA, known as mtDNA (Nass and Nass, 1963). The major task of mitochondria is to produce adenosine triphosphate (ATP) through the electron transport chain (ETC), which is located at the mitochondrial inner membrane (Alberts *et al.*, 2025). Besides this, mitochondria are involved in the amino acid production (Kohlhaw, 2003; Xu *et al.*, 2006), the iron-sulfur cluster synthesis (Braymer and Lill, 2017), the heme homeostasis (Hoffman *et al.*, 2003), and the redox state of the cell (Alberts *et al.*, 2025). The important functions in the cell explain the importance of mitochondria and the reason for their involvement in various diseases.

This also highlights the relevance of understanding mitochondria and mtDNA in detail, whose regulation is only partially known so far. A commonly used model organism to study mitochondria is *Saccharomyces cerevisiae.* The well-studied so-called "budding yeast" has several advantages justifying its use for this study. Most importantly, budding yeast can be easily cultivated and genomically manipulated (Guthrie and Fink, 1991; Duina *et al.*, 2014). Its ability to grow in fermentable media, even without containing functional mtDNA (Ephrussi and Slonimski, 1955; Schatz *et al.*, 1964), additionally opens up huge possibilities when studying mtDNA.

Mitochondria in budding yeast are shaped like a network, which pervades the whole cell (Hermann *et al.*, 1998). The network includes relatively equally distributed nucleoids (Osman *et al.*, 2015), which package the mtDNA with a variety of proteins (Williamson and Fennell, 1975; Kukat *et al.*, 2011). One of these proteins is the major packaging factor Abf2 (Zelenaya-Troitskaya *et al.*, 1995), whose homolog in mammals is known as TFAM (Ekstrand *et al.*, 2004). The mtDNA is replicated by its own replication machinery, consisting of different proteins such as the mtDNA polymerase, in budding yeast known as Mip1 (Genga *et al.*, 1986) and in mammals as PolG (Foury, 1989). Furthermore, mtDNA in budding yeast encodes eight proteins, which are mainly part of the ETC (Foury, 1989).

Interestingly, mtDNA is not strictly coupled to the cell cycle as nuclear DNA (nDNA). By contrast, as the length of the mitochondrial network (mtNetwork) and the number of nucleoids, it has been shown that the mtDNA copy number is also regulated cell volume dependently (Rafelski *et al.*, 2012; Osman *et al.*, 2015; Seel *et al.*, 2023). Previous studies could even

identify two major limiting factors of mtDNA copy number: Abf2 and Mip1 (Seel *et al.*, 2023). The cell volume-dependent regulation of the amount of those nuclear-encoded proteins limits the mtDNA copy number in budding yeast (Seel *et al.*, 2023).

A previous study has shown the dependency of mtDNA copy number on Abf2 and Mip1 in hemizygous deletion strains, but an addition of the two genes could not completely explain the cell volume-dependent regulation of the mtDNA copy number (Seel *et al.*, 2023). That is why it remains open whether other additional factors might limit mtDNA copy number in budding yeast. Also, it is unclear whether a cell volume-dependent regulation of the mtDNA copy number occurs independently of the described limiting-machinery. This study aims to answer these two questions to better understand the details of mtDNA copy number regulation. Additionally, it aims to reveal how altered mtDNA concentrations affect cell function. This thesis also answers the question whether mtDNA copy number influences the mitochondrial network length and number of nucleoids in budding yeast.

Before going into details of the results, important background information about mitochondria and mtDNA will be highlighted in the following sections of chapter 1, and the material and methods used are described in chapter 2. After explaining the results in chapter 3, they will be discussed in chapter 4.

1.1. The structure and cell cycle of budding yeast

The model organism of choice in this study was *Saccharomyces cerevisiae*, which is a unicellular eukaryotic organism. This class of cells contains highly organized cytoplasmic organelles such as the nucleus and mitochondria (Alberts *et al.*, 2025). As visualized in Figure 1, budding yeast cells are surrounded by a cell membrane and a cell wall, which contains the cell components and the cytoplasm (Alberts *et al.*, 2025). As their name already indicates, budding yeast form small daughter cells, so-called “buds”, during cell cycle progression.

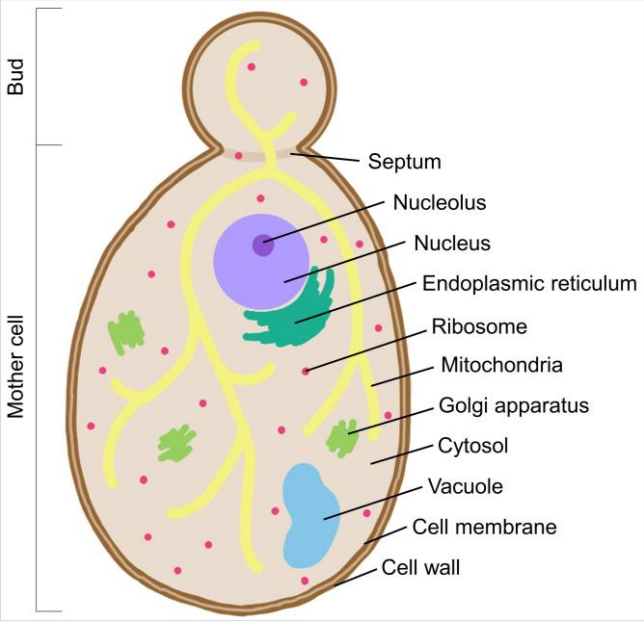

Figure 1: The structure of budding yeast. A budding yeast cell is covered by a cell wall and cell membrane (dark brown). The cytosol (light brown) contains different organelles: Nucleus (including nucleolus; purple), endoplasmic reticulum (dark green), Golgi apparatus (light green), ribomsome (pink), mitochondria (yellow) and vacuole (blue). The junction between mother and daughter cell (“bud”) is called septum.

Besides sexual reproduction by mating, budding yeast can also reproduce asexually by undergoing the cell cycle (Figure 2) (Duina *et al.*, 2014). During the so-called G1-phase, the cell increases in size (Morgan, 2007). Before being able to switch into S-phase, the cell has to pass the *Start*-check point (Jorgensen *et al.*, 2002). The correlation between the cell cycle regulators Whi5 (Jorgensen *et al.*, 2002), Bck2 and Cln3 (Mortimer *et al.*, 1992; Bastajian *et al.*, 2013) plays an essential role here: While Whi5 is inhibiting, Bck2 and Cln3 are activating the SBF-transcription factor involved in G1/S-transition. As Whi5 is regulated independently of the cell size, its protein concentration decreases with increasing size. On the other hand, Bck2 and Cln3 are kept at constant protein concentrations, as they are regulated cell size-dependently (Schmoller *et al.*, 2015; Chen *et al.*, 2020). The increasing cell size during G1-phase therefore results in a progressive Whi5-dilution, increasing the probability of the start of S-phase. During S-phase, DNA is replicated and the yeast mother cell creates a small attached bud. The next cell cycle phases are G2- and M-phase, where mitosis and cytokinesis take place. Here, two regulatory commitment points are reported: a G2/M-checkpoint also called “morphogenesis”-checkpoint (Lew and Reed, 1995; McMillan *et al.*, 1998) and the metaphase-anaphase transition control (Yang *et al.*, 1997). In the G2/M-phase, the bud increases in size and is provided with all necessary components by its mother cell, such as a nucleus and mitochondria (Morgan, 2007). The cytokinesis in *S. cerevisiae* is an asymmetrical division of the daughter (bud) from its mother (Hartwell and Unger, 1977). Both cells, mother and daughter, continue their own cell cycle by going into G1-phase next (Morgan, 2007). As the cell size of the daughter is smaller than the cell size of the mother, the daughter cell will stay longer in its first G1-phase (Hartwell and Unger, 1977). Additionally, the transcription factors Ace2 and Ash1, which are expressed in the daughter cells, repress *CLN3* and therefore support a longer initial G1-phase (Di Talia *et al.*, 2009).

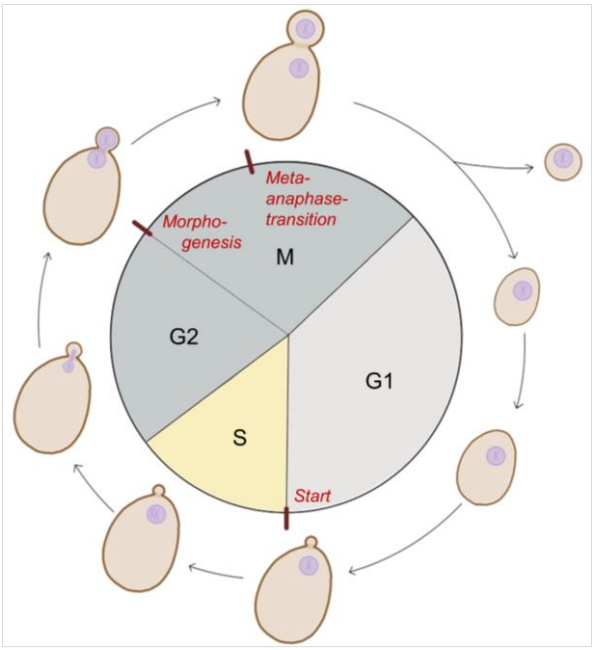

Figure 2: The asexual cell cycle of budding yeast. Budding yeast cells increase their cell size in G1-phase until they can proceed through the checkpoint “Start”. In S-phase they replicate their nuclear DNA and start forming a small daughter cell, the so-called “bud”. In G2/M-phase, the bud increases in size while mitosis takes place and divides from the mother during cytokinesis. Two known checkpoints regulate the progression during G2/M-phase: the “morphogenesis”-checkpoint and the metaphase-anaphase transition control. After the bud divides from its mother asymmetrically, both go into G1-phase independently.

1.2. Advantages of using *Saccharomyces cerevisiae* as a model organism to study mitochondria

As briefly mentioned in the beginning, the model organism *Saccharomyces cerevisiae* brings a wide range of advantages for this study: First, the possibility to analyze both haploid (single set of chromosomes) and diploid (two sets of chromosomes) strains. Also, the yeast strain W303, which is used as background in this study, is already sequenced completely (Ralser *et al.*, 2012), and the manipulation of genes in yeasts is relatively easy (Guthrie and Fink, 1991; Duina *et al.*, 2014). Moreover, it is even possible to do genomic manipulations of mtDNA when using budding yeast (Fox *et al.*, 1991). The relatively fast and simple growth conditions of this model organism enable various experimental designs. Budding yeast can perform mitochondria-independent fermentation to generate energy or switch into respiration, where mitochondria are needed (Crabtree, 1929; Feldmann, 2012; Ben Galeota-Sprung *et al.*, 2022). This makes *S. cerevisiae* capable of growing in both fermentable and non-fermentable media, which is a very useful tool for studying mitochondria, as intended here. The fact that yeast lacking (ρ^0) or containing non-functional (ρ^-) mtDNA can survive in fermentable media by using fermentation for energy production enabled researchers to identify mtDNA and its involvement in the respiratory functions of cells (Ephrussi and Slonimski, 1955; Schatz *et al.*, 1964). Another advantage is the existence of an already established system to visualize mtDNA in yeast: the LacI-LacO system uses the aim of the mNeon-tagged LacI repressor to bind the mitochondrial-integrated LacO-repeats to visualize the nucleoids (Osman *et al.*, 2015; Seel *et al.*, 2023). Moreover, as a lot of proteins are highly conserved from budding yeast to different eukaryotic cells, like mammals, the results can easily be used as a starting point to study human disease. Interestingly, more than 50% of the mitochondrial-related proteins in yeast (Prokisch *et al.*, 2004; Reinders *et al.*, 2006) are reported to have a homolog in mammals (Pagliarini *et al.*, 2008). All in all, this high number of advantages justifies the choice to use budding yeast to study mtDNA, as intended in this thesis.

1.3. The organelle mitochondria and its mtDNA

1.3.1. The structure of mitochondria

Mitochondria are, as shown in Figure 3, organelles that generally consist of two membranes: the permeable outer membrane (non-specifically permeable for proteins smaller than 5.000 Da) covers the non-permeable inner membrane (Lemasters, 2007). The transport through the inner membrane can only occur with the help of exchangers and transporters. To maximize its surface, the inner membrane is laid in several folds called “cristae” structures (Alberts *et al.*, 2025). In most organisms, including yeast, mitochondria are formed like a network that is distributed throughout the whole cell. In some cell types, they might appear differently, for example, in liver tissue: here the shape of mitochondria shifts between spherical, doughnut- or C-shaped forms (Ding *et al.*, 2012; Jenkins *et al.*, 2024). The mitochondrial network in budding yeast is highly flexible and can be changed by fission or fusion. While fusion describes the merging of two mitochondria, fission represents the division of a mitochondrial tube into two parts. Selective degradation can occur by detaching defined parts of the network using fission (Youle and van der Bliek, 2012).

According to the endosymbiosis theory, mitochondria are semi-autonomous organelles in both yeast and mammals, harbouring their own DNA (Nass and Nass, 1963). Over the years, the genome of the incorporated alphabacterium was shrunk by the loss of unnecessary or repetitive genes. Additionally, some genes were incorporated into the nuclear DNA of the host cell. The remaining genes form the mtDNA, which is replicated, transcribed and translated inside the matrix of mitochondria (Alberts *et al.*, 2025).

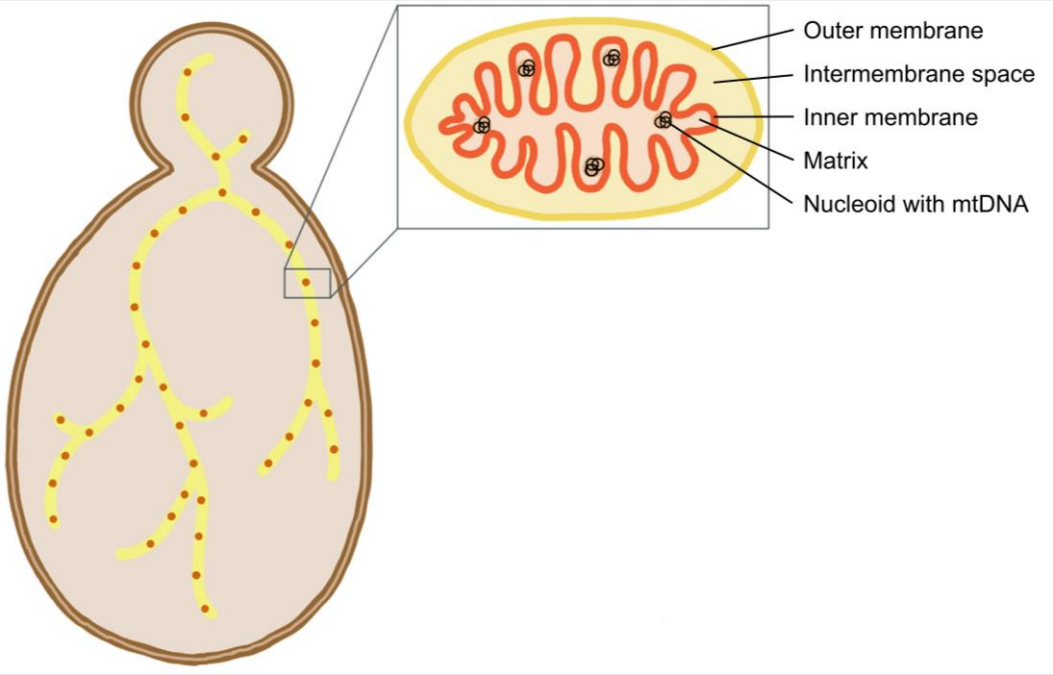

Figure 3: The structure of mitochondria in budding yeast. The mitochondria in budding yeast are shaped like a network permeating the entire cell (yellow). This network includes an outer and inner membrane, separated by the intermembrane space. The inner membrane of mitochondria is layered in cristae, leading to a maximation of surface. Inside the inner membrane, the mitochondrial matrix harbours “nucleoids” including the mtDNA. The nucleoids are equally distributed throughout the mitochondrial network.

1.3.1. The functions of mitochondria

Besides their roles in metabolic processes, by producing amino acids (Kohlhaw, 2003; Xu *et al.*, 2006), the synthesis of iron-sulfur clusters (Braymer and Lill, 2017) and heme (Hoffman *et al.*, 2003) mitochondria are responsible for the redox state and, most importantly, the major ATP producer in the cell. The principle for providing energy for the cell through the ETC takes place at the inner membrane of mitochondria. The ETC in mammals includes five enzyme complexes, as well as cytochrome c and ubiquinone (Nolfi-Donegan *et al.*, 2020). However, in *S. cerevisiae* complex I of the ETC is replaced by two NADH dehydrogenases (Vries and Marres, 1987). Still, the essence of the production of ATP at the ETC is conserved from mammals to yeasts, as shown in Figure 4. Through different pathways, pyruvate is generated and transported into the mitochondria, where it is converted into acetyl-CoA. Which is further metabolised in the citric acid cycle (TCA) to generate the two-electron donors needed. In budding yeast, these are nicotinamide adenine dinucleotide (NADH) and succinate, whereas in mammalian cells NADH and flavin adenine dinucleotide ($FADH_2$) provide the electrons which go through the ETC. The exergonic process of the electron flow through the ETC includes a translocation of protons (H^+) from the mitochondrial matrix into the intermembrane space, generating an electrochemical gradient between these two. This so-called "mitochondrial membrane potential" ($\Delta\Psi$) drives the phosphorylation of adenosine diphosphate (ADP) to ATP by the ATP-synthase (Complex V). Located in the inner membrane, the ATP-synthase transports the excess protons from the intermembrane space back into the matrix and thereby generates energy in the form of ATP.

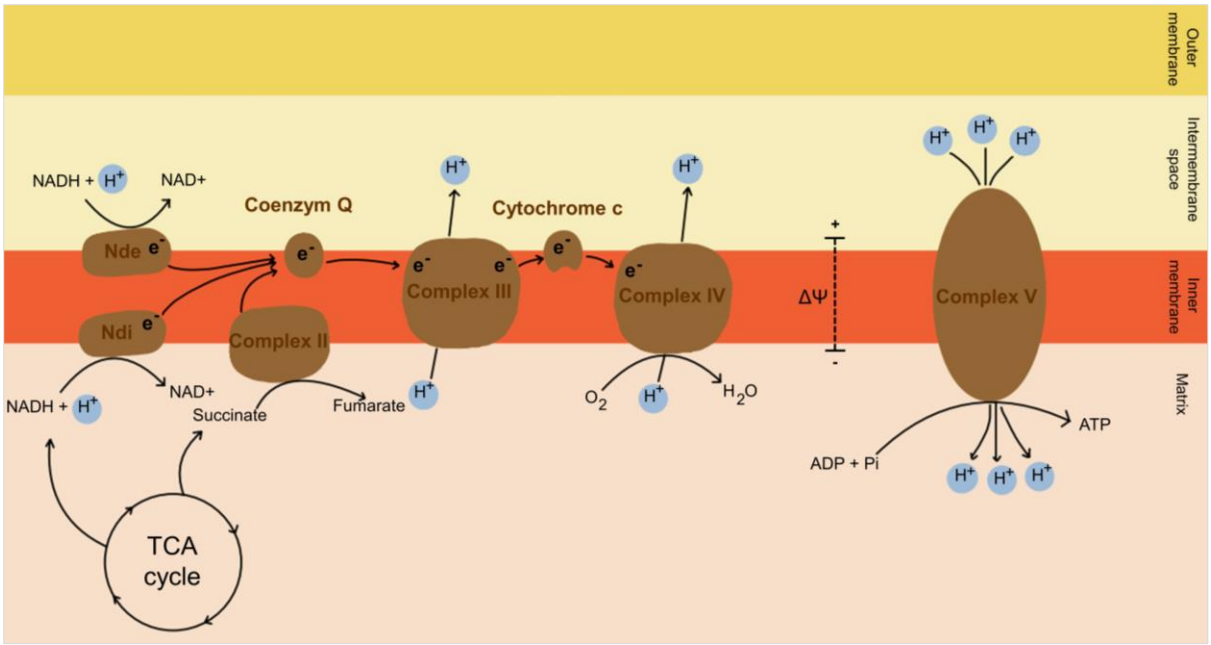

Figure 4: The electron transport chain at the inner membrane of budding yeast mitochondria. As yeasts do not have a complex I as mammals do, the first step at the ETC is performed by two NADH dehydrogenases (Nde and Ndi). To produce ATP by the ETC, different pathways serve acetyl-CoA first. This can be metabolized in the citric acid cycle (TCA) to generate two-electron donors needed for the ETC: In budding yeast, these are NADH and succinate. Through an exergonic process, the electrons flow through the different complexes of ETC along the mitochondrial inner membrane, leading to a translocation of protons (H+) into the mitochondrial intermembrane space. Thereby, an electrochemical gradient (mitochondrial membrane potential, ΔΨ) is generated along the mitochondrial inner membrane. This potential drives the ATPase (Complex V), which phosphorylates ADP into ATP.

As mentioned above, through reactive oxygen species (ROS), mitochondria are also responsible for the redox state of the cell. The ETC can also lead to ROS production, such as hydrogen peroxide (H_2O_2) or superoxide anion radical ($O_2^{\bullet-}$) (Nolfi-Donegan *et al.*, 2020). These substances can lead to signal transduction involved in cell growth and differentiation (Sauer *et al.*, 2001). Moreover, it is speculated that ROS are participating in the induction of mtDNA replication (see chapter 1.3.3.2.) (Hori *et al.*, 2009).

1.3.2. Their role in human disease highlights the importance of studying mitochondria and mtDNA

Many studies in humans have shown diseases related to mitochondria, known as primary mitochondrial diseases (PMD) or secondary mitochondrial diseases (SMD) (Niyazov *et al.*, 2016). As the name already indicates, PMDs are characterized by a dysfunction of mitochondria's primary function (Niyazov *et al.*, 2016), which often leads to reduced ATP levels and increased ROS (Ceccatelli Berti *et al.*, 2021). PMDs are caused by mutations in mtDNA and/or nDNA affecting genes encoding members of the ETC (Niyazov *et al.*, 2016). On the other hand, SMDs are described as diseases based on mutations affecting mitochondria outside their energy supply through ATP-production (Niyazov *et al.*, 2016). For example, damage impairing mitochondrial fission and fusion is associated with diseases such as Alzheimer's, Parkinson's (Keogh and Chinnery, 2015), or cardiovascular disease (Ahuja *et al.*, 2013). Mitochondrial disease can further be divided into two sub-groups: single large-scale deletions (SLSD) and mtDNA maintenance disorders (MMD) (Bernardino Gomes *et al.*, 2024). SLDS occur sporadically and mostly early in development or as an accumulation over time (Chen *et al.*, 2011; Pitceathly *et al.*, 2012).

To focus on MMD, these diseases can be associated with either complete mtDNA depletion, the clustering of multiple mtDNA deletions or, far less frequently, duplications of mtDNA (Bernardino Gomes *et al.*, 2024). While these duplications are mainly described in diabetes (Poulton *et al.*, 1989; Rötig *et al.*, 1992; Dunbar *et al.*, 1993) or Kearns-Sayre syndrome (Tang et al., 2000), complete or partial deletions of mtDNA are associated with a large variety of diseases. Deletions of mtDNA can lead to changes in mtDNA replication, dynamics, or its nucleotide metabolism (Bernardino Gomes *et al.*, 2024). Diseases associated with reduced mtDNA copy numbers are for example breast cancer, type-2 diabetes or liver disease (Clay Montier *et al.*, 2009). The accumulated presence of mtDNA mutations in human diseases highlights the importance of studying mtDNA homeostasis.

1.3.3. The structure, replication and regulation of mtDNA

1.3.3.1. The structure of mitochondrial DNA

In mammals and yeast, mitochondria contain their own DNA (Nass and Nass, 1963), which is packaged into DNA-protein complexes, so-called "nucleoids" (Williamson and Fennell, 1975; Kukat *et al.*, 2011). The nucleoids are distributed throughout the mtNetwork at an almost uniform distance of 800 nm on average in yeast (Osman *et al.*, 2015) and between 500 and 2000 nm in mammalian cells (Kukat *et al.*, 2011). To ensure this distribution and control the inheritance of the mtDNA, nucleoids are speculated to be anchored at the inner membrane of mitochondria (Nunnari *et al.*, 1997; Cho *et al.*, 1998). As also shown in Figure 5, this takes place near the mitochondrial contact sites complexes (MICOS), which stabilize the contact of nucleoids at the Cristae junctions, where the inner and outer membranes come close (Harner *et al.*, 2011). Based on different literature, a nucleoid contains one or multiple copies of mtDNA (Miyakawa *et al.*, 2004; Lipinski *et al.*, 2010; Kukat *et al.*, 2011). Additionally, different proteins

help package and stabilize mtDNA in the nucleoids. The major packaging factor of mtDNA in yeast is Abf2 (Zelenaya-Troitskaya *et al.*, 1995), whose homologue in mammals is known as TFAM (Ekstrand *et al.*, 2004). The structure of mtDNA can be in a linear or circular form (Shapiro *et al.*, 1968). While linear mtDNA is described as not tightly packed and loosely bound by Abf2 (Brewer *et al.*, 2003), the protein helps wrap circular mtDNA into supercoils (Diffley and Stillman, 1992). Recent studies in HeLa cells have reported two nucleoid types with different accessibilities shaped by their TFAM levels (Isaac *et al.*, 2024). The nucleoids containing tightly packaged mtDNA with high TFAM amounts seem to be hardly accessible for the replication machinery and are therefore categorized as “inactive nucleoids” (Isaac *et al.*, 2024). In contrast to the “active nucleoids”, which are bound by a smaller amount of TFAM and are frequently replicated, the inactive version is speculated to be a genetic reservoir or regulator for the location of mtDNA replication within the network (Isaac *et al.*, 2024). In yeast, Abf2 has an antagonist called Cim1, which is also described to be part of the mitochondrial HMG-box family (Schrott and Osman, 2023). Additionally, proteins that are part of mtDNA replication and transcription are present in nucleoids. In budding yeast, this includes the helicases Hmi1 (Sedman *et al.*, 2000) and Pif1 (Ramanagoudr-Bhojappa *et al.*, 2013), the mtDNA polymerase Mip1 (Genga *et al.*, 1986), the RNA polymerase Rpo41 (Lisowsky and Michaelis, 1989), and the single-strand DNA (ssDNA) binding protein Rim1 (van Dyck *et al.*, 1992). The role of these proteins will be highlighted in the chapters 1.3.3.2. and 1.3.3.3. Mammalian nucleoids also contain mitochondrial helicases, the best known of which is TWINKLE, which has no direct homolog in yeast (Spelbrink, 2010). All of the other named yeast proteins have mammalian homologs that are also associated with the human nucleoid: PolG for the mtDNA polymerase (Lodi *et al.*, 2015), POLRMT for the mitochondrial RNA polymerase (Sultana *et al.*, 2017), and SSBP1 for the ssDNA-binding protein (Spelbrink, 2010).

In yeast, the mtDNA is approximately 86 kb long, encodes eight proteins (Foury *et al.*, 1998) and contains eight origin-like elements (oris) (Tzagoloff and Myers, 1986), 24 non-coding transfer RNAs and ribosomal RNAs (Zamaroczy and Bernardi, 1986b). Whereas mammal mtDNA encodes for 13 proteins in its approximately 16.6 kb (Anderson *et al.*, 1981). Another major difference is the presence of introns in yeast mtDNA, which are not found in human mtDNA (Tzagoloff and Myers, 1986). Moreover, coding regions of mtDNA in yeast are separated by AT-rich regions, while the genes consist of around 30% GC-rich regions (Zamaroczy and Bernardi, 1986a).

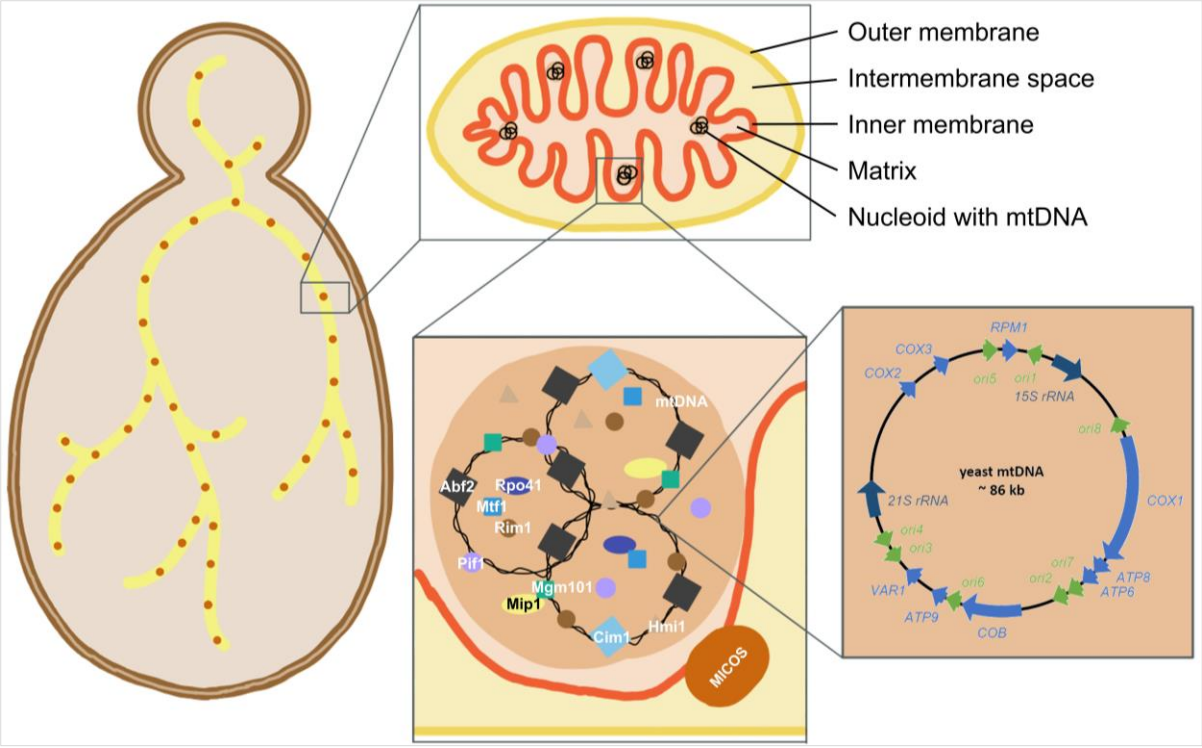

Figure 5: The structure of mitochondria in budding yeast. Left: the mitochondrial network with equally distributed nucleoids. Upper middle: a detailed slice of mitochondria. Bottom middle: the detailed structure of nucleoids, including mtDNA and associated proteins. Right: a schematic representation of circular mtDNA.(partially adapted from (Seel, 2022))

1.3.3.2. The replication and quality control of mtDNA

The replication of mtDNA, in contrast to nuclear DNA (nDNA), is not strictly coupled to the cell cycle and is not completely understood yet. In some eukaryotic organisms, such as budding yeast, the so-called rolling-circle replication (RCR) is assumed (Maleszka *et al.*, 1991; Backert *et al.*, 1996; Lewis *et al.*, 2015). If the mtDNA is present as concatemers in a linear shape, it first has to become circular by intermolecular recombination (Figure 6). The first step of the initiation is to unwind the mtDNA by its helicases Pif1, Rrm3 and Hmi1 (Sedman *et al.*, 2005; Ramanagoudr-Bhojappa *et al.*, 2013). The next step of priming the replication can occur in a transcription-dependent manner (Lecrenier and Foury, 2000) by the RNA-polymerase Rpo41 (Lisowsky and Michaelis, 1989), whose complex to the promoter is stabilized by Mtf1 (Sanchez-Sandoval *et al.*, 2015). As studies have documented mtDNA maintenance in cells lacking Rpo41 (Fangman *et al.*, 1990b), there has to be at least one alternative pathway to initiate mtDNA replication. The so-called “recombination-mediated rolling circle replication” is a common alternative model. Here, the priming happens with the help of homologous priming of a concatemeric mtDNA. This linear mtDNA is created by a double-strand break induced by the enzyme Ntg1 (Maleszka *et al.*, 1991; Bendich, 1996; Ling *et al.*, 2007), potentially activated by ROS (Hori *et al.*, 2009). The linear single-stranded mtDNA is stabilized by Rim1 (Mbantenkhu *et al.*, 2011). By processing the 5’-tail through the exonuclease Din7 (Ling *et al.*, 2013), the mitochondrial homologous recombinase Mhr1 can recognize and bind the mtDNA (Ling and Shibata, 2002). The recombination can additionally be catalyzed by the protein Mgm101 (Hayward *et al.*, 2013), with the help of ssDNA-binding protein Rim1 (Mbantenkhu *et al.*, 2011). Moreover, Mgm101 is speculated to recruit the mtDNA polymerase Mip1 in yeast (Meeusen and Nunnari, 2003). Independent of how the mtDNA replication was primed, the

next steps of elongation and termination are carried out by the only mtDNA polymerase in yeast: Mip1 (Genga *et al.*, 1986).

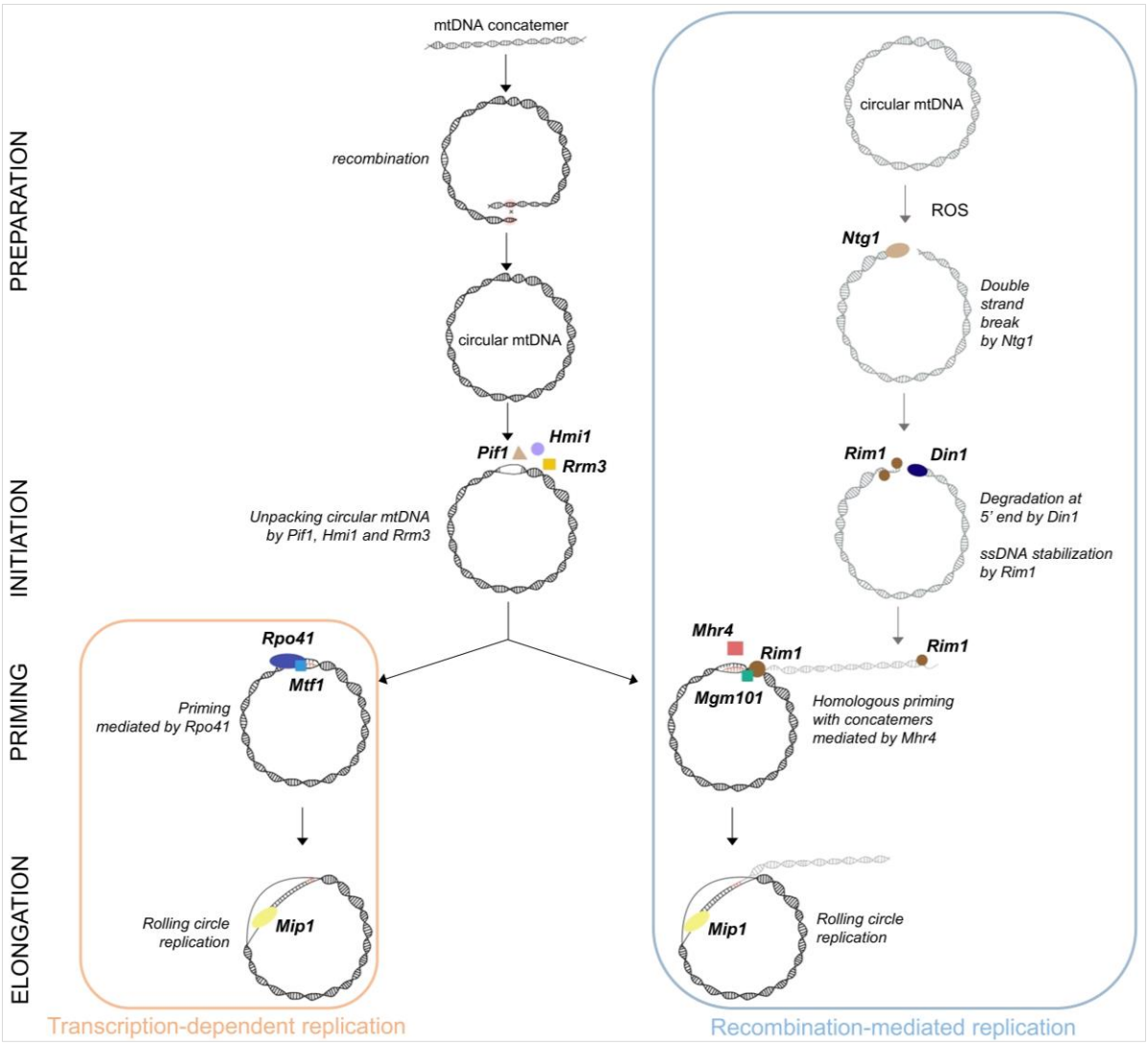

Figure 6: Proposed mechanisms of mtDNA replication in budding yeast. After preparation of mtDNA into its circular form by recombination (if needed), the replication is initiated by unwinding through the helicases Hmi1, Pif1 and Rrm3. Next, priming can be mediated by Rpo41 called "transcription-dependent replication" (left; orange). The Rpo41-promotor complex is stabilized by Mtf1. Alternatively, priming can be mediated by recombination (right; blue): The homologous linear mtDNA is created by a double-strand break mediated by ROS and Ntg1. Din1 degrades the 5'-end and Rim1 stabilizes the single strand of mtDNA. Afterwards, this mtDNA sequence is used for homologous priming by Mhr4 with the help of Rim1 and Mgm101. The elongation takes place via rolling circle replication by the mtDNA polymerase Mip1 (partially adapted from (Seel, 2022))

Due to a lower number of repair mechanisms, the chance of mutations is noticeably higher in mtDNA than in nDNA (Haag-Liautard *et al.*, 2008; Lynch *et al.*, 2008). Incorrect replication (Stumpf *et al.*, 2010) or damaged mtDNA due to other influences such as ROS (Doudican *et al.*, 2005) can become problematic for the cell, especially if the mutations interfere with the function of mitochondria (Park and Larsson, 2011). The first control of mutations is done by Mip1, which is, besides replicating mtDNA, also in charge of proofreading mtDNA using its exonuclease activity (Foury and Vanderstraeten, 1992).

In humans, mutations in mtDNA can be particularly problematic, as they can cause multiple diseases (see chapter 1.3.2.). Due to mutation events, multiple versions of mtDNA can exist in a cell in parallel, which is called “heteroplasmy” (Stewart and Chinnery, 2021). If the proportion of mutated mtDNA copies exceeds a certain threshold in a cell or tissue, the mutations are sufficient to trigger the appearance of a phenotypic disease (Rossignol *et al.*, 2003). Moreover, the degree of heteroplasmy, indicating the variability of mtDNA, can change throughout a lifetime in mammalian cells (Zhang *et al.*, 2017; Wengert *et al.*, 2024) and yeast (Kauppila *et al.*, 2017). Recent studies found a fast adjustment of heteroplasmic populations of budding yeast to homoplasmic states (Roussou *et al.*, 2024). This approach is documented to be related to the mtDNA copy distribution during cell division, as well as the fission and fusion events of the mtNetwork (Roussou *et al.*, 2024). Former theoretical modelling suggested the heteroplasmy to be influenced by the number of cell divisions (Johnston *et al.*, 2015; Johnston, 2019), mitochondrial network and/or mitochondrial dynamics (Kowald and Kirkwood, 2011; Tam *et al.*, 2013; Glastad and Johnston, 2023), supporting those results.

Generally, fission and fusion are part of the quality and quantity control system of the mitochondria (Nunnari *et al.*, 1997). These events also play a role in mtDNA inheritance and segregation (Roussou *et al.*, 2024). Previous papers have shown a selective and controlled inheritance of mtDNA from the mother to the daughter cells in yeast (Okamoto *et al.*, 1998), influencing the cell fitness (Kotrys *et al.*, 2024) and preferring the transfer of intact mtDNA (Jakubke *et al.*, 2021).

1.3.3.3. Regulatory proteins of mtDNA in budding yeast

As previously mentioned, due to its ability to grow on fermentable carbon sources even if they contain only non-functional mtDNA (ρ^-) or lack mtDNA completely (ρ^0) (Ephrussi and Slonimski, 1955), budding yeast is a suitable model organism to study mtDNA and its homeostasis. Several proteins have been identified to be involved in the mtDNA homeostasis of budding yeast over the last decades. The proteins listed in this chapter are only a part of the factors influencing mtDNA, which were selected to mention due to their importance for this study. Probably best known is the mtDNA polymerase Mip1, whose deletion leads to a complete loss of mtDNA (ρ^0) (Foury, 1989). Moreover, a hemizygous deletion in a diploid strain reduces the mtDNA copy number by approximately 36% compared to the wild type when cultured in non-fermentable media (Seel *et al.*, 2023). In line with that, increasing the *MIP1* gene copy number results in higher mtDNA concentrations (Seel *et al.*, 2023). Another well-studied example is the packaging factor Abf2, whose deletion in a haploid strain results in reduced mtDNA (Diffley and Stillman, 1991; Zelenaya-Troitskaya *et al.*, 1998). Also, a diploid hemizygous deletion results in approximately 31% reduced mtDNA concentrations when grown in non-fermentable media (Seel *et al.*, 2023). Similar to Mip1, increased Abf2 concentrations lead to higher mtDNA concentrations (Seel *et al.*, 2023). The following proteins have been identified to be involved in mtDNA replication (see chapter 1.3.3.2.) and are also known to impact mtDNA: Rim1 (van Dyck *et al.*, 1992), Mgm101 (Chen *et al.*, 1993), Hmi1 (Monroe *et al.*, 2005), Rpo41 (Greenleaf *et al.*, 1986; Fangman *et al.*, 1990a), Mtf1 (Lisowsky and Michaelis, 1988), Mhr1 (Ling *et al.*, 1995) and Pif1 (Foury and Kolodynski, 1983; Lahaye *et al.*, 1991). Hemizygous deletions of the genes coding for these proteins in diploid yeast strains have shown reduced mtDNA concentrations to various degrees (Seel *et al.*, 2023) and complete deletions result in ρ^- or ρ^0 yeasts. The effect of increased expression of these proteins was not studied in detail, but it does not necessarily lead to increased mtDNA, for example shown for Rpo41 (Schrott *et al.*, 2025). By contrast, other factors whose decrease or

deletion leads to an increase in mtDNA have been identified. Within this category, the mitochondrial ribosome-associated proteins Mrx6 and Mam33 and the packaging protein Cim1 have to be mentioned (Göke *et al.*, 2020; Schrott and Osman, 2023; Schrott *et al.*, 2025). Overexpression of Cim1 is also reported to reduce mtDNA content (Schrott and Osman, 2023), whereas Mrx6-overexpression does not (Göke *et al.*, 2020). The influence of Cim1 on the mtDNA copy number could also be explained by the fact that it is the antagonist of Abf2 (Schrott and Osman, 2023). The downregulation of mtDNA copy number in *abf*2*Δ*-strains could be rescued by an additional *cim1*-deletion (Schrott and Osman, 2023).

1.3.4. Mitochondria and mtDNA in different contexts

Due to its high relevance for the cell, especially through the ATP production, it is important to maintain the mitochondria and their mtDNA at certain levels. The exact mechanism of how the cell regulates its mitochondrial homeostasis is still unclear. This chapter will therefore give a short overview of the dependency of mitochondria, including mtDNA, on three different factors: nutrient availability, cell cycle and cell size. It has to be mentioned that a complete separation of these three topics is not possible, as they also show dependencies on each other. For example, nutrient availability affects the cell size and cell cycle (Broach, 2012; Pérez-Hidalgo and Moreno, 2016), and the cell size influences the progression of the cell cycle (Di Talia *et al.*, 2007).

1.3.4.1. Mitochondria and nutrient availability

As briefly mentioned above, budding yeast can grow on different carbon sources. These can generally be divided into fermentable and non-fermentable carbon sources. The most prominent fermentable carbon source is glucose, whereas typical non-fermentable carbon sources are for example ethanol and glycerol (Feldmann, 2012). The availability of the carbon source determines the pathway of energy production performed by the cell. During fermentation, the carbon source glucose gets converted into ethanol and carbon dioxide. On the other hand, non-fermentable carbon sources are used for respiration to generate energy (Feldmann, 2012). As *S. cerevisiae* is a Crabtree-positive organism, it prefers fermentation even under aerobic conditions (Crabtree, 1929; Feldmann, 2012). When yeast cells grown on glucose have fermented their preferred carbon source completely, they face the so-called “diauxic shift” to switch completely into respiration of the present ethanol (Ben Galeota-Sprung *et al.*, 2022).

Generally, changing nutrient availability leads to an adjustment of transcriptome and proteome in budding yeast (Bleeg *et al.*, 1972) and mammalian cell lines (Kilberg *et al.*, 2005; Gameiro and Struhl, 2018). Especially, the presence of glucose triggers a downregulation of specific metabolic pathways necessary for the metabolism of other carbon sources. This effect is described as “glucose repression” (Bleeg *et al.*, 1972) and influences expression, especially on transcriptional levels (Gancedo, 1998). It has been reported that the mitochondrial volume per cell volume is lower in fermentable media than in non-fermentable media, proving variability in different media (Seel *et al.*, 2023). Also, there are fewer nucleoids and mtDNA copies per cell for cells grown in fermentable media compared to those grown on non-fermentable media (Ulery *et al.*, 1994; Seel *et al.*, 2023). Glucose repression affects some of the proteins that were reported to influence mtDNA, for example Abf2, Rim1, Rpo41, Mtf1, Mhr1 and Mgm101 (Morgenstern *et al.*, 2017), and could therefore be the main driver of nutrient-dependent mtDNA regulation. Studies of the mtDNA copy number during the diauxic shift have revealed an interesting regulation in yeast: While mtDNA copy number is relatively stable when growing in glucose, it starts to increase shortly before complete glucose exhaustion (Ben Galeota-Sprung *et al.*, 2022). The increase of mtDNA copy number is bigger during the diauxic shift but still continues during respiration (Ben Galeota-Sprung *et al.*, 2022). Interestingly, a decreased level of Mip1 and Pif1 has also been described in early phases of the diauxic shift (Murphy *et al.*, 2015). By contrast, Abf2 and Rpo41 protein levels are increasing with decreasing glucose concentrations until the diauxic shift, from whereon they stay constant (Murphy *et al.*, 2015). Experiments where yeasts were transferred into fresh glucose-based media after performing respiration showed the opposite effect, confirming the

results: mtDNA copy number decreases within six hours and replication of mtDNA seems to be stopped completely for the first three hours (Ben Galeota-Sprung *et al.*, 2022).

1.3.4.2. Mitochondria and the cell cycle

As an appropriate transfer of mitochondria from the mother to the daughter cell is important, an accurate inheritance of them is a critical part of the cell cycle. As visualized in Figure 7, the mitochondrial inheritance is coordinated during cell division as follows: In late G1-phase, the mitochondrial network is organized along polarized actin cables (Boldogh *et al.*, 2001). During S-phase, the protein Myo2 transports the mitochondria along these actin cables (Altmann *et al.*, 2008; Förtsch *et al.*, 2011) by binding to the network with the help of Mmr1 and Ypt11 (Itoh *et al.*, 2002). To ensure the allocation, mitochondria are anchored in the tip of the bud through the protein of Mmr1 (Swayne *et al.*, 2011), and at the cell cortex of the mother cell with the help of Num1 and Mdm36 (Klecker *et al.*, 2013; Lackner *et al.*, 2013) or Mfb1 (Pernice *et al.*, 2016). After the poleward movement in S- and G2-phase (Simon *et al.*, 1997), the cell can undergo cytokinesis in M-phase and mitochondria are then detached from the poles (Boldogh *et al.*, 2001).

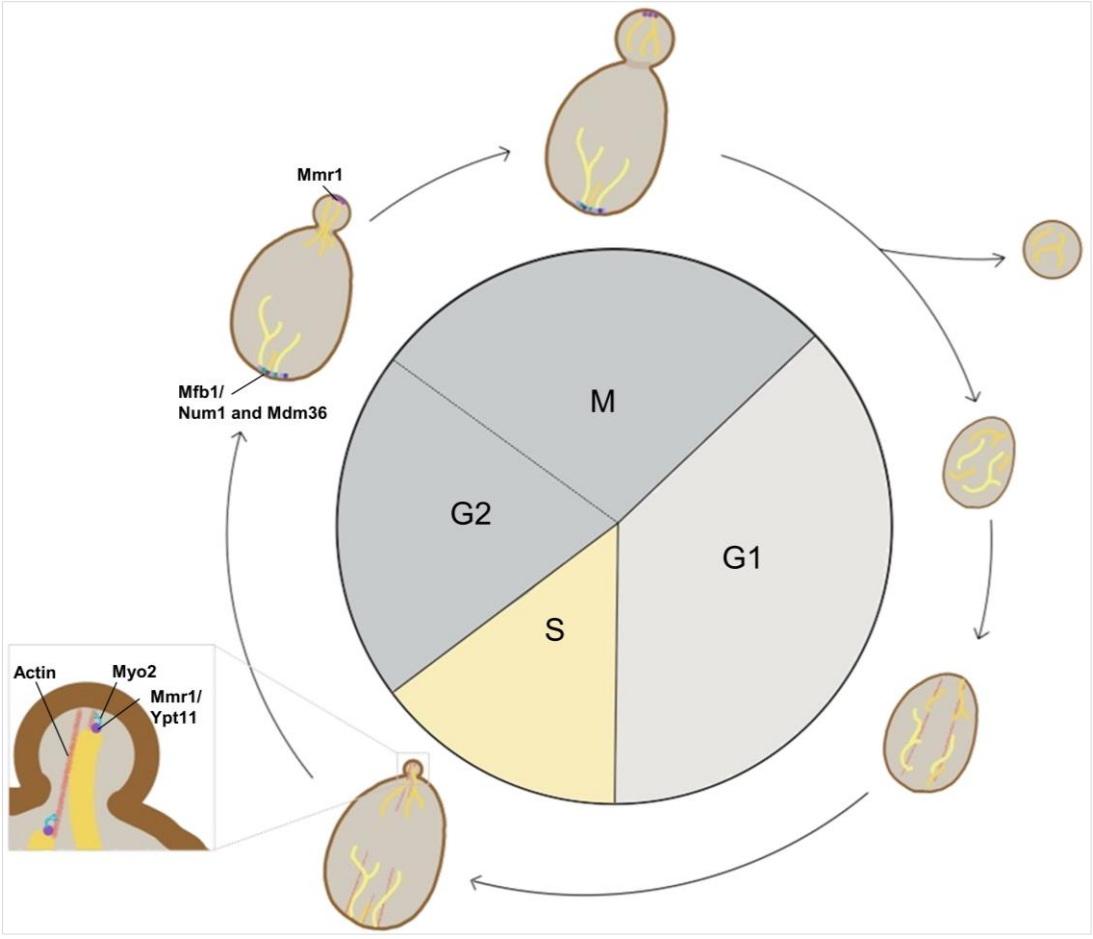

Figure 7: Mitochondrial regulation during the cell cycle of budding yeast. Starting in late G1-phase, the mitochondrial network (orange and yellow) is organized along actin cables (red). In S-phase, Myo2 (turquoise) transports them along these cables. They transport the reduced mitochondria (orange), which are described to have a better quality, faster into the bud than low-quality oxidized mitochondria (yellow). The mitochondrial network will bind the bud tip with the help of Mmr1 (purple) and the mother cell cortex by Mbf1 (green) or Num1 and Mdm36 (blue). After poleward movement in S/G2-phase, cytokinesis takes place in M-phase and mitochondria can detach from the poles.

Interestingly, studies in budding yeast have shown an asymmetric inheritance of mitochondria as well as a quality control to ensure healthy daughter cells. As described above, the mother cell provides mitochondria for the daughter cell by intracellular transport. This leads to the effect of changing mitochondria-to-cell-size ratios in mother and bud. Throughout the cell cycle, the mitochondrial concentration in the mother cell decreases, simultaneously leading to an increase in the bud (Rafelski *et al.*, 2012). The final mitochondria-to-cell-size ratio inside the daughter cell is reached at around half of its final size and is fixed independently of the mothers' age (Rafelski *et al.*, 2012). The lower mitochondrial concentration in the mother cell is restored by homeostasis (Rafelski *et al.*, 2012). Also, the quality of the mitochondria transferred to the daughter cells is shown to be higher, as they exhibit a higher $\Delta\Psi$ as well as a lower concentration of ROS (McFaline-Figueroa *et al.*, 2011; Pernice *et al.*, 2016). The exact mechanism of this daughter-oriented quality control is still unknown (Aretz *et al.*, 2020), but it has been speculated that Mfb1 and Mmr1 participate by preferred anchoring (McFaline-Figueroa *et al.*, 2011; Pernice *et al.*, 2016) and Tpm2 for selective transport (Higuchi *et al.*, 2013). One potential mechanism is based on the observation that reduced mitochondria, which are characterized as healthier, are transported faster into the daughter cell by Myo2 than oxidized mitochondria with lower quality (Nyström, 2013).

Moreover, some cell-cycle-dependent events support mitochondrial biogenesis. One example is the TOM-complex, which promotes mitochondrial import of necessary nuclear-encoded proteins. The phosphorylation of Tom6 by Cdc28 is enhanced within M-phase of the cell cycle, which enables for example the import of Mgm1 (Harbauer *et al.*, 2014). Mgm1, together with Fzo1 and Ugo1, is necessary for mitochondrial fusion (Tilokani *et al.*, 2018). Naturally, mitochondrial fusion and fission play a role in mitochondrial inheritance. Mitochondrial fission in *S. cerevisiae* is mediated by Dnm1, which creates homomultimeric complexes encircling the potential fission site (Mears *et al.*, 2011).

Another important aspect is the inheritance of mtDNA inside the mitochondria. Studies have documented a high but not exclusive connection between mtDNA and ER-associated mitochondrial division (ERMD) in budding yeast (Murley *et al.*, 2013) as well as mammals (Lewis *et al.*, 2016). The associated proteins, which form a complex called "ER-mitochondria encounter structure" (ERMES complex), are Mdm10, Mdm34, Mdm12 and Mmm1 (Kornmann *et al.*, 2009). Interestingly, the mtDNA copies are segregated into both resulting tips after mitochondrial fission in only 60% of the cases (Aretz *et al.*, 2020). In contrast to nuclear DNA, mtDNA replication is documented throughout the whole cell cycle (Conrad and Newlon, 1982). Also, mtDNA replication occurs independently of nDNA replication as shown in cell cycle mutants (Newlon and Fangman, 1975).

Taken together, previous studies have documented a partial dependency of mitochondria on the cell cycle, but the mtDNA seems to be regulated independently.

1.3.4.3. Mitochondria and cell size

A relationship between cell size and organelle sizes, as well as subcellular structures as the contractile ring in *S. cerevisiae*, is widely known. Studies have shown increased sizes of nucleolus (Weber and Brangwynne, 2015), nucleus (Jorgensen *et al.*, 2007), centrosomes (Decker *et al.*, 2011) or the mitotic spindle (Hara and Kimura, 2009) with increasing cell volumes in various model organisms. It has also been shown that yeast cells with higher cell volumes exhibit higher RNA amounts (Zhurinsky *et al.*, 2010) and total protein amounts (Newman *et al.*, 2006). This can be explained by a cell size-dependent transcription and translation rate as well as mRNA degradation rates (Wu *et al.*, 2010; Padovan-Merhar *et al.*, 2015; Swaffer *et al.*, 2023). While the mitochondrial diameter is reported to be cell size-independent (Seel, 2022), the majority of mitochondrial components showed a dependency on cell volume in several studies: Higher cell volumes lead to increased mtNetwork volume (Rafelski *et al.*, 2012; Seel *et al.*, 2023), higher amounts of nucleoids (Osman *et al.*, 2015; Jajoo *et al.*, 2016; Seel *et al.*, 2023) and increased mtDNA copy numbers (Seel *et al.*, 2023). Previous experiments tried to answer the question of how this cell volume-dependency of the mtDNA copy number is regulated. The theoretical idea was that a nuclear-encoded and cell volume-dependently regulated protein is the reason. This would suggest that the mtDNA copy number increases with increasing amounts of the protein. In theory, if one protein is perfectly limiting the mtDNA copy number, it is expected that a diploid hemizygous deletion of the encoding gene (equals - 50%) leads to a halving of the mtDNA copy number (equals - 50%). The analysis of around 10 different genes, encoding for proteins that are documented to have an effect on mtDNA copy number, did not result in the expected 50% reduction of mtDNA copy number (Seel *et al.*, 2023). This indicated that it is not a single factor limiting mtDNA cell volume-dependently. The two most limiting proteins of this screen have been identified to be Abf2 and Mip1 (Seel *et al.*, 2023). A combination of those two factors in a diploid hemizygous deletion of *ABF2* and *MIP1* reduced the mtDNA concentration significantly (Figure 8) with a resulting value close to the aimed 50% reduction (Seel *et al.*, 2023). In theory, if all mtDNA-limiting factors were added to a haploid strain once (equals 200%), the mtDNA copy number is expected to increase to around 200% compared to wild type. In fact, when adding one gene copy of both *ABF2* and *MIP1* in a haploid strain, the mtDNA copy number is only increased to around 150% (Figure 8; (Seel *et al.*, 2023)). This finding hints towards one or several additional factors that limit the mtDNA copy number by supporting Mip1 and Abf2.

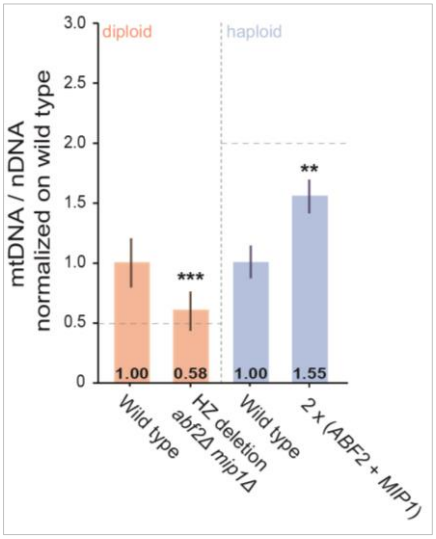

Figure 8: Mitochondrial DNA copy number per cell normalized on the respective wild type. Diploid strains include wild type and hemizygous deletion of *abf2Δ* and *mip1Δ* (left; orange), Haploid strains include wild type and double addition strain with one additional copy of *ABF2* and *MIP1* (right; blue). The indicated mean values are calculated based on at least three replicates. Statistical significances were calculated using a two-tailed two-handed t-tests. Statistical significances compared to wild type are indicated as * for $p < 0.05$, ** for $p < 0.01$ and *** for $p < 0.005$. Values acquired from (Seel, 2022).

As verified at least on RNA level, it was assumed that the genomic manipulations have the expected effect on gene expression. Also, data from various studies have confirmed the increased RNA and protein amounts of those two potential mtDNA-limiting proteins with increasing cell volumes (Parts *et al.*, 2014; Swaffer *et al.*, 2021; Seel *et al.*, 2023), further supporting the theory. If the limiting machinery model is correct, the shown result (Figure 8) would suggest that Abf2 and Mip1 are two major limiting proteins of mtDNA copy number, but one or several factors of the limiting machinery seem to be missing. All in all, as visualized in Figure 9, the current model says: With increasing cell volume, the amount of specific nuclear-encoded proteins increases, which then regulates mtDNA replication and stability, leading to higher mtDNA copy numbers (Seel *et al.*, 2023).

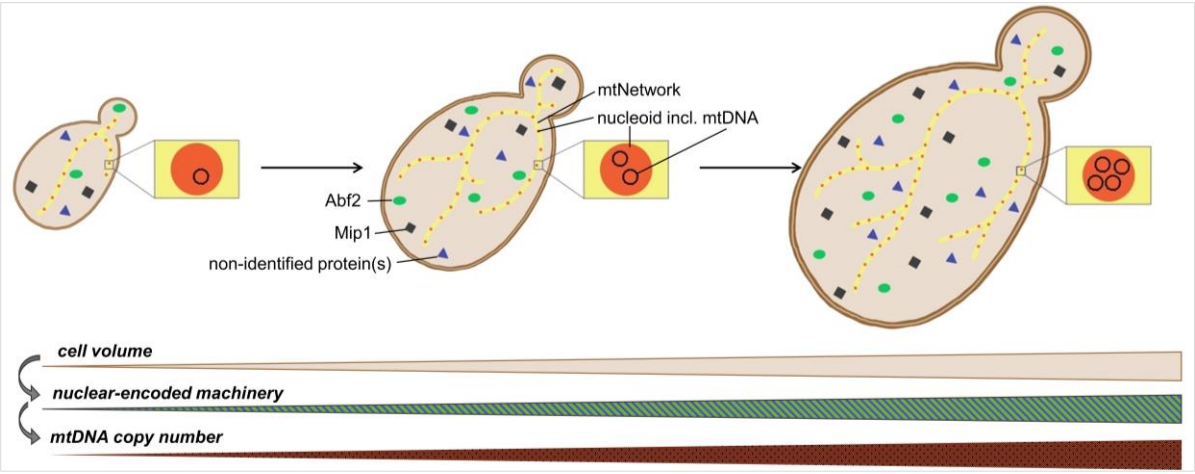

Figure 9: Model of cell volume-dependent regulation of mitochondria and mtDNA in budding yeast. With increasing cell volume, the amount of the nuclear-encoded limiting machinery is increasing and therefore leading to increased mtDNA copy numbers.

1.4. Aim of this study

As illustrated in the previous chapters, mitochondria and especially mtDNA are important factors of eukaryotic cells, which can be studied very well using the model organism budding yeast. In the past, the influence of nutrients and the cell cycle on mitochondria and their genome has been studied. More importantly, the modulation of mitochondria through cell volume has been shown and mtDNA regulation is explained by a cell volume-dependent regulation of nuclear-encoded genes necessary for mtDNA copy number (Seel *et al.*, 2023). As previous results could not fully explain the regulation of mtDNA copy number through the two most limiting proteins Abf2 and Mip1 alone, this study aims to determine the missing factors of the limiting machinery. Another aim of this thesis was to answer the question, whether cell volume influences the mtDNA copy number also independently of the limiting machinery. The ideal strain for this purpose would maintain constant amounts of all proteins of the limiting machinery with increasing cell volumes. With this strategy, the direct influence of the cell size on the mtDNA copy number would become detectable.

While it is known that mtDNA misregulations are common in various human diseases (see chapter 1.3.2.), the actual molecular mechanisms remain unclear. Also, little is known about the effect of mtDNA misregulation on the cell physiology of budding yeast. A third objective of this thesis therefore is to study it through selected strains with increased or decreased mtDNA concentrations. Using the ability to modify the mtDNA copy number through genomic manipulation of the gene copy numbers of the limiting machinery, it is possible to study the effect of mtDNA on different cell physiologies. In addition to the analysis of cell volume, budding behavior, growth and respiratory capacity, this work also aims to examine single-cell behavior in various microscopy and aging experiments. To study the effects of altered mtDNA copy numbers on the expression of mitochondrial-encoded genes, a comparison of RNA and protein concentrations in the strains was done. Additionally, the results of those RNA-Seq and mass spectrometry experiments should provide further information about the impact of mtDNA copy number changes on nuclear gene regulation. Overall, the analysis of cell physiologies and expression levels might reveal potential coping mechanisms in strains with altered mtDNA copy numbers. By performing experiments in both fermentable (carbon source: glucose) and non-fermentable media (carbon source: glycerol and ethanol), it is also intended to gain further insights into nutrient-dependent differences.

As already mentioned, not only does mtDNA copy number depend on cell volume, but also the mitochondrial network and the number of nucleoids are regulated in a cell size-dependent manner (Rafelski *et al.*, 2012; Jajoo *et al.*, 2016; Seel *et al.*, 2023). Nevertheless, the dependency of these three on each other has not yet been conclusively clarified, as previous studies focused on cell volume changes. An analysis of the mtNetwork length and the number of nucleoids in strains with increased mtDNA copy numbers and constant cell volumes could reveal an existence of a dependency of them on the mtDNA copy number.

2. Material and methods

2.1. Chemicals and Consumables

Table 1: Chemicals and consumables used in this study.

Chemicals or consumables	Supplier
µ-Slide 8 Well, ibi-Treat	ibidi, Gräfelfing, Germany
Acetic acid optima LC/MS	Fisher Scientific GmbH, Schwerte, Germany
Aceton	Roth, Karlsruhe, Germany
Acetonitril	Sigma-Aldrich, St. Louis, USA
Agarose SERVA Wide Range	Serva Electrophoresis, Heidelberg, Germany
Albumin fraction V	Roth, Karlsruhe, Germany
Amino acids	Sigma-Aldrich, St. Louis, USA
Ammonium sulfate	Schubert & Weiß Omnilab, München, Germany
Ampicillin	Roth, Karlsruhe, Germany
Chlorophorm	Thermo Fisher Scientific, Waltham, USA
Concanavalin A TYPE IV	Sigma-Aldrich, St. Louis, USA
Coverslips (24 x 50 mm)	Gerhard Menzel GmbH, Braunschweig, Germany
D(+) Glucose	Sigma-Aldrich, St. Louis, USA
Difco Agar, granulated	Schubert & Weiß Omnilab, München, Germany
Dithiothreitol (DTT)	Thermo Fisher Scientific, Waltham, USA
EDTA	Sigma-Aldrich, St. Louis, USA
Ethanol	Sigma-Aldrich, St. Louis, USA
Glycerol	Th. Greyer, Renningen, Germany
Halt™ Protease & Phosphatase Inhibitor Cocktail (100X)	Thermo Fisher Scientific, Waltham, USA
HEPES solution	Sigma-Aldrich, St. Louis, USA
Hygromycine	Serva Electrophoresis, Heidelberg, Germany
Iodacetamide	Serva Electrophoresis, Heidelberg, Germany
Isoton II Diluent	Beckman Coulter, Krefeld, Germany
Kanamycin	Roth, Karlsruhe, Germany
LB Broth (Lennox)	Sigma-Aldrich, St. Louis, USA
LB-Agar (Lennox)	Sigma-Aldrich, St. Louis, USA
LightCycler 480 Multiwell Plate 96	Roche, Basel, Switzerland
Lithium acetate dihydrate	Schubert & Weiß Omnilab, München, Germany
Microscope slides	Gerhard Menzel GmbH, Braunschweig, Germany
Nourseothricin (clonNAT)	Jena Bioscience GmbH, Jena Germany
Peptone, BD Bacto™	Biozol, Eching, Germany
Phenol/ Chloroform/ Isoamyl alcohol (25:24:1)	Thermo Fisher Scientific, Waltham, USA
Phenylmethylsulfonyl Fluoride (PMSF)	Thermo Fisher Scientific, Waltham, USA
Pierce™ Trypsin Protease	Thermo Fisher Scientific, Waltham, USA
Polyethylene glycol, (PEG), BIOXTRA	Sigma-Aldrich, St. Louis, USA
SDS 10%	Invitrogen, Thermo Fisher Scientific, Waltham, USA

Sodium chloride (NaCl),5M	Promega, Madison, USA
Sodium hydroxide (NaOH)	Thermo Fisher Scientific, Waltham, USA
Sybr® Safe DNA Gel Stain	Invitrogen, Thermo Fisher Scientific, Waltham, USA
Tergitol	Sigma-Aldrich, St. Louis, USA
Trifluoroacetic acid (TFA), LC-MS	Thermo Fisher Scientific, Waltham, USA
Tris acetate	Sigma-Aldrich, St. Louis, USA
Tris/HCl	Sigma-Aldrich, St. Louis, USA
Urea proteomics grade	VWR International GmbH, Darmstadt, Germany
Water optima LC/MS	Thermo Fisher Scientific, Waltham, USA
Yeast extract, BD Bacto™	Biozol, Eching, Germany
Yeast nitrogen base	Schubert & Weiß Omnilab, München, Germany
β-estradiol	Sigma-Aldrich, St. Louis, USA

2.2. Devices

Table 2: Devices used in this study.

Device	Supplier
CytoFlex S Flow Cytometer	Beckman Coulter, Krefeld, Deutschland
Ecotron shaking incubator	Infors HT, Bottmingen, Switzerland
FastPrep™-24 5G Bead-Beater	MP Biomedicals Germany GmbH, Eschwege, Germany
LightCycler® 96	Roche, Basel, Switzerland
microfluidic device	costume
Mini-BeadBeater 24, 230V	BioSpec Products, Oklahoma, USA
miVac Speed vac	Genevac Ltd.
NanoDrop OneC	Thermo Fisher Scientific, Waltham, USA
Nikon Eclipse Ti-E microscope	Nikon Instruments Inc.
U:Genius3 Transilluminator	Syngene, Bengaluru, Karnataka, India
Z2 Coulter Particle Count and Size Analyzer	Beckman Coulter, Krefeld, Deutschland
Zeiss LSM 800 microscope	Zeiss Germany, Oberkochen, Germany

2.3. Kits

Table 3: Kits used in this study.

Kit	Supplier/Source
High-capacity cDNA Reverse Transcription Kit with RNase Inhibitor	Life Technologies, Carlsbad, California, USA
NucleoSpin Gel and PCR Clean-up	Macherey-Nagel, Düren, Germany
NucleoSpin Plasmid	Macherey-Nagel, Düren, Germany
Pierce™ BCA Protein Assay Kit	Thermo Fisher Scientific, Waltham, USA
YeaStar RNA Kit	Zymo Research, Freiburg, Germany

2.4. Strains

Table 4: List of strains used in this study. All strains derived from W303 background and sorted alphabetically.

Name	Genotype	Description	Origin	Figures
AFY002-4	*Mat α; ADE2, whi5::kanMX6-LexApr-WHI5-ADH1term-LEU2, his3::LexA-ER-AD-TF-HIS3, abf2::TRP1-HTB1pr-mCITRINE-P2A-ABF2-ABF2term*	*HTB1pr-mCitrine-P2A-ABF2* in *ABF2*-Locus	This study	22,23
AFY003-1	*Mat α/a; ADE2/ADE2, mip1::TRP1/MIP1, abf2::clonNAT/ABF2, rim1::HIS3/RIM1*	Triple hemizygous deletion *mip1 abf2 rim1*	This study	11,13,15,17, 18,20, 27-35,38, 40-43, 45-49, 53-58,60
AFY004-3	*Mat α/a; ADE2/ADE2, mip1::TRP1/MIP1, abf2::clonNAT/ABF2, mhr1::HIS3/MHR1*	Triple hemizygous deletion *mip1 abf2 mhr1*	This study	15,38,40
AFY005-1	*Mat α/a; ADE2/ADE2, mip1::TRP1/MIP1, abf2::clonNAT/ABF2, hmi1::HIS3/HMI1*	Triple hemizygous deletion *mip1 abf2 hmi1*	This study	15,38,40
AFY006-3	*Mat α/a; ADE2/ADE2, mip1::TRP1/MIP1, abf2::clonNAT/ABF2, mgm101::HIS3/MGM101*	Triple hemizygous deletion *mip1 abf2 mgm101*	This study	15,38,40
AFY007-7	*Mat α/a; ADE2/ADE2, mip1::TRP1/MIP1, abf2::clonNAT/ABF2, pif1::HIS3/PIF1*	Triple hemizygous deletion *mip1 abf2 pif1*	This study	15,38,40
AFY008-1	*Mat α/a; ADE2/ADE2, mip1::TRP1/MIP1, abf2::clonNAT/ABF2, rpo41::HIS3/RPO41*	Triple hemizygous deletion *mip1 abf2 rpo41*	This study	15,38,40
AFY009-2	*Mat α/a; ADE2/ADE2, mip1::TRP1/MIP1, abf2::clonNAT/ABF2, mtf1::HIS3/MTF1*	Triple hemizygous deletion *mip1 abf2 mtf1*	This study	15,38,40
AFY010-1	*Mat α; ADE2, whi5::kanMX6-LexApr-WHI5-ADH1term-LEU2, his3::LexA-ER-AD-TF-HIS3, ura3::TRP1-HTB1pr-mCITRINE-P2A-ABF2-ADH1term-URA3*	*HTB1pr-mCitrine-P2A-ABF2-ADH1term* in *URA3*-Locus	This study	22,23
AFY011-1	*Mat α/a; ADE2/ADE2, abf2::clonNAT/ABF2, rim1::HIS3/RIM1*	Double hemizygous deletion *abf2 rim1*	This study	15,38,40
AFY012-1	*Mat α/a; ADE2/ADE2, abf2::clonNAT/ABF2, mhr1::HIS3/MHR1*	Double hemizygous deletion *abf2 mhr1*	This study	15,38,40
AFY013-1	*Mat α/a; ADE2/ADE2, abf2::clonNAT/ABF2, hmi1::HIS3/HMI1*	Double hemizygous deletion *abf2 hmi1*	This study	15,38,40

AFY014-1	*Mat α/a; ADE2/ADE2, abf2::clonNAT/ABF2, mgm101::HIS3/MGM101*	Double hemizygous deletion *abf2 mgm101*	This study	15,38,40
AFY015-1	*Mat α/a; ADE2/ADE2, abf2::clonNAT/ABF2, pif1::HIS3/PIF1*	Double hemizygous deletion *abf2 pif1*	This study	15,38,40
AFY016-1	*Mat α/a; ADE2/ADE2, abf2::clonNAT/ABF2, rpo41::HIS3/RPO41*	Double hemizygous deletion *abf2 rpo41*	This study	15,38,40
AFY017-1	*Mat α/a; ADE2/ADE2, abf2::clonNAT/ABF2, mtf1::HIS3/MTF1*	Double hemizygous deletion *abf2 mtf1*	This study	15,38,40
AFY018-1	*Mat α/a; ADE2/ADE2, mip1::TRP1/MIP1, rim1::HIS3/RIM1*	Double hemizygous deletion *mip1 rim1*	This study	15,38,40
AFY019-1	*Mat α/a; ADE2/ADE2, mip1::TRP1/MIP1, mhr1::HIS3/MHR1*	Double hemizygous deletion *mip1 mhr1*	This study	15,38,40
AFY020-1	*Mat α/a; ADE2/ADE2, mip1::TRP1/MIP1, hmi1::HIS3/HMI1*	Double hemizygous deletion *mip1 hmi1*	This study	15,38,40
AFY021-1	*Mat α/a; ADE2/ADE2, mip1::TRP1/MIP1, mgm101::HIS3/MGM101*	Double hemizygous deletion *mip1 mgm101*	This study	15,38,40
AFY022-1	*Mat α/a; ADE2/ADE2, mip1::TRP1/MIP1, pif1::HIS3/PIF1*	Double hemizygous deletion *mip1 pif1*	This study	15,38,40
AFY023-1	*Mat α/a; ADE2/ADE2, mip1::TRP1/MIP1, rpo41::HIS3/RPO41*	Double hemizygous deletion *mip1 rpo41*	This study	15,38,40
AFY024-1	*Mat α/a; ADE2/ADE2, mip1::TRP1/MIP1, mtf1::HIS3/MTF1*	Double hemizygous deletion *mip1 mtf1*	This study	15,38,40
AFY025-1	*Mat α/a; ADE2/ADE2, mip1::TRP1/MIP1, abf2::clonNAT/ABF2, rim1::HIS3/RIM1, hmi1::KanMX6/HMI1*	Quadruple hemizygous deletion *mip1 abf2 rim1 hmi1*	This study	11,17, 27-35,38, 40-43,45-49, 53-57
AFY027-1	*Mat α; ADE2, whi5::kanMX6-LexApr-WHI5-ADH1term-LEU2, his3::LexA-ER-AD-TF-HIS3, ura3::TRP1-HTB1pr-mCITRINE-P2A-ABF2-ADH1term-URA3, abf2::hphMX6*	*HTB1pr-mCitrine-P2A-ABF2-ADH1term* in *URA3*-Locus + deletion *abf2*	This study	22,23
AFY030-1	*Mat α; ADE2, whi5::kanMX6-LexApr-WHI5-ADH1term-LEU2, his3::LexA-ER-AD-TF-HIS3, ura3::TRP1-HTB1pr-ABF2-ADH1term-clonNAT-URA3*	*HTB1pr-ABF2-ADH1term* in *URA3*-Locus	This study	22,23

AFY031-2	*Mat α; ADE2, whi5::kanMX6-LexApr-WHI5-ADH1term-LEU2, his3::LexA-ER-AD-TF-HIS3, ura3::TRP1-HTB1pr-ABF2-ADH1term-clonNAT-URA3, abf2::hdhMX6*	*HTB1pr-ABF2-ADH1term* in *URA3*-Locus + deletion *abf2*	This study	22,23
AFY033-1	*Mat α; ADE2, trp1::MIP1-TRP1, his3::HMI1-HIS3*	Haploid WT with additional copies *MIP1 HMI1*	This study	16,39,40
AFY034-2	*Mat α; ADE2, ura3::ABF2-URA3, trp1::MIP1-TRP1, his3::HMI1-HIS3*	Haploid WT with additional copies *ABF2 MIP1 HMI1*	This study	16,39,40
AFY036-1	*Mat α; ADE2, whi5::kanMX6-LexApr-WHI5-ADH1term-LEU2, his3::LexA-ER-AD-TF-HIS3, trp1::HTB1pr-MIP1-ADH1term-TRP1*	*HTB1pr-MIP1-ADH1term* in *TRP1*-Locus	This study	26
AFY037-1	*Mat α; ADE2, leu2::RIM1-LEU2*	Haploid WT with additional copy *RIM1*	This study	16,19,39,40, 51
AFY037-2	*Mat α; ADE2, leu2::RIM1-RIM1-LEU2*	Haploid WT with two additional copies *RIM1*	This study	19
AFY037-3	*Mat α; ADE2, leu2::RIM1-LEU2*	Haploid WT with additional copy *RIM1*	This study	19
AFY041-2	*Mat α; ADE2, whi5::kanMX6-LexApr-WHI5-ADH1term-LEU2, his3::LexA-ER-AD-TF-HIS3, ura3::HTB1pr-ABF2-MBF1term-URA3*	*HTB1pr-ABF2-MBF1term* in *URA3*-Locus	This study	24
AFY042-1	*Mat α; ADE2, whi5::kanMX6-LexApr-WHI5-ADH1term-LEU2, his3::LexA-ER-AD-TF-HIS3, ura3::HTB1pr-ABF2-ALR2term-URA3*	*HTB1pr-ABF2-ALR2term* in *URA3*-Locus	This study	24
AFY043-1	*Mat α; ADE2, whi5::kanMX6-LexApr-WHI5-ADH1term-LEU2, his3::LexA-ER-AD-TF-HIS3, ura3::HTB1pr-ABF2-KKQ8term-URA3*	*HTB1pr-ABF2-KKQ8term* in *URA3*-Locus	This study	24
AFY044-2	*Mat α; ADE2, whi5::kanMX6-LexApr-WHI5-ADH1term-LEU2, his3::LexA-ER-AD-TF-HIS3, trp1::HTB1pr-MIP1-ADH1term-TRP1, mip1::clonNAT*	*HTB1pr-MIP1-ADH1term* in *TRP1*-Locus + deletion *mip1*	This study	26
AFY046-1	*Mat α; ADE2, whi5::kanMX6-LexApr-WHI5-ADH1term-LEU2, his3::LexA-ER-AD-TF-HIS3, ura3::HTB1pr-ABF2-SUT1term-URA3*	*HTB1pr-ABF2-SUT1term* in *URA3*-Locus	This study	24
AFY048-2	*Mat α; ADE2, whi5::kanMX6-LexApr-WHI5-ADH1term-LEU2, his3::LexA-ER-AD-TF-HIS3, ura3::HTB1pr-ABF2-SUT1term-URA3, abf2::clonNAT*	*HTB1pr-ABF2-SUT1term* in *URA3*-Locus + deletion *abf2*	This study	24,25

AFY053-2	*Mat α; ADE2, ura3::ABF2-URA3, his3::HMI1-HIS3*	Haploid WT with additional copies *ABF2 HMI1*	This study	16,39,40
AFY054-4	*Mat α; ADE2, his3::HMI1-HIS3*	Haploid WT with one additional copy *HMI1*	This study	16,19,39,40, 51
AFY054-7	*Mat α; ADE2, his3::HMI1-HMI1-HIS3*	Haploid WT with two additional copies *HMI1*	This study	19
AFY054-9	*Mat α; ADE2, his3::HMI1-HMI1-HMI1-HIS3*	Haploid WT with three additional copies *HMI1*	This study	19
AFY055-5	*Mat α; ADE2, ura3::ABF2-URA3, trp1::MIP1-TRP1, leu2::RIM1-LEU2, his3::HMI1-HIS3*	Haploid WT with additional copies *ABF2 MIP1 RIM1 HMI1*	This study	12,17, 27-35, 39-43, 45-48,51
AFY056-2	*Mat α; ADE2, ura3::ABF2-URA3, leu2::RIM1-LEU2*	Haploid WT with additional copies *ABF2 RIM1*	This study	16,39,40
AFY057-1	*Mat α; ADE2, ura3::ABF2-URA3, trp1::MIP1-TRP1, leu2::RIM1-LEU2*	Haploid WT with additional copies *ABF2 MIP1 RIM1* clone A	This study	12,16-19, 27-36,39-43, 45-51, 53-60
AFY058-2	*Mat α; ADE2, leu2::RIM1-RIM1-RIM1-LEU2*	Haploid WT with three additional copies *RIM1*	This study	19
AFY059-2	*Mat α; ADE2, leu2::RIM1-RIM1-RIM1-RIM1-LEU2*	Haploid WT with four additional copies *RIM1*	This study	19
AFY060-1	*Mat α; ADE2, trp1::MIP1-TRP1, leu2::RIM1-LEU2*	Haploid WT with additional copies *MIP1 RIM1*	This study	16,39,40
AFY061-1	*Mat α; ADE2, whi5::kanMX6-LexApr-WHI5-ADH1term-LEU2, his3::LexA-ER-AD-TF-HIS3, trp1::HTB1pr-MIP1-SUT1term-TRP1*	*HTB1pr-MIP1-SUT1term* in *TRP1*-Locus	This study	26
AFY067-1	*Mat α; ADE2, his3::LexA-ER-AD-TF-HIS3, ura3::LexApr-ABF2-CYC1term-URA3, abf2::hphMX*	Abf2-inducible strain + deletion *abf2*	This study	19
AFY070-5	*Mat α; ADE2, mt-LacO, Pucp1-Su9-2xNEON-LacI-Pgk1-Su9-mKate2:KanMX4, ura3::ABF2-URA3*	Haploid microscopy strain with additional copy *ABF2*	This study	61

AFY072-1	Mat α; ADE2, TRP1, URA3, LEU2, HIS3	Reference strain haploid WT corrected *TRP1, URA3, LEU2, HIS3*	This study	29,42
AFY074-1	*Mat α; ADE2, ura3::ABF2-ABF2-URA3, trp1::MIP1-TRP1, his3::MIP1-HIS3, leu2::RIM1-RIM1-LEU2*	Haploid WT with two additional copies *ABF2 MIP1 RIM1*	This study	12,20, 27-29,35, 39-43, 45-49,53-60
AFY082-2	*Mat α; ADE2, ura3::ABF2-URA3, trp1::MIP1-TRP1, his3::MGM101-HIS3*	Haploid WT with additional copies *ABF2 MIP1 MGM101*	This study	16,39,40
AFY083-1	*Mat α; ADE2, ura3::ABF2-URA3, trp1::MIP1-TRP1, leu2::RIM1-LEU2, his3::MGM101-HIS3*	Haploid WT with additional copies *ABF2 MIP1 RIM1 MGM101*	This study	17,39,40
AFY085-1	*Mat α; ADE2, trp1::AmpR-TRP1*	Reference strain haploid WT including empty *TRP1-AMPR*-Vector	This study	36,42
AFY086-1	Mat α; ADE2, TRP1, URA3	Reference strain haploid WT corrected *TRP1, URA3*	This study	29,42
AFY087-1	*Mat α; ADE2, ura3::ABF2-URA3, trp1::MIP1-TRP1, leu2::RIM1-LEU2, cim1::clonNAT*	Haploid WT with additional copies *ABF2 MIP1 RIM1* + deletion *cim1*	This study	36,39-42,51
AFY088-1	*Mat α; ADE2, ura3::ABF2-URA3, trp1::MIP1-TRP1, leu2::RIM1-LEU2, mrx6::hphMX6*	Haploid WT with additional copies *ABF2 MIP1 RIM1* + deletion *mrx6*	This study	36,39-42,51
AFY089-1	*Mat α; ADE2, cim1::clonNAT*	Haploid deletion *cim1*	This study	36,39-42,51
AFY090-1	*Mat α; ADE2, mrx6::hphMX6*	Haploid deletion *mrx6*	This study	36,39-42,51
AFY092-1	Mat α; ADE2, TRP1, URA3, LEU2	Reference strain haploid WT corrected *TRP1, URA3, LEU2*	This study	29,36,42
AFY094-1	*Mat α; ADE2, sir2::clonNAT*	Haploid deletion *sir2*	This study	50,51
AFY095-1	*Mat α; ADE2, ura3::ABF2-URA3, trp1::MIP1-TRP1, leu2::RIM1-LEU2, sir2::clonNAT*	Haploid WT with additional copies *ABF2 MIP1 RIM1* + deletion *sir2*	This study	50,51

AFY098-1	*Mat α; ADE2, ura3::ABF2-URA3, trp1::MIP1-TRP1*	Haploid WT with additional copies *ABF2 MIP1 clone B*	This study	11,27-29,35, 39-42, 45-49, 52-60
AFY098-2	*Mat α; ADE2, ura3::ABF2-URA3, trp1::MIP1-TRP1*	Haploid WT with additional copies *ABF2 MIP1 clone C*	This study	11,27-29,35, 39-42, 45-49, 52-60
AFY099-1	*Mat α; ADE2, mt-LacO, Pucp1-Su9-2xNEON-LacI-Pgk1-Su9-mKate2:KanMX4, ura3::ABF2-URA3, his3::MIP1-HIS3*	Haploid microscopy strain with additional copy *ABF2 MIP1*	This study	61
AFY100-1	*Mat α; ADE2, mt-LacO, Pucp1-Su9-2xNEON-LacI-Pgk1-Su9-mKate2:KanMX4, ura3::ABF2-URA3, his3::MIP1-HIS3, leu2::RIM1-LEU2*	Haploid microscopy strain with additional copy *ABF2 MIP1 RIM1*	This study	61
AFY101-2	*Mat α; ADE2, ura3::ABF2-URA3, trp1::MIP1-TRP1, leu2::RIM1-LEU2*	Haploid WT with additional copies *ABF2 MIP1 RIM1* clone B	This study	12,27-29,35, 39-42, 45-49, 53-60
AFY102-1	*Mat α; ADE2, ura3::ABF2-URA3, trp1::MIP1-TRP1, leu2::RIM1-LEU2*	Haploid WT with additional copies *ABF2 MIP1 RIM1* clone C	This study	12,27-29,35, 39-42, 45-49, 53-60
ASY014-1	*Mat α; ADE2, mt-LacO, PUCP1-Su9-2xNEON-LacI-PGK1-SU9-mKATE2:KanMX4*	Haploid microscopy WT strain	Anika Seel, Schmoller lab	61
ASY020-1	*Mat α/a; ADE2/ADE2*	Diploid WT	Anika Seel, Schmoller lab	8,11,15,17,18, 20,27-35,38, 40-43, 45-49, 53-58,60
ASY024-1	*Mat α/a; ADE2/ADE2, mip1::TRP1/MIP1*	Diploid hemizygous deletion *mip1*	Anika Seel, Schmoller lab	38,40
ASY033-1	*Mat α/a; ADE2/ADE2, pif1::TRP1/PIF1*	Diploid hemizygous deletion *pif1*	Anika Seel, Schmoller lab	15,38,40
ASY046-2	*Mat α/a; ADE2/ADE2, mip1::TRP1/MIP1, abf2::clonNAT/ABF2*	Double hemizygous deletion *abf2 mip1*	Anika Seel, Schmoller lab	8,11,15,17,20, 27-35,38, 40-43, 45-49, 53-58,60
ASY051-2	*Mat α; ADE2, ura3::ABF2-URA3*	Haploid WT with additional copy *ABF2*	Anika Seel, Schmoller lab	16,39,40,51
ASY057-3	*Mat α; ADE2, trp1::MIP1-TRP1*	Haploid WT with additional copy *MIP1*	Anika Seel, Schmoller lab	16,39,40,51

ASY059-4	*Mat α; ADE2, ura3::ABF2-URA3, trp1::MIP1-TRP1*	Haploid WT with additional copy ABF2 *MIP1*	Anika Seel, Schmoller lab	8,11,16,27-35, 39-42,45-60
ASY075-1	*Mat α; ADE2, his3::LexA-ER-AD-TF-HIS3, ura3::LexApr-MIP1-CYC1term-URA3, mip1::clonNAT*	Mip1-inducible strain + deletion *mip1*	Anika Seel, Schmoller lab	19
JE611-c	*Mat α; cln1Δ, cln2Δ, cln3::leu2, lexOpr-Cln1-Leu2, ADE2, his3::cyc1-Pr-lexO TF-his3*	Cln1-inducible strain	Jennifer Ewald, Skotheim lab	14
KSY244-1	*Mat α/a; ADE2/ADE2, abf2::TRP1/ABF2*	Diploid hemizygous deletion *abf2*	Anika Seel, Schmoller lab	38,40
KSY246-1	*Mat α/a; ADE2/ADE2, hmi1::TRP1/HMI1*	Diploid hemizygous deletion *hmi1*	Anika Seel, Schmoller lab	15,38,40
KSY253-1	*Mat α/a; ADE2/ADE2, rpo41::TRP1/RPO41*	Diploid hemizygous deletion *rpo41*	Anika Seel, Schmoller lab	15,38,40
KSY254-1	*Mat α/a; ADE2/ADE2, mtf1::TRP1/MTF1*	Diploid hemizygous deletion *mtf1*	Anika Seel, Schmoller lab	15,38,40
KSY255-1	*Mat α/a; ADE2/ADE2, mhr1::TRP1/MHR1*	Diploid hemizygous deletion *mhr1*	Anika Seel, Schmoller lab	15,38,40
KSY256-1	*Mat α/a; ADE2/ADE2, mgm101::TRP1/MGM101*	Diploid hemizygous deletion *mgm101*	Anika Seel, Schmoller lab	15,38,40
KSY257-1	*Mat α/a; ADE2/ADE2, rim1::TRP1/RIM1*	Diploid hemizygous deletion *rim1*	Anika Seel, Schmoller lab	15,38,40
KSY302-4	*Mat α; ADE2, whi5::kanMX6-LexApr-WHI5-ADH1term-LEU2, his3::LexA-ER-AD-TF-HIS3, abf2::TRP1-HTB1pr-ABF2-ABF2term*	*HTB1pr-ABF2-ABF2term* in *ABF2*-Locus	Anika Seel, Schmoller lab	21,23
KSY303-1	*Mat α; ADE2, whi5::kanMX6-LexApr-WHI5-ADH1term-LEU2, his3::LexA-ER-AD-TF-HIS3, abf2::URA3-HTB1pr-MIP1-MIP1term*	*HTB1pr-MIP1-MIP1term* in *MIP1*-Locus	Anika Seel, Schmoller lab	26
KSY313-1	*Mat α; ADE2, whi5::kanMX6-LexApr-WHI5-ADH1term-LEU2, his3::LexA-ER-AD-TF-HIS3, abf2::TRP1-HTB2pr-ABF2-ABF2term*	*HTB2pr-ABF2-ABF2term* in *ABF2*-Locus	Anika Seel, Schmoller lab	21,23
KSY314-4	*Mat α; ADE2, whi5::kanMX6-LexApr-WHI5-ADH1term-LEU2, his3::LexA-ER-AD-TF-HIS3, abf2::TRP1-HTB1pr-ABF2-ADH1term-URA3*	*HTB1pr-ABF2-ADH1term* in *ABF2*-Locus	Anika Seel, Schmoller lab	21,23

KSY315-4	*Mat α; ADE2, whi5::kanMX6-LexApr-WHI5-ADH1term-LEU2, his3::LexA-ER-AD-TF-HIS3, abf2::TRP1-HTB2pr-ABF2-ADH1term-URA3*	*HTB2pr-ABF2-ADH1term* in *ABF2*-Locus	Anika Seel, Schmoller lab	21,23
MMY116-2c	*Mat α; ADE2*	Haploid WT	Skotheim lab stock	8,10,11, 16-20, 27-37, 39-43,45-60
MSY63-1	*Mat a; ADE2, whi5Δ::kanMX6-LexAprom-WHI5-ADH1term-LEU2, his3::LexA-ER-AD-TF-HIS3*	Haploid *WHI5*-inducible WT	Matthew Swaffer, Skotheim lab	14,21-26

2.5. Enzymes

Table 5: Enzymes used in this study.

Enzyme	Supplier/Source
Alkaline phosphatase (CIP)	New England Biolabs GmbH, Frankfurt a.M., Germany
DNase I	Life Technologies, Carlsbad, California, USA
Phusion polymerase	Schmoller Lab stock
Q5 polymerase	New England Biolabs GmbH, Frankfurt a.M., Germany
Restriction Enzymes	New England Biolabs GmbH, Frankfurt a.M., Germany
RNase A	Sigma-Aldrich, St. Louis, USA
T4 DNA Ligase	Thermo Fischer Scientific (Schwerte/Germany)
Gibson assembly Master Mix	New England Biolabs GmbH, Frankfurt a.M., Germany

2.6. Plasmids

Table 6: List of plasmids used for transformation in this study.

Plasmid	Description	Origin
ASE002-2	*MIP1pr-MIP1-MIP1term* in pRS404 (*TRP1*)	Anika Seel, Schmoller lab
ASE003-1	*ABF2pr-ABF2-ABF2term* in pRS406 (*URA3*)	Anika Seel, Schmoller lab
pAF001G	*RIM1pr-RIM1-RIM1term* in pRS405 (*LEU2*)	This study
pAF002G	*HMI1pr-HMI1-HMI1term* in pRS403 (*HIS3*)	This study
pAF015-11	*MIP1pr-MIP1-MIP1term* in pRS403 (*HIS3*)	This study
pAF020-1	*MGM101pr-MGM101-MGM101term* in pRS403 (*HIS3*)	This study

Table 7: Plasmids used for knock-out transformations in this study.

Plasmid	Description	Origin
pPP2960/ pFA6a-Cgla*TRP1*	knock-out template with *C. glabrata TRP1* gene	Peter Pryciak Lab
pPP2961/ pFA6a-Klac*URA3*	knock-out template with *K. lactis URA3* gene	Peter Pryciak Lab
pPP3129/ pFA6a-Cgla*LEU2*	knock-out template with *C. glabrata LEU2* gene	Peter Pryciak Lab
pCA12	plasmid with *KanMX* gene	Jan Skotheim Lab
pCA13	plasmid with *natMX* gene	Jan Skotheim Lab
pCA14	plasmid with *hdhMX* gene	Jan Skotheim Lab

2.7. Oligonucleotides

Table 8: Primer for qPCR used in this study. Ordered from Sigma-Aldrich.

Gene	Primer direction	Primer Sequence (5‘-3‘)	Origin
ABF2	forward reverse	CCAACCTTACGTCCTGCTG CGTCAAACTCCTTCTTCGCC	This study
ACT1	forward reverse	AGTTGCCCCAGAAGAACACC GGACAAAACGGCTTGGATGG	Kora-Lee Claude, Schmoller lab
AMPR	forward reverse	TTACCAATGCTTAATCAG CCCTTCCGGCTGGCTGGTTTA	This study
COX2	forward reverse	GTTGATGCTACTCCTGGTAGATT TTGCATGACCTGTCCCACAC	Anika Seel, Schmoller lab
COX3	forward reverse	TTGAAGCTGTACAACCTACC CCTGCGATTAAGGCATGATG	Anika Seel, Schmoller lab
HMI1	forward reverse	GGTTCTCTTTGACGGCGGTA ACACAGTTCATGGGTTGGCT	This study
mCITRINE	forward reverse	GAGCTGAAGGGCATCGACTT TTCTGCTTGTCGGCCATGAT	Kora-Lee Claude, Schmoller lab
MGM101	forward reverse	GGCATACCAACTGCTACAG GGATATTCAACTTGTCTGTC	This study
MHR1	forward reverse	GATTCCGCCCCGCTTCATGG CAAGTTCACTACACACATAC	This study
MIP1	forward reverse	CCATCACAAGCAAGAACGGC GTCCCTTTCCAGCTCAACCA	Anika Seel, Schmoller lab
MRX6	forward reverse	CATCCGACGTGGTGCTCTTA TCTCATCTCTCCCTCCACCC	Anika Seel, Schmoller lab
MTF1	forward reverse	GCAAATTCTAAAAAGAGATC CATCTTTACTTTACCAAACC	This study
PIF1	forward reverse	GTTAGACGCAGAACTGCTTG CCTTTTGTAGCATAATCGTC	This study

RDN18	forward reverse	AACTCACCAGGTCCAGACACAATAAGG AAGGTCTCGTTCGTTATCGCAATTAAGC	Kora-Lee Claude, Schmoller lab
RIM1	forward reverse	GTATATGTTGAAGCAGATG GCATTTTCTTGGCCCTCAGC	This study
RPO41	forward reverse	GGCAAGAATTATTAAACAG GACTGTTTCTCAATACTG	This study
SIR2	forward reverse	GCCGTATCAAAGACTAGCG GCCACTTCTCCGAGCGCAG	This study

2.8. Buffer and Media

Table 9: Buffer used in this study. Storage of all buffers on room temperature.

Buffer	Composition
0.1 M TE/Lithium acetate	0.1 M Lithium acetate 10 mM Tris/HCl 1 mM EDTA
1 M TE/Lithium acetate	1 M Lithium acetate 10 mM Tris/HCl 1 mM EDTA
Alkylating solution	0.5M Iodacetamide 1M Tris-HCl (pH8.0)
C18-Buffer A	0.1 % TFA
C18-Buffer D	80 % (v/v) acetonitrile 0.1 % (v/v) acetic acid
C18-Buffer C	0.1 % acetic acid
Detergent Lysis Buffer pH 8.0	100 mM NaCl 10 mM Tris/HCl 1 mM EDTA 2 % (v/v) Triton X-100 1 % (w/v) SDS
Mass Spec Lysis Buffer	50 mM Tris-HCl (pH 8.0) 0.2 % (v/v) Tergitol 150 mM NaCl 5 mM EDTA 1 % (v/v) Protease Inhibitor 1 % (v/v) PMSF

PPT solution	50 % (v/v) acetone 49.9 % (v/v) ethanol 0.1 % (v/v) acetic acid
TAE-Buffer pH 8.5	40 mM Tris acetate 1 mM EDTA
Tris/NaCl solution	50 mM Tris-HCl (pH 8.0) 150 mM NaCl
Urea/Tris solution	8 M Urea 50 mM Tris-HCl (pH8.0)

Table 10: Media used in this study. All media stored at 4°C. The glucose, glycerol and ethanol stock were sterile filtered, all other media were autoclaved.

Media	Composition
YPD	2.0 % (w/v) Peptone 1.0 % (w/v) Yeast extract 2.0 % (w/v) Glucose
SCD	0.1385 % (w/v) Synthetic complete mix (see Table 12) 0.17 % (w/v) Yeast nitrogen base 0.5 % (w/v) Amonium sulfate 2.0 % (w/v) Glucose
SCGE	0.1385 % (w/v) Synthetic complete mix (see Table 12) 0.17 % (w/v) Yeast nitrogen base 0.5 % (w/v) Amonium sulfate 2.0 % (v/v) Glycerol 1 % (v/v) Ethanol (sterile filtered)
SMMD	10 % (v/v) 10X Yeast salts (see Table 13) 0.95 % (w/v) Sorbitol 0.05 % (w/v) Glucose 10 % (w/v) 5 M potassium hydrogen phthalate 0.5 % (v/v) 1 M TRP1 0.5 % (v/v) 1 M HIS3 0.5 % (v/v) 1 M LEU2 0.5 % (v/v) 1 M URA3
LB	2.0 % (w/v) Peptone
SOC	1.0 % (w/v) Peptone 0.5 % (w/v) Yeast extract

Table 11: Amount of the respective synthetic complete dropout mix.

SC Mix	% (w/v)
SC complete	0.1385
SC-HTLUA Met	0.1085
SC-HTLUA	0.1105
SC-Met	0.1365
SC-Ade	0.1345
SC-Ura	0.1365
SC-His	0.1365
SC-Leu	0.1265
SC-Trp	0.1305

Table 12: Composition of synthetic complete mix. The supplements were mixed and stored at 4°C until use. For dropout plates, the respective amino acid was left out.

Composition (w/v)	Amino acid/supplement
0.01 %	Aspartic acid
0.005 %	Gluatmic acid
0.003 %	Phenylalanine
0.0375 %	Lysine
0.02 %	Serine
0.015 %	Threonine
0.003 %	Valine
0.0375 %	Tyrosine
0.003 %	Isoleucine
0.002 %	Arginine
0.002 %	Methionine
0.004 %	Adenine
0.002 %	Uracile
0.002 %	Histidine
0.012 %	Leucine
0.008 %	Tryptophan

Table 13: Composition of 10X Yeast salt mixture used for SMMD media.

10X Yeast salts % (w/v)
5 % (w/v) Ammonium sulfate
1.7 % (w/v) Yeast nitrogen base

Table 14: Agar-plates used in this study. Plates were stored at 4°C until usage.

Agar-plates	Composition
LB plates	3.5 % (w/v) LB agar
YPD plates	2.0 % (w/v) Peptone 1.0 % (w/v) Yeast extract 2.0 % (w/v) Agar 1 pellet NaOH per litre (autoclaved) 2.0 % (w/v) Glucose
YPG plates	2.0 % (w/v) Peptone 1.0 % (w/v) Yeast extract 2.0 % (w/v) Agar 1 pellet NaOH per litre 3.0 % (w/v) Glycerol (autoclaved)
YPG + 0.1% D (indicator) plates	2.0 % (w/v) Peptone 1.0 % (w/v) Yeast extract 2.0 % (w/v) Agar 1 pellet NaOH per litre 3.0 % (w/v) Glycerol (autoclaved) 0.1 % (w/v) Glucose
SCD plates	x % (w/v) Synthetic complete mix (see Table 12) 0.17 % (w/v) Yeast nitrogen base 0.5 % (w/v) Ammonium sulfate 2.0 % (w/v) Agar 1 pellet NaOH per litre (autoclave) 2% (w/v) Glucose

SCGE plates	x % (w/v) Synthetic complete mix (see Table 12) 0.17 % (w/v) Yeast nitrogen base 0.5 % (w/v) Ammonium sulfate 2.0 % (w/v) Agar 1 pellet NaOH per litre 2% (w/v) Glycerol (autoclave)

2.9. Cultivation of yeast

Long-term storage of the budding yeast took place at - 80°C. For this purpose, they were dissolved in SC-medium containing 15% (v/v) glycerol solution. Before culturing the strains, they were plated on YPD plates at 30°C for two days. The yeast could then be stored at 6 to 8°C in a fridge for up to two weeks.

2.9.1. Basic cultivation procedure

The basic cultivation procedure starts by inoculating the appropriate strain into the culture media of interest. They were cultured at 30°C and 250 rpm in a shaking incubator for approximately 4 to 6 hours, depending on the media (SCD for 4 hours; SCGE for 6 hours). For proper dilution for an overnight culture, a spectrophotometer (NanoDrop One© in Cuvette mode) was used to identify the optical density. The dilution was calculated according to the growth rate of the strain to achieve exponential growth within 17 to 24 hours (Formula 1).

Formula 1: Dilution for yeast cultivation.

$$V_{strain\ add\ to\ fresh\ culture} = \frac{V_{fresh\ culture} \times OD_{want\ for\ harvest}}{2^{\left(\frac{T_{until\ harvest}}{T_{doubling}}\right)} \times OD_{currently(strain)}}$$

When hormone-inducible strains were used, the appropriate β-estradiol concentration between 0 and 15 nM was added, too. Experiments were performed when the cells were in log-phase (OD_{600} < 1), controlled by optical density measurements using the spectrophotometer (NanoDrop One©).

2.9.2. Cultivation with induction for histone-promoter experiments

The first step for the cultivation of the histone-promoter strains (see Table 20) differs from the basic cultivation procedure, as the yeast were inoculated in 3 mL YPD first. Next, the cells were grown at 30°C and 250 rpm overnight, washed twice and transferred into their target media. 50 µL of each strain was filled into 30 mL of fresh target media and grown until the next day (30°C, 250 rpm). After measuring the optical density with a spectrophotometer (NanoDrop One©), cells were diluted to achieve cell concentrations of cells in exponential growth for the next day and transferred into fresh media, including the respective β-estradiol concentration. The strains were cultured in the media supplemented with the appropriate hormone concentration at 30°C and 250 rpm until the next day. Before the continuation of the experiment, an OD_{600}-value below 1 was confirmed.

2.10. Cultivation of bacteria

For long-term storage of *Escherichia coli*, the strains were kept in LB medium containing 25% (v/v) glycerol solution at - 80°C. Bacteria were cultured in LB medium including 100 µg/mL ampicillin at 37°C and 250 rpm in a shaking incubator. Plasmid isolation was performed using the NucleoSpin Plasmid Kit according to instructions for high-copy DNA isolation from *E. coli*.

2.11. Transformation of cells

2.11.1. Transformation of *Saccharomyces cerevisiae*

The yeast was inoculated in YPD and grown until stationary phase upon the next day (30°C, 250 rpm), diluted and grown to log-phase for four more hours. After harvesting, the cells were washed in ddH_2O and 800 µL 0.1 M TE/Lithium acetate and transferred into 400 µL 0.1 M TE/Lithium acetate. The competent cells were stored on ice. A mixture of 25 µL salmon sperm

carrier DNA solution (2 mg/mL), 240 µL of 50% PEG and 32 µL of 1 M TE/Lithium acetate was prepared. 50 µL of the yeast cell suspension and 1 µg of insert-DNA (linearized plasmid or PCR product) were added to the solution. After gentle homogenizing by vortexing, the mixture was incubated at 30°C and 250 rpm for 30 min. Next, a heat-shock was performed at 42°C for 20 min. The sample was then centrifuged at 3.500 g for 30 secs, washed with ddH_2O and plated onto appropriate selective medium plates. For antibiotic selection, the transformed cells were first plated onto YPD plates and then replica-plated onto a plate containing the respective antibiotics after 24 hours. After incubating the selection-plate at 30°C for about 48 hours, single colonies were picked and streaked onto fresh plates containing the selective medium or antibiotics. The single-picking was repeated once more after 24 to 48 hours of incubation at 30°C.

2.11.2. Transformation of *Escherichia coli*

For the transformation of *E. coli*, competent bacteria were prepared in advance (Inoue *et al.*, 1990) and thawed on ice. After adding the plasmid DNA (volume ratio 1:20) to the cells, they were incubated for 30 min on ice. Next, a heat-shock at 42°C for 2 min was performed, followed by cooling down the mixture on ice for 2 min. Then it was solved in 800 µL SOC media and incubated at 37°C and 250 rpm for around 1 hour. Next, the cells were spun down by centrifugation at 3000 rpm for 3 min, followed by dissolving the pellet into 100 µL fresh SOC media. The final volume was then plated on LB plates including 100 µg/mL ampicillin and incubated at 37°C overnight. Single clones were solved in 10 µL ddH_2O for control colony PCR or further procedure.

2.12. Cloning, DNA purification and sequencing

2.12.1. Polymerase Chain Reaction and purification

A Polymerase Chain Reaction (PCR) was performed to amplify specific DNA fragments using specific oligonucleotides. For this, all components were mixed as given in Table 15 and a PCR program was performed as shown in Table 16: As the first step of the program, the DNA was denatured at 95°C for 3 min. This was followed by 30 cycles of denaturation (95°C; 30 sec), primer-annealing (variable temperature; 30 sec) and elongation (72°C; variable time). As the melting temperature of individual primers differs, the annealing temperature was calculated depending on their length and GC content. The elongation time was chosen according to the product size (1 min/kb). Ending the program with a final extension at 72°C for 10 min, the reaction was stored at 4°C. For purification of the PCR product, the NucleoSpin Gel and PCR Clean-up Kit was used according to the manual.

Table 15: Components for Polymerase chain reaction.

PCR components		
75 µL		Nuclease-free H_2O
20 µL		5 x HF Phusion Buffer
2 µL	0.2 mM	dNTPs
0.5 µL	1 µM	Forward primer
0.5 µL	1 µM	Reverse primer
1 µL	50 – 100 ng	Template DNA
1 µL	1.25 U	Phusion-polymerase
100 µL		

Table 16: Program for Polymerase chain reaction.

PCR program			
95 °C	3 min	Initial denaturation	
95 °C	30 sec	Denaturation	30 cycles
x °C	30 sec	Annealing	
72 °C	x min	Elongation	
72 °C	10 min	Final extension	

2.12.2. Agarose gel electrophoresis

To check the PCR product size as a control, agarose gel electrophoresis was done. The concentration of the agarose was chosen depending on the expected length of the DNA fragments: For small fragments < 800 bp 1.5 % (w/v) agarose was dissolved in 1x TAE, for products between 500 and 4000 bp 1 % (w/v) agarose and for large fragments > 4000 bp 0.5 % (w/v) agarose was used. After heating the gel completely, the stain (1 x Sybr safe DNA gel stain) was added, and the gel was poured into trays with combs. Placing the cool and solid gel into the electrophoresis tank, it was ready to load the samples, mixed with 6 x loading dye. To be able to determine the length of the bands afterwards, one pocket of the gel was loaded with a DNA marker. The gel was then run for 30 to 45 min at 100 V. Visualization of the bands was done using UV-light (U:Genius3 Transilluminator).

2.12.3. Digestion with restriction enzymes and ligation

The classical procedure to linearize a plasmid for yeast transformation or to modify it, for example by inserting or changing specific regions, is to digest it with restriction enzymes (RE) followed by ligation. The alternative way used was Gibson assembly, which is described in the next section (see chapter 2.12.4.).

Before digesting with enzymes, the insert DNA sequence was amplified via PCR using specific primers, which added the needed restriction sites to the fragment. Afterwards, the insert and the plasmid were digested using the same restriction enzymes. After mixing the reaction (Table 17) it was incubated at an enzyme-specific temperature for 3 hours. By adding calf intestinal alkaline phosphatase (CIP), it was ensured that the plasmid was unable to re-ligate with its own ends. The incubation was then continued for 45 min. Both the digested insert and the digested plasmid were then purified using the NucleoSpin Gel and PCR Clean-up Kit.

Table 17: Components of digestion by restriction enzymes.

RE digestion components		
x µL		Nuclease-free H_2O
10 µL	1 x	Enzyme specific buffer
1 µL	1 U	Restriction enzyme(s)
x µL	1000 ng	DNA/Plasmid
0.5 µL	0.5 U	Phosphatase (CIP)
50 µL		

For merging the plasmid and insert, a ligation step was performed. For that, a ligation mixture of T4 DNA Ligase, the appropriate Buffer, the digested plasmid and the digested insert was created (Table 18). The ratio of the plasmid to insert was variable, but usually a ratio of 1:3 was used. The ratio was changed if optimizations were needed. Ligation was done at room temperature for 15 min. To inactivate the ligase, a heat-shock was performed at 65°C for 10 min. After cooling down on ice, 2 µL of the freshly ligated plasmid was used for *E. Coli* transformation (see chapter 2.11.2.).

Table 18: Components for ligation.

Ligation components		
x µL		Nuclease-free H_2O
2 µL	10 x	T4 DNA Ligase Buffer
1 µL	400 units	T4 DNA Ligase
x µL	100 ng	Digested plasmid
x µL	300 ng	Digested insert DNA
20 µL		

2.12.4. Gibson Assembly

An alternative way to assemble two or more fragments to a new plasmid is Gibson Assembly (GA). For that, the insert-DNA and the linearized plasmid were amplified via PCR using specifically designed primers to add matching overhangs to the fragments. Afterwards, the GA was mixed on ice using the insert(s), the plasmid-fragment and the GA-Master Mix (Table 19). Then, a 15 min incubation at 50°C was performed. The reaction was then stored on ice upon further procedure by diluting it in a ratio of 1:4 with nuclease-free water. Finally, 2 µL of the diluted samples was used for bacterial transformation (see chapter 2.11.2.).

Table 19: Components for Gibson assembly.

Gibson assembly components		
x µL		Nuclease-free H_2O
x µL	100 ng	Linearized plasmid
x µL	300 ng	Insert DNA
10 µL	2 x	Gibson assembly Master-Mix
20 µL		

2.12.5. Genomic sequencing

For control purposes, control PCR sequences and new plasmids were sent for sequencing to Eurofins Genomics Germany GmbH (Ebersberg). For this, the samples were diluted to 50 – 100 ng/µL (plasmid DNA) or 10 ng/µL (purified PCR product) in 20 µL. Specific primers for Sequencing were diluted to 10 nM in 50 µL.

2.13. Molecular biological methods to construct yeast strains

2.13.1. Gene deletion in yeast

To delete genes in yeast, the open reading frame was replaced by a selectable marker by homologous recombination. For that, the cassette of the marker was amplified via PCR using primers to add overhangs encoding the flanking regions of the target gene. These primers were designed with the following attributes: a total length of around 80 bp, including approximately 60 bp of the region of interest and 20 bp of the marker sequence. The forward primer included the sequence upstream of the start codon, whereas the reverse primer contained the sequence downstream of the stop codon. The auxotrophic markers used to generate knock-outs were the *C. glabrata TRP1* gene, *K. lactis URA3*, *C. glabrata LEU2* and/or *S. cerevisiae HIS3* (Table 7). As an alternative to the auxotrophic markers, antibiotic resistances were used, specifically natMX (against clonNAT), hphMX (against hygromycin B) and/or kanMX (against G418) (Table 7). After creating the insert using PCR (see chapter 2.12.1), it was purified and used for yeast transformation (see chapter 2.11.1.). The deletion was confirmed by at least two control PCRs and sequencing (see chapter 2.12.5.). Also, the hemizygous deletions were controlled to still include one copy of the gene, while one copy was deleted successfully.

2.13.2. Gene addition in yeast

The first step for adding genes to yeast was to create a plasmid including the respective gene sequence, an auxotrophic marker (*TRP1*, *URA3*, *LEU2* or *HIS3*) and an ampicillin-resistance. For that, either classical digestion by REs and ligation (see chapter 2.12.3.) or Gibson cloning (see chapter 2.12.4.) was performed, followed by an *E. Coli* transformation (see chapter 2.11.2.). The target gene was chosen to include 1000 bp upstream and at least 200 bp downstream of the coding sequence. After linearization of the final plasmid by enzymatic digestion, it was ready for yeast transformation (see chapter 2.11.1.) to integrate the gene through homologous recombination at the corresponding marker region. As multiple insertions of the plasmid are possible, a control qPCR was performed (see chapter 2.14.2.) in addition to the common control PCR, using primers for the gene-of-interest, to check the number of integrations. Before measuring strains, the newly integrated region was sequenced to exclude mutations (see chapter 2.12.5.).

2.13.3. Modification of promoter or terminator sequences in yeast

For testing the effect of histone-promoters on the expression of *ABF2* and *MIP1*, a plasmid with the corresponding gene sequence, including a histone promoter, the gene of interest and a chosen terminator was created. After a successful control PCR and sequencing of the plasmid, which additionally contains an ampicillin resistance and the sequence of an auxotrophic marker, the plasmid was ready for yeast transformation. For strains that were intended to test the effect in the endogenous locus, the promoter-gene-terminator sequence was amplified using PCR accompanied by adding homologous regions of the endogenous locus. This insert was used for yeast transformation (see chapter 2.11.1.). Alternatively, if the sequence was planned to be inserted into a marker region, the complete plasmid was linearized by digestion with the corresponding RE's (see chapter 2.12.3.) and then used for yeast transformation (see chapter 2.11.1.). If needed, a second transformation was performed to delete the endogenous gene of interest (see chapter 2.13.1.). Successfully transformed clones were again confirmed using control PCR and sequencing. An overview of the strains

and the included promoter, gene of interest, terminator as well as the transformed region, is shown in table 20.

Table 20: Overview of strains for histone-promoter experiments.

Strains for histone-promoter experiments					
Strain	Promoter	Gene of interest	Terminator	Trans-formed region	Additional deletion
KSY302	*HTB1*	*ABF2*	*ABF2*	*ABF2*	
KSY314	*HTB1*	*ABF2*	*ADH1*	*ABF2*	
KSY313	*HTB2*	*ABF2*	*ABF2*	*ABF2*	
KSY315	*HTB2*	*ABF2*	*ADH1*	*ABF2*	
AFY002-4	*HTB1*	*mCITRINE-P2A-ABF2*	*ABF2*	*ABF2*	
AFY010	*HTB1*	*mCITRINE-P2A-ABF2*	*ADH1*	*URA3*	
AFY027	*HTB1*	*mCITRINE-P2A-ABF2*	*ADH1*	*URA3*	*abf2*Δ
AFY030	*HTB1*	*ABF2*	*ADH1*	*URA3*	
AFY031-2	*HTB1*	*ABF2*	*ADH1*	*URA3*	*abf2*Δ
AFY041-2	*HTB1*	*ABF2*	*MBF1*	*URA3*	
AFY042	*HTB1*	*ABF2*	*ALR2*	*URA3*	
AFY043	*HTB1*	*ABF2*	*KKQ8*	*URA3*	
AFY046	*HTB1*	*ABF2*	*SUT1*	*URA3*	
AFY048-2	*HTB1*	*ABF2*	*SUT1*	*URA3*	*abf2*Δ
KSY303	*HTB1*	*MIP1*	*MIP1*	*MIP1*	
AFY036	*HTB1*	*MIP1*	*ADH1*	*TRP1*	
AFY044-2	*HTB1*	*MIP1*	*ADH1*	*TRP1*	*mip1*Δ
AFY061	*HTB1*	*MIP1*	*SUT1*	*TRP1*	

2.14. Measuring mtDNA concentration

2.14.1. DNA extraction

When DNA needed to be extracted for controls after transformations, single colonies were used directly and an extraction without RNase digestion step was done. In case the sample was used for mtDNA analysis, two rounds of DNA extraction were separated by an RNase digestion step. For these purposes, a volume of 10 mL of a cell culture was harvested by

centrifugation at 3434 g for 5 min at 4°C. After washing the cell pellet in nuclease-free water, the sample was frozen in liquid nitrogen and stored at - 20°C or immediately used for extraction.

The phenol-chloroform-isoamyl alcohol (PCI) extraction started by adding 200 µL DNA extraction buffer (pH 8.0), 200 µL PCI and approximately 250 µg glass beads to the sample. By vortexing 30 sec at 3000 oscillations in a Mini-BeadBeater 24, cells were disrupted mechanically. Next, the samples were centrifuged at 11600 g for 5 min, resulting in a phase separation of the sample. The transparent top layer (approximately 200 µL) was then transferred into 500 µL ethanol (100%). This was followed by another centrifugation under the same conditions as before. Afterwards, 700 µL Ethanol (70%) was used to wash the sample by adding it to the pellet and another centrifugation step. After removing the ethanol from the sample, it was incubated with open lid at 50°C to let the alcohol evaporate completely. Then, the pellet was dissolved in 50 µL nuclease-free water.

If necessary, RNA was digested by adding RNase A (DNase-free; 1 mg/mL) to the sample and incubating at 37°C for 30 min. Afterwards, the PCI extraction was repeated, starting by adding the extraction buffer and PCI as described above. As the sample only contains DNA, no glass beads and oscillation were needed anymore; instead, a short vortex-step was performed. After the extraction was finished, samples were stored at - 20°C until further analysis. If necessary, the DNA concentration of the samples was measured using a spectrophotometer (NanoDrop One©) at 260 nm and 280 nm.

2.14.2. qPCR measurements

To determine the mtDNA copy numbers or the DNA concentration of a certain gene, quantitative PCR measurements were performed. This was done in a LightCycler 480 Multiwell Plate 96 (Roche) using NA-binding fluorescent dye (BioRad, SsoAdvanced Universal SYBR Green Supermix). As the fluorescence intensity increases in proportion to the amount of amplified sequence by binding the double-stranded DNA, a quantitative analysis is possible.

The master mix (Table 21) for qPCR consists of SsoAdvanced Universal SYBR® Green Supermix and 0.5 µM of appropriate primer pairs (see Table 8). After pipetting the master mix, 8 µL of it was transferred into each well, followed by adding 2 µL DNA sample (1 ng). Each sample was analyzed in three technical replicates, measuring each sample of each biological replicate three times on the same plate. Calculations later on were based on the mean value of the three technical replicates. In case one of the technical replicates showed an outlier leading to a standard deviation higher than 0.5, this questionable replicate was excluded from the analysis.

Table 21: Components of qPCR master mix.

qPCR master mix components		
2 µL		Nuclease-free H_2O
5 µL		SsoAdvanced Universal SYBR® Green Supermix
0.5 µL	0.5 µM	Primer forward
0.5 µL	0.5 µM	Primer reverse
2 µL	1 ng	DNA sample
10 µL		1 reaction (well)

The qPCR was performed on a Light Cycler® 96 with the following steps (Table 22).

Table 22: Program of qPCR for DNA samples.

qPCR program			
95 °C	10 min	Polymerase activation	1 x
95 °C	10 sec	Denaturation	40 cycles
60 °C	30 sec	Annealing	
95 °C	60 min	Melting	1 x

If a specific gene should be measured, the required primer pair was designed for a sequence of approximately 200 bp. For each gene, three primer pairs were compared regarding their efficiency for qPCR by performing calibration dilution series to obtain standard curves. The primer pair with the best coefficient of determination of a linear fit was then used for qPCR analysis. The primer pairs of the following genes were adopted from previous studies of the lab: *COX2 (Seel et al., 2023)*, *COX3 (Seel et al., 2023)*, *ACT1 (Claude et al., 2021)*, *MRX6 (Seel et al., 2023)*, *MIP1 (Seel et al., 2023), RDN18 (Claude et al., 2021)*, *ABF2* (Seel *et al.*, 2023). The calibration standard curves of *COX2*, *COX3*, *MRX6* and *MIP1* can be found in (Seel, 2022). The calibration standard curves of some of the previously used and all of the newly designed primer pairs can be seen in Figure 10.

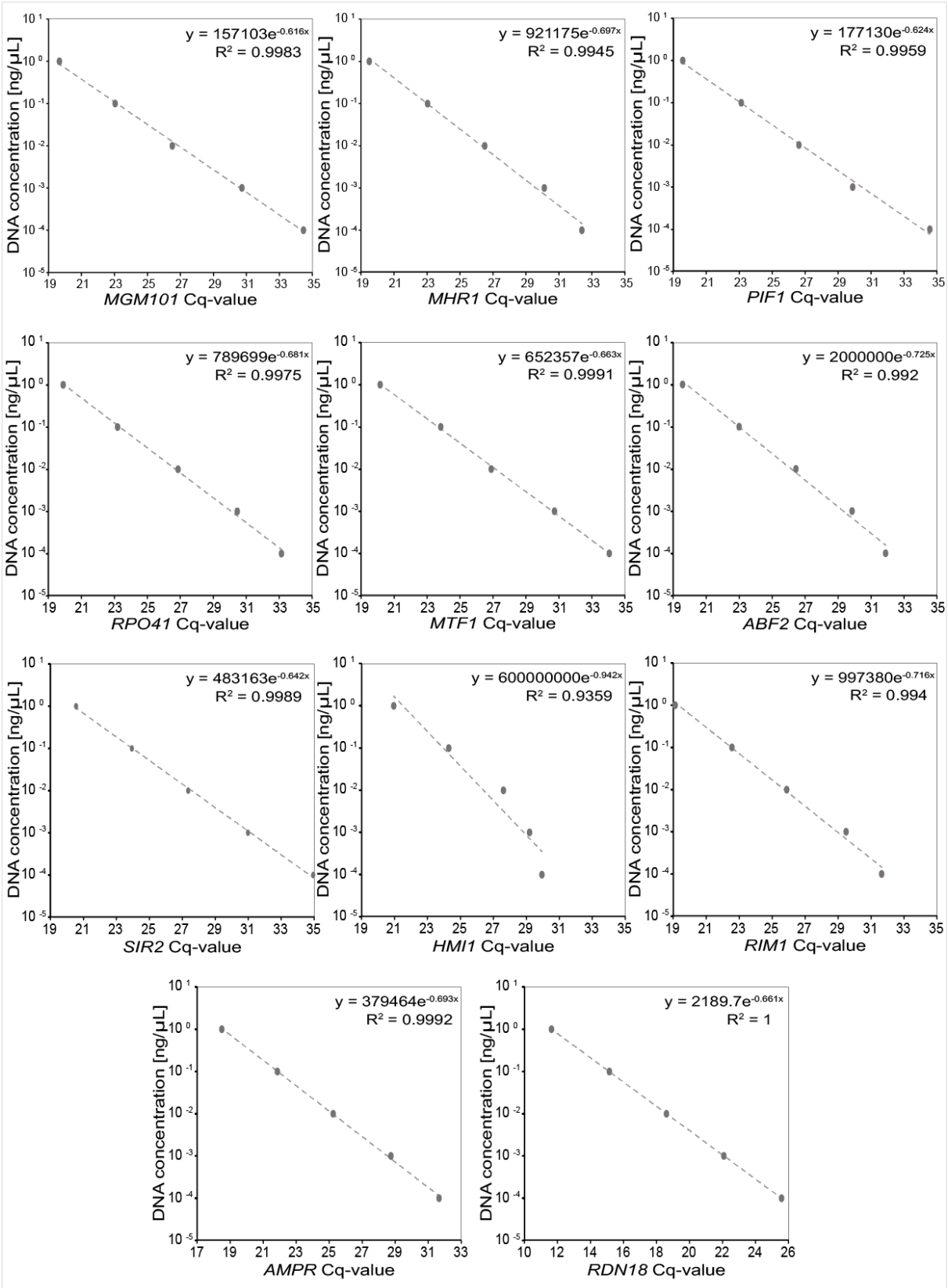

Figure 10: Calibration curves of newly designed primer pairs for qPCR. Standard curves were measured for *MGM101*, *MHR1*, *PIF1*, *RPO41*, *MTF1*, *ABF2*, *SIR2*, *HMI1*, *RIM1*, *AMPR* and *RDN18*. Dilution series was based on 1 ng/µL wild type DNA. Best fitted primer pair out of three tested pairs per gene was selected for experiments and shown in this Figure.

For calculating the mtDNA concentration, each sample was measured using the four primer pairs of *COX2*, *COX3*, *ACT1* and *MRX6*. Using the mean value of the two primer pairs of *ACT1* and *MRX6,* the nDNA concentration, and the mean value of the two primer pairs of *COX2* and *COX3,* the mtDNA concentration, was measured. By normalizing the mtDNA on nDNA, the relative mtDNA copy number per nDNA was calculated. After averaging the results of mtDNA copy number per nDNA of at least three biological replicates (three experiments performed identical on three independent days), the mean cell volume (see chapter 2.16.1.) and mean nuclear DNA copy number (see chapter 2.16.2.) were used to calculate the mtDNA concentration per cell (Formula 2).

Formula 2: mtDNA concentration per cell.

$$\text{mtDNA concentration per cell} = \frac{\left(\frac{\text{mtDNA}}{\text{nDNA}}\right) \times \text{ nDNA copy number per cell}}{\text{cell volume}} = \frac{\text{mtDNA copies per cell}}{\text{cell volume}}$$

2.15. Measuring RNA concentrations

2.15.1. RNA extraction and cDNA synthesis

After culturing the yeast, 10 mL of each sample was harvested by centrifugation at 3434 g for 5 min at 4°C. The pellet was washed with nuclease-free water and centrifuged at 11600 g for 1 min. After the supernatant was removed carefully, the RNA was extracted using the YeaStar RNA Kit (Zymo Research) according to the instructions of the kit. The final RNA pellet was then stored at - 20°C (short term) or - 80°C (long term). If necessary, RNA concentrations were determined using a NanoDrop One©.

To exclude possible DNA contamination, a DNase digestion step was performed using DNase I (858 U per sample; Life Technologies). The DNase I Buffer and DNase I were added to 100 ng of RNA sample as shown in Table 23. Except for the histone-promoter strains, where only 83.3 ng of RNA was used. After 15 min of DNase-incubation at room temperature, 25 mM EDTA was added to the sample to inactivate the reaction while incubating at 65°C for 10 min.

The samples were then reverse transcribed into cDNA using the high-capacity cDNA reverse-transcription kit and its protocol (Thermo Fisher Scientific).

Table 23: Components of DNase digestion of RNA.

DNase digest components		
x µL		Nuclease-free H_2O
3.3 µL		DNase I Buffer
3.3 µL	1 U/µl	DNase I
x µL	100 ng	RNA sample
3 µL	25 mM	EDTA
33 µL		1 reaction (well)

2.15.2. RT-qPCR measurements of RNA samples

For RT-qPCR, the cDNA samples, representing the RNA, were diluted in two ways: for *RDN18* measurements, the samples were diluted 1:100 to 10 ng, whereas for all other primer pairs, the samples were diluted 1:10 to 100 ng. Besides that, the master mix of qPCR was the same as for DNA qPCR (see Table 21). The primer pairs used for RT-qPCR were dependent on the

purpose of the experiment and were created as described before (see chapter 2.14.2.). A measurement using *RDN18* primers was always included for subsequent normalization. Again, a total of three technical replicates on the same plate were measured per sample. Using a Light Cycler® 96, the RT-qPCR was performed as described in Table 24.

Table 24: Program of RT-qPCR for cDNA samples.

RT-qPCR program			
95 °C	1 min	Polymerase activation	1 x
95 °C	10 sec	Denaturation	40 cycles
60 °C	30 sec	Annealing	
95 °C	60 min	Melting	1 x

To calculate the RNA concentration of a specific gene in a sample, the technical replicates were averaged (excluding questionable replicates leading to standard deviation > 0.5). Afterwards, the result was normalized on the *RDN18*-concentration of the same sample.

For the histone-promoter strains, a Volume-Dependence-Parameter (VDP) was determined as described in (Claude *et al.*, 2021). This parameter gives insights into the expression of a gene regarding its cell-volume dependency: constant concentrations with increasing cell volumes are represented by a VDP of around 0, whereas constant amounts are represented by a VDP of around -1.

2.16. Measurements of cell physiologies

2.16.1. Cell volume

To determine the cell volume, a Coulter counter was used. For the separation of individual cells, 1 mL of the cultured yeast was sonicated before measuring. To achieve a total number of counted cells between 20.000 and 50.000 cells, a volume of 100 to 1000 µL (depending on the OD_{600}- value) was added to 10 mL Isoton II Diluent in a cuvette. Cells in a range of 10 to 328 fL were measured at a gain of 256 and a current of 0.707 mA. In case the cells were induced to higher cell volumes, a second range between 328 to 1856 was measured (Gain 256, Current 0.125 mA). Then, the combined cell volume of both ranges was calculated by using the number of cell counts as shown below (Formula 3). Otherwise, the mean cell volume is calculated from the distribution of range 1.

Formula 3: Total cell volume for measurements in two ranges with a Coulter counter.

$$\text{cell volume}_{\text{total}} = \text{cell volume}_{\text{range 1}} \times \left(\frac{\text{cell number}_{\text{range 1}}}{\text{cell number}_{\text{total}}}\right) + \text{cell volume}_{\text{range 2}} \times \left(\frac{\text{cell number}_{\text{range 2}}}{\text{cell number}_{\text{total}}}\right)$$

2.16.2. Mean nDNA copy number

To measure the nDNA copy number and track the budding behavior, 1 mL of the sample was sonicated and diluted 1:10 in fresh media. The number of budding cells was determined by visual inspection using a microscope. A total number of at least 100 cells (per person) was counted independently by two persons. After averaging the two results, the nDNA copy number was calculated dependent on the ploidy of the strain as follows (Formulas 4 and 5):

Formula 4: nDNA copy number per cell for haploid strains.

$$\text{nDNA copy number per cell}_{\text{haploids}} = \frac{(2 \times \text{N(Buds)}) + (1 \times \text{N(noBuds)})}{\text{N(total)}}$$

Formula 5: nDNA copy number per cell for diploid strains.

$$\text{nDNA copy number per cell}_{\text{diploids}} = \frac{(4 \times \text{N(Buds)}) + (2 \times \text{N(noBuds)})}{\text{N(total)}}$$

2.16.3. Growth rate

For analysis of the growth rate, the optical density was determined by spectrophotometry at 600 nm. By measuring every 30 min for OD_{600} values between 0.1 and 1, a growth curve was created. The doubling time could then be obtained by quantifying the slope of a linear fit through the data when plotting the logarithmic value over time (linear). The growth curves per strain grown in SCGE media are shown in Figures 11 and 12.

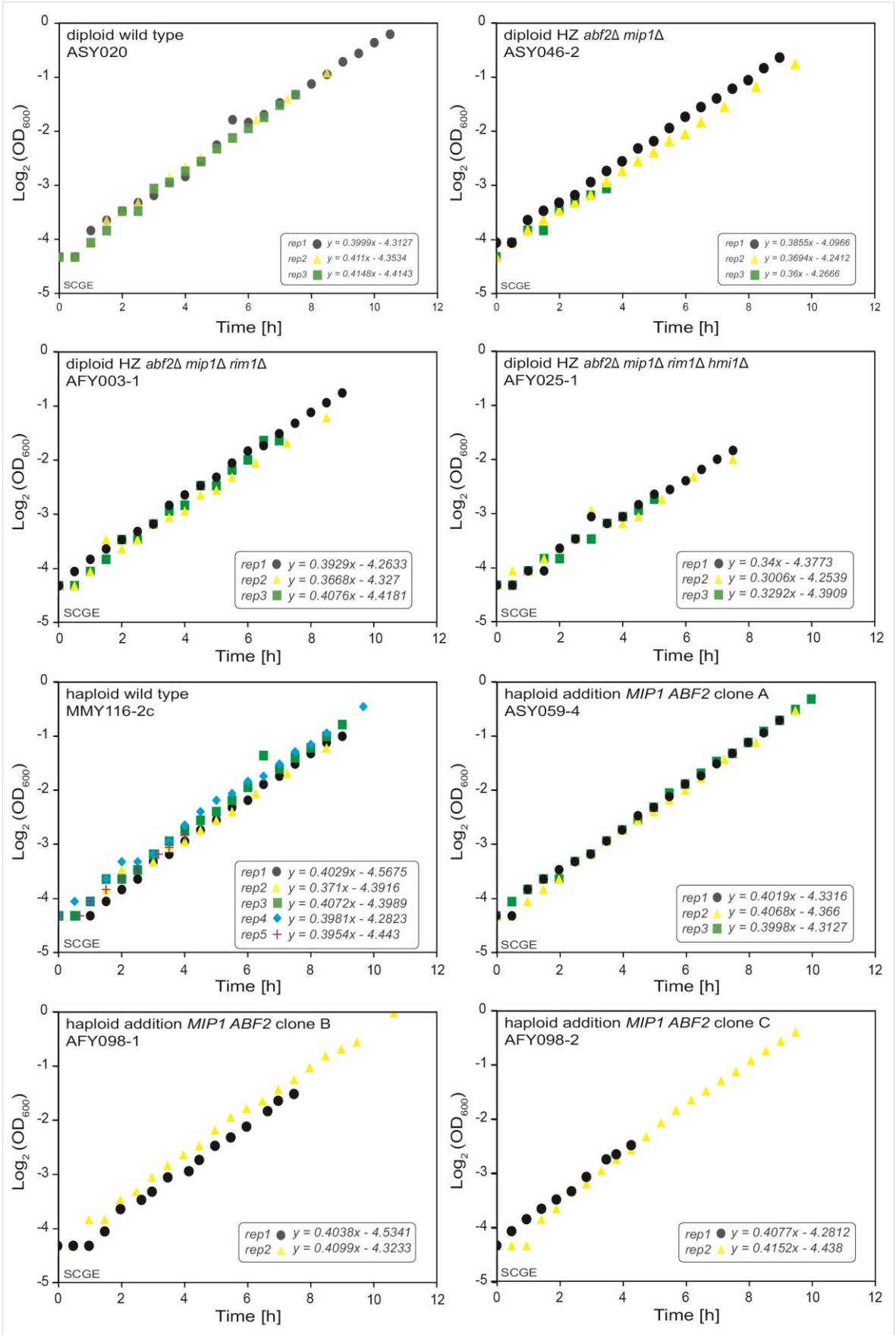

Figure 11: OD-Growth curves for calculations in SCGE 1. Log2 of optical density at OD600 over time. For each strain, at least 2 replicates were performed.

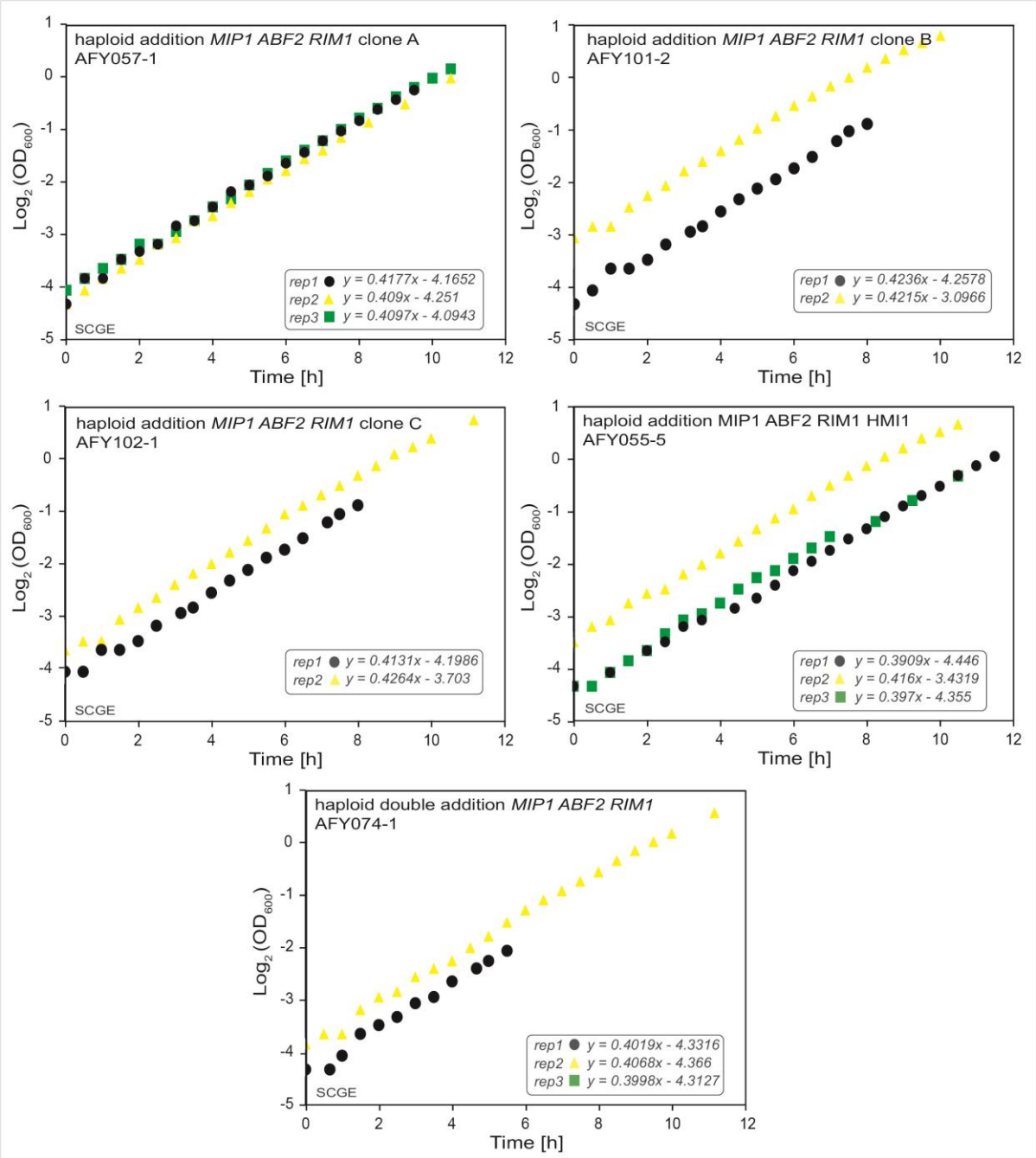

Figure 12: OD-Growth curves for calculations in SCGE 2. Log2 of optical density at OD600 over time. For each strain, at least 2 replicates were performed.

2.16.4. Competition assay

To confirm the growth rate measurements (see chapter 2.16.3.), competition assays were performed for selected strains. Before mixing, the strains were cultivated individually in 30 mL SCGE at 30°C with 250 rpm in a shaking incubator overnight. After determining the optical density of each sample with the NanoDrop One©, each strain was diluted to an OD_{600} of 0.3 with fresh media in 10 mL. Next, a sample of the pure strain was created by harvesting 7 mL of the diluted culture. Afterwards, each strain was mixed in a 25%/75% ratio with its corresponding wild type with corrected auxotrophic markers (reference strain). Again, a sample of 7 mL was taken from the homogenously mixed sample, harvested and stored for DNA extraction (T = 0 h). The last step was to dilute the mixture in fresh media for growth in

log-phase until the next day (30°C, 250 rpm). Samples were harvested daily for 5 to 8 days by diluting to an OD_{600} of 0.3, collecting 7 mL of each mixture and using the rest for diluting in fresh media. After extracting the DNA of all samples (see chapter 2.14.1.), they were analyzed using qPCR with *ACT1*- and *AMPR*-primers (see chapter 2.14.2.). This way, as only the strain-of-interest contains the *AMPR*-Sequence (due to the plasmid for gene addition; see chapter 2.13.2.), the fraction of it in the mixed culture was determined. For this, the *AMPR*-concentration per *ACT1*-concentration was calculated and the result of each time point was then normalized on the corresponding pure strain sample.

2.16.5. Assay of petite frequency

This assay was used to determine the frequency of petite colonies, which indicates the probability of a strain losing its respiratory capacity. After inoculation of the strain in 4 mL YPD and growth at 30°C, 250 rpm overnight, 50 µL of it were transferred into 7 mL fresh YPD media and incubated under the same conditions for two more hours. Next, the optical density was measured with the NanoDrop One©, the cells were washed and diluted to OD_{600} = 1 in 1 mL ddH_2O. A volume of 150 µL of the cells was then plated onto an indicator plate (YPG + 0.1 % Glucose). For each strain, two plates were prepared and then incubated at 30°C for around 48 hours. All cells can ferment the present glucose and start growing on the plate first. However, as soon as the glucose is consumed completely, only the cells with intact mtDNA can use the glycerol as carbon source, switch to respiration, and continue to grow. This is why two different sizes of colonies become visible on the plate after 48 hours: The small ("petite") colonies with no respiratory capacity (ρ^- and ρ^0) and the large (ρ^+) colonies with respiratory capacity (Figure 13). The number of petite colonies was counted by visual inspection of at least 500 colonies per biological replicate.

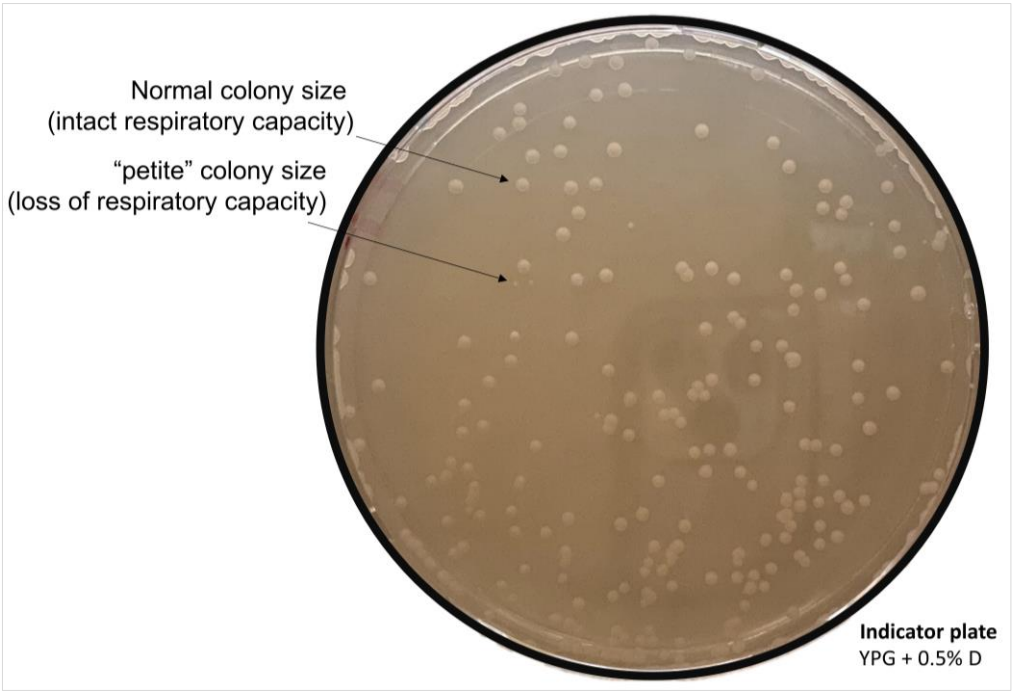

Figure 13: Exemplary indicator plate of a petite frequency assay. YPG-Plate including 0.5% glucose to indicate the respiratory capacity of each colony. Cells with intact respiratory capacity switch into respiration when glucose is consumed completely, continue to grow and form normal colony sizes. Cells without respiratory capacity stop growing when glucose is consumed completely and therefore result in smaller "petite" colony size. The exemplary plate shown here was used to test the strain AFY003-1.

2.16.6. Stress spot assay

First, the strains were inoculated in 4 mL YPD and grown over night at 30°C and 250 rpm. After measuring the optical density using a Nano Drop One©, the sample was diluted to OD_{600} = 1. It was then washed by centrifugation at 11600 g for 1 min and resuspended in 1 mL ddH_2O. A 1:10 dilution series of 5 dilutions was created starting from this sample. 5 µL of each dilution was then plated onto the specific plate using a multichannel pipette.

The plates (YPD, SCD or SCG) for the temperature assay did not include any further additions. These plates were incubated at 23, 30 or 37°C for at least 48 hours. For all other assays, the stress-inducing chemical was added before pouring the plates. To test the strains under osmotic stress, 5 nM NaCl were included in YPD plates. 50 or 100 nM hydroxyurea were added to SCD plates to monitor the growth under replicative stress. The chemical stress assay plates were incubated at 30°C for at least 48 hours. Each stress assay was stopped as soon as the wild type showed adequate colony growth. The pictures of each plate were taken by a Transilluminator without UV light. Evaluation of the results was performed by three individual persons under masked conditions to conclude unbiased results.

2.16.7. Chronological aging

Chronological aging experiments were performed to determine the survival of a strain without any nutrient supply. Starting with inoculation of a 7 mL YPD culture, each strain was grown at 30°C, 250 rpm for approximately 4 hours. Afterwards, the cells were diluted to grow into stationary phase using the same conditions until the next day. When an optical density of OD_{600} = 3 was reached as measured with the NanoDrop One©, the cultures were diluted to OD_{600} = 0.01 in 10 mL H_2O. Afterwards, the cells were incubated in water at 30°C with 250 rpm in a shaking incubator. Samples were taken every 48 hours by plating a defined volume onto a YPD plate. This plate was then incubated at 30°C for 48 hours, and single colonies were counted by visual inspection.

2.17. Single-cell analysis

2.17.1. Replicative aging

The replicative aging experiment was conducted by Jurgita Paukštytė (Saarikangas lab, University of Helsinki, Finland) as described in (Paukštytė *et al.*, 2023).

2.17.2. Time-lapse microscopy

In order to phenotype cells on the single-cell level, time-lapse microscopy was performed. For this, the cells were cultured in the appropriate media for at least 24 hours before diluting them to OD_{600} = 0.1 in 5 mL. In order to avoid clogging, it is important to use filtered media. The experiment was performed with different media depending on the aim of the experiment: For investigation of the steady-state growth and confirming bulk experiment results, the cells were cultured in SCGE for the complete experiment. Additionally, a media switch experiment was performed to analyze the cells' behavior when facing low-glucose stress. For this, the cells were cultured in SCD pre-microscopy as well as for the first two hours of microscopy. Afterward, the media was switched to a minimal media, which contained 0.05 % Glucose and 0.95 % Sorbitol. Additionally, 1 % of each of the four amino acids, which were corrected in some of the strains (1% tryptophan, 1% histidine, 1% leucine, 1% uracil) were supplemented. This serves to avoid potential differences in the growth of strains with corrected auxotrophic markers due to their transformations.

The time-lapse microscopy was performed with a custom microfluidic device (Kukhtevich *et al.*, 2022), with which single cells can be trapped while allowing a continuous supply of media. 20 µL/min growth media is supplied during the experiment and a constant temperature of 30°C was guaranteed by an objective heater. For the media switch experiment, it has to be noted that it takes approximately 30 min until the second media is distributed in the device completely. The microscope used was a Nikon Eclipse Ti-E microscope (NIS-Elements software) with an Andor iXon Ultra 888 camera and SPECTRA X light engine illumination. To generate a time-lapse video, phase-contrast images were obtained with a plan-apo λ 100×/1.45 Na Ph3 oil immersion objective (with additional magnification 1.5x) and 100 ms exposure time, every 3 min.

For each strain and replicate, five positions were measured in parallel. To prevent overcrowding of the cells, each position was ensured to include a number as minimal as possible with a maximum of six cells.

2.17.3. Live-cell confocal microscopy for analysis of mtNetwork and nucleoids

For analysis of mitochondrial network volume and nucleoids, live-cell confocal microscopy was performed. Before adding the cells, the slides (µ-Slide 8 Well, ibi-Treat) were coated with Concanavalin A (ConA, 1 mg/mL in H_2O). For this, 200 µL ConA was added and incubated for 10 min at room temperature. After two steps of washing the slides, they were dried on air. The cells were cultured (see 2.9.1.) and washed in the appropriate media twice by centrifugation at 17000 g for 1 min. Next, 200 µL of the cells were added to the slide and incubated for 5 min at room temperature to settle down. After removing the supernatant, the slide was washed again twice and covered with 200 µL of fresh medium.

The live-cell microscopy was performed using a Zeiss LSM 800 microscope (software: Zen 2.3, blue edition) with a Zeiss Axiocam 506 camera. The following settings were used: confocal mode, 63x /1.4 Oil DIC objective, 0.35 µm z-stack steps with a depth of 15.05 µm. The visualization of the mitochondrial network was done using mKate2 (excitation 561 nm; detection 610-700 nm), whereas the nucleoids were visualized with 2xmNeon (excitation 488 nm; detection 410-546 nm). In addition to the fluorescent channels, bright-field images were obtained using the transmitted light detector (T-PMT).

2.17.4. Analysis of microscopy data

Time-lapse microscopy data were analyzed using the open-source software Cell-ACDC (Padovani *et al.*, 2022). This includes the first step of prepping the data by aligning and cropping the region of interest. Afterwards, by using the contrast channel, cells were automatically segmented and tracked by YeaZ (Dietler *et al.*, 2020). Next, the results were corrected manually and buds were assigned to their mothers. In addition, the cell division was labelled in the appropriate frame. For downstream analysis, the final dataset was exported and mainly analyzed by code published by (Chadha *et al.*, 2024b). The analysis of the network and nucleoids was done via spotMAX (Padovani *et al.*, 2024) inside the Cell-ACDC software.

2.18. Analysis of expression with variable mtDNA concentrations

2.18.1. RNA sequencing

In order to analyze transcription and check expression on RNA level, RNA was extracted as described in chapter 2.15.1. After the DNase digestion step, the RNA samples were stored at - 80°C. The RNA-Seq was conducted by Novogene Co., Ltd. After quality control

measurements including Agilent 5400 Bioanalyzer, Agarose gel electrophoresis and NanoDrop One© measurements, samples that showed residuals of DNA or an Integrity value below 3 were excluded. All included samples resulted in an Integrity value higher than 7.6, except for four samples (Integrity values between 4.7 and 6.7). If Poly-A Enrichment is used for RNA Seq, mitochondrial RNA would be excluded from the analysis, as yeast mtRNA does not include Poly-A (Groot *et al.*, 1974). The protocol therefore included an rRNA depletion step instead. After the RNA was depleted and reverse transcribed into cDNA, an end repair and A-Tailing, adaptors were ligated and libraries were amplified. Again, a quality control of the final library was performed. The sequencing data were analyzed by Kim Job (Scialdone Lab, Helmholtz Munich, Germany). Genes with fewer than 30 counts in at least three samples were excluded. Gene expression counts were normalized using transcripts per million (TPM). The 500 most highly variable genes were selected using Scanpy and $\log_{10}$-transformed for principal component analysis (PCA). Differential expression analysis was performed using pyDESeq2 and genes with an adjusted p-value < 0.1 were classified as differentially expressed.

2.18.2. Proteomics by mass spectrometry

To quantify the composition of the proteome in strains with altered mtDNA concentrations, mass spectrometry was performed. For this purpose, the cells were cultured in 50 mL SCGE, and the cell pellets were harvested and stored at - 80°C until further procedure. Peptide extraction was performed by Luisa Hernández Götz (Schmoller Lab, Helmholtz Munich, Germany) as described in (Lanz *et al.*, 2023): For this, cells were lysed using a buffer containing 50 mM Tris-HCl (pH 8.0), 0.2% Tergitol, 150 mM NaCl, and 5 mM EDTA, with protease inhibitors. Lysates were disrupted using glass beads, clarified by centrifugation, and protein concentrations were determined using the BCA assay. Proteins were denatured with 1% SDS and 5 mM DTT at 65°C for 10–15 min, then alkylated with iodoacetamide at room temperature for 15 min. Proteins were precipitated with a solution of 50% acetone, 49.9% ethanol, and 0.1% acetic acid, then resuspended in 8 M urea with 50 mM Tris-HCl (pH 8.0) and diluted with NaCl. Proteins were digested overnight with trypsin (1:50 enzyme:protein) at 37°C. Digests were desalted using C18 columns. Peptides were eluted in 80% acetonitrile with 0.1% acetic acid, dried, and resuspended in water for storage at - 20°C. Mass spec and downstream analysis were conducted by Michael Lanz (Skotheim Lab, Stanford University, USA) as published in (Lanz *et al.*, 2023).

To test the dependency of a protein on mtDNA, the values of single proteins were calculated as follows: The mean of the appropriate wild type measured within the same batch was calculated from two replicates per batch. Next, the value of a single replicate for each strain was normalized to the mean of the appropriate wild type. Afterwards, the two normalized values were used to calculate a mean for this specific protein and strain. The dependency could then be evaluated by plotting the mean normalized protein value as a function of the mtDNA concentration normalized to wild type. By creating a linear regression through all of the included values, the slope and the coefficient of determination (R^2) could be identified. A slope of 0 represents no dependency of the relative protein concentration on the mtDNA concentration, while a slope of 1 would represent a perfect linear dependency. A negative slope of -1 means that the relative protein concentration linearly decreases with increasing mtDNA concentrations. Moreover, the R^2-value displays the accuracy of the linear regression. The closer the R^2-value is to 1, the more precisely the individual values fit the linear regression.

3. Results

3.1. G1 arrest leads to increasing mtDNA copy numbers with rising cell volumes

As described before, previous experiments in the lab have demonstrated the cell volume-dependency of mtDNA copy number (Seel, 2022) by increasing cell volume using a β-estradiol-inducible Whi5-system (Schmoller *et al.*, 2015). The cell cycle regulator Whi5 inhibits the SBF transcription and therefore the cells stay longer in the G1-Phase and gain more cell volume, dependent on the hormone concentration. This approach to achieve bigger cell volumes is no permanent arrest and the cells can cycle through their cell cycle with normal doubling times afterwards again. While the results obtained by this strategy suggest a dependency of mtDNA copy number on the cell volume, an additional influence of the hormone or Whi5 itself can not be excluded. That is why an alternative approach to increase the cell volumes, including a permanent arrest in G1-Phase, was performed. For this, a haploid strain with a triple deletion of the three G1 cyclins *cln1*, *cln2* and *cln3,* as well as a β-estradiol-inducible *CLN1* was used to measure mtDNA copy number (Ewald *et al.*, 2016). As Whi5, also Cln1/2/3 are cell-cycle regulators influencing the SBF transcription (Richardson *et al.*, 1989), as shown in Figure 14a. Cln1 in particular is involved in inhibiting Whi5, which subsequently inhibits the SBF-Transcription (Costanzo *et al.*, 2004). In the described strain, the cells can perform their cell cycle unrestricted, as long as β-estradiol is available in the media. After removing the β-estradiol, the cells will face a G1-arrest, leading to higher cell volumes over time. Collecting samples every hour opened up the possibility to track mtDNA copy number with increasing cell volumes. Cells grown in SCGE and SCD were analyzed regarding their cell volume, nDNA copy number per cell and mtDNA copy number. The G1-arrest was observed when checking the nDNA copy number per cell (Figure 14b): After two hours of arrest, the cells grown in SCD only show one copy of nDNA per cell, indicating there is no replication of nDNA taking place. For cells grown in SCGE, this is achieved around three hours after starting the arrest. These are also the times when the cells start to increase their cell volume (Figure 14c). In line with previous results (Seel *et al.*, 2023), the cells cultured in non-fermentable media contain higher amounts of mtDNA (Figure 14d). This can be explained by the fact that mtDNA is not needed in SCD, as fermentation can be used to generate energy. As shown in Figure 14d, the mtDNA copies per cell increased with rising cell volumes, independently of the media. The results generated with the *cln1/2/3* mutant together with the β-estradiol-inducible Whi5-system results support the conclusion of an increasing mtDNA copy number with increasing cell volume.

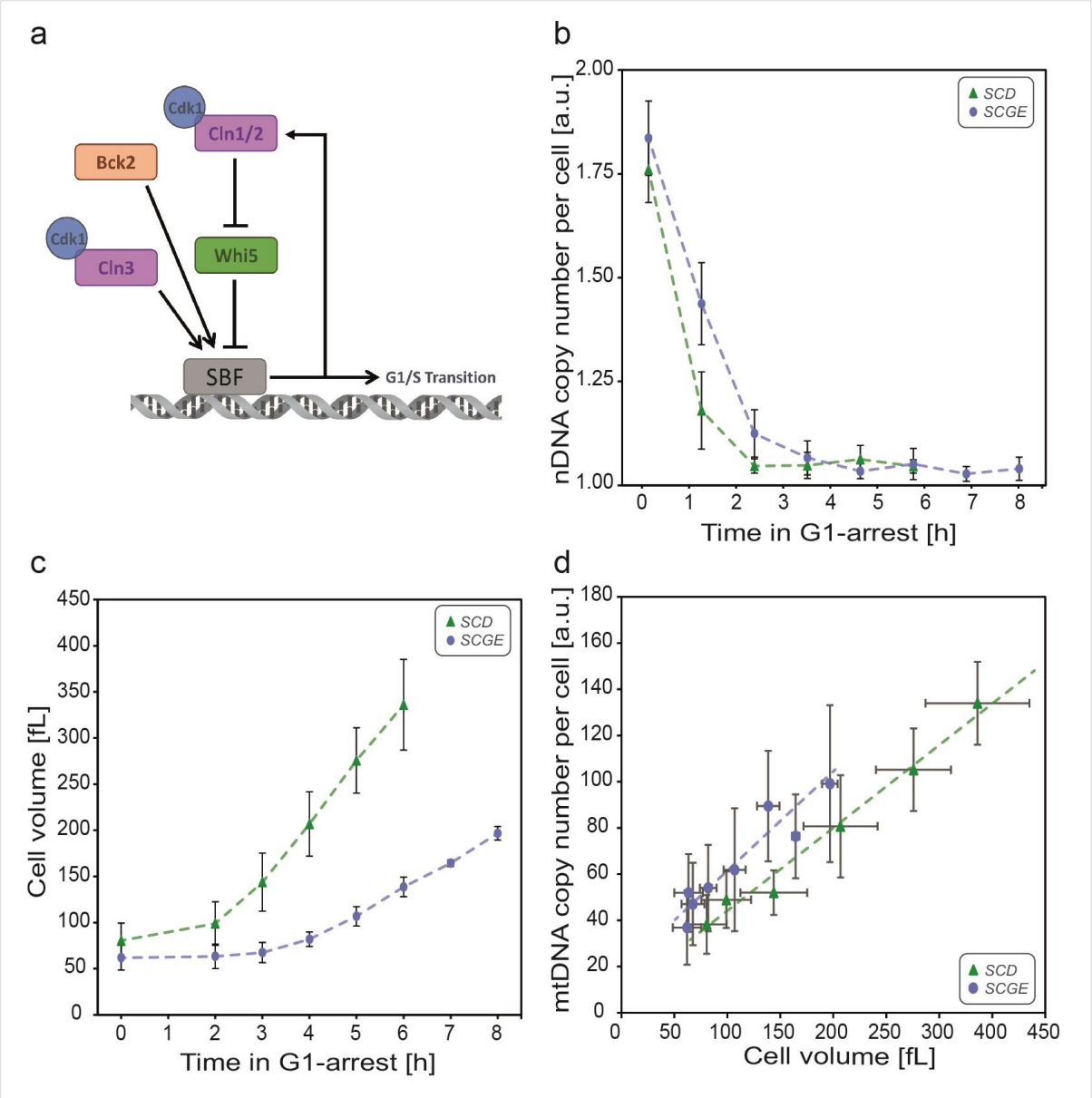

Figure 14: Increasing cell volumes by G1-arrest in c*ln1/2/3*-deletion and β-estradiol-inducible *CLN1*-strain leading to increasing mtDNA copy numbers. a) Schematic representation of included cell-cycle regulators involved in G1/S-Transition. **b)** nDNA copy number per cell decreases over time after the G1-arrest started for growth in SCD (green triangle) and SCGE (blue dot), measured in three replicates per media. **c)** Cell volume increases over time after the G1-arrest started for growth in SCD (green triangle) and SCGE (blue dot) for three replicates per medium. **d)** Increasing cell volume leads to increasing mtDNA copy number per cell, measured in SCD (green triangle) and SCGE (blue dot), measured in three replicates per medium.

3.2. Identification of the cell volume-dependent machinery limiting mtDNA copy number

3.2.1. The nuclear-encoded cell volume-dependent machinery limiting mtDNA copy number comprises *MIP1*, *ABF2* and *RIM1*

Mitochondrial DNA copy number is not strictly coupled to the cell cycle as nDNA (Conrad and Newlon, 1982), but is regulated in a cell volume-dependent manner as mentioned before (see chapter 1.3.4.3.; (Seel *et al.*, 2023)). The proposed model is that cell volume drives the amount of a nuclear-encoded machinery, which then influences the mtDNA copy number. Previous experiments in the lab have identified two major limiting genes for mtDNA as part of this machinery to be *MIP1*, encoding the mitochondrial polymerase, and *ABF2*, encoding the packaging factor for mtDNA (Seel *et al.*, 2023). However, as the upregulation of both of these genes to two-fold only increases the mtDNA concentration to 1.5-fold (see Figure 8), it can be speculated that one or several genes that additionally limit mtDNA copy number in yeast are missing. This leads to the question: What are these additional factors that limit mtDNA copy number?

Several nuclear or mitochondrial-encoded genes are reported to be essential for mtDNA (see chapter 1.3.3.3.). Here, it was decided to focus on seven nuclear-encoded genes, which showed slight limiting effects on mtDNA in hemizygous deletion strains before (Seel *et al.*, 2023): *HMI1*, *MGM101*, *MHR1*, *MTF1*, *PIF1*, *RIM1* and *RPO41*. It has to be noted that deleting one gene copy of the gene of interest was assumed to lead to the reduction of its protein concentration to 50%. As no feedback regulations are known in yeast so far, it was taken for granted first and checked for the final candidate(s) later (see Figure 15 and chapter 3.8.1).

In theory, if all nuclear-encoded mtDNA-limiting protein amounts are reduced to 50%, it is expected to lead to a 50% reduction of mtDNA copy number. To test this, various hemizygous deletions based on either only the gene of interest, a double deletion of the gene of interest in combination with *mip1Δ* or with *abf2Δ* or a triple deletion of the gene of interest, *mip1Δ* and *abf2Δ*, were created and their mtDNA concentration was measured in SCGE and SCD media (Figure 15).

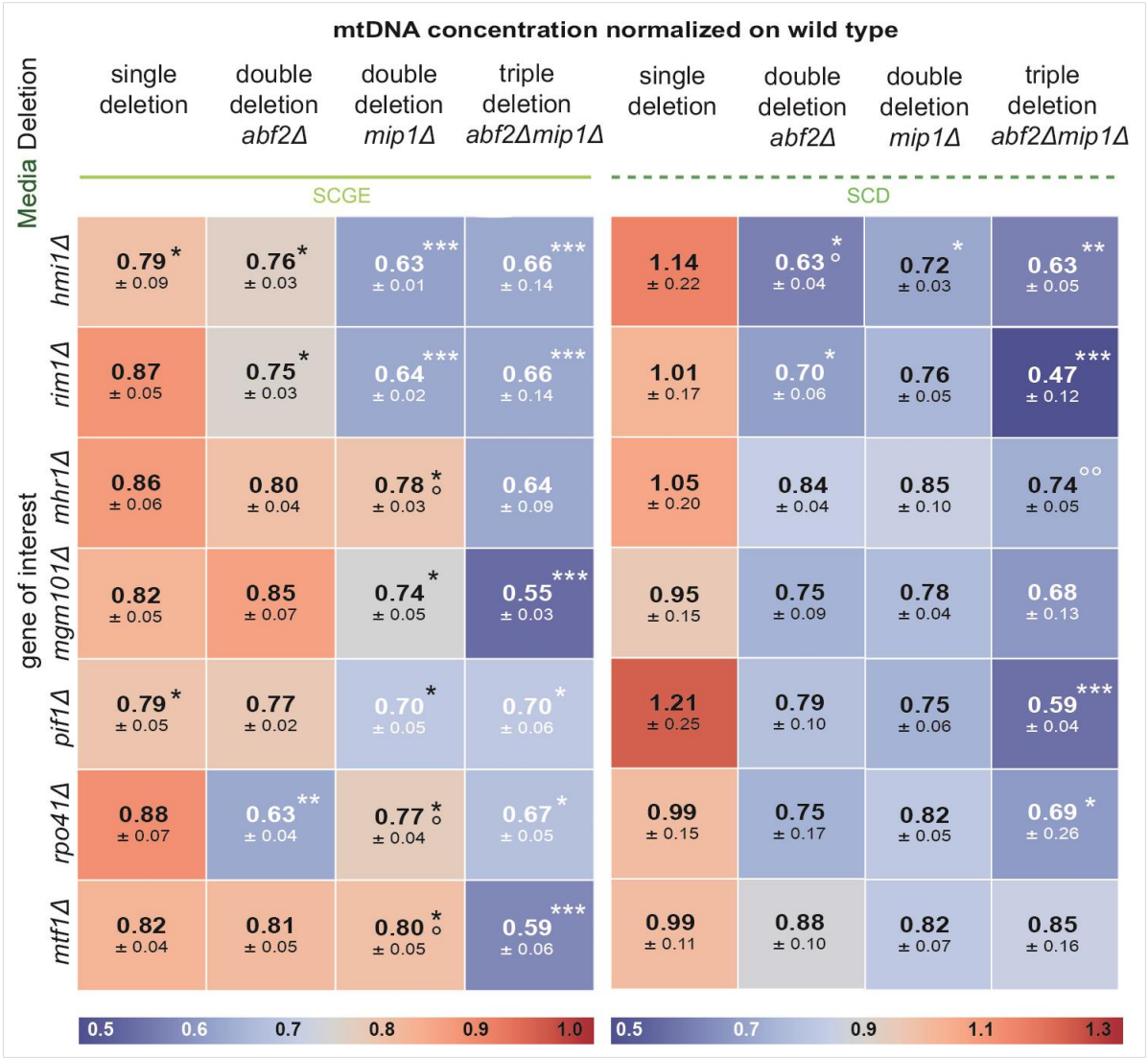

Figure 15: Heatmap of mtDNA concentration normalized on wild type for hemizygous deletion strains in SCGE and SCD. Two heatmaps showing the mean of mtDNA concentration normalized on the diploid wild type and the standard deviation for at least three replicates per strain. The color of the tiles ranges from dark blue (lowest value) to dark red (highest value). The two heatmaps represent the results for the strains cultured in non-fermentable SCGE media (left; continuous line) and in fermentable SCD media (right; dashed line). The four columns of each heatmap represent the type of hemizygous deletion: a hemizygous deletion of a single gene, the hemizgyous double deletion of a gene in combination with *abf2Δ*, the hemizgyous double deletion of a gene in combination with *mip1Δ*, the gene in a hemizygous triple deletion in combination with *abf2Δ* and *mip1Δ* (from left to right). The rows of the heatmap represent the gene of interest included in the respective hemizygous deletion. Statistical significances were calculated using a two-tailed two-handed t-test and if no symbol is given, no significant effect was obtained. Statistical significances compared to wild type are indicated as * for $p < 0.05$, ** for $p < 0.01$ and *** for $p < 0.005$ and statistical significances compared to the background deletion strain are indicated as ° for $p < 0.05$, °° for $p < 0.01$ and °°° for $p < 0.005$.

When culturing the yeast in SCGE media, the single deletions all showed a reduction of mtDNA concentration of around 10 to 20 %. None of the double deletions with *mip1Δ* or a*bf2Δ* led to a significantly lower mtDNA concentration than the hemizygous double deletion of *mip1Δ* and *abf2Δ* itself (mtDNA concentration normalized on WT was 0.66 with a standard deviation of 0.15). The hemizygous double deletions of *mhr1Δ* and *rpo41Δ* in combination with

mip1Δ even ended up in significantly higher mtDNA concentrations than the hemizygous single deletion of *mip1Δ* in SCGE. The triple deletions did nearly all show a significantly lower value than the wild type, but none of the hemizygous deletions measured in SCGE lowered the mtDNA significantly compared to the double deletion of *mip1Δ* and *abf2Δ*. As the hemizygous triple deletion of *mip1Δ*, *abf2Δ* and *mgm101Δ* showed the lowest mtDNA concentration with a reduction to 55% normalized on wild type in SCGE, *MGM101* was selected as a potential candidate as the third factor limiting mtDNA.

For the results measured in SCD media, the hemizygous single deletions showed no significant difference to wild type. Additionally, none of the hemizygous deletions lowered the mtDNA concentration below that of their background strain. By contrast, the hemizygous triple deletion of *mip1Δ*, *abf2Δ* and *mhr1Δ* even showed a significantly higher value. In SCD, the strongest reduction of mtDNA concentration was measured in the hemizygous triple deletion of *mip1Δ*, *abf2Δ* and *rim1Δ*, and therefore *RIM1* was selected as an additional potential third limiting factor. In addition, *HMI1* was also chosen for further analysis because its deletions resulted in the lowest normalized mtDNA concentration in half of all tested deletion categories. The list of potential candidates has therefore been narrowed to the three genes *HMI1*, *MGM101* and *RIM1*.

In theory, if the amount of a mtDNA-limiting factor is decreased, it is expected to result in decreased mtDNA copy number. Additionally, if the amount is increased, the mtDNA copy number should also increase. As no single factor limits mtDNA copy number but rather a machinery of multiple factors, the copy number of mtDNA is expected to be regulated according to the amount of these factors. If all proteins of the genes limiting mtDNA would be increased to two-fold in concentration, one would expect a corresponding increase of the mtDNA concentration to two-fold. To investigate the effect of upregulating the potential third factors, haploid strains with additional copies of defined genes were created. *HMI1* and *RIM1* were added to the haploid wild type and a strain with two copies of *MIP1* or *ABF2*. Additionally, triple addition strains of *HMI1*, *RIM1* or *MGM101* in combination with *MIP1* and *ABF2* were created and analyzed. While adding *HMI1* to the given strains did not lead to a significant increase in mtDNA concentration, the *RIM1*-addition to the wild type showed a slight increase in all media. As Figure 16 shows, adding *HMI1* or *MGM101* to the strain carrying extra copies of *MIP1* and *ABF2*, did not add a noteworthy effect on the mtDNA concentration. When cultured in SCD, it even resulted in reduced mtDNA concentrations compared to the double addition of *MIP1* and *ABF2*. While the triple addition strain of *MIP1*, *ABF2* and *RIM1* increased the mtDNA concentration to nearly two-fold independently of the media. Taken together, it can be concluded that the third factor of the nuclear-encoded machinery influencing the mtDNA besides *MIP1* and *ABF2* is *RIM1.*

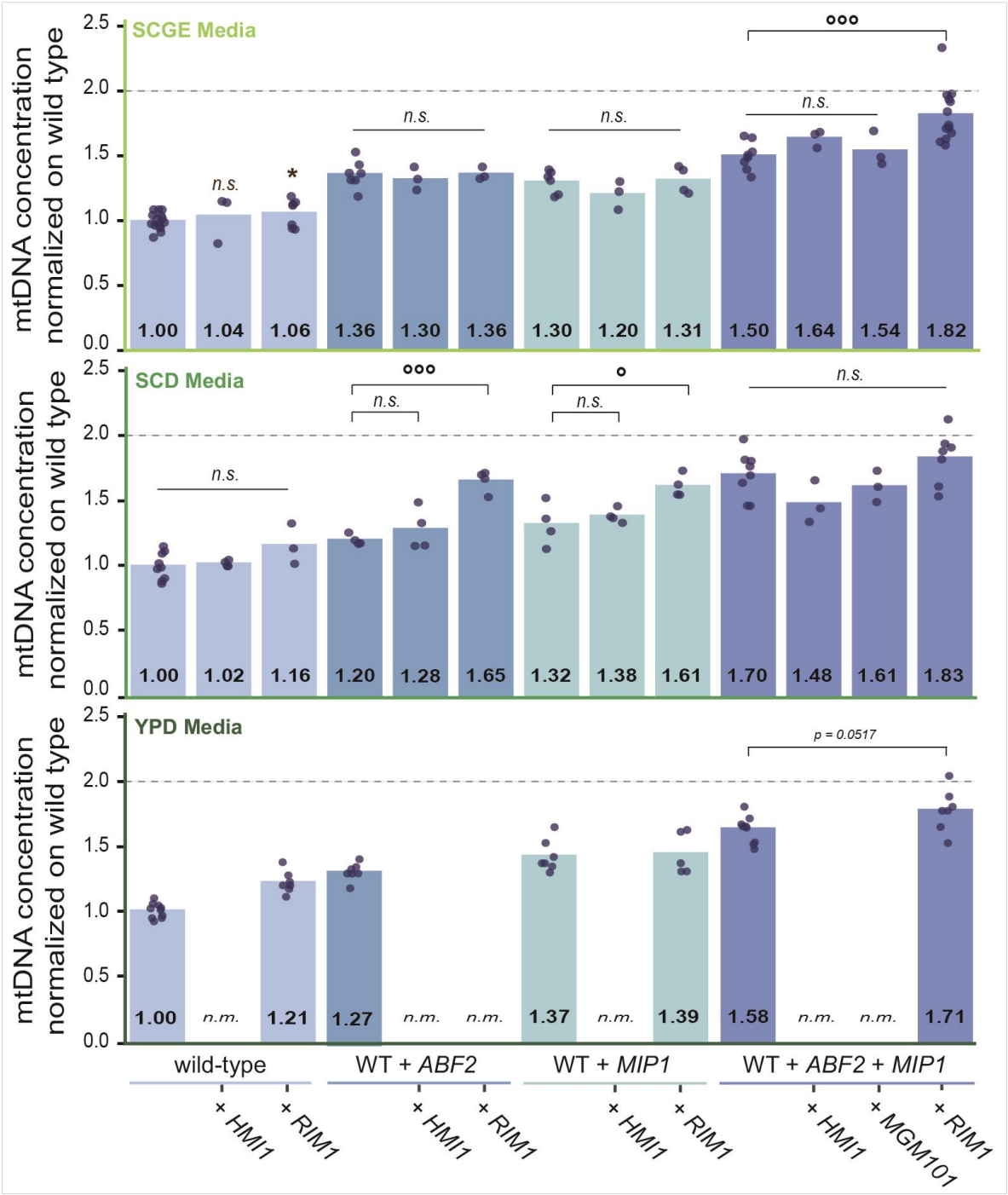

Figure 16: Mitochondrial DNA concentration normalized on wild type for haploid additional copy strains grown in SCGE, SCD and YPD. mtDNA concentrations normalized on haploid wild type for each strain, in three culture media: non-fermentable SCGE media (top; light green), fermentable SCD media (middle; green) and fermentable YPD media (bottom; dark green). Haploid background strains were either the wild type, the wild type including one additional copy of *ABF2*, the wild type including one additional copy of *MIP1*, or the wild type including one additional copy of both *ABF2* and *MIP1*. One extra gene copy of either *HMI1*, *RIM1* or *MGM101* was added to the background strains. The indicated mean values are calculated based on at least three replicates. Strains that were not measured are marked as "n.m.". Statistical significances were calculated using a two-tailed two-handed t-tests and if no symbol is given, no significant effect was obtained. Statistical significances compared to wild type are indicated as * for $p < 0.05$, ** for $p < 0.01$ and *** for $p < 0.005$ and statistical significances compared to the background deletion strain are indicated as ° for $p < 0.05$, °° for $p < 0.01$ and °°° for $p < 0.005$.

Next, it was investigated whether the two remaining potential factors *HMI1* and *MGM101* have an additional effect on the mtDNA copy number together with *ABF2*, *MIP1* and *RIM1* (Figure 17). For testing *HMI1* as an element of the limiting machinery, a diploid hemizygous quadruple deletion of *mip1Δ*, *abf2Δ*, *rim1Δ* and *hmi1Δ* was analyzed, as well as a haploid strain including two copies of these four genes. The result did not indicate any further limiting effect of *HMI1* on the mtDNA. Adding *MGM101* as the fourth factor to the triple addition strain of *MIP1*, *ABF2* and *RIM1*, did not show higher mtDNA concentrations in both media. Taken together, the data do not support these two genes to be a fourth factor of the mtDNA-limiting machinery.

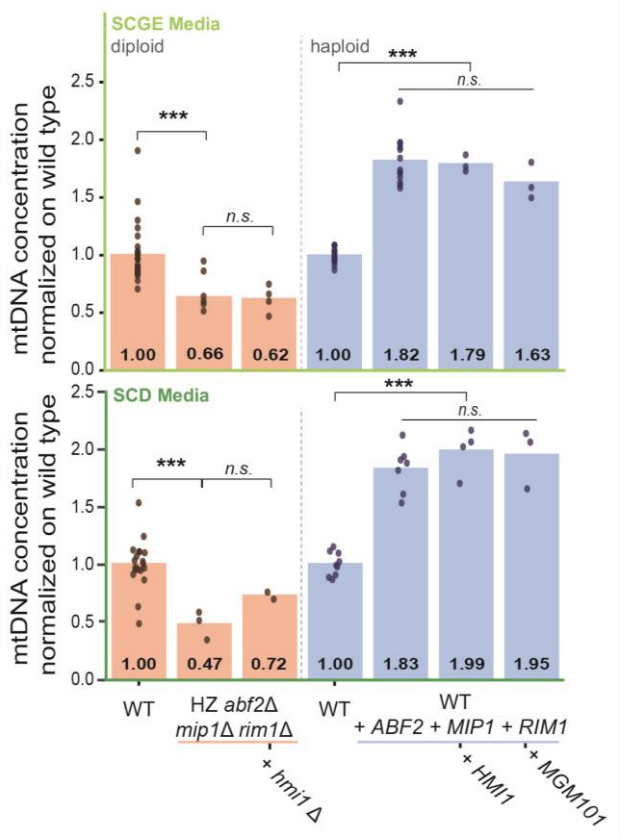

Figure 17: Mitochondrial DNA concentration normalized on wild type for testing potential fourth limiting factors grown in SCGE and SCD. Mitochondrial DNA concentration normalized on the corresponding wild type for two growth media: non-fermentable SCGE media (top; light green) or fermentable media (bottom; green). Diploid strains include wild type, hemizygous deletion of *abf2Δ, mip1Δ* and *rim1Δ* and hemizygous quadruple deletion of *abf2Δ, mip1Δ, rim1Δ* and *hmi1Δ* (left; orange), Haploid strains include wild type, triple addition strain with one additional copy of *ABF2, MIP1* and *RIM1*, quadruple addition strain with one additional copy of *ABF2, MIP1, RIM1* and *HMI1* or *MGM101* (right; blue). The indicated mean values are calculated based on at least three replicates. Statistical significances were calculated using a two-tailed two-handed t-tests and if no symbol is given, no significant effect was obtained. Statistical significances compared to wild type are indicated as * for $p < 0.05$, ** for $p < 0.01$ and *** for $p < 0.005$.

In summary, the measured values of mtDNA concentrations matched the model very well when considering *MIP1*, *ABF2* and *RIM1* to be the nuclear-encoded limiting machinery: For a hemizygous deletion the expected concentration would be decreased to 50% and indeed the strain showed a reduction to 66 ± 14 % and 47 ± 12% (SCGE or SCD media), respectively. Based on the model, the addition of all three genes is expected to increase mtDNA to 200% and the actual measurement demonstrated approximately 182, 171 and 183% (SCGE, YPD or SCD media) in the respective media. To ensure that the *RIM1* transcript concentrations are

indeed in- or decreasing according to their genotype in the mentioned strains, the RNA levels of *RIM1* were studied using RT-qPCR (Figure 18): The RIM1 RNA-levels are decreased to approximately 50% in the diploid hemizygous deletions and increased to around 200% in the haploid strains, where *RIM1* was added. Additionally, the results of the RNA-Seq analysis, as well as the proteomics shown in chapter 3.8.1., support the documented results on RNA- and Protein-level. This supports the finding that *RIM1* is the third mtDNA-limiting factor, as it fulfills both set criteria: the protein synthesis is regulated according to the genotype and the mtDNA concentration decreases to approximately 50% in a diploid hemizygous deletion of *abf2Δ*, *mip1Δ* and *rim1Δ*.

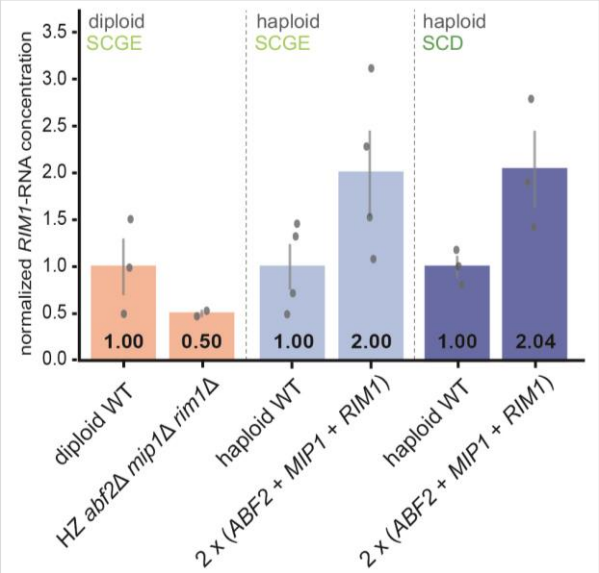

Figure 18: *RIM1*-RNA concentration in hemizygous deletion and triple addition strain in SCGE and SCD. RNA-concentration analyzed by qPCR and calculating *RIM1* normalized on *RDN18*. Diploid strains include wild type and hemizygous triple deletion of *abf2Δ, mip1Δ* and *rim1Δ* (left; orange), Haploid strains include wild type and triple addition strain with one additional copy of *ABF2, MIP1* and *RIM1* (middle and right; blue). The haploid strains were measured in non-fermentable SCGE media (middle; light blue) and fermentable SCD media (right; dark blue). The indicated mean values are calculated based on at least three replicates.

3.2.2. *MIP1*, *ABF2* and *RIM1* are limiting mtDNA maintenance independently and to varying degrees

To better understand the dependency of mtDNA on the concentration of the individual factors, strains with hormone-inducible promoters for *MIP1* and *ABF2* were created. The genes are driven by a β-estradiol-promoter, leading to increased expression of the gene with increasing hormone concentration. As shown in Figure 19a and b, the mtDNA concentration increases with rising RNA concentrations of *MIP1* or *ABF2*. Overexpression of *MIP1* results in a higher upper limit of mtDNA concentration of around two-fold compared to overexpression of *ABF2*, which leads to a maximum increase of approximately 20% compared to wild type. In line with previous studies (Zelenaya-Troitskaya *et al.*, 1998), it was only possible to overexpress *ABF2* around 10-fold, without causing changes in phenotype. A higher overexpression resulted in increased cell volumes, reduced nDNA copy numbers per cell and reduced mtDNA concentrations. On the other hand, *MIP1* can be overexpressed up to 40-fold without detrimental effects. It has to be mentioned that the leakiness of the hormone-promoter leads to the expression of the genes even if no β-estradiol is supplemented, resulting in RNA concentrations below wild type.

As constructing the hormone-inducible *RIM1*-strain was not successful, an alternative way to investigate the effect of increasing *RIM1* RNA-concentrations was performed: a series of strains with multiple *RIM1* copies were created and measured. Also, a multicopy-strain series for *HMI1* was created and analyzed to compare the effect. Overexpression of *RIM1* up to 10-fold increases mtDNA concentration up to around 50% compared to wild type in SCGE (Figure 19c). By contrast, Hmi1 overexpression led to a constant mtDNA concentration in both media (Figure 19c and d).

Besides further supporting that the three genes *MIP1*, *ABF2* and *RIM1* limit mtDNA copy number, this also indicates that this effect is to varying degrees. The individual overexpression of one of the three factors increases mtDNA concentrations, which reach individual upper limits. These limits might be explained by the other factors, which become fully limiting.

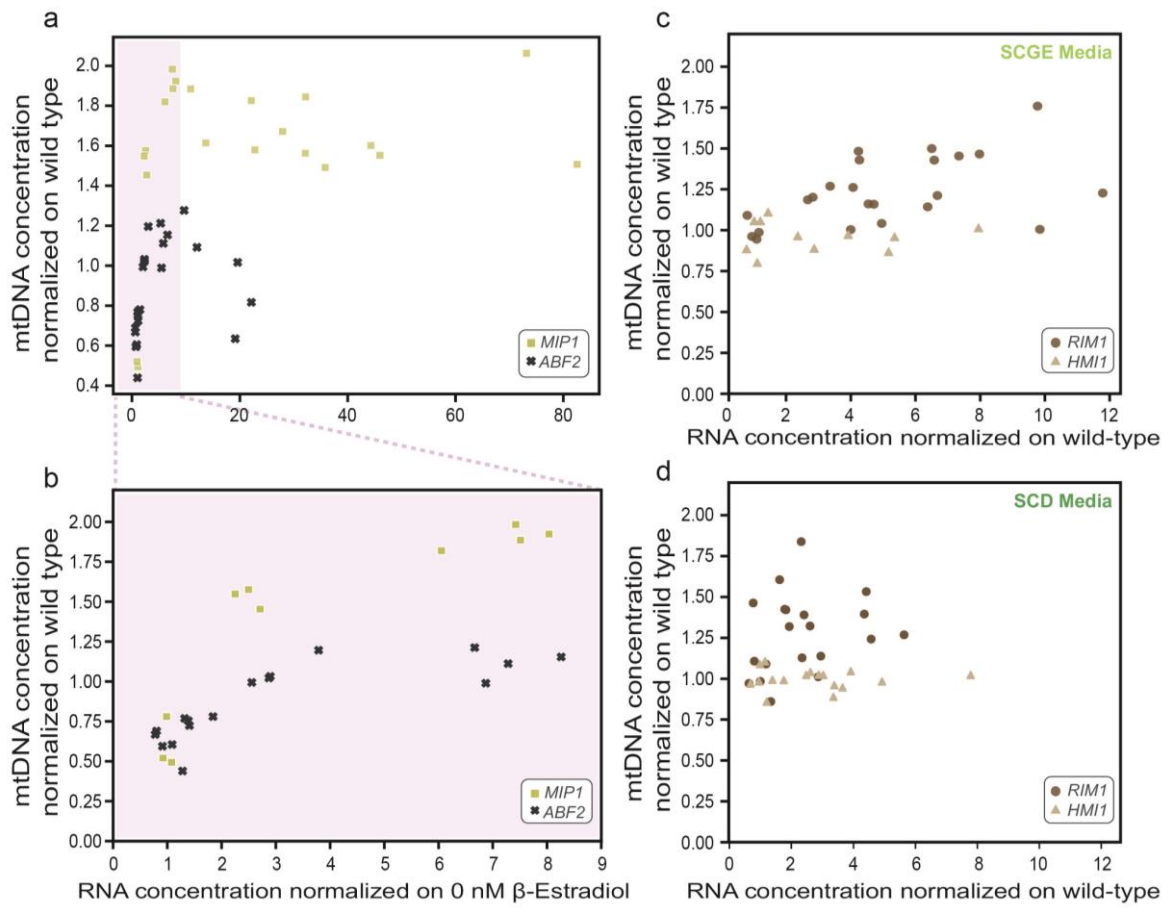

Figure 19: Mitochondrial DNA concentration normalized on wild type with increasing RNA concentrations of hormone-inducible *ABF2*- and *MIP1*-strains as well as multicopy strains of *RIM1* and *HMI1*. mtDNA concentration and RNA concentration normalized on non-induced measurement. **a)** Quantification of all measured concentrations of hormone-inducible *MIP1* (yellow square)- and *ABF2 (black cross)*-strain for two replicates in non-fermentable SCGE media. **b)** detailed view of hormone-inducible *MIP1* (yellow square)- and *ABF2* (black cross)-strain for two replicates in non-fermentable SCGE for RNA-concentrations between 0 and 9. **c)** multi-copy strains of *RIM1* (brown dots) and *HMI1* (beige triangle) for at least three replicates in non-fermentable SCGE media. **d)** multi-copy-strains of *RIM1* (brown dots) and *HMI1* (beige triangle) for at least three replicates in fermentable SCD media.

3.2.3. Stronger overexpression of the total limiting machinery results in even higher mtDNA concentrations

The next obvious question was: Is it possible to increase mtDNA concentrations higher than by overexpressing one single of the three factors? To study this, a strain with three copies of *MIP1*, *ABF2* and *RIM1* was created and measured. As shown in Figure 20, this strain increases the mtDNA concentration even higher than the two-fold *MIP1*, *ABF2* and *RIM1* strain, to a normalized concentration of around 225% compared to wild type. This proves the possibility for even higher mtDNA concentrations than the individual limits of the three factors. When considering the normalized mtDNA concentration as a function of the gene copy number of the limiting machinery (*ABF2*, *MIP1*, *RIM1*), a non-proportional increase is visible (Figure 20). This indicates that the mtDNA copy number might already be close to saturation with three copies of the limiting machinery.

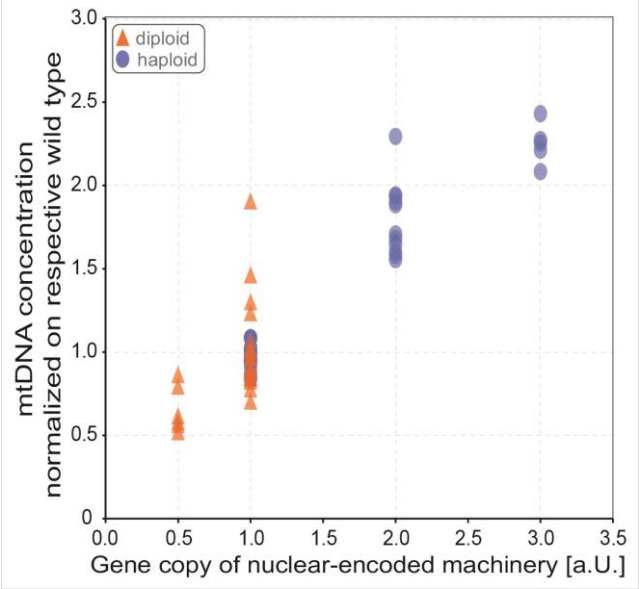

Figure 20: Mitochondrial DNA concentration normalized on wild type as a function of the gene copy number of the nuclear-encoded mtDNA-limiting machinery in SCGE. Diploid strains include diploid wild type and hemizygous triple deletion of *mip1Δ, abf2Δ* and *rim1Δ* (orange triangle) and haploid strains include haploid wild type, a strain including one extra copy of *ABF2, MIP1* and *RIM1* and a strain including two additional copies of *MIP1, ABF2* and *RIM1* (blue dots). Each single datapoint represents one replicate.

3.3. First evidence hints towards no cell volume-dependent regulation of mtDNA copy number in the absence of its limiting machinery-dependency

As shown so far, the nuclear-encoded machinery limits mtDNA and thereby drives its cell volume-dependency. However, there is no information on whether the cell volume can influence the mtDNA copy number independently of the nuclear-encoded machinery. Thus, the aim of the next experiments was to uncouple the amount of the three factors from cell volume and measure the mtDNA copy number with increasing cell volumes. The strategy is based on the following finding: the cell volume-dependency of proteins can be influenced by the promoter driving the expression of a gene (Claude *et al.*, 2021). The fluorescent protein mCitrine shows constant mRNA-concentrations with increasing cell volumes when using an *ACT1*-promoter. As Claude et al. revealed, this cell volume-dependency largely disappears when using a histone promoter for mCitrine, leading to decreasing RNA concentrations with increasing cell volume. The idea now was to use a histone promoter for the three factors limiting mtDNA, to achieve constant amounts even with increasing cell volumes. Implementing this into a β-estradiol-inducible Whi5-strain additionally gives the opportunity to increase cell volumes. As Whi5 is a cell cycle-regulator that inhibits SBF-dependent transcription, cells with higher Whi5-concentrations will stay longer in G1-phase and therefore gain more cell volume before continuing their regular cell cycle again (Schmoller *et al.*, 2015). This would allow to increase cell volumes at constant Mip1, Abf2 and Rim1 amounts, and to evaluate the direct effect of cell volume on mtDNA copy number.

3.3.1. Constant amounts of *ABF2*-mRNA lead to reduced cell-volume dependency of mtDNA

To obtain a strain with constant amounts of the limiting machinery with increasing cell volumes, a first optimization to drive the three genes by a histone promoter was done individually, starting with *ABF2*. One way to quantify whether the gene stays constant in amounts or concentrations is by calculating the Volume-Dependence-Parameter (VDP) (Claude *et al.*, 2021). The VDP represents the slope of a linear regression to the logarithm of RNA-concentration as a function of the logarithm of cell volume (Claude *et al.*, 2021). If the VDP shows a value around 0, this means that the mRNA-concentration stays constant with cell volume changes. On the other hand, if the VDP is -1, the mRNA stays at constant amounts with increasing cell volumes. To conclude, the aim was to achieve a VDP of around -1 for the limiting factors expressed from histone promoters. The constant amounts of the factors are used to answer the question of whether the cell volume has a direct factor-independent influence on mtDNA copy number.

As visualized in Figure 21, replacing the endogenous promoter of *ABF2* by an *HTB1*- or *HTB2*-promoter did not lead to any difference in the VDPs compared to wild type. Next, the endogenous terminator of *ABF2* was replaced by the *ADH1*-terminator, which also resulted in a wild-type-like VDP.

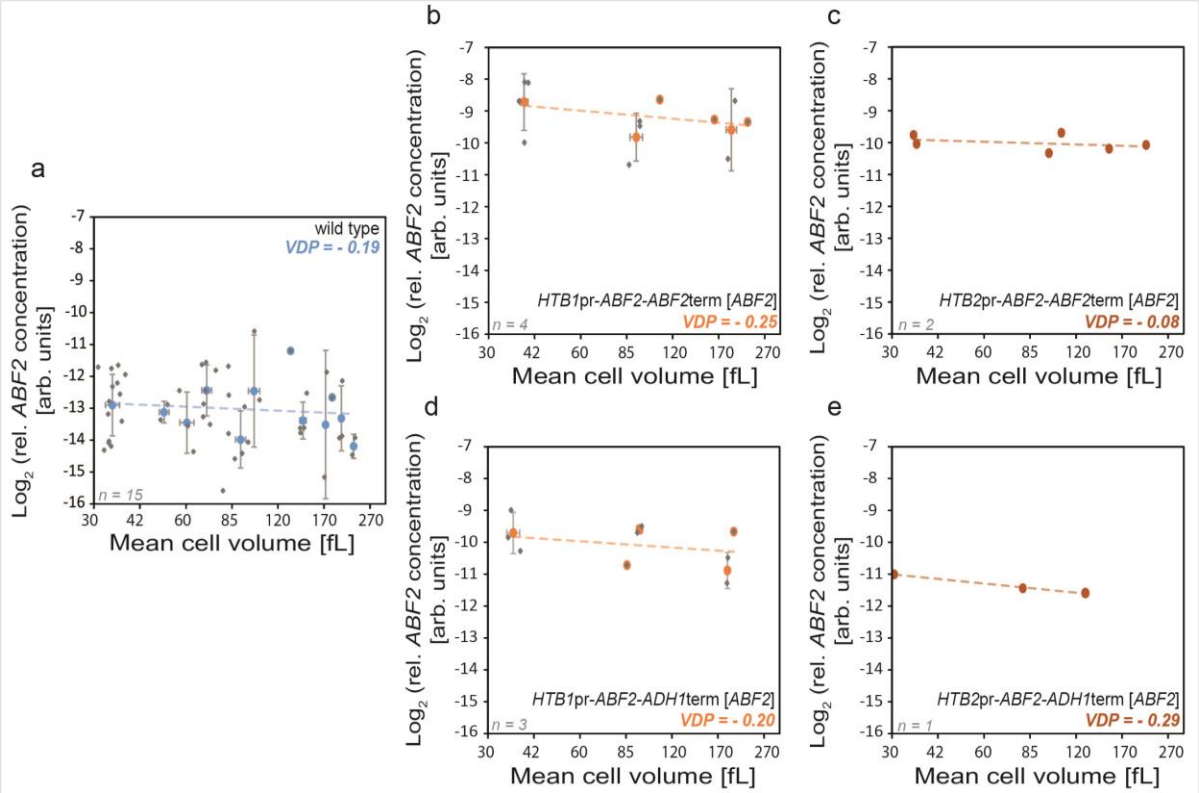

Figure 21: *ABF2* mRNA-concentration with increasing cell volumes – Replacement of endogenous promoter by promoter of *HTB1* or *HTB2* and of endogenous terminator through *ADH1*-terminator. Double logarithmic plots showing the relative *ABF2* mRNA-concentration (in arb. units) as a function of the mean cell volume (in fL). Inside the chart, the Volume-Dependence-Parameter VDP (slope; colored according to strain) as well as the number of replicates (left bottom; light grey) and strain name are displayed. Colored dots represent the mean values of replicates in the same cell volume range (10 fL) and grey dots represent the single replicates. Strains included in this figure: **a)** wild type (VDP = -0.19, n = 15, light blue), **b)** *HTB1*pr-*ABF2*-*ABF2*term in *ABF2*-locus (VDP = -0.25, n = 4, orange), **c)** *HTB2*pr-*ABF2*-*ABF2*term in *ABF2*-locus (VDP = -0.08, n = 2, red), **d)** *HTB1*pr-*ABF2*-*ADH1*term in *ABF2*-locus (VDP = -0.20, n = 3, orange), **e)** *HTB2*pr-*ABF2*-*ADH1*term in *ABF2*-locus (VDP = -0.29, n = 1, red).

As mentioned before, a previous study (Claude *et al.*, 2021) observed a negative VDP when using *HTB1*-promoter and *ADH1*-terminator for *mCITRINE.* What if the cell volume-independent behavior is specific to the open reading frame (ORF) of *mCITRINE* following the histone promoter? To check this, a short 2A-peptide-sequence of *porine eschovirus-1* (P2A) (Ryan *et al.*, 1991; Ryan and Drew, 1994), which has a high self-cleavage efficiency, was used. It allows to drive the expression of two individual proteins by a single promoter and terminator. The ribosome stops translation of the first protein right before the last amino acid of the P2A-Sequence and starts translation of the second protein starting with the last P2A-Aminoacid Proline (Ryan *et al.*, 1999; Donnelly *et al.*, 2001; Atkins *et al.*, 2007). Using this approach, the following sequence was created inside the *ABF2*-Locus: *HTB1*pr-*mCITRINE*-P2A-*ABF2*-*ABF2*term. While the mRNA-concentration of *mCitrine* seems to decrease with increasing cell volumes, unfortunately, the *ABF2* mRNA-concentration behaves similarly to wild type (see Figure 22). As all of the tested strains so far included gene manipulations directly at the endogenous *ABF2*-gene and earlier research (Claude *et al.*, 2021) focused on strains that mostly used the auxotrophic-marker region of *URA3*, the next strategy was to change the region. For this, the P2A and *ABF2*-Sequence were added into the *HTB1*pr-*mCITRINE*-*ADH1*term sequence in the *URA3*-Locus of strains from Claude et al. As shown in Figure 22,

the result indeed led to a VDP of close to -1 if measured across a cell volume range between 30 and 200 fL. Next, the endogenous *ABF2*-gene was deleted to eliminate its additional influence on *ABF2*-mRNA expression and the mtDNA copy number. Surprisingly, this resulted in an increase of the VDP to a value around –0.5 for both m*Citrine* and *ABF2*. Whether this is due to measurement errors or hints towards a potential feedback on transcriptional stability remains unclear.

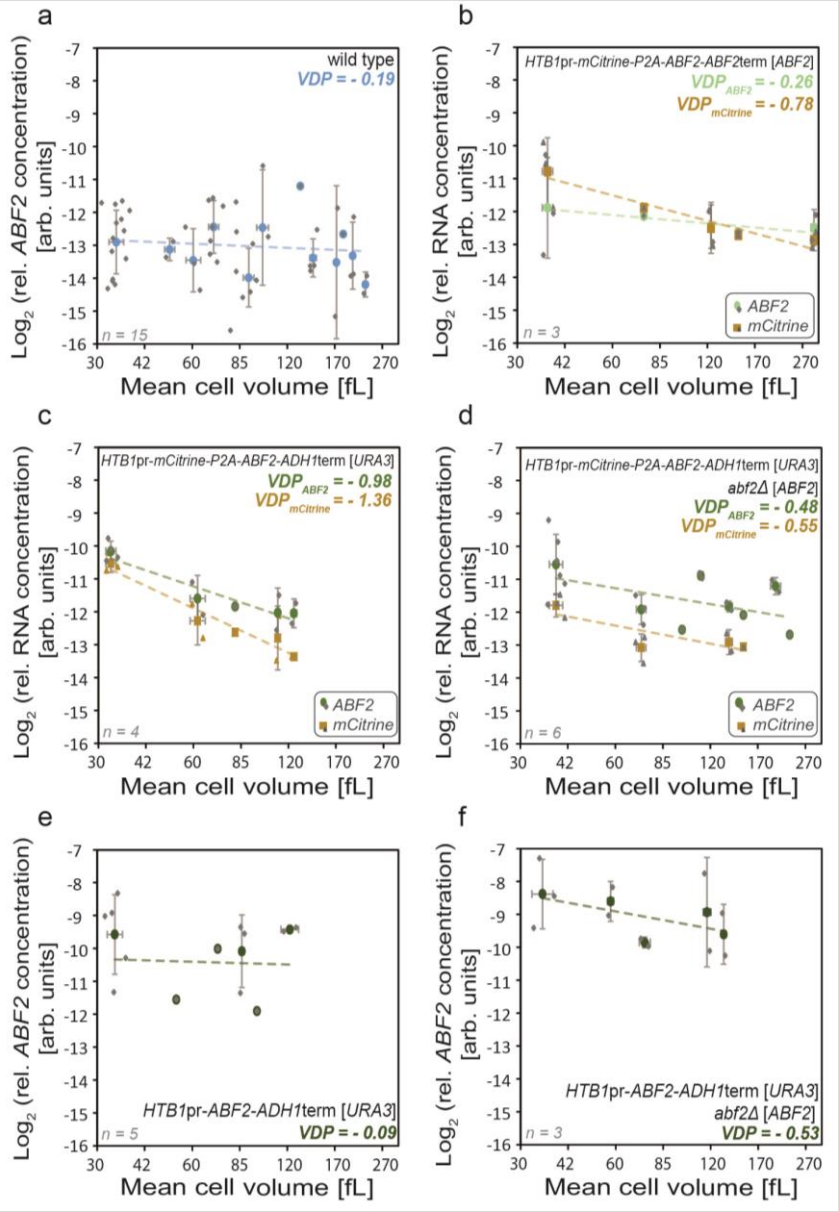

Figure 22: *ABF2* & *mCITRINE* mRNA-concentration with increasing cell volumes – P2A strategy in *ABF2* and *URA3* locus, revealing a locus dependency of the promoter effect. Double logarithmic plots showing the relative mRNA-concentration (in arb. units) as a function of the mean cell volume (in fL). Inside the chart, the Volume-Dependence-Parameter VDP (slope; colored according to strain) as well as the number of replicates (left bottom; light grey) and the strain name are displayed. Colored dots represent the mean value of single replicates in the same cell volume range (10 fL) and grey dots represent the single replicates. Charts **b,c** and **d** show two mRNA-concentrations as a function of cell volume: *ABF2* (green) and *mCITRINE* (yellow). Strains included in this figure: **a)** wild type (VDP = -0.19, n = 15, light blue), **b)** *HTB1*pr-*mCITRINE*-P2A-*ABF2-ABF2*term in *ABF2*-locus (VDP for *ABF2* = -0.26, VDP for mCITRINE = -0.78, n = 3), **c)** *HTB1*pr-*mCITRINE*-P2A-*ABF2-ADH1*term in *URA3*-locus (VDP for *ABF2* = -0.98, VDP for mCITRINE = -1.36, n = 4),

d) *HTB1*pr-*mCITRINE*-P2A-*ABF2*-*ADH1*term in *URA3*-locus and additional deletion of endogenous *abf2Δ* (VDP for *ABF2* = -0.48, VDP for mCITRINE = -0.55, n = 6), **e)** *HTB1*pr-*ABF2*-*ADH1*term in *URA3*-locus (VDP = -0.09, n = 5, green), **f)** .*HTB1*pr-*ABF2*-*ADH1*term in *URA3*-locus and additional deletion of endogenous *abf2Δ* (VDP = -0.53, n = 3, green).

Changing the locus led to a decreased VDP. As *mCITRINE* and the P2A-sequence are potentially unnecessary additional components, which could influence the mtDNA results, another strain was created without those. In this strain, the *HTB1*-promoter followed by the *ABF2*-gene and the *ADH1*-terminator were added into the *URA3*-locus. Again, to eliminate its effects, the endogenous *ABF2* was knocked out in a second step. This resulted in a similar VDP to the last described strain (see Figure 22), indicating that *mCITRINE* is not needed to achieve the cell-volume-independent effect. Besides, another surprising result can be observed when comparing the last two mentioned strains: The deletion of the endogenous *ABF2*-gene leads to an unexpected increase in its mRNA-concentration. In combination with the previously documented surprising changes in VDP when deleting the endogenous *ABF2*-gene in the *HTB1*pr-*mCITRINE*-P2A-*ABF2*-*ABF2*term strain, this could indeed hint towards a feedback mechanism influencing the transcriptional stability of *ABF2*.

The two most interesting strains regarding the initial aim were the *HTB1*pr-*mCITRINE*-P2A-*ABF2*-*ABF2*term strain and the *HTB1pr-ABF2-ADH1*term strain inside *URA3* with a knockout of the endogenous *ABF2*-gene. Looking into the detailed cell volume-dependence of the *ABF2* mRNA-concentration for the successful strains compared to wild type, the *ABF2*-mRNA-concentration decreases drastically, especially in the beginning, and stays more or less constant for higher cell volumes (Figure 22). To set the focus of the study on physiological cell volume ranges, the VDPs were recalculated for cell volumes up to only 115 fL. As shown in Figure 23, only the four strains, which drive *ABF2* by the histone-promoter in the *URA3*-locus result in VDPs lower than -0.6. This confirmed the strategy to set a focus on these strains.

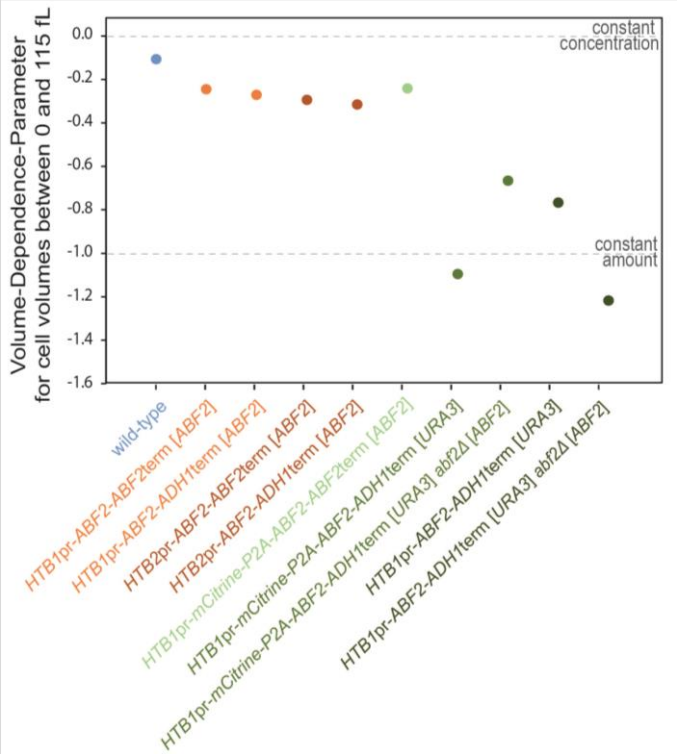

Figure 23: Volume-Dependence-Parameter of strains with different histone-promoters and different terminators in different locations for small cell volumes until 115 fL. VDP was calculated based on the slope in a double logarithmic plot of mRNA-concentration of *ABF2* as a function of cell volumes between 0 and 115 fL. VDP close to 0 indicates a constant concentration with increasing cell volumes and a VDP close to -1 indicates a constant amount with increasing cell volumes. Genomic manipulation of the strain is indicated by the color: wild type (VDP = -0.11; light blue), *HTB1*pr-*ABF2*-*ABF2*term in *ABF2*-locus (VDP = -0.25, orange), *HTB1*pr-*ABF2*-*ADH1*term in *ABF2*-locus (VDP = -0.28, orange), *HTB2*pr-*ABF2*-*ABF2*term in *ABF2*-locus (VDP = -0.3, red), *HTB2*pr-*ABF2*-*ADH1*term in *ABF2*-locus (VDP = -0.32, red), *HTB1*pr-*mCITRINE*-P2A-*ABF2*-*ABF2*term in *ABF2*-locus (VDP = -0.25, light green), *HTB1*pr-*mCITRINE*-P2A-*ABF2*-*ADH1*term in *URA3*-locus (VDP = -1.1, green), *HTB1*pr-*mCITRINE*-P2A-*ABF2*-*ADH1*term in *URA3*-locus and additional deletion of endogenous *abf2Δ* (VDP -0.67, green), *HTB1*pr-*ABF2*-*ADH1*term in *URA3*-locus (VDP = -0.77, dark green), *HTB1*pr-*ABF2*-*ADH1*term in *URA3*-locus and additional deletion of endogenous *abf2Δ* (VDP = -1.22, dark green).

The next challenge was set when comparing the mRNA-concentrations of the two most promising strains with wild type at small cell volumes. The *ABF2*-mRNA-concentration at small cell volumes is higher than the wild type for the *HTB1*pr-*mCITRINE*-P2A-*ABF2*-*ABF2*term strain and the *HTB1pr-ABF2-ADH1*term strain. As demonstrated in previous experiments of this study (see chapter 3.2.2.), the three limiting factors of mtDNA influence mtDNA concentration individually. Especially *ABF2* has been shown to reach a saturation state of mtDNA concentration already upon moderate overexpression. This highlights the importance of achieving wild-type-like mRNA-concentrations for the histone-promoter strain. Yamanishi et al. described the effect of different terminators on the expression levels of fluorescent proteins. Using their results (Yamanishi *et al.*, 2013), the terminators of the four genes *MBF1*, *ALR2*, *KKQ8* and *SUT1* were chosen due to their lower mRNA-concentrations and used to replace the *ADH1*-terminator used so far.

As shown in Figure 24, all of the tested terminators resulted in a lower starting concentration of *ABF2*-mRNA compared to the strain using an *ADH1*-terminator, with *MBF1*- and *SUT1*-terminator showing the lowest starting mRNA-concentration of *ABF2*. After identifying the *SUT1*-terminator to show the lowest mRNA-concentration, again the endogenous *ABF2*-gene was knocked out in this strain to eliminate its effects on mtDNA copy number. As expected the deletion of ABF2 leads to a slight decrease in the mRNA starting-concentration. More importantly, this strain shows slightly higher mRNA-concentrations at small cell volumes compared to wild type, which decrease to wild-type level, with a VDP of -0.33 when inducing cell volumes up to 200 fL.

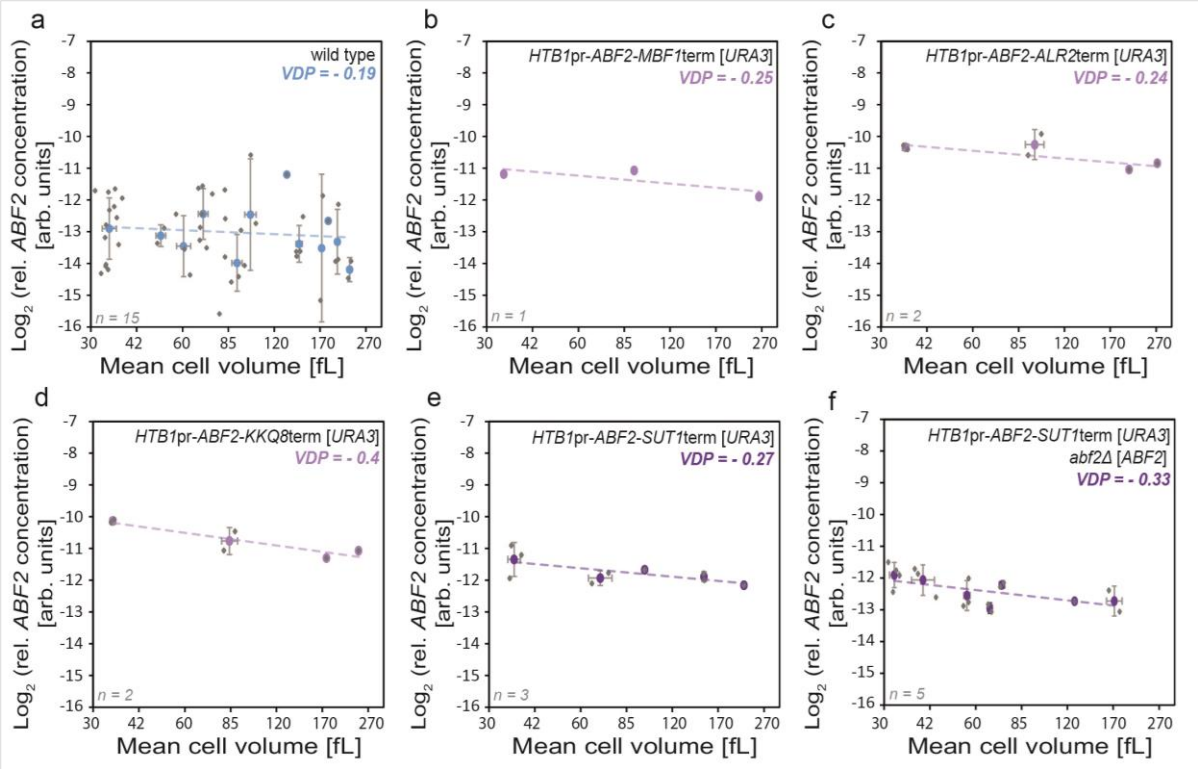

Figure 24: *ABF2* mRNA-concentration with increasing cell volumes – Exchange of terminator sequence to aim for lower mRNA-concentrations close to wild type. Double logarithmic plots show the relative mRNA-concentration (in arb. units) as a function of the mean cell volume (in fL). Inside the chart, the Volume-Dependence-Parameter VDP (slope; colored according to strain) as well as number of replicates (left bottom; light grey) and strain name are displayed. Colored dots represent the mean value of single replicates in the same cell volume range (10 fL) and grey dots represent the single replicates. Strains included in this figure: **a)** wild type (VDP = -0.19, n = 15, light blue), **b)** *HTB1*pr-*ABF2-MBF1*term in *URA3*-locus (VDP = -0.25, light purple), **c)** *HTB1*pr-*ABF2-ALR2*term in *URA3*-locus (VDP = -0.24, light purple), **d)** *HTB1*pr-*ABF2-KKQ8*term in *URA3*-locus (VDP = -0.4, light purple), **e)** *HTB1*pr-*ABF2-SUT1*term in *URA3*-locus (VDP = -0.27, dark purple), **f)** *HTB1*pr-*ABF2-SUT1*term in *URA3*-locus and additional deletion of endogenous *abf2Δ* (VDP = -0.33, dark purple).

For detailed analysis of the optimized strain (*HTB1*pr-*ABF2-SUT1*term in *URA3*-locus + *abf2Δ*), additional experiments resulting in mean cell volumes between 28 and 115 fL were performed. As shown in Figure 25a, the *ABF2*-mRNA-concentration decreases drastically first and then matches the wild-type level. The wild type stays constant as expected with a VDP of 0.07. As the strain was optimized now, the next step was to investigate the behavior of mtDNA. In theory, if all limiting factors stay constant in their amount as cell volume increases and cell volume does not additionally influence the mtDNA copy number, it is expected that the mtDNA amount also stays constant. So far in this strain, only *ABF2* has a roughly constant amount, especially in small cell volumes, which is why it's not possible to draw a final conclusion about the additional influence of cell volume on the mtDNA copy number independently of the limiting machinery. However, a first indication can be obtained when estimating the expected change and comparing it to the experimental results.

The expected change of mtDNA concentration is calculated using three parameters: the VDP of the constructed strain (here: -0.4), the scale of the cell volume change (difference of $\log_2$ cell volumes; here: 1.5) and the effect on mtDNA copy number of an *abf2Δ* single hemizygous deletion strain (here: -31%). By multiplying the VDP and the scale of cell volume change, the

expected difference of ABF2-mRNA is calculated first (here: -0.6). Afterwards, by multiplying the result with the single hemizygous *abf2Δ*-effect, the expected change of mtDNA copy number within the scope of the given changes in *ABF2*-mRNA in the strain is estimated. For the analysed strain (*HTB1*pr-*ABF2*-*SUT1*term in *URA3*-locus including an additional deletion of endogenous *abf2Δ*), the expected change of mtDNA copy number is approximately -19%. The effect measured in the experiment (see Figure 25) was calculated as follows: First the ratio of the mtDNA concentration between the strain and the wild type was calculated individually for small cell volumes (25 – 35 fL; 0 nM β-estradiol) as well as for big cell volumes (65 – 115 fL; 12 nM β-estradiol). Afterwards, the ratio between those two resulting ratios was calculated to obtain the relative change of mtDNA copy number in the given cell volume range. According to this calculation, the measured effect of mtDNA copy number in the strain is approximately -9.4%. As the expected and the measured effect of a constant *ABF2*-amount are of a similar magnitude, this supports the model that the cell-volume-dependency is regulated through the limiting machinery (*ABF2*, *MIP1* and *RIM1*) and there is no evidence for an additional effect of cell volume independent of this machinery.

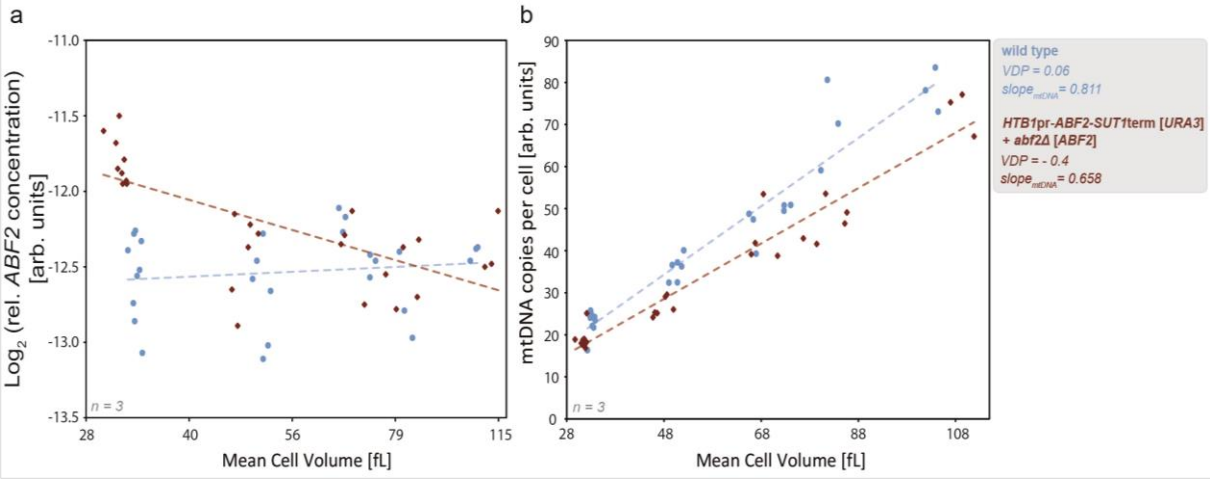

Figure 25: *ABF2* mRNA concentration and mtDNA copies per cell with increasing cell volumes for wild type and *ABF2*-optimized strain *HTB1pr-ABF2-SUT1term* [*URA3*] + *abf2Δ* [*ABF2*]. Included strains were measured in three biological replicates including three technical replicates for wild type (VDP = 0.06, mtDNA-slope = 0.811; light blue) and *HTB1*pr-*ABF2*-*SUT1*term in *URA3*-locus including an additional deletion of endogenous *abf2Δ* (VDP = -0.4, mtDNA-slope = 0.658; red). **a)** double logarithmic plot of ABF2 mRNA-concentration with increasing cell volume indicates the VDP (slope). **b)** mtDNA copies per cell with increasing cell volume, resulting in a slope indicating the dependency.

At this point, it is still unclear why the concentration of *ABF2*-mRNA in the *HTB1pr-ABF2-ADH1*term+*abf2Δ* strain decreases perfectly in cell volumes smaller than 60 fL but stays more or less constant for higher cell volumes. Moreover, the actual direct influence of cell volume on mtDNA has to be tested by adding constant amounts of *MIP1* and *RIM1* to the optimized *ABF2*-strain.

3.3.2. Constant amounts of *MIP1* can be achieved through histone-promoter strategy

The next aim was to construct a strain with constant amounts of *MIP1*-mRNA. As before, replacing the endogenous promoter in the *MIP1*-locus with an *HTB1*-promoter was the first strategy. As this resulted in a VDP of –0.3 for cell volume changes up to 365 fL and a VDP of –0.1 for smaller cell volume changes up to 120 fL (Figure 26b and f), the strategy was modified based on previous optimizations on *ABF2*. The next strain carried the *HTB1*-promoter, followed by the *MIP1*-gene and *ADH1*-terminator in the auxotrophic marker region of *TRP1* (Figure 26c). *MIP1* was knocked out in the next step to eliminate the effects of the endogenous gene. The strain resulted in a VDP between –0.8 and –1.2, depending on the cell volume range (Figure 26d), which shows a decrease in *MIP1*-mRNA concentration, which is consistent with a constant *MIP1* amount. Again, the histone-promoter leads to higher expressions of *MIP1* than in the wild type, which is why a *SUT1*-terminator was chosen as additional optimization to decrease the *MIP1*-mRNA concentration. This resulted in minor changes in the VDP, but unfortunately also in even higher mRNA-concentrations of *MIP1* than the *HTB1pr-MIP1-ADH1*term strain (Figure 26e).

In summary, further optimizations are needed to decrease the *MIP1*-mRNA-concentration of this strain close to that of wild-type levels. As *MIP1* is generally much less expressed than, for example *ABF2*, this could be challenging to achieve. Additional terminator changes or differences in 5’ or 3’-UTRs would be possible strategies for the future. Also, the use of a lower-expressing promoter that may lead to constant amounts is a conceivable strategy. An example of this could be the *HHO1*-promoter, which is reported to be lower-expressing than the promoter of *HTB1* (Claude *et al.*, 2021). As these elaborative optimizations exceeded the scope of this work, future studies have to continue at this point.

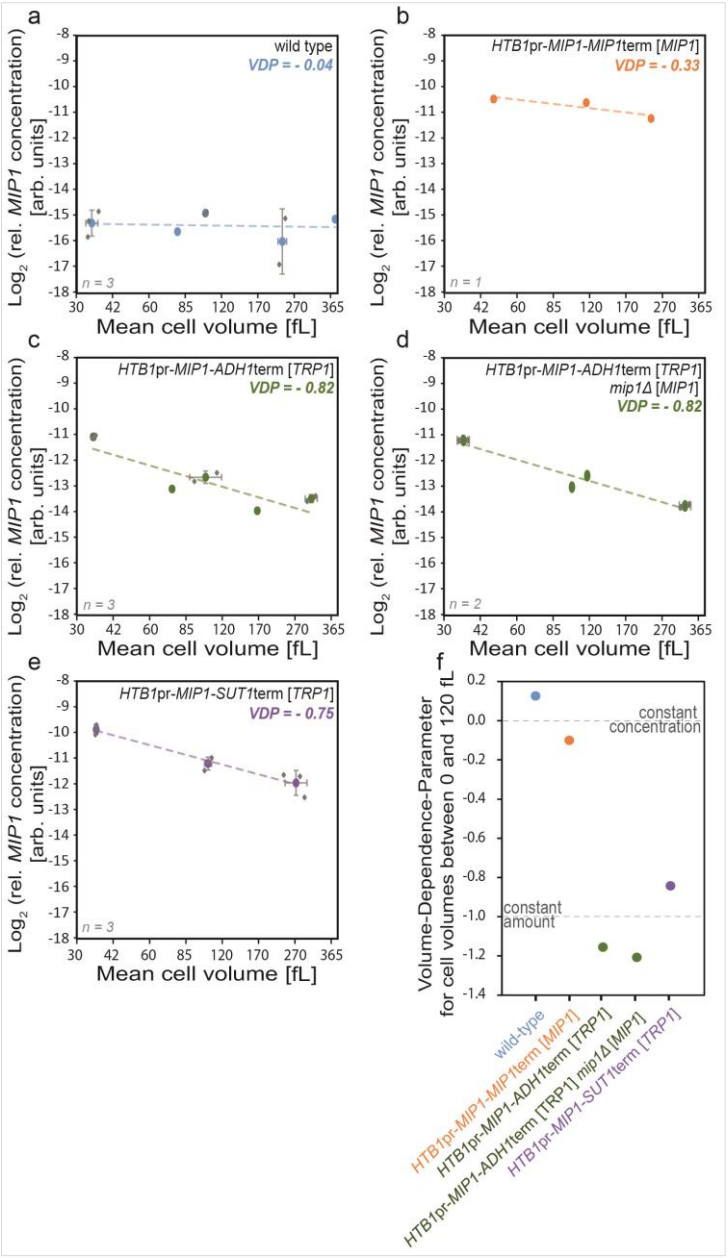

Figure 26: *MIP1* mRNA-concentration with increasing cell volumes – Exchange of promoter and terminator to aim for constant amounts with increasing cell volumes. a – e) Double logarithmic plots showing the relative *MIP1* mRNA-concentration (in arb. units) as a function of the mean cell volume (in fL). Inside the chart, the Volume-Dependence-Parameter VDP (slope; colored according to strain) as well as the number of replicates (left bottom; light grey) and strain name are displayed. Colored dots represent the mean value of single replicates in the same cell volume range (10 fL) and grey dots represent the single replicates. Strains included in this figure: **a)** wild type (VDP = -0.04; n = 3; light blue), **b)** *HTB1*pr-*MIP1*-*MIP1*term in *MIP1*-locus (VDP = -0.33; n = 1; orange), **c)** *HTB1*pr-*MIP1*-*ADH1*term in *TRP1*-locus (VDP = -0.82; n = 1; green), **d)** *HTB1*pr-*MIP1*-*ADH1*term in *TRP1*-locus and additional deletion of endogenous *mip1Δ* (VDP = -0.82; n = 2; green), **e)** *HTB1*pr-*MIP1*-*SUT1*term in *TRP1*-locus (VDP = -0.75; n = 3; purple). **f)** VDP calculated based on the slope in a double logarithmic plot of mRNA-concentration of *MIP1* as a function of cell volumes between 0 and 120 fL: wild type (VDP = 0.13; light blue), *HTB1*pr-*MIP1*-*MIP1*term in *MIP1*-locus (VDP = -0.1; orange), *HTB1*pr-*MIP1*-*ADH1*term in *TRP1*-locus (VDP = -1.16; green), *HTB1*pr-*MIP1*-*ADH1*term in *TRP1*-locus and additional deletion of endogenous *mip1Δ* (VDP = -1.21; green), *HTB1*pr-*MIP1*-*SUT1*term in *TRP1*-locus (VDP = -0.84; purple). A VDP close to 0 indicates a constant concentration with increasing cell volumes and a VDP close to -1 indicates a constant amount with increasing cell volumes.

3.3.3. Proposed strategy to achieve constant amounts of *RIM1*

The last limiting factor that remains to be genetically manipulated in the future, such that it stays constant in its amount in increasing cell volumes, is *RIM1*. Following the findings of the optimizations performed here for *ABF2* and *MIP1*, the initial strategy would be to use *HTB1*-promoter for *RIM1* in an auxotrophic marker locus. As the expression levels of *ABF2* and *RIM1* are comparable, using the *SUT1*-terminator could lead to suitable *RIM1*-mRNA-concentrations.

3.3.4. Constant amounts of the three factors limiting mtDNA need to be investigated further in the future

Last but not least, the optimized cell volume-independent alleles for all of the three factors limiting mtDNA need to be introduced into one single strain containing the β-estradiol-inducible *WHI5*-gene. Since this cell size-inducible strain has only two usable selectable marker regions (*URA3* and *TRP1*), *ABF2* and *RIM1* might need to be combined by using the P2A-Sequence as described before (see chapter 3.3.1.). This way, the two genes could be driven by the same promoter and terminator, to achieve constant amounts with increasing cell volume of *ABF2* and *RIM1* simultaneously. When analyzing the P2A strain described in chapter 3.3.1. in more detail, it can be seen that the first gene is expressed a bit lower than the second one. The order of ABF2 and RIM1 should be planned accordingly.

Taken together, to obtain a strain with cell volume-independent mtDNA-limiting factors (*ABF2*, *MIP1* and *RIM1*), whose cell size can be increased due to a β-estradiol-inducible *WHI5*-gene, would open up a lot of possibilities to study mtDNA copy number. The work presented here demonstrated that the use of a histone-promoter can be a successful strategy to achieve cell volume-independence for the genes, as shown in chapter 3.3.1. for *ABF2* and in chapter 3.3.2. for *MIP1*. Many adjustments of the genetic manipulation are necessary to ensure an appropriate VDP and mRNA-concentrations similar to wild type, as aimed for in this study. This work verifies that the target strain is possible in principle, but the extensive adaptations needed are beyond the scope of this thesis. However, the preparatory work of this project, which has been done so far, not only proved the concept but also gave rise to preliminary conclusions. As described in chapter 3.3.1., when analyzing a strain with almost constant amounts of *ABF2*-mRNA, the estimated and experimental behavior of mtDNA concentration with increasing cell volume agree closely. This suggests that in this strain, the cell volume-dependence of the mtDNA copy number is only influenced by the two remaining cell volume-dependent genes *MIP1* and *RIM1*, and no further influence of the cell volume itself was detectable. Future work will be needed to break the cell volume-dependence of all of the three factors, allowing conclusive experiments to test the influence of cell volume on mtDNA copy number independently of the limiting machinery.

3.4. Budding yeast is robust against variation in mtDNA concentration

Due to its involvement in various critical regulations, especially the ATP production through the ETC, mitochondria play an important role in the cell (Foury *et al.*, 1998; Hoffman *et al.*, 2003; Kohlhaw, 2003; Xu *et al.*, 2006; Braymer and Lill, 2017). Also, the mtDNA is a central part of this importance, as described in detail in chapter 1.3. It is associated with a variety of human diseases, but its homeostasis and precise contribution to those remain poorly understood. With the help of the model organism budding yeast, which can be genetically manipulated more easily than mammalian cell lines, important questions regarding mtDNA can be answered. As shown in this study, a model on how mtDNA is regulated in a cell volume-dependent manner was established: Increasing cell volume leads to increasing amounts of the nuclear-encoded limiting machinery (Abf2, Mip1 and Rim1) and subsequently leads to an increase of mtDNA copy number. To reach this conclusion, a large number of genetically manipulated strains were created and measured. Depending on the manipulations, these strains result in different mtDNA copy numbers, but mostly show wild-type-like cell volumes. These strains open up a wide range of possibilities to study mtDNA copy numbers, especially independently of cell volume. The second part of this thesis will therefore try to answer the question: Does the mtDNA concentration have an impact on the cell physiology of budding yeast? First, the cell volume and nDNA copy number will be analyzed. Next, the cell growth under normal and stress conditions, as well as the respiratory capacity, will be investigated.

To this end, 13 strains were selected for phenotyping. These strains are listed in Table 25 and include diploid strains with hemizygous deletions, as well as haploids with additional copies of specific genes. For simplicity, the strains have been assigned acronyms (Table 25), which will be used throughout the rest of this thesis. For instance, the strain “ASY059-4” is referred to as the “double addition” strain, based on the fact that this haploid strain carries an addition of the two genes *ABF2* and *MIP1*. This strain also has a supplementary name, “clone A, " since three individual “double addition” strains were created and measured (see chapter 3.7.4.). The triplicate of strains with the same genotype was performed for the double and triple addition strains. Unless otherwise indicated, the results presented in this chapter were obtained from cultivation in SCGE media. A comparison to cultivation in other media will be discussed later in chapter 3.6. The mtDNA concentrations of the thirteen selected strains measured in SCGE are summarized in Figure 27.

Table 25: Overview of strains included in phenotyping experiments.

Strains for phenotyping				
Strain name	Ploidy	Description	**Acronym**	clone
ASY020	diploid	Wild type	**WT diploid**	
ASY046-2	diploid	Hemizygous deletion *abf2 mip1*	**Double deletion**	
AFY003-1	diploid	Hemizygous deletion *abf2 mip1 rim1*	**Triple deletion**	
AFY025-1	diploid	Hemizygous deletion *abf2 mip1 rim1 hmi1*	**Quadruple deletion**	
MMY116-2c	haploid	Wild type	**WT haploid**	
ASY059-4	haploid	One additional copy *ABF2 MIP1*	**Double addition**	A
AFY098-1	haploid	One additional copy *ABF2 MIP1*	**Double addition**	B
AFY098-2	haploid	One additional copy *ABF2 MIP1*	**Double addition**	C
AFY057-1	haploid	One additional copy *ABF2 MIP1 RIM1*	**Triple addition**	A
AFY101-2	haploid	One additional copy *ABF2 MIP1 RIM1*	**Triple addition**	B
AFY102-1	haploid	One additional copy *ABF2 MIP1 RIM1*	**Triple addition**	C
AFY055-5	haploid	One additional copy *ABF2 MIP1 RIM1 HMI1*	**Quadruple addition**	
AFY074-1	haploid	Two additional copies *ABF2 MIP1 RIM1*	**Triple Triple addition**	

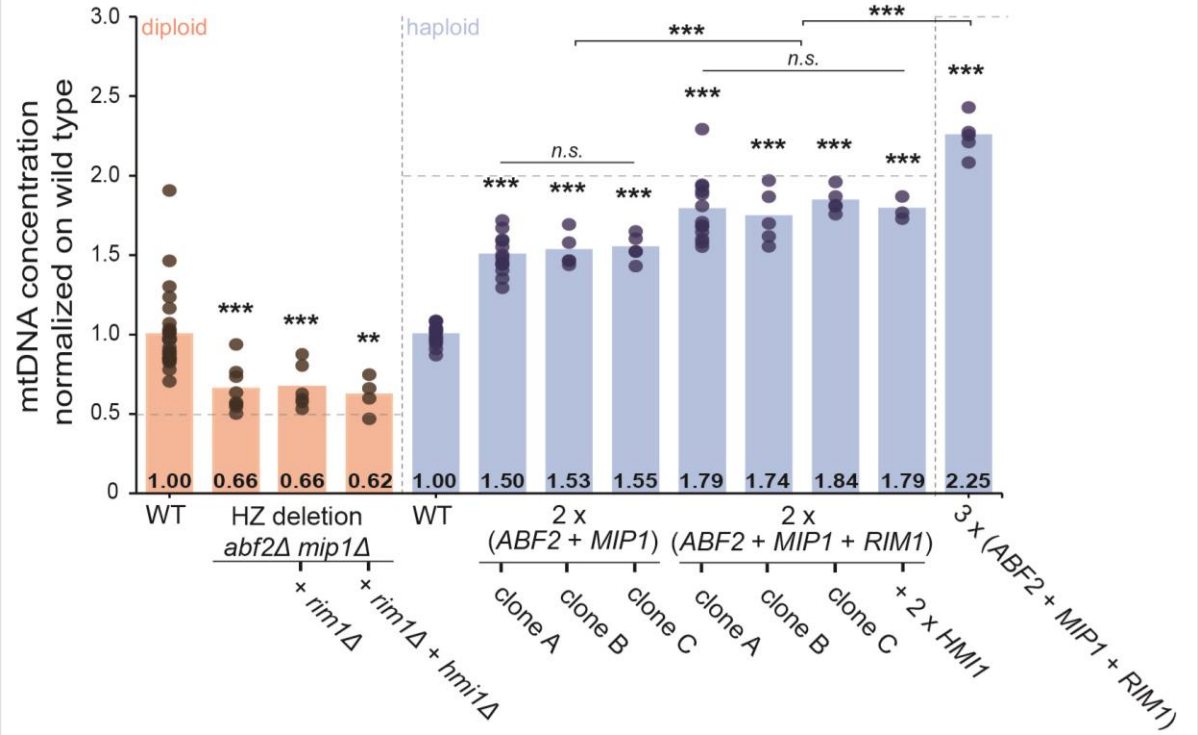

Figure 27: Mitochondrial DNA concentration normalized on wild type of selected strains for phenotyping experiments measured in SCGE. MtDNA concentration normalized on the corresponding wild type grown in non-fermentable SCGE media, separated by ploidy: Diploid strains include wild type, hemizygous double deletion of *abf2* and *mip1,* hemizygous triple deletion of *abf2, mip1* and *rim1* and hemizygous quadruple deletion of *abf2, mip1, rim1* and *hmi1* (left; orange), Haploid strains include wild type, 3 individual clones A-C of double addition strains including one additional copy of *ABF2* and *MIP1*, 3 individual clones A-C of triple addition strains with one additional copy of *ABF2, MIP1* and, quadruple addition strain with one additional copy of *ABF2, MIP1, RIM1* and *HMI1,* triple triple addition strain including two additional copies of *ABF2, MIP1* and *RIM1* (right; blue). The bars indicate the mean values, calculated based on at least three replicates. Individual replicates are shown as dots. Statistical significances were calculated using a two-tailed two-handed t-tests and if no symbol is given, no significant effect was obtained. Statistical

significances compared to wild type are indicated as * for p < 0.05, ** for p < 0.01 and *** for p < 0.005. No significant difference was obtained between the three clones with identical genotype and the triple addition strains are all significantly higher than the corresponding double addition strain (*** for p < 0.005). The triple triple addition strain appears significantly higher than all of the triple addition strains (*** for p < 0.005).

3.4.1. Mitochondrial DNA concentration does not affect cell volume or nDNA copy number

Given the tight coupling between cell volume and mtDNA copy number, it was first tested whether the cell volume was affected by the changes in mtDNA copy number. For this, the first experiment was Coulter counter measurements. As shown in Figure 28a, no significant changes were observed except for a slightly higher cell volume for the quadruple deletion and the triple triple addition strain. It has to be noted that this observation is not significant after performing multiple hypothesis testing by Benjamini-Hochberg-correction. Comparing the three clones of the double and triple additions, it becomes clear that clone A in both cases appears slightly smaller, while clone C is a bit bigger, but none of the clones shows significant differences to wild type. The next analysis included the budding behavior by analyzing bud counts. For this, it is assumed that a cell in G1-phase, which does not have a bud, only contains one copy of nDNA and a cell in S/G2/M-phase (including a bud) contains two copies of nDNA. Counting the budding cells inside a culture can then give information about the nDNA copy number per cell. As shown in Figure 28b, there are no changes in the mean nDNA copy number per cell compared to the corresponding wild type.

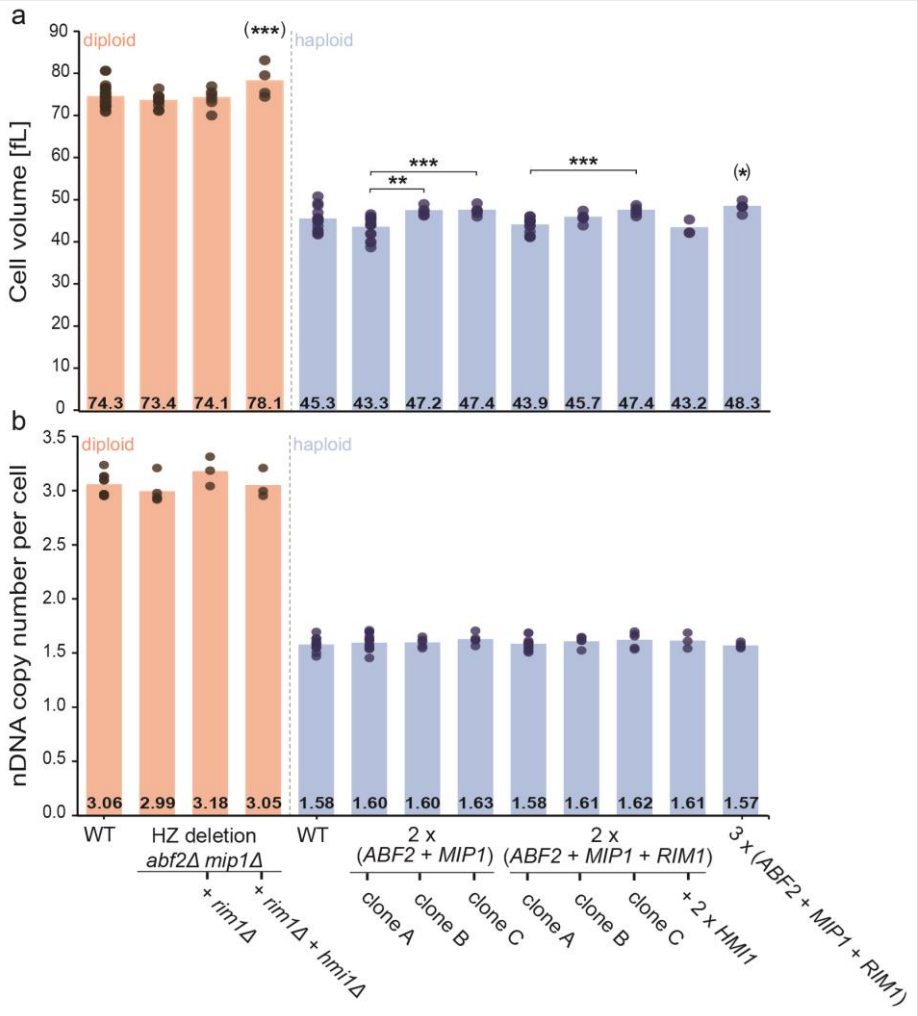

Figure 28: Cell volume measured by Coulter counter and nDNA copy number per cell measured by visual inspection for selected strains grown in SCGE. a) Cell Volume in fL measured by Coulter Counter and **b)** nDNA copy number per cell for selected strains measured by visual inspection ("Bud counts") with the use of a microscope. **a-b)** Diploid strains include wild type, hemizygous double deletion of *abf2* and *mip1,* hemizygous triple deletion of *abf2, mip1* and *rim1* and hemizygous quadruple deletion of *abf2, mip1, rim1* and *hmi1* (left; orange), Haploid strains include wild type, 3 individual clones A-C of double addition strains including one additional copy of *ABF2* and *MIP1*, 3 individual clones A-C of triple addition strains with one additional copy of *ABF2, MIP1* and *RIM1*, quadruple addition strain with one additional copy of *ABF2, MIP1, RIM1* and *HMI1,* triple triple addition strain including two additional copies of *ABF2, MIP1* and *RIM1* (right; blue). The bars indicate the mean values, calculated based on at least three replicates. Individual replicates are shown as dots. Statistical significances were calculated using a two-tailed two-handed t-tests and if no symbol is given, no significant effect was obtained. Statistical significances compared to wild type are indicated as * for $p < 0.05$, ** for $p < 0.01$ and *** for $p < 0.005$. When including multiple-hypothesis testing by Benjamini-Hochberg-correction, the cell volume-differences of the quadruple deletion and the triple triple addition strains against the appropriate wild type are not significant.

3.4.2. Higher mtDNA concentrations lead to slightly faster cell growth in non-fermentable SCGE media

Next, a growth analysis was done by OD_{600}-measurements over time. For this, the optical density of the cultures was measured at 600 nm every 30 minutes for at least 5 hours for values between 0.1 and 1. When plotting the measured OD_{600}-values in logarithmic scale over time, the slope of a linear fit represents the growth rate (see chapter 2.16.3.; Figures 11 and 12). As shown in Figure 29a, decreasing mtDNA led to slower growth, whereas increasing mtDNA resulted in faster growth.

The slower growth in non-fermentable media for strains with lower mtDNA concentrations seems logical, as a lower ATP production through the ETC seems plausible. More surprisingly, strains with higher mtDNA concentrations result in faster cell growth than wild type. However, as the difference is only around 10 minutes, additional competition assays were performed for the haploid strains. To better understand the aim of this experiment, the intention and two theoretical outcomes are explained first. For this experiment, two individually cultured strains are mixed in a defined ratio, then cultured and diluted over time, while samples are taken every day. The DNA of these samples was extracted and the proportion of the additional copy strain was quantified by qPCR measurements using *AMPR*-primers. The (bacterial) Ampicillin Resistance is only inserted into strains, which were genomically manipulated through yeast transformation, introducing a plasmid containing the gene of interest and the Ampicillin Resistance (see chapter 2.13.2.). As the wild type does not include the Ampicillin Resistance gene, measuring the occurrence of it inside the mixture, the fraction of the contained addition strain could be determined. Two possible scenarios can happen inside the mixture: In scenario 1, the ratio of the two strains stays more or less constant over time, indicating that they have (nearly) the same doubling time. In scenario 2 the fraction of one strain increases over time until a certain time point, where this one strain outcompetes the other strain, meaning that this strain is growing faster.

As already mentioned, the addition strains were constructed using plasmids (see chapter 2.13.2.). Besides the to-be-added gene and the bacterial Ampicillin Resistance cassette, this plasmid also contains an auxotrophic marker. It can not be excluded that these markers are influencing cell growth. To rule out these potential effects, strains without gene addition but corrected corresponding auxotrophic markers were used as reference strains in the competition assay. The Figures 29b to 29d show the fraction of the addition strains over time: As expected, a starting fraction of 25% was measured for all of the strains. On the time scale of the experiment, they show a continuous increase of the fraction until reaching around 100%. The double and triple addition strains take over the media around 100 hours after mixing with the corresponding reference strains (Figure 29b and c). No obvious differences between the three clones of the same genotype were observed here. A closer look at the result of the triple triple addition strain (Figure 29d) reveals a slower takeover of the mixture for this strain. This result stands in contrast to the growth rate measurements (Figure 29a), in which the triple triple addition strain was the fastest growing strain. This could hint towards an involvement of the auxotrophic markers used in this strain, helping the cells to grow faster. The triple triple addition strain contains corrections for the selectable markers of *LEU2*, *URA3*, *HIS3* and *TRP1*. As the quadruple addition strain includes corrections of the identical four selectable markers and shows a growth rate similar to wild type in the OD-measurements (Figure 29a), the selectable markers cannot be the main reason for the contrary results of the triple triple addition strain. A competition assay with a mixture of the reference strain and the haploid wild

type could provide more information, but it is impossible for the designed experiment, as neither of these two strains includes the Ampicillin Resistance.

However, all of the strains tested via competition assay outcompeted their reference strains. These results support that strains with increased mtDNA concentrations grow faster in non-fermentable media.

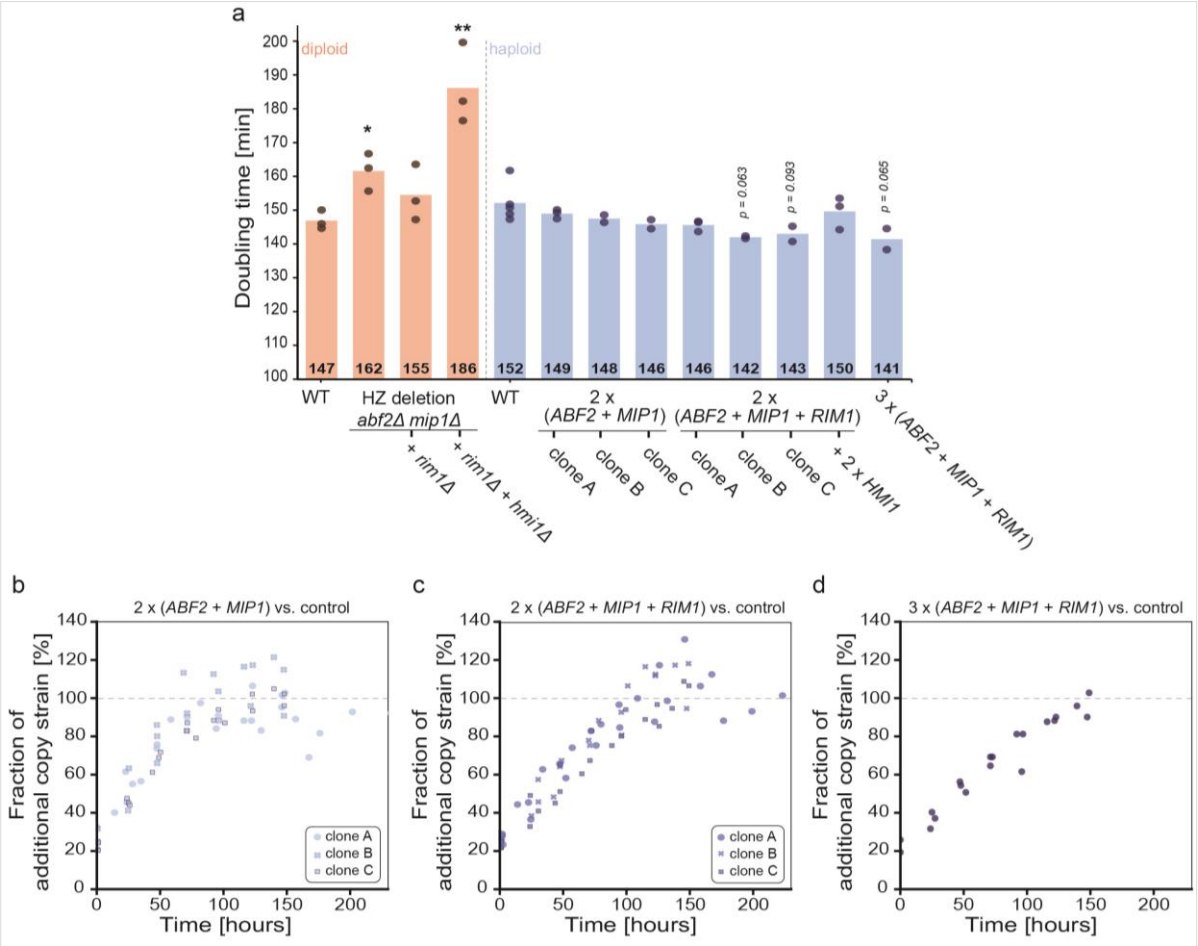

Figure 29: Cell growth in SCGE media at 30 °C. a) Doubling time in minutes calculated through the slope of a time course of optical density at 600 nm. Strains were grown in non-fermentable SCGE media, separated by ploidy: Diploid strains include wild type, hemizygous double deletion of *abf2* and *mip1,* hemizygous triple deletion of *abf2, mip1* and *rim1* and hemizygous quadruple deletion of *abf2, mip1, rim1* and *hmi1* (left; orange), Haploid strains include wild type, 3 individual clones A-C of double addition strains including one additional copy of *ABF2* and *MIP1*, 3 individual clones A-C of triple addition strains with one additional copy of *ABF2, MIP1* and *RIM1*, quadruple addition strain with one additional copy of *ABF2, MIP1, RIM1* and *HMI1,* triple triple addition strain including two additional copies of *ABF2, MIP1* and *RIM1* (right; blue). The bars indicate the mean values, calculated based on at least three replicates. Individual replicates are shown as dots. Statistical significances were calculated using a two-tailed two-handed t-tests and if no symbol is given, no significant effect was observed. Statistical significances compared to wild type are indicated as * for $p < 0.05$, ** for $p < 0.01$ and *** for $p < 0.005$. **b-d)** showing the fraction of the additional copy strain in percent over time in hours measured in a competition assay using qPCR (with *AMPR*- and *ACT1*-primers) for **b)** the double addition strains against reference strain (corrected auxotrophic markers: *TRP1*, *URA3*). Clone A (dot), clone B (cross) and clone C (square) contain at least 2 replicates per clone. **c)** the triple addition strains against reference strain (corrected auxotrophic markers: *TRP1*, *URA3*, *LEU2*). Clone A (dot), clone B (cross) and clone C (square) contain at least 2 replicates per clone. **d)** the triple triple addition strains against reference strain (corrected auxotrophic markers: *TRP1, URA3, LEU2, HIS3*) contain 3 replicates.

3.4.3. Variation in mtDNA copy numbers do not cause a clear phenotype in cells facing temperature-, osmotic- or replicative stresses

As shown in this study, budding yeast with increased mtDNA concentrations grow faster when cultured in standard lab conditions at 30 °C on SCGE media. Next, the question arose whether increasing mtDNA concentrations could be a disadvantage in certain conditions. For this, stress spot assays were performed with 8 of the 13 selected strains (Table 25). The assays include all diploid hemizygous deletion strains and one clone of each haploid addition strain, except for the triple triple addition strain. The unbiased evaluation of the results was done with masked conditions by three individual scientists.

First, a temperature assay was performed on various growth media. For the rich media YPD, three temperatures of cold 23 °C, normal 30 °C and hot 37 °C conditions were tested (Figure 31). Additionally, for the defined fermentable media SCD and non-fermentable media SCG, two temperatures of normal 30 °C and hot 37 °C conditions were tested (Figures 30 and 32).

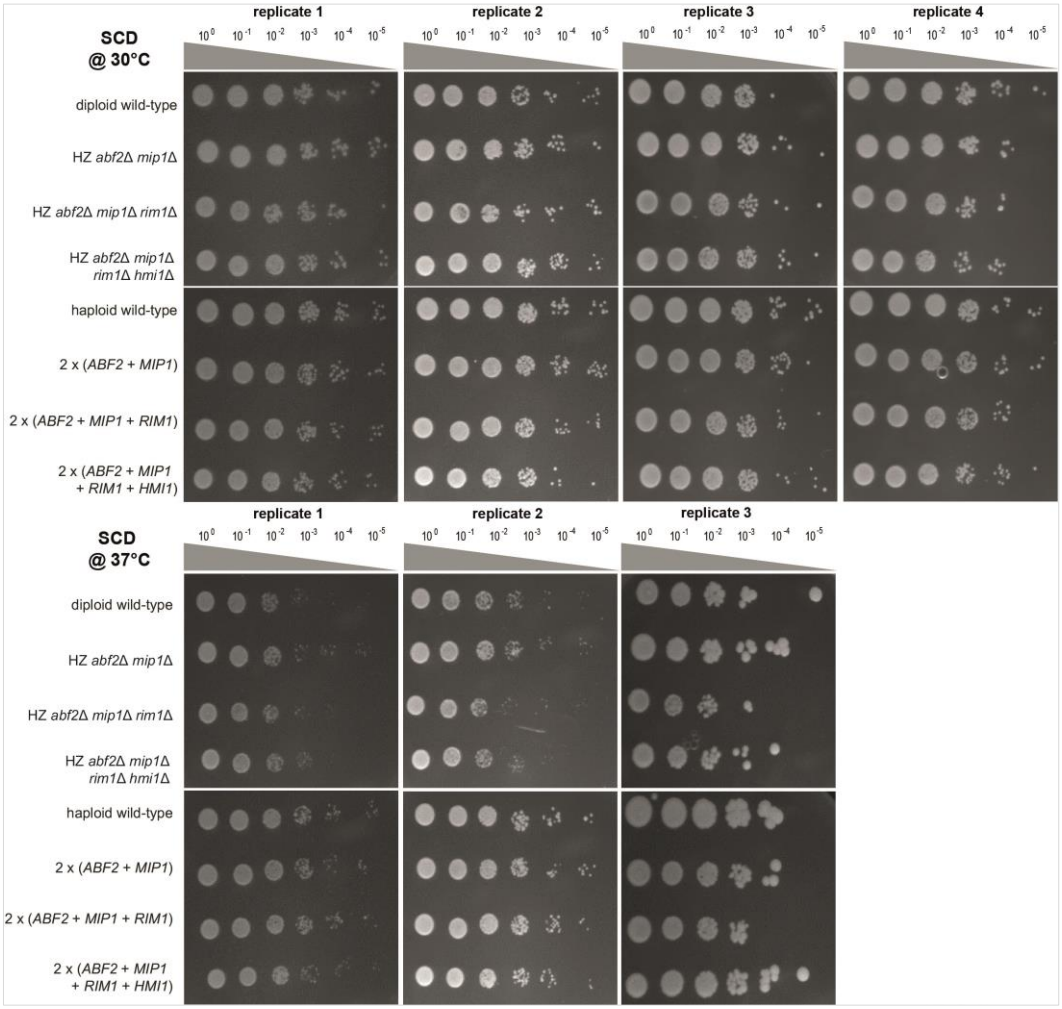

Figure 30: Growth in stress spot assays on SCD plates at various temperatures. Selected strains were plated in a six-fold 1:10 dilution series starting with OD_{600}=1 on a SCD plate and incubated at 30°C (top) or 37°C (bottom). For each ploidy, the corresponding wild type strain was included on the same plate for all of the at least three replicates. Diploid strains include wild type, hemizygous double deletion of *abf2* and *mip1*, hemizygous triple deletion of *abf2, mip1* and *rim1* and hemizygous quadruple deletion of *abf2, mip1, rim1* and *hmi1*. Haploid strains include wild type, double addition strains including one additional copy of *ABF2* and *MIP1* (clone A), triple addition strains with one additional copy of *ABF2, MIP1* and *RIM1* (clone A), quadruple addition strain with one additional copy of *ABF2, MIP1, RIM1* and *HMI1*.

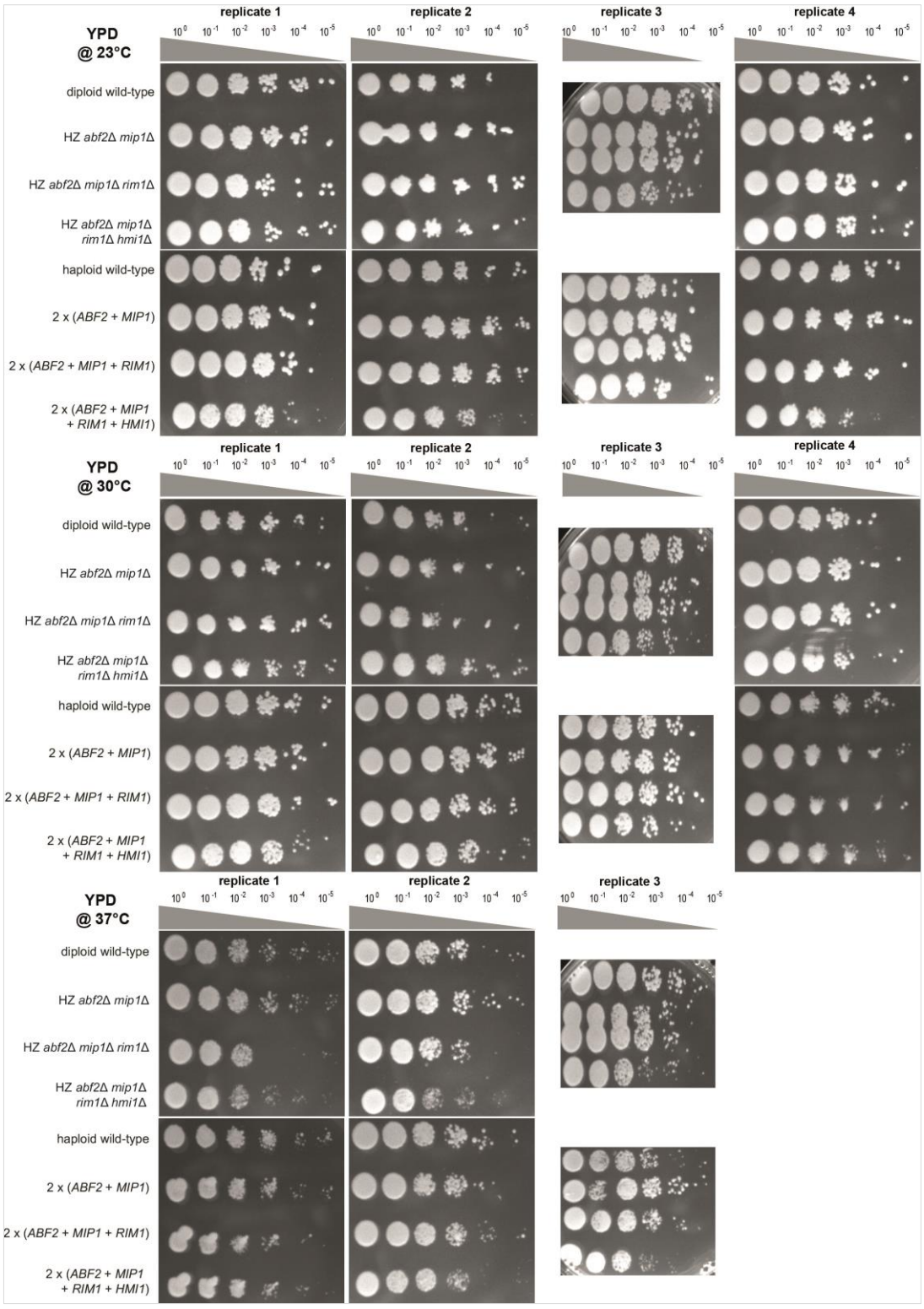

Figure 31: Growth in stress spot assays on YPD plates at various temperatures. Selected strains grown in fermentable YPD media, plated in a six-fold 1:10 dilution series starting with OD_{600}=1, and incubated at 23 °C (top), 30°C (middle) or 37°C (bottom). For each ploidy, the corresponding wild type strain was included on the same plate for all of the at least three replicates. Diploid strains include wild type, hemizygous double deletion of *abf2* and *mip1,* hemizygous triple deletion of *abf2, mip1* and *rim1* and hemizygous quadruple deletion of *abf2, mip1, rim1* and *hmi1.* Haploid strains include wild type, double addition strains including one additional copy of *ABF2* and *MIP1* (clone A), triple addition strains with one additional copy of *ABF2, MIP1* and *RIM1* (clone A), quadruple addition strain with one additional copy of *ABF2, MIP1, RIM1* and *HMI1.*

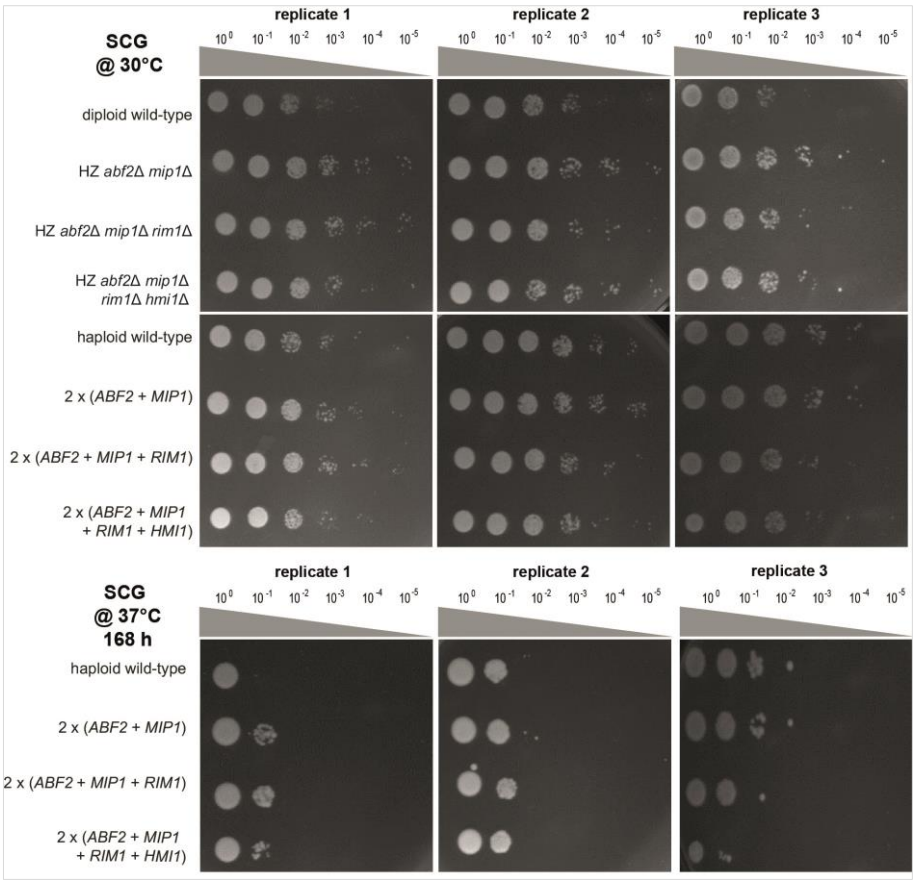

Figure 32: Growth in stress spot assays on SCG plates at various temperatures. Selected strains were plated in a six-fold 1:10 dilution series starting with OD_{600}=1 on SCG plates and incubated at 30°C (top) or 37°C (bottom). For each ploidy, the corresponding wild type strain was included on the same plate for all of the at least three replicates. Diploid strains include wild type, hemizygous double deletion of *abf2* and *mip1*, hemizygous triple deletion of *abf2, mip1* and *rim1* and hemizygous quadruple deletion of *abf2, mip1, rim1* and *hmi1*. Haploid strains include wild type, double addition strains including one additional copy of *ABF2* and *MIP1* (clone A), triple addition strains with one additional copy of *ABF2, MIP1* and *RIM1* (clone A), quadruple addition strain with one additional copy of *ABF2, MIP1, RIM1* and *HMI1*. Pictures of the diploid strains grown on SCG plates at 37°C for 168 hours are not included, as no growth was visible.

As Figures 30 to 32 show, there is no clearly visible growth difference between the strains when cultured at 30 °C on glucose media plates (YPD and SCD). This could be explained by the fact that budding yeast can ferment glucose, so there is no need for respiration and mtDNA. For the same temperature and growth on non-fermentable media (SCG), the haploid strains with increased mtDNA copy number show no drastic differences to the corresponding wild type. By contrast, the diploid strains with decreased mtDNA copy number seem to grow slightly faster compared to wild type. While no major effect is visible when culturing the cells at 23 °C (cold) on YPD, culturing at 37 °C (hot) leads to differences between the strains: the triple deletion strain showed slightly slower growth compared to the corresponding wild type at 37 °C. Also, the triple addition strain seems to grow worse than the haploid wild type when cultured at 37 °C on YPD plates but not on SCD plates.

When the strains were cultured on SCG plates at 37 °C, a generally slower growth than for all other tested conditions was observed (Figure 32). As no colonies were visible for any of the diploid strains after 96 hours, the plates were discarded. The haploid strains cultured in these conditions were grown until approximately 168 hours, to ensure enough colony growth for

comparison. As shown in Figure 32, the three replicates resulted in very inconsistent effects. Summarizing the temperature assays, no major differences between the strains were observed, besides the fact that the deletion of all three factors leading to decreased mtDNA concentrations causes poorer growth at increased temperatures.

In addition to the temperature assays, spot assays with stress-inducing chemicals were performed at 30 °C. Adding sodium chloride (NaCl) to cells induces ion toxicity and osmotic stress (Logothetis *et al.*, 2007). To test the effect of mtDNA copy number on growth when facing these stresses, they were cultured on YPD plates including 5 nM NaCl. As shown in Figure 33, no drastic differences were observed, except for the quadruple addition strain, which seems to grow fewer colonies than the other strains.

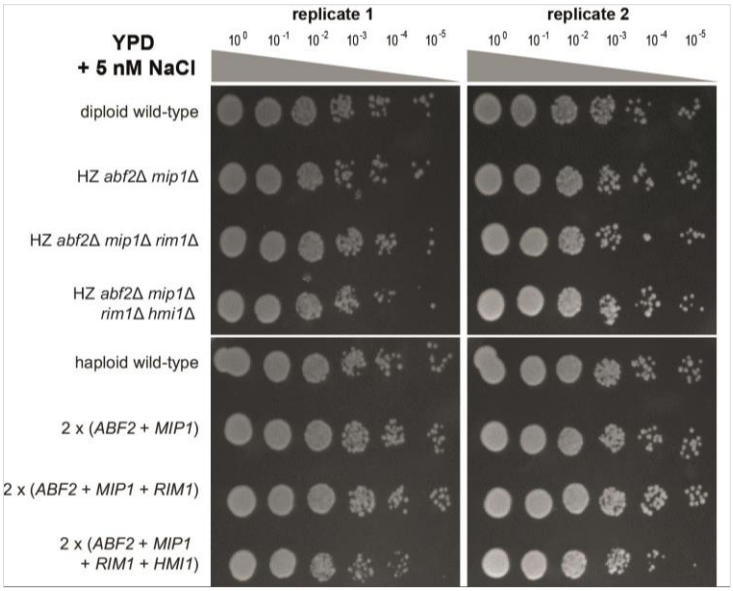

Figure 33: Growth in stress spot assays on YPD plates supplemented with 5 nM NaCl. Selected strains were plated in a six-fold 1:10 dilution series starting with OD_{600}=1 on YPD plates supplemented with 5 nM NaCl at 30°C. For each ploidy, the corresponding wild type strain was included on the same plate for all of the two replicates. Diploid strains include wild type, hemizygous double deletion of *abf2* and *mip1*, hemizygous triple deletion of *abf2, mip1* and *rim1* and hemizygous quadruple deletion of *abf2, mip1, rim1* and *hmi1*. Haploid strains include wild type, double addition strains including one additional copy of *ABF2* and *MIP1* (clone A), triple addition strains with one additional copy of *ABF2, MIP1* and *RIM1* (clone A), quadruple addition strain with one additional copy of *ABF2, MIP1, RIM1* and *HMI1*.

Another stress condition tested was replicative stress induced by the addition of hydroxyurea (HU) (Young and Hodas, 1964; Shaw *et al.*, 2024). As 50 nM HU did not show any different growth comparing the strains, the experiments were also repeated with 100 nM HU. Here, no striking differences were visible when comparing the diploid strains (Figure 34). Regarding the haploid strains, the triple and quadruple addition strains grew slower than the wild type. Interestingly, the number of colonies seems to be comparable to the wild type, but the size of the colonies is visibly smaller. This indicates that there is no change in survival but a disadvantage in growth with increased mtDNA.

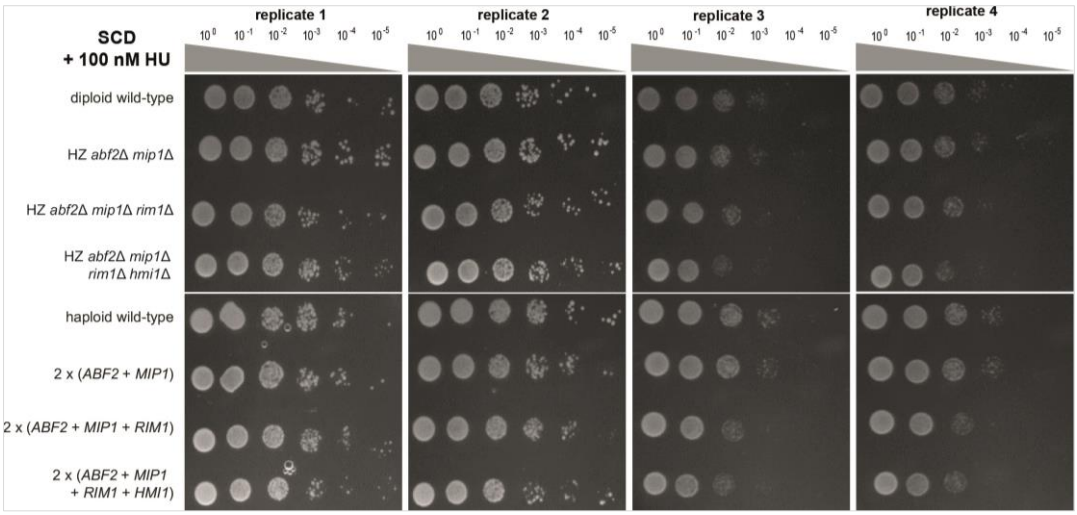

Figure 34: Growth in stress spot assays on SCD plates supplemented with 100 nM ydroxyurea. Selected strains were plated in a six-fold 1:10 dilution series starting with OD_{600}=1 on SCD plates supplemented with 100 nM Hydroxyurea at 30°C. For each ploidy, the corresponding wild type strain was included on the same plate for all of the four replicates. Diploid strains include wild type, hemizygous double deletion of *abf2* and *mip1*, hemizygous triple deletion of *abf2, mip1* and *rim1* and hemizygous quadruple deletion of *abf2, mip1, rim1* and *hmi1*. Haploid strains include wild type, double addition strains including one additional copy of *ABF2* and *MIP1* (clone A), triple addition strains with one additional copy of *ABF2, MIP1* and *RIM1* (clone A), quadruple addition strain with one additional copy of *ABF2, MIP1, RIM1* and *HMI1*.

3.4.4. The loss of respiratory capacity is dependent on mtDNA copy number

When there is no glucose for fermentation available, budding yeast switches to respiration to generate ATP (Turcotte *et al.*, 2010; Ben Galeota-Sprung *et al.*, 2022). As mentioned before, mtDNA is essential for budding yeast to be able to respire (Ephrussi and Slonimski, 1955). When losing their mtDNA completely, budding yeast become petite and subsequently lose their respiratory capacity. Petites can be caused by mutations directly in the mtDNA itself or indirectly by mutations in the nDNA, which subsequently lead to a loss of mtDNA (Contamine and Picard, 2000). Examples of nDNA mutations causing petite's are the mtDNA-limiting factors, as reports have documented an influence of Abf2 (Gichner, 1982), Mip1 (Genga *et al.*, 1986; Foury, 1989; Hu *et al.*, 1995; Lecrenier and Foury, 1995) and Rim1 (van Dyck *et al.*, 1992) on the respiratory capacity. It therefore seems to be logical to also analyze the petite frequency in strains with different mtDNA copy numbers.

When performing a petite assay, the strains are growing on an indicator plate, which contains glycerol and a very low and limiting concentration of glucose as carbon sources. This enables all colonies to start growing by fermenting the glucose. After the glucose is consumed completely, only the glycerol on the plate can be used as an alternative. Cells that contain dysfunctional mtDNA (ρ^-) or are lacking the mtDNA completely (ρ^0) are now unable to continue to grow (Ephrussi and Slonimski, 1955; Faye *et al.*, 1973; Gichner, 1982; Contamine and Picard, 2000), whereas cells containing functional mtDNA (ρ^+) switch into respiration and proceed growing (see chapter 2.16.5.; Figure 13). The frequency of the petite colonies therefore represents the respiratory capacity of a strain. The results (Figure 35a) show a significant increase in petite colonies when decreasing the mtDNA concentrations in the diploid strains. On the other hand, an increase in mtDNA concentration leads to a significantly decreased frequency of petite colonies. When comparing the clones of identical genotypes with each other, no significant difference can be observed. Moreover, when pooling the results

of the three clones harbouring the identical genotype (for double and triple addition strains individually), a significantly lower frequency of petite cells is observed in the triple additions compared to the double addition strains. As reported by previous studies (Stuart *et al.*, 2006), haploid wild type cells showed higher petite frequencies than diploid wild type cells (Figure 35a). Another recent study has documented that slightly decreased mtDNA copy numbers in an *mmr1*-deletion strain coincide with significantly higher frequencies of petite colonies (Ray *et al.*, 2025). This is in line with the observation in this study that mtDNA copy number influences the petite frequency in budding yeast. Interestingly, the percentage of petite colonies for the triple addition strain is comparable to that of the diploid wild type strain. These two strains contain approximately the same number of mtDNA copies per cell. Also, the triple deletion and the haploid wild type contain a similar amount of mtDNA and have a similar frequency of petite colonies.

In summary, this indicates that the loss of respiratory capacity decreases with increasing mtDNA copy number (Figure 35b). This might be explained by the stochastic loss of mtDNA at cell division.

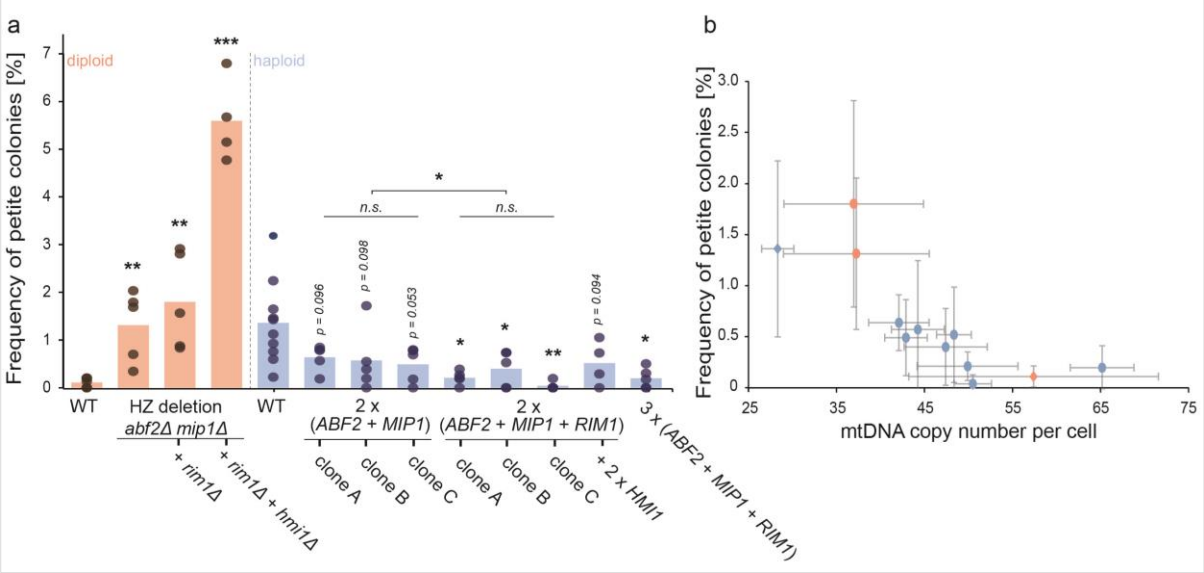

Figure 35: Petite frequency in selected strains. Selected strains were plated onto an indicator plate (SCG + 0.1% Glucose), where glucose limitation leads to the formation of two colony sizes: strains capable of respiratory growth (big colonies) and strains unable to respire (small "petite" colonies, lacking functional mtDNA). At least 500 colonies were visually counted and classified for all of the at least three replicates. Diploid strains (left; orange) including wild type, hemizygous double deletion of *abf2* and *mip1,* hemizygous triple deletion of *abf2, mip1* and *rim1* and hemizygous quadruple deletion of *abf2, mip1, rim1* and *hmi1.* Haploid strains (right; blue) including wild type, 3 individual clones A-C of double addition strains including one additional copy of *ABF2* and *MIP1,* 3 individual clones A-C of triple addition strains with one additional copy of *ABF2, MIP1* and *RIM1*, quadruple addition strain with one additional copy of *ABF2, MIP1, RIM1* and *HMI1,* triple triple addition strain including two additional copies of *ABF2, MIP1* and *RIM1.* **a)** The frequency of petite colonies (percentage) is shown for each strain. The bars indicate the mean values, calculated based on at least three replicates. Individual replicates are shown as dots. Statistics were calculated using a two-tailed two-handed t-tests and if no symbol is given, no significant effect was obtained. Statistical significances compared to wild type are indicated as * for $p < 0.05$, ** for $p < 0.01$ and *** for $p < 0.005$. **b)** Frequency of petite colonies in percentage, as a function of the mtDNA copy number per cell. Each datapoint represents the mean value of one strain for the diploid (orange) and haploid (blue) strains. The hemizygous quadruple deletion is not included in this chart.

3.5. Increasing mtDNA concentrations by alternative strategies confirms the discovered phenotypes

Besides manipulation of the nuclear-encoded machinery, it is also possible to obtain higher mtDNA concentrations by genomic manipulations of other genes, such as the deletion of *MRX6 (Göke et al., 2020)* or *CIM1 (Schrott and Osman, 2023).* While deletion of the nuclear gene *MRX6*, encoding for a mitochondrial ribosome-associated protein, leads to higher mtDNA copy number, there is no difference in mtDNA copy number when adding additional copies of *MRX6 (Göke et al., 2020).* On the other hand, deleting *CIM1* results in a higher mtDNA copy number, whereas adding additional copies of CIM1 results in lower mtDNA copy numbers (Schrott and Osman, 2023). Besides leading to higher mtDNA copy numbers, deleting *CIM1 c*an rescue the negative effects of an *abf2Δ*-deletion-strain (Schrott and Osman, 2023). To better understand the mtDNA-related phenotypes measured in experiments in SCGE (see chapter 3.4.), alternative strains to increase mtDNA copy number were created by deleting *MRX6* or *CIM1*. Moreover, to test whether the two strategies used to increase mtDNA copy number (adding mtDNA-limiting machinery and *cim1Δ*-deletion or *mrx6Δ*-deletion) are additive or not, another two strains were created. For this, the two strategies were combined by adding the deletion of *MRX6* or *CIM1* to the triple addition strain. The six strains compared in this chapter are listed below (Table 26). As before, the documented acronyms will be used from here on for simplicity.

Table 26: Overview of strains included in alternative strategies to increase mtDNA copy number, to confirm measured results.

Strains for phenotyping by alternative strategies to increase mtDNA copy number			
Strain name	Ploidy	Description	**Acronym**
MMY116-2c	haploid	Wild type	**WT haploid**
AFY057-1	haploid	One additional copy *ABF2 MIP1 RIM1*	**Triple addition**
AFY089-1	haploid	*cim1* deletion	***cim1Δ***
AFY090-1	haploid	*mrx6* deletion	***mrx6Δ***
AFY087-1	haploid	One additional copy *ABF2 MIP1 RIM1* plus *cim1* deletion	**Triple addition *cim1Δ***
AFY088-1	haploid	One additional copy *ABF2 MIP1 RIM1* plus *mrx6* deletion	**Triple addition m*rx6Δ***

The mtDNA concentration normalized on wild type for the *mrx6Δ*-strain was 1.80 and the *cim1Δ*-strain was 1.91 (Figure 36a). The mtDNA concentrations are therefore comparable to those in the triple addition strain. Deleting one of the two genes (*CIM1* or *MRX6*) in the triple addition strain leads to even higher wild-type-normalized mtDNA concentrations of around 2.42 and 2.12, respectively (Figure 36a). This indicates that these two ways to increase mtDNA copy number act independently. However, the effect of deleting *MRX6* or *CIM1* does not seem to be perfectly additive to the triple addition in the strain, as the increase upon the triple addition is lower than this would suggest. A strain containing three copies of all factors of the mtDNA-limiting machinery was shown to increase mtDNA concentration to comparable concentrations around 2.25 normalized on wild type (Figure 20). It was speculated before that this mtDNA concentration could already be close to saturation (see chapter 3.2.3.). The absence of an additive effect when combining the two strategies to increase mtDNA copy number (increasing the amount of the limiting machinery and deletion of *CIM1* or *MRX6*) supports this assumption: The mtDNA copy number might be constrained by an unknown factor leading to a not perfectly scalable additional effect and assuming a mtDNA-saturation in the nucleoids. The slightly weaker effect of a *cim1Δ*-deletion in strains with higher mtDNA-

concentrations, such as the triple addition strain, compared to the effect in wild type, might also be explainable by the antagonist effect of Cim1 and Abf2 (Schrott and Osman, 2023). As the triple addition strain includes higher Abf2 concentrations than the wild type strain, the effect of deleting *CIM1* could be weakened.

The alternative strategies to increase mtDNA concentration confirm the previously mentioned absence of major changes in cell volume or budding behavior (Figure 36b and c). The strains containing multiple copies of the mtDNA-limiting machinery with increasing mtDNA concentrations resulted in faster cell growth in SCGE (Figure 29). When measuring the OD at 600 nm over time for the strains of the alternative strategy to increase mtDNA copy number, it becomes clear that the *cim1Δ*- and *mrx6Δ*-strain show comparable doubling times to the triple addition strain and therefore also grow faster than wild type (Figure 36d). This confirms the dependency of cell growth on mtDNA concentrations. The triple addition containing a *cim1Δ*- or *mrx6Δ*-deletion shows higher doubling times than the triple addition strain, which are anyway still lower than the wild type doubling time (Figure 36d). As mentioned before, these effects are so small that a more detailed experimental analysis is needed to confirm it. To better understand cell growth of the triple addition strain containing a *cim1Δ*- or *mrx6Δ*-deletion, competition assays against the corresponding reference strain with corrected auxotrophic markers were performed. Interestingly, the triple addition strain containing a *mrx6Δ*-deletion showed a slower growth than expected from the OD-measurements (see Figure 36d) and could not outcompete the reference strain within the first approximately 125 hours. A negative control was performed by measuring an empty vector control against the same reference strain as used for the triple addition strain containing a *mrx6Δ*-deletion. The difference between the negative control and the haploid wild type is only the empty vector, which includes the Ampicillin Resistance, needed for the experimental procedure, and the marker-correction of *TRP1*. The fraction over time of the empty vector and the triple addition containing a *mrx6Δ*-deletion shows very similar results, indicating that the increased mtDNA concentration of the triple addition containing a *mrx6Δ*-deletion does not lead to a faster growth rate, as expected (Figure 36f). This leads to the question of why the triple addition containing a *mrx6Δ*-deletion does not show the faster cell growth as all other strains with comparable mtDNA concentrations? Among other things, Schrott et al measured transcript amounts of genes encoded by mtDNA in *mrx6Δ*-deletion and *cim1Δ*-deletion strains (Schrott and Osman, 2023). The results showed no difference in mitochondrial-encoded transcripts compared to wild type for the *mrx6Δ*-deletion strain (Schrott and Osman, 2023), which indicates that the mtDNA increase does not result in functional mtDNA. By contrast, the *cim1Δ*-deletion strain showed increased transcript amounts for the mitochondrial-encoded genes compared to wild type (Schrott and Osman, 2023). This indicates that only an increase in mtDNA copy number that also leads to increased transcription results in faster cell growth. This is also supported by the competition assay of the triple addition strain containing a *cim1Δ*-deletion, which shows faster cell growth than the corresponding reference strain. Interestingly, the fraction over time is very similar to that of the triple triple addition strain (Figure 36e and Figure 29d). As described before, these two strains need slightly longer to outcompete the reference strain than the other strains with increased mtDNA copy number, which seems to be due to their similarly high mtDNA concentrations. All strains with increased functional mtDNA concentrations showed a faster cell growth (see Figure 26 and 36), but strains with a more drastic increase of mtDNA concentration (as in the triple triple addition strain or the triple addition strain containing a *cim1Δ*-deletion) seem to grow slower than strains with a moderate increase of mtDNA copy number (as in the double and triple addition strain).

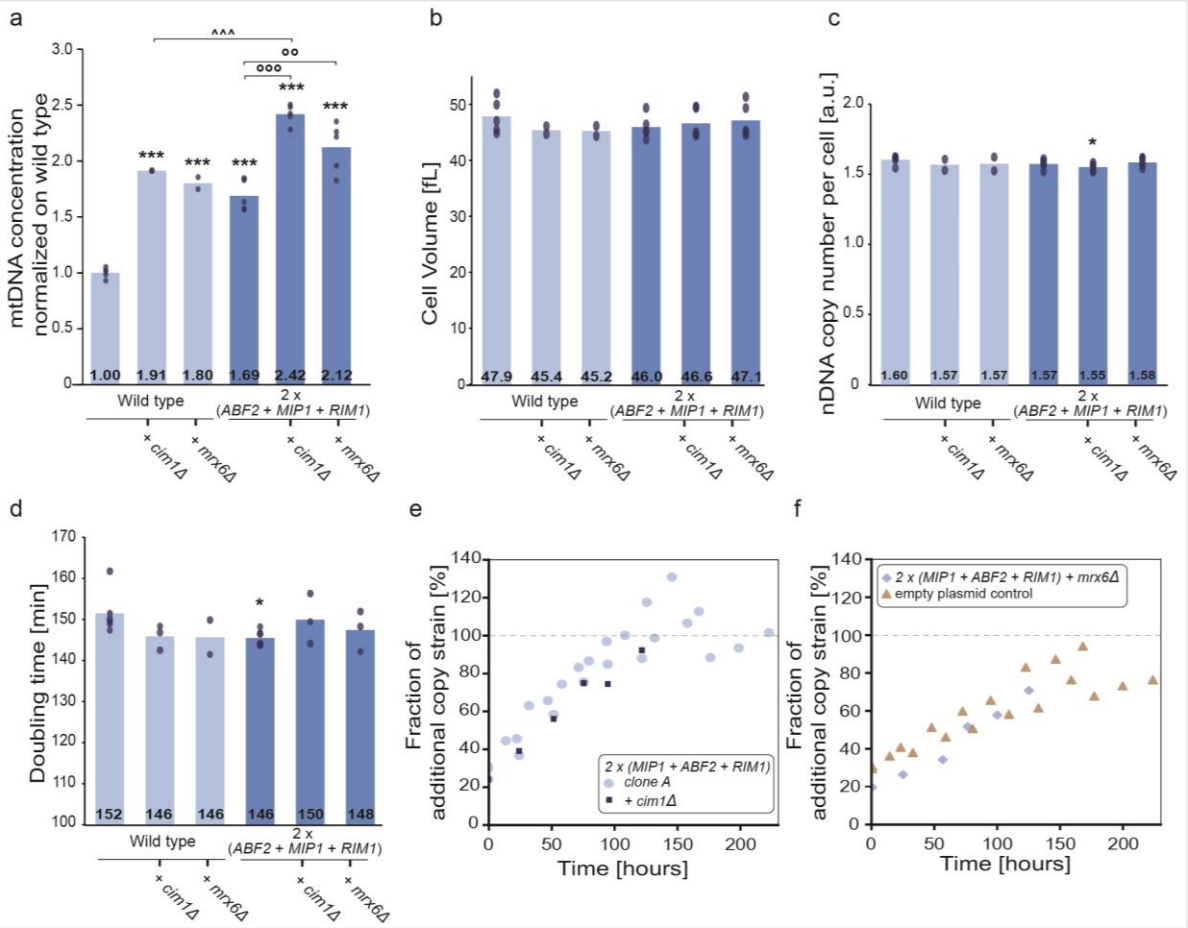

Figure 36: Analysis of an alternative strategy to increase mtDNA concentration by deleting *cim1* or *mrx6*. **a - d)** The six strains included in the analysis are differently coloured based on the background strains: wild type and the wild type including *cim1Δ*-deletion or *mrx6Δ*-deletion (left; light blue) or triple addition strain and the triple addition strain including *cim1Δ*-deletion or *mrx6Δ*-deletion (right; dark blue). The bars indicate the mean values, calculated based on at least two replicates. Individual replicates are shown as dots. Statistical significances were calculated using a two-tailed two-handed t-tests and if no symbol is given, no significant effect was observed. Statistical significances compared to wild type are indicated as * for $p < 0.05$, ** for $p < 0.01$ and *** for $p < 0.005$ and statistical significances compared to the triple addition strain are indicated as ° for $p < 0.05$, °° for $p < 0.01$ and °°° for $p < 0.005$. Plots for strains grown in non-fermentable SCGE media, representing the **a)** mtDNA concentration normalized on the haploid wild type measured by qPCR, **b)** Cell Volume in fL measured by Coulter counter, **c)** nDNA copy number per cell for selected strains measured by visual inspection ("Bud counts") with the use of a microscope and **d)** Doubling time in minutes calculated by the slope of optical density at 600 nm over time. **e – f)** Fraction of the additional copy strain in percent over time in hours measured in a competition assay using qPCR (with *AMPR*- and *ACT1*-Primers) for **e)** the triple addition strain including *mrx6*-deletion (diamond; light blue; 1 replicate) and empty plasmid control (insert includes *AMPR*-Sequence and correction for *TRP1;* triangle; light brown; 2 replicates) against reference strain (corrected auxotrophic markers: *TRP1*, *URA3*, *LEU2*). **f)** the triple addition strain clone A (dot; light blue; 3 replicates) and the triple addition strain including a *cim1*-deletion (square; dark blue; 1 replicate) against the reference strain (corrected auxotrophic markers: *TRP1*, *URA3*, *LEU2*).

When testing stress spot assays for the strains with increased mtDNA concentration due to an addition of the limiting machinery, one major finding was a slower growth than wild type when facing replicative stress (Figure 34). To test whether this is an mtDNA-dependent effect, this stress spot assay was repeated with the alternative strategy to increase mtDNA by deleting *CIM1* or *MRX6*. Additionally, the *cim1Δ*- and *mrx6Δ*-deletions in the triple addition

strain were included in the analysis to see the effect in strains with even higher mtDNA concentrations. The strains were grown on SCD plates with and without supplementation of 100 nM HU at 30°C. When comparing the colony growth on SCD without additional supplementation (Figure 37a), the *cim1Δ*-deletion seems to grow slightly faster than the *mrx6Δ*-deletion, independently of the background strain. This could again be explainable by the increase on transcript level of mtDNA-encoded genes for the Δ*cim1*-deletion, which is missing in the *mrx6Δ*-deletion (Schrott and Osman, 2023). When inducing replicative stress by adding HU to the plates, it can be observed that the deletions in wild type background grow slightly better than the deletions in the triple addition strain. This goes hand in hand with the fact that the triple addition strain shows a negative growth phenotype in this assay, as mentioned before (see chapter 3.4.3.). However, the fact that the single deletions do not show a visible difference to wild type, even though they contain similar mtDNA concentrations as the triple addition strain, could be an indication that this observed phenotype is not based on the mtDNA copy number but the three limiting factors themselves.

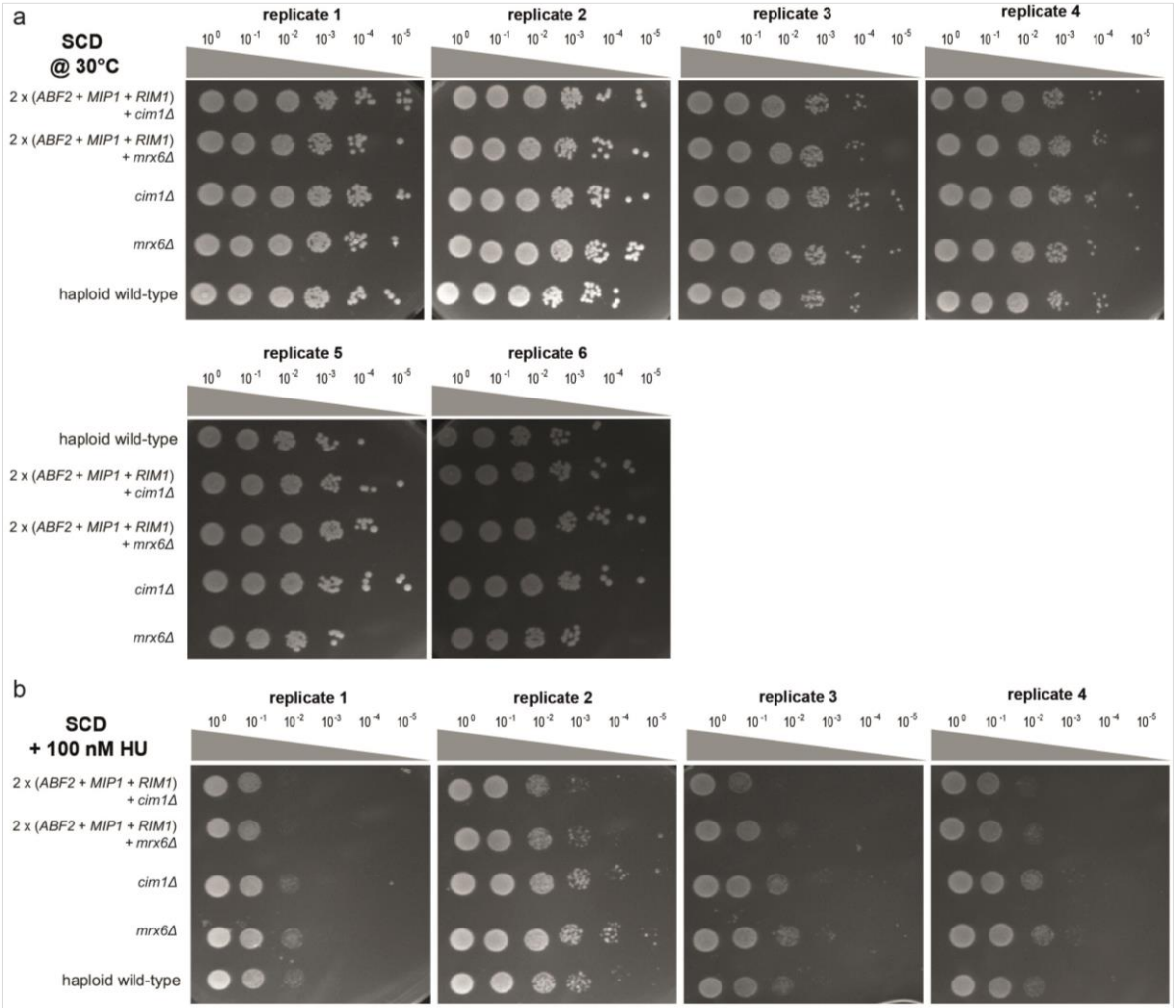

Figure 37: Stress spot assays of an alternative strategy to increase mtDNA concentration by deleting *cim1* or *mrx6* on SCD plates supplemented with 100 nM Hydroxyurea. Selected strains were plated in a six-fold 1:10 dilution series starting with OD_{600}=1 on **a)** SCD plates or **b)** SCD plates supplemented with 100 nM Hydroxyurea at 30°C. The six strains included in the analysis: wild type and the wild type including *cim1*-deletion or *mrx6*-deletion and the triple addition strain including *cim1*-deletion or *mrx6*-deletion.

Another major result when analyzing the strains with overexpression of the limiting machinery resulting in increased mtDNA copy numbers was a decreased frequency of petite cells with increasing mtDNA copy numbers (Figure 35). This is supported by previous studies, which have described a decreased frequency of petite colonies in a *cim1Δ*-deletion strain (Schrott and Osman, 2023). It has to be noted that no information about the petite frequency in the *mrx6*Δ-deletion strain is given so far.

In conclusion, an increase of mtDNA concentration by deleting *MRX6* does not lead to higher mtDNA transcript concentrations (Schrott and Osman, 2023), which makes it harder to use this strain as confirmation experiments as intended in this study. However, the alternative way to increase mtDNA concentration in budding yeast by deleting *CIM1* results in increased mtDNA transcripts and confirms the two major observed phenotypes: strains with increasing mtDNA show a slightly faster growth rate and a lower chance of losing their mtDNA. When inducing the mtDNA concentrations higher than 2-fold, the faster growth rate seems to be impaired, as shown for the triple triple addition (see chapter 3.4.2.) and the triple addition strain containing a *cim1Δ*-deletion. The reduced growth rate when facing replicative stress shown in the triple addition strain could not be confirmed in the *cim1Δ*-deletion, pointing towards a specific dependency on the limiting factor.

3.6. Growth in fermentable media modifies observed phenotypes

The phenotyping documented so far was based on cells cultured in non-fermentable SCGE media (see chapters 3.4. and 3.5.), where mitochondria and their DNA are necessary for growth. To test whether the observed phenotypes are independent of the media, the measurements of cell volume, nDNA copy number per cell and growth rate were repeated in fermentable SCD media.

3.6.1. Only mild differences in cell volume to wild type when comparing growth in fermentable and non-fermentable media

A previous study has reported that cells grown in rich media, such as SCD, are bigger than cells grown in poor media, such as SCGE (Broach, 2012). To confirm this difference and also compare the strains' cell volumes to the corresponding wild type, Coulter counter measurements were performed for all strains included in the search for the third factor that limits mtDNA (see chapter 3.2.1.). Besides confirming bigger cell volumes in SCD than in SCGE in general (Figures 38 and 39), only small changes in cell volume between the strains are visible. As a lot of data are compared in this analysis, multiple-hypothesis testing is conducted by adjusting the alpha-value with the Benjamini-Hochberg procedure (Benjamini and Hochberg, 1995). As a result, only a few differences in cell volume are significant.

The most dominant increase in cell volume is observable for the hemizygous double deletion of *abf2Δ* and *rpo41Δ,* in both media. Interestingly, no other hemizygous deletion strain results in any significant difference to wild type when cultured in fermentable SCD media. On the other hand, when cultured in non-fermentable SCGE media, more hemizygous deletion strains show significant differences to wild type regarding their cell volume. Interestingly, especially the diploid strains containing a hemizygous deletion of *rpo41Δ* or *hmi1Δ* show deviating results to wild type in SCGE. In contrast to the hemizygous deletion combination of *rpo41Δ* with *abf2Δ*, the combination with *mip1Δ,* as well as the hemizygous triple deletion of *abf2Δ mip1Δ* and *rpo41Δ*, result in significantly smaller cell volumes when measured in SCGE. These small changes could be linked to the relation between Rpo41 and Mip1: It is known that Rpo41 is the mitochondrial RNA-polymerase, which is stabilized by Mtf1 and synthesizes primers for mitochondrial replication (Sanchez-Sandoval *et al.*, 2015). Its role of priming Mip1 could explain the smaller cell volume upon hemizygous deletion of both of the genes: As the mitochondrial DNA- and RNA-polymerase are reduced, it can be assumed that the replication as well as transcription are limited. Due to low mitochondrial protein levels, this could ultimately also lead to reduced ATP-levels, potentially resulting in a smaller cell volume. Moreover, the diploid hemizygous triple deletion of *abf2Δ mip1Δ* and *mtf1Δ* shows significantly higher cell volumes when cultured in SCGE media. As mentioned before, Mtf1 stabilizes Rpo41 for mitochondrial transcription (Sanchez-Sandoval *et al.*, 2015), which might be a reason for the observed phenotype.

As already mentioned, the diploid hemizygous double deletions of *hmi1Δ* in combination with *abf2Δ* or *mip1Δ* show significantly bigger cell volumes for cells cultured in non-fermentable SCGE media. Studies revealed that a deletion of *HMI1* causes the formation of long concatemeric mtDNA, which is related to a decreased number of nucleoids in ρ^0-yeast cells (Sedman *et al.*, 2005). They also showed that mutations in *HMI1* lead to fragmented mtDNA (Sedman *et al.*, 2005). This allows speculations about the hemizygous *hmi1Δ*-deletions possibly leading to disrupted nucleoid to network ratios, causing problems in the mtDNA regulation that are accompanied by increased cell volumes.

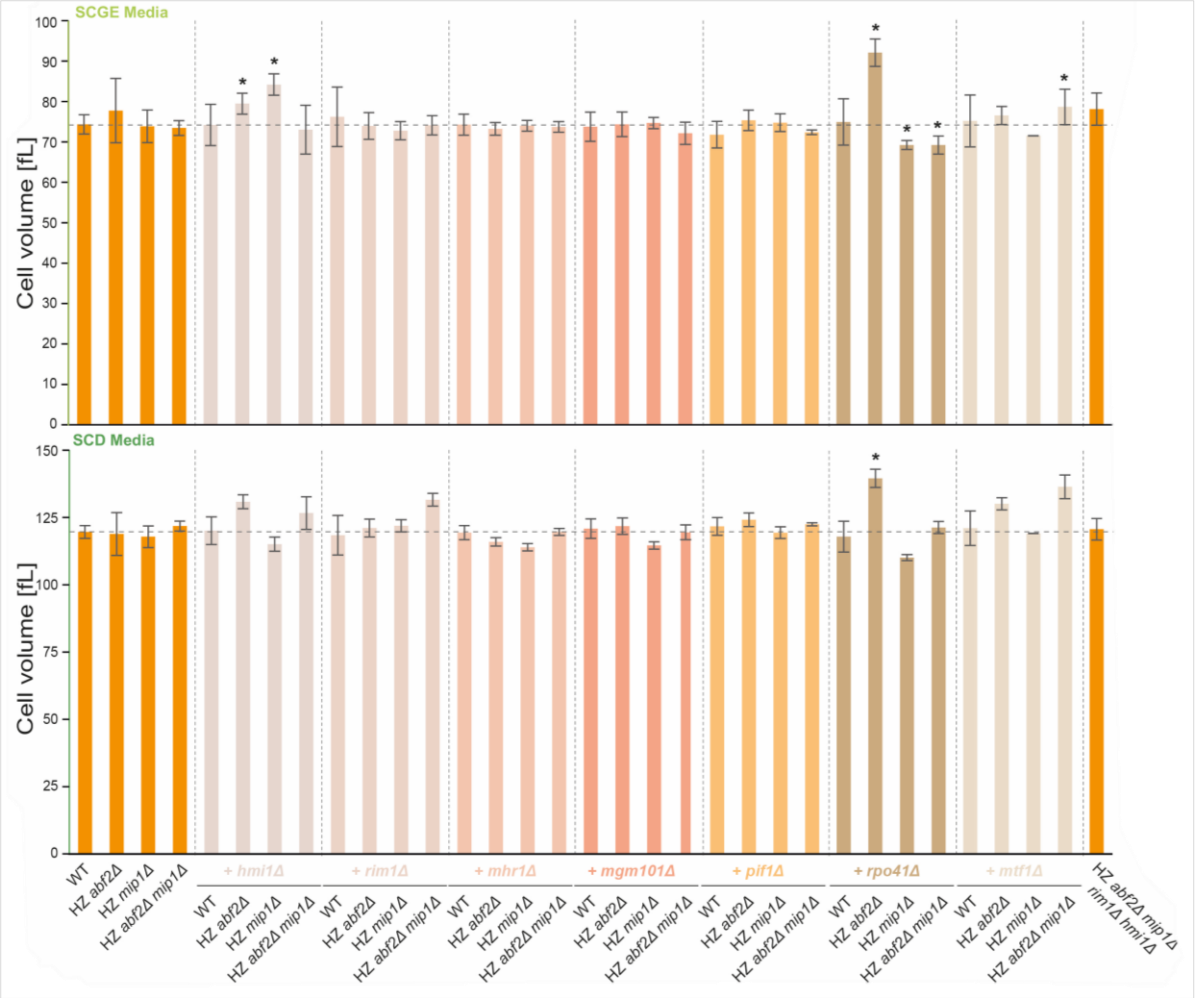

Figure 38: Comparison of cell volumes for diploid strains grown in SCGE or SCD. Cell volume in fL measured by Coulter counter. The bars indicate the mean values, calculated based on at least three replicates. Error bars indicate the standard deviation. Statistical significances were calculated by two-tailed two-handed t-test against the wild type including multiple-hypothesis testing by Benjamini-Hochberg-correction. If no symbol is given, no significant effect was obtained, whereas * indicates significantly different results. Diploid strains include all combinations of hemizygous single, double and triple deletions as well as diploid wild type and quadruple deletion of *abf2*, *mip1*, *rim1* and *hmi1*. Chart separated into growth in non-fermentable SCGE media (top) and fermentable SCD media (bottom).

Interestingly, when comparing the cell volumes of the haploid strains containing variable additions to wild type (Figure 39), only one strain shows significantly different cell volumes after the Benjamini-Hochberg-correction for multiple-hypothesis testing: The strain with an additional copy of *ABF2* and *HMI1* results in significantly higher cell volumes when cultured in fermentable SCD media. No significant difference is observed for any strain when cultured in non-fermentable SCGE media.

Generally, no big difference in cell volume compared to wild type was observed in both media. It also has to be highlighted that no significant difference was shown for any of the thirteen selected strains for detailed phenotyping (see chapter 3.4.), confirming the previously shown result in SCGE media (Figure 28) also to be true in SCD media (Figures 38 and 39).

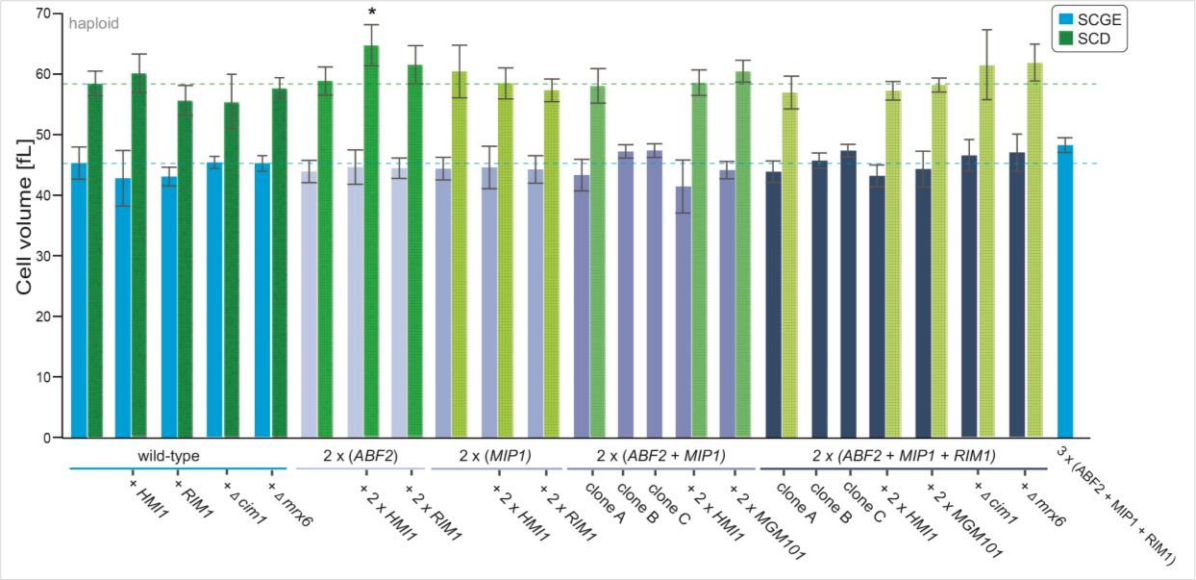

Figure 39: Comparison of cell volumes for haploid strains grown in SCGE or SCD. Cell volume in fL measured by Coulter counter. The bars indicate the mean values, calculated based on at least three replicates. Error bars indicate the standard deviation. Statistical significances were calculated by two-tailed two-handed t-test against the wild type including multiple-hypothesis testing by Benjamini-Hochberg-correction. If no symbol is given, no significant effect was obtained, whereas * indicates significantly different results. Haploid strains include combinations of different single, double or triple additions as well as the haploid wild type and the triple triple addition strain. Strains grown in non-fermentable SCGE media (left; blue) and fermentable SCD media (right; green).

3.6.2. Only mild differences in nDNA copy number per cell to wild type when growing in fermentable and non-fermentable media

Another characteristic that had to be tested was the nDNA copy number, which is quantified by bud counts using a microscope by two individual scientists. This is a common method in the field to measure the cell cycle status. As for the cell volume comparison (see chapter 3.6.1.), a multiple-hypothesis testing was performed by adjusting the alpha-value with the Benjamini-Hochberg procedure (Benjamini and Hochberg, 1995). When comparing the nDNA copy number per cell (Figure 40), no strain showed a significantly different nDNA copy number per cell when cultured in non-fermentable SCGE media. When cultured in fermentable SCD media, only four strains have to be mentioned to show minor significantly higher nDNA copies per cell: The diploid hemizygous single deletion of *mip1Δ*, the hemizygous double deletion of *abf2Δ hmi1Δ*, as well as the two hemizygous triple deletions of *abf2Δ* and *mip1Δ* in combination with *hmi1Δ* or *mgm101Δ*.

All in all, no big differences in nDNA copy number per cell could be observed in fermentable or non-fermentable media. Importantly, the thirteen strains selected for detailed phenotyping (see chapter 3.4.) show wild-type-like copy numbers of nDNA per cell, which confirms the previously shown phenotype measured in SCGE media (see Figure 28) also to be true in SCD media (Figure 40).

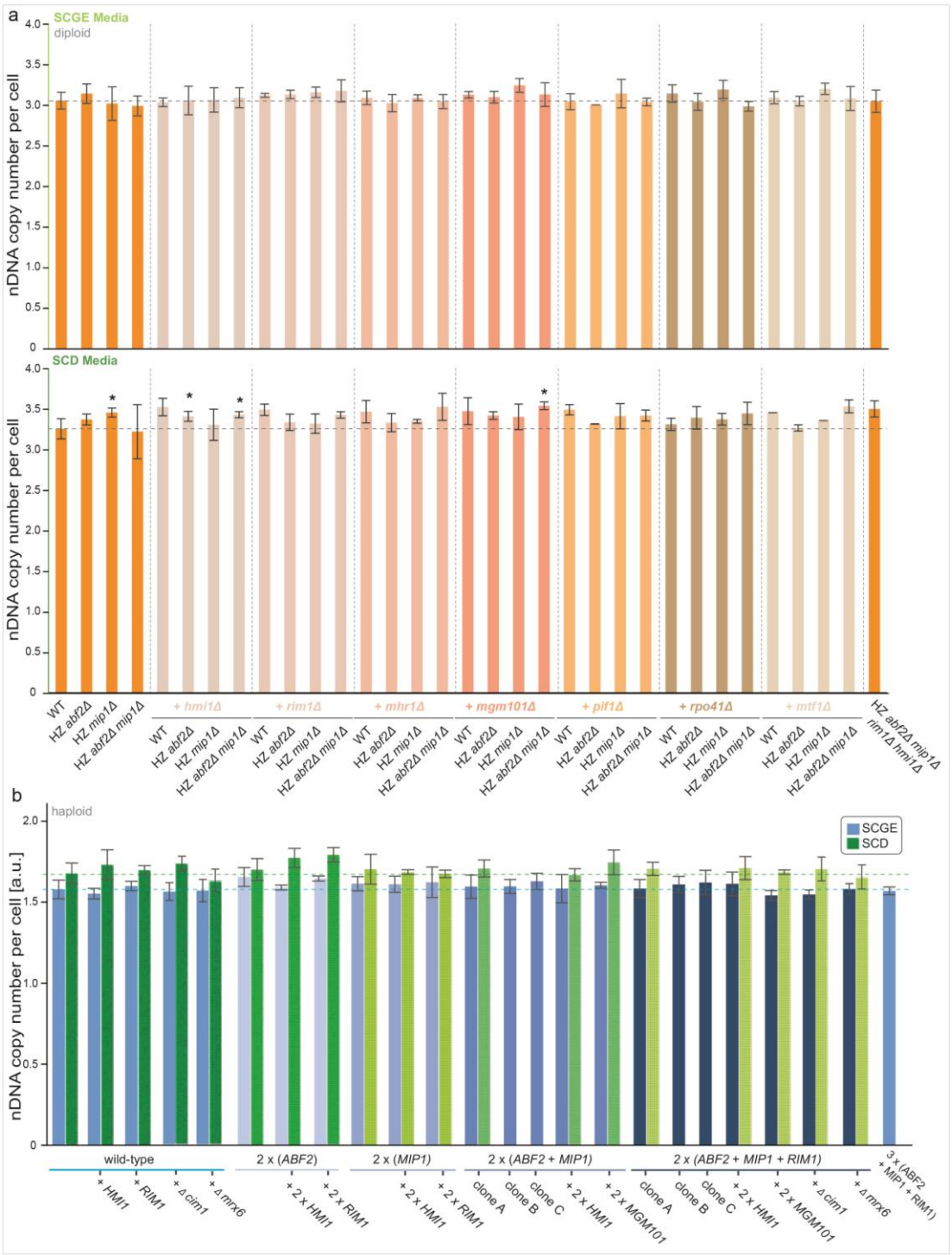

Figure 40: Comparison of nDNA copy number per cell for strains gown in SCGE or SCD. nDNA copy number per cell for selected strains measured by visual inspection ("Bud counts") with the use of a microscope. The bars indicate the mean values, calculated based on at least three replicates. Error bars indicate the standard deviation. Statistical significances were calculated by two-tailed two-handed t-test against the wild type including multiple-hypothesis testing by Benjamini-Hochberg-correction. If no symbol is given, no significant effect was obtained, whereas * indicates significantly different results. **a)** Diploid strains include all combinations of hemizygous single, double and triple deletion as well as diploid wild type and quadruple deletion of *abf2*, *mip1*, *rim1* and *hmi1*. Chart separated into growth in non-fermentable SCGE media (top) and fermentable SCD media (bottom). **b)** Haploid strains include combinations of different single, double or triple additions as well as haploid wild type and triple triple addition strain. Strains grown in non-fermentable SCGE media (left; blue) and fermentable SCD media (right; green).

3.6.3. The limiting machinery influences mtDNA copy number independent of growth media

Of course, the focus of this study still remains on the mtDNA concentration of the 13 strains selected for detailed analysis (see chapter 3.4.). Comparing the mtDNA concentration of each strain measured in SCGE with the mtDNA concentration measured in SCD, only small changes between the fold-changes are observed (Figure 41). Generally, the same trend of mtDNA concentration normalized on wild type can be observed when culturing the cells in fermentable SCD media, as previously shown for SCGE media (see Figures 41 and 27). This confirms that the limiting machinery (*ABF2*, *MIP1* and *RIM1*) influences mtDNA copy number without changing the cell volume or nDNA copy number, independently of whether the cells grow on SCGE or SCD media.

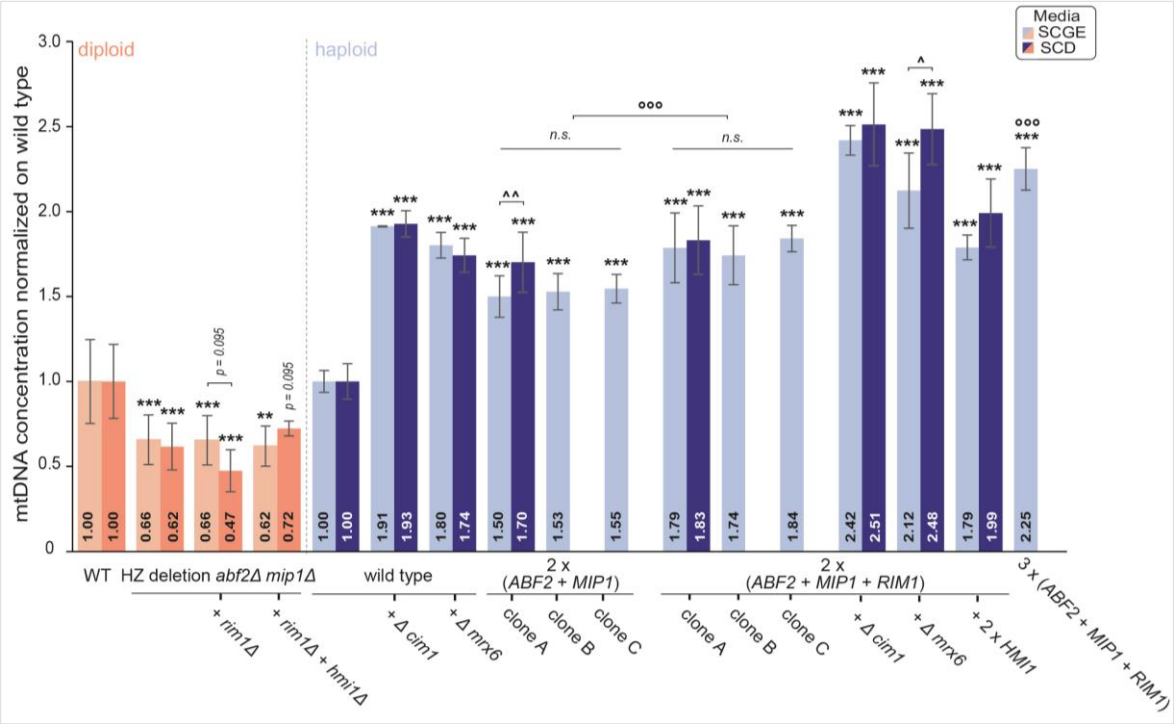

Figure 41: Comparison of mtDNA concentration normalized on the corresponding wild type for strains grown in SCGE or SCD. mtDNA concentration normalized on corresponding wild type measured by qPCR. The bars indicate the mean values, calculated based on at least three replicates. Error bars indicate the standard deviation. Statistical significances were calculated using a two-tailed two-handed t-tests against the corresponding wild type and if no symbol is given, no significant effect was obtained. Statistical significances are indicated as * for $p < 0.05$, ** for $p < 0.01$ and *** for $p < 0.005$, Statistical significances compared to the background strain are indicated as ° for $p < 0.05$, °° for $p < 0.01$ and °°° for $p < 0.005$ and statistical significances comparing the results of both media within one strain are indicated as ^ for $p < 0.05$, ^^ for $p < 0.01$ and ^^^ for $p < 0.005$. Strains were grown in non-fermentable SCGE media (left; light color) and fermentable SCD media (right; dark color). Diploid strains include wild type, hemizygous double deletion of *abf2* and *mip1,* hemizygous triple deletion of *abf2, mip1* and *rim1* and hemizygous quadruple deletion of *abf2, mip1, rim1* and *hmi1* (orange), Haploid strains include wild type, 3 individual clones A-C of double addition strains including one additional copy of *ABF2* and *MIP1*, 3 individual clones A-C of triple addition strains with one additional copy of *ABF2, MIP1* and *RIM1*, triple addition strain with one additional copy of *ABF2, MIP1* and *RIM1* including *cim1*-deletion or *mrx6*-deletion, quadruple addition strain with one additional copy of *ABF2, MIP1, RIM1* and *HMI1,* triple triple addition strain including two additional copies of *ABF2, MIP1* and *RIM1* (blue).

3.6.4. Faster cell growth in yeast with increasing mtDNA concentration is specific to SCGE media

One of the major findings of the experiments for phenotyping in SCGE was a faster growth rate for yeast with increasing mtDNA (see chapter 3.4.2.). To check whether this is also true when culturing the strains in fermentable media, the OD_{600}-measurements and the competition assays were repeated in SCD media. For time reasons, only clone A of the double and triple additions were included and the triple triple addition strain was not included in the OD-measurements for media comparison.

As shown in Figure 42a, none of the diploid or haploid strains showed a significantly different doubling time compared to wild type. Again, the *cim1Δ*- and *mrx6Δ*-deletion strains were tested to check their doubling time. Additionally, the deletions were introduced into the triple addition strain to observe possible additive effects. No significant changes were observed for any of the mutants, comparing their doubling time to wild type (Figure 42b), but the *mrx6Δ*-deletion showed slightly higher doubling times in both backgrounds. This could again be explained by the difference between the two strains in obtaining increased transcription of mtDNA-encoded genes, which was observable for the *cim1Δ*-deletion but not for the *mrx6Δ*-deletion (Schrott and Osman, 2023).

To confirm the absence of a difference in cell growth when culturing the strains in fermentable media, a competition assay was performed for the haploid strains. This was done by quantifying the fraction of the strain in a defined mixture with the corresponding reference strain (including the identical corrections of auxotrophic markers) over time. When culturing the strains in SCGE media, the double and triple addition strains, as well as the triple addition strain containing a *cim1Δ*-deletion, were able to outcompete their reference strain within approximately 100 hours (Figures 29 and 36). Repeating this experiment in SCD, as shown in Figure 42c to 42f, gave very inconsistent results overall. However, it is clearly visible that those three strains were not able to outcompete the reference strain at the same pace as in SCGE media. This confirms the result of the OD-measurement that the strains containing higher mtDNA concentrations do not grow that much faster than the wild type, as they do in SCGE media.

All in all, the results indicate that cells with increasing mtDNA concentrations do not grow faster when they are facing glucose as a carbon source. This could be explained by the fact that their energy production is mainly based on fermentation when being cultured in SCD, where mtDNA is not needed (Turcotte *et al.*, 2010). By contrast, culturing the strains in non-fermentable SCGE media requires mitochondria and their DNA to generate ATP (Ephrussi and Slonimski, 1955). In SCGE, higher concentrations of mtDNA might therefore lead to increased amounts of ATP, which could be the reason for the faster growth rate (Figures 29 and 36).

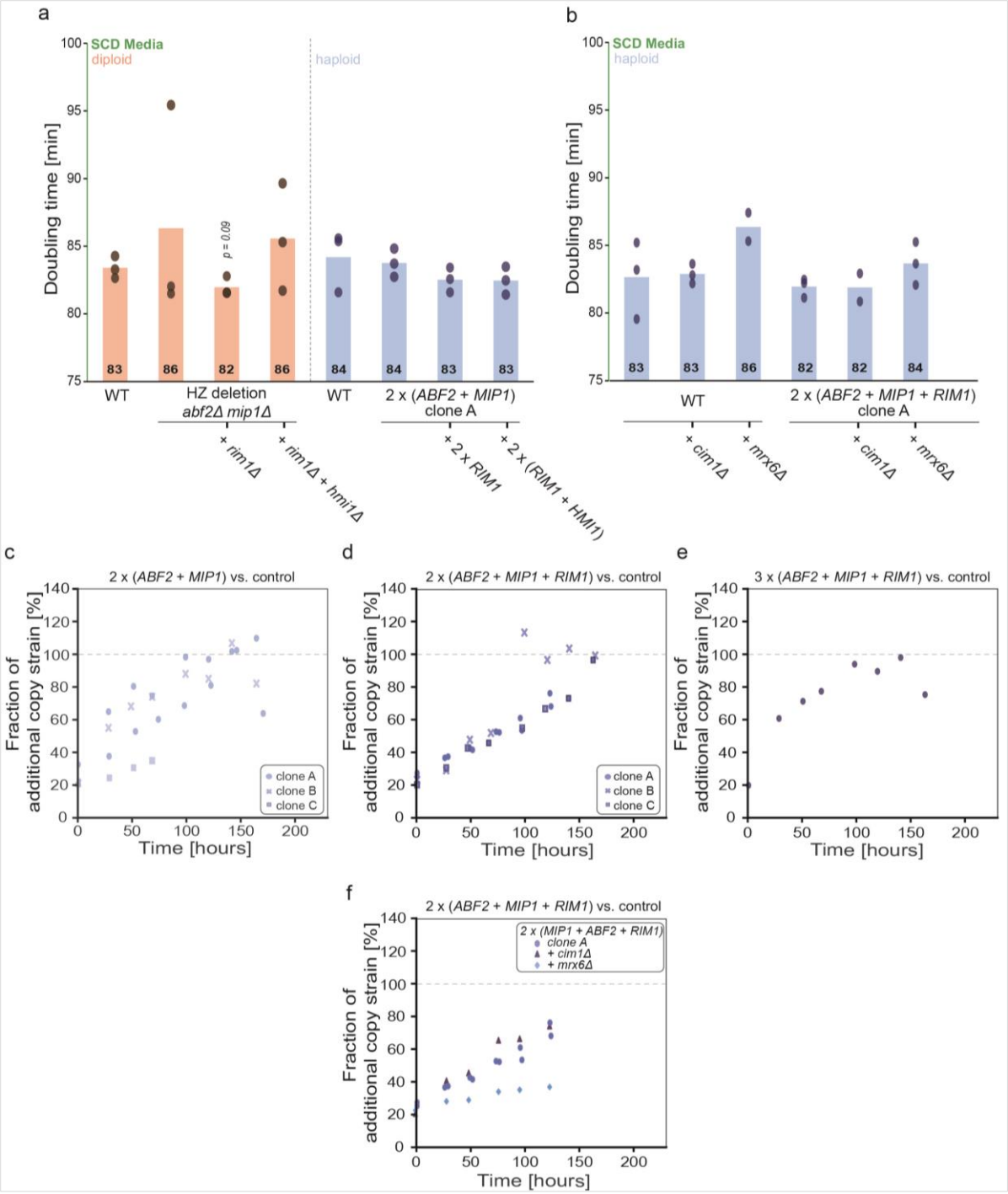

Figure 42: Cell growth in SCD media at 30 °C. a-b) Doubling time in minutes calculated through the slope of a time course of optical density at 600 nm. The bars indicate the mean values, calculated based on at least three replicates. Individual replicates are shown as dots. Statistical significances were calculated using a two-tailed two-handed t-tests and if no symbol is given, no significant effect was obtained. Statistical significances compared to wild type are indicated as * for $p < 0.05$, ** for $p < 0.01$ and *** for $p < 0.005$. **a)** Diploid strains include wild type, hemizygous double deletion of *abf2* and *mip1,* hemizygous triple deletion of *abf2, mip1* and *rim1* and hemizygous quadruple deletion of *abf2, mip1, rim1* and *hmi1* (left; orange), Haploid strains include wild type, double addition strain including one additional copy of *ABF2* and *MIP1* clone A, triple addition strain with one additional copy of *ABF2, MIP1* and *RIM1* clones A, quadruple addition strain with one additional copy of *ABF2, MIP1, RIM1* and *HMI1* (right; blue). **b)** Haploid wild type and the wild type including *cim1Δ*-deletion or *mrx6Δ*-deletion, triple addition strain and the triple addition strain including *cim1Δ*-deletion or *mrx6Δ*-deletion.**c-f)** Fraction of the additional

copy strain (percent) as a function of time (hours) measured in fermentable SCD media during a competithe tion assay using qPCR (with *AMPR*- and *ACT1*-Primers) for **c)** the double addition strains against reference strain (corrected auxotrophic markers: *TRP1*, *URA3*). Clone A (dot), clone B (cross) and clone C (square). **d)** the triple addition strains against thereference strain (corrected auxotrophic markers: *TRP1*, *URA3*, *LEU2*). Clone A (dot), clone B (cross) and clone C (square). **e)** the triple triple addition strains against reference strain (corrected auxotrophic markers: *TRP1, URA3, LEU2, HIS3*). **f)** the triple addition strain clone A (dot) and the triple addition strain including *cim1Δ*-deletion (triangle) or *mrx6Δ*-deletion (diamond).

3.6.5. No notable phenotype in strains with mild mtDNA concentration changes when grown in fermentable media

Summing up, the SCD results confirm the three factors that limit mtDNA to be *ABF2*, *MIP1* and *RIM1* (Figure 41). The changes in mtDNA copy number achieved through deletion or addition of this nuclear-encoded machinery did not lead to major changes in cell volume or nDNA copy number per cell (Figures 38 to 40). While increasing mtDNA concentrations leads to faster cell growth in SCGE media (Figures 29 and 36), no growth advantage can be observed when culturing the strains in SCD media (Figure 42), likely because mtDNA is not required in fermentable media.

3.7. Single-cell analysis partially confirms previous experiments

After several phenotyping experiments mainly focusing on bulk level (Chapter 3.4.), additional experiments on single-cell level were performed. This should give insights about possible heterogeneous subpopulations within a strain, as well as answer the question of whether the observed phenotypes could be co-dependent. It is known that petite cells grow slower (Ephrussi B, Hottinguer H, Tavlitzki J., 1949), and as the frequency of petite colonies is mtDNA-dependent (Figure 35), they could affect the doubling time when measured in bulk experiments. Cells lacking functional mtDNA (petites) are unable to grow in SCGE but can survive in fermentable media as SCD (Ephrussi and Slonimski, 1955). The slower growth of the petites when growing in SCD media could influence the mean doubling time, potentially making it impossible to see a slightly faster cell growth of the ρ^+-cells. Further insights are therefore obtained by microscopy experiments on single-cell level. Additionally, the experiments are conducted to receive more information about the cell morphology and cell cycle phase lengths. The first experiment was performed in SCGE media, while the second experiment was performed in SCD media and included a switch to a low-glucose minimal media. This aims to answer the question of the potential co-dependency as well as analyze the strains in another stress condition on a single-cell level.

3.7.1. Single-cell analysis of steady-state growth in SCGE confirms bulk experiment results

The time-lapse microscopy was performed using a customized microfluidic device (Kukhtevich *et al.*, 2022), which traps the cells in dedicated chambers with the possibility of constant growth media supply. The strains were grown at steady-state growth in SCGE, which excludes potential cell growth of petite cells, for the complete experiment. After analysis of the data using Cell ACDC (Padovani *et al.*, 2022), and a variety of information, such as the cell volume, cell growth or budding can be evaluated for multiple cell cycles.

First of all, the cell volumes were compared (Figure 43a). Generally, as expected, the diploid cells are bigger than the haploids. The single-cell analysis also makes it possible to distinguish between mother and daughter cells. Consistent with previous knowledge (Hartwell and Unger, 1977), the cells divide unequally, with mothers being approximately twice as big as their daughters', consistently throughout the strains (Figure 43a). Comparing the haploid strains, there is no major difference regarding their cell volumes for both mothers and daughters. Consistent with the bulk-experiment (Figure 28), the quadruple deletion strain is bigger than the diploid wild type, especially when comparing mother cells.

Next, the cell cycle length was analyzed. By defining the time of division, as well as bud emergence, the G1-phase was distinguished from the rest of the cell cycle stages (S/G2/M-phase). As expected (Hartwell and Unger, 1977), the daughter cells show longer cell cycles than the mother cells (Figure 43b). This can mainly be explained by the longer G1-phase of the daughters (Hartwell and Unger, 1977; Johnston *et al.*, 1977; Di Talia *et al.*, 2009). When comparing the diploid mother cells to their wild type, the deletion strains show a slightly longer cell cycle of a few minutes, confirming the documented results of this thesis (Figure 29). Also, the quadruple deletion again shows the highest variability of the strains. Regarding the haploid strains, the results in Figure 43b validate the faster growth rate of the triple addition strain compared to wild type in both mother and daughter cells. Moreover, it can be noted that the faster cell cycle length is based on a faster G1-phase as well as a faster S/G2/M-phase. For the double addition strain, both mother and daughter cells show a slightly faster G1-phase but

also a slightly longer S/G2/M-phase length, resulting in a comparable total cell cycle length to wild type.

All in all, the single-cell analysis confirmed the previous results of cells cultured in non-fermentable media (Figures 28 and 29). It has to be noted that the quadruple deletion strain consistently appears to have a high variability, indicating difficulties based on the multiple deletions. The OD-measurements (Figure 29a), the competition assays (Figure 29b and c) and the time-lapse single-cell analysis of the cells (Figure 43b) growing in SCGE media demonstrate a slightly faster growth rate with increasing mtDNA concentrations.

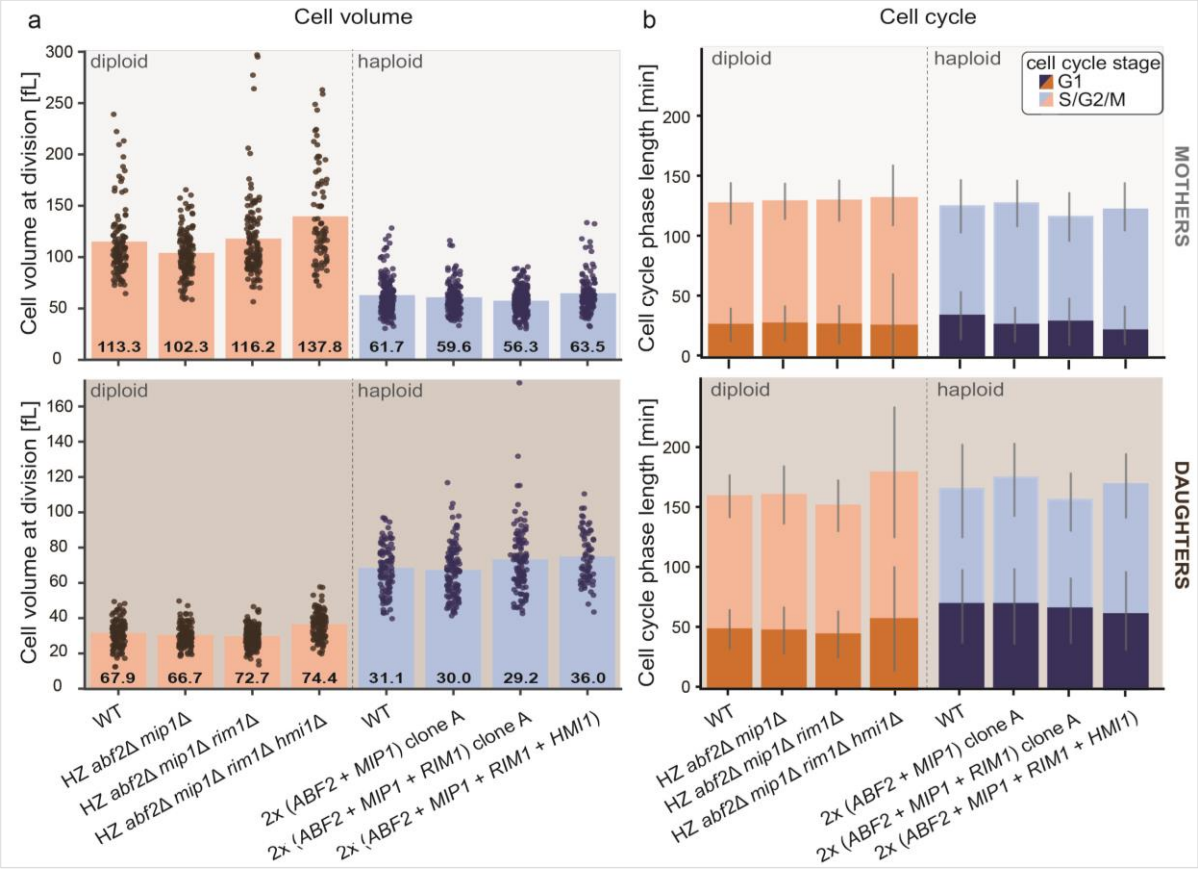

Figure 43: Single cell analysis by microscopy for steady state growth in SCGE. Strains were cultured in filtered non-fermentable SCGE media and grown in steady state under the microscope. Imaging with a frame rate of 3 minutes for 10 hours and evaluation of the resulting videos with Cell-ACDC allows detailed single cell analysis. Diploid strains include wild type, hemizygous double deletion of *abf2* and *mip1,* hemizygous triple deletion of *abf2, mip1* and *rim1* and hemizygous quadruple deletion of *abf2, mip1, rim1* and *hmi1* (left; orange), Haploid strains include wild type, double addition strain including one additional copy of *ABF2* and *MIP1* clone A, triple addition strain with one additional copy of *ABF2, MIP1* and *RIM1* clones A, quadruple addition strain with one additional copy of *ABF2, MIP1, RIM1* and *HMI1* (right; blue). The chart is separated into two rows representing the mother cells (top; light grey) or daughter cells (bottom; light brown) and into two columns. The columns are **a)** Cell volume at the time of division of mother and bud in fL; The bars indicate the mean values, calculated based on at least three replicates. Individual replicates are shown as dots. and **b)** Length of the cell cycle stage in minutes, distinguishing between G1-phase (dark colour) and S/G2/M-phase (light colour). The bars indicate the mean values, calculated based on at least three replicates. Error bars indicate the standard deviation.

3.7.2. Changing mtDNA concentrations lead to a mild phenotype in low-glucose-minimal-media switch experiment

By testing the response of the strains to low glucose stress, the aim of the next experiment was to track potential limitations of cells with aberrant mtDNA concentrations. The experiment was based on the idea that applying stress in a glucose-based media, such as SCD, could lead to difficulties when excessive mtDNA concentrations are present. Understanding the behavior in strains with reduced mtDNA concentrations could additionally give insights into the need for defined mtDNA concentrations. The experiment was done using the same time-lapse microscopy setup as described before (see chapter 3.7.1.). However, the difference was that the cells were cultured in SCD media for the first two hours of microscopy. Afterwards, the media was switched to a minimal media containing low glucose concentrations. In addition to the 0.5 % glucose and 0.95% sorbitol, the minimal media was supplemented with 1 % of each of the four amino acids that were used as markers during the transformation for some of the strains. This aims to eliminate potential advantages due to the auxotrophic marker corrections. As the second media takes around 30 minutes until it is distributed into the chambers completely, the switch time point for downstream analysis was set to 2.5 hours. While analyzing the switch-experiment, the cells were assigned to different categories, as explained in Figure 44 (adapted from (Chadha *et al.*, 2024b)). First of all, the cells that face the switch are divided into G1- and S/G2/M-switchers, depending on whether they are budding at this time point of the switch or not. The daughter cells that were born during the switch cell cycle are defined as “first daughter cells”.

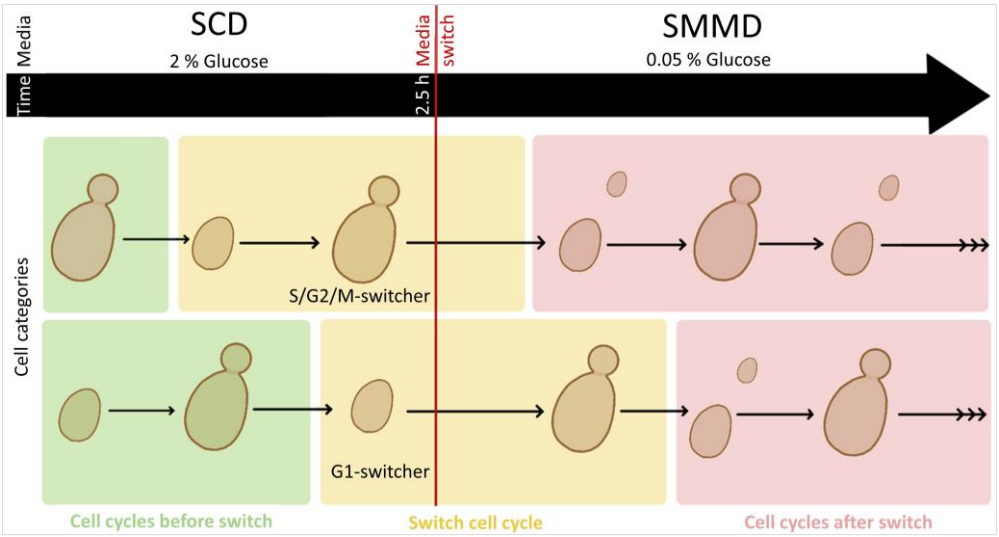

Figure 44: Cell categories of the nutrient switch live-cell microscopy. Taking pictures of the cells every 3 minutes and evaluation of the resulting video via Cell ACDC allows detailed single-cell analysis. Strains were cultured in filtered fermentable SCD media (containing 2% glucose) for the first 2 hours, the media was then switched into minimal SMMD media (containing 0.05% glucose, 0.95% sorbitol, 1% Tryptophan, 1% Histidine, 1% Leucine and 1% Uracil). As the distribution of the second media within the chamber takes approximately 30 minutes, the time of the switch is set to 2.5 hours for downstream analysis. Cell cycles are distinguished into three different parts for downstream analysis: Cell cycle before the switch, where the cells finish their cell cycle stages in SCD media (green), Switch cell cycle, which describes the cell cycle in which the cell faces the switch from SCD into SMMD media (yellow) and cell cycles after the switch (red), where the cells complete their cell cycle completely within the second SMMD media. Also, the cells are categorized into two lines: S/G2/M-switcher describe the cells, which face the switch while they are in S/G2/M-phase (i.e. they have a bud) and G1-switchers are facing the media switch without a bud, indicating to be in G1-phase at this time point. Adapted from (Chadha *et al.*, 2024b).

3.7.2.1. Analysis of the cell cycle before the switch confirms wild-type-like cell growth in SCD media

As mentioned before, the cells were grown in SCD media without any limitation for the first two hours of the experiment. This opens up the possibility of comparing SCD steady-state growth on a single cell level to previous results (Figure 42). Comparing the cell cycle length of the diploid strains to the corresponding wild type, there is nearly no difference for the triple deletion (Figure 45). By contrast, the double deletion strain has the longest cell cycle, with an increase of a few minutes, closely followed by the quadruple deletion strain. Consistent with previous experiment results (Figure 42), the haploid strains show very similar cell cycle lengths in SCD (Figure 45). This again confirms the minor influence of mtDNA concentration on cell growth in glucose-based media.

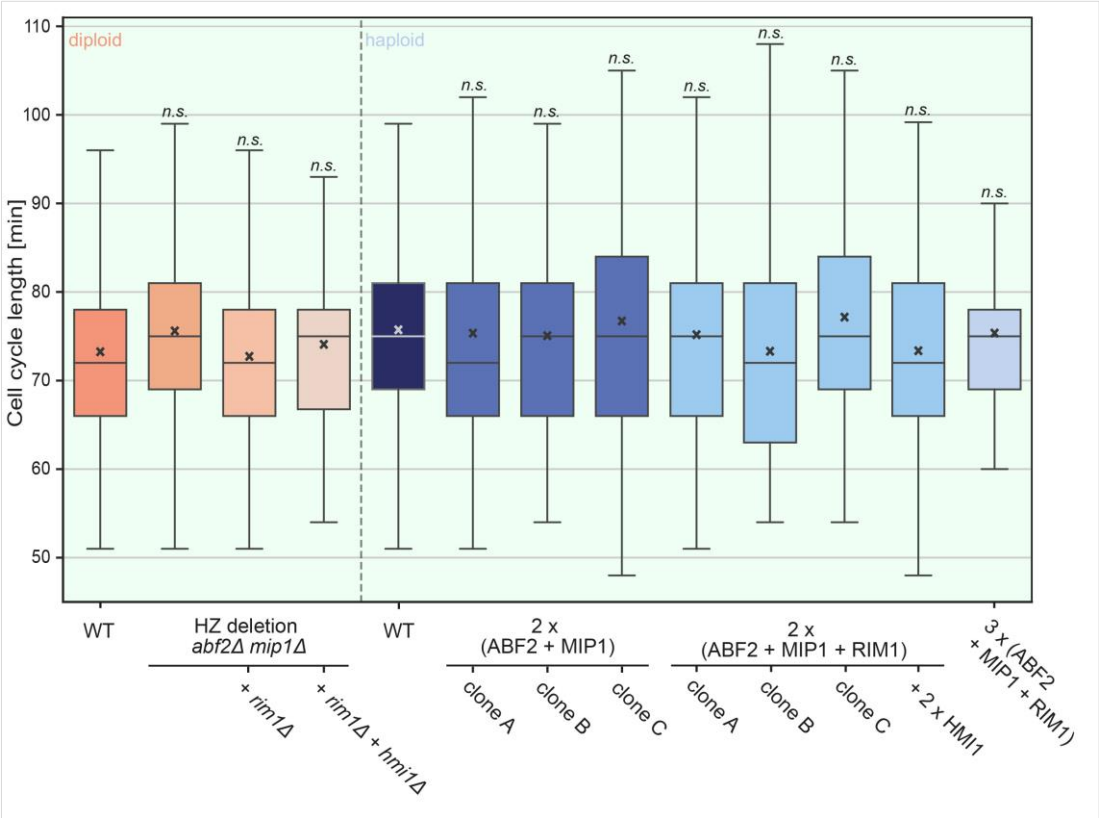

Figure 45: Steady state growth in SCD media on single cell level in nutrient switch experiment for the cell cycle before the switch. Total cell cycle length in minutes in the cell cycles before the switch in fermentable SCD media. Boxplot including the interquartile range (box), total range of data (whisker), median (undashed line inside the box) and mean (cross inside the box). Statistical significances were calculated using a two-tailed two-handed t-tests and no significant effect was obtained for any strain compared to the corresponding wild type. Diploid strains (left; orange) include diploid wild type (96 analyzed cells), hemizygous double deletion of *abf2* and *mip1* (84 analyzed cells), hemizygous triple deletion of *abf2, mip1* and *rim1* (74 analyzed cells) and hemizygous quadruple deletion of *abf2, mip1, rim1* and *hmi1* (46 analyzed cells). Haploid strains (right; blue) include haploid wild type (185 analyzed cells) , 3 individual clones A-C of double addition strains including one additional copy of *ABF2* and *MIP1* (clone A 179 analyzed cells, clone B 95 analyzed cells and C 73 analyzed cells), 3 individual clones A-C of triple addition strains with one additional copy of *ABF2, MIP1* and *RIM1* (clone A 135 analyzed cells ,clone B 78 analyzed cells and C 68 analyzed cells), quadruple addition strain with one additional copy of *ABF2, MIP1, RIM1* and *HMI1* (101 analyzed cells) , triple triple addition strain including two additional copies of *ABF2, MIP1* and *RIM1* (50 analyzed cells).

3.7.2.2. No major cell volume-differences between the strains during low-glucose stress

Next, the switchers were analyzed regarding their cell volumes and phase lengths. Considering only the G1-Switchers, no significant difference regarding the total cell volume of mother and buds can be seen (Figure 46). On the other hand, comparing the S/G2/M-switchers of the haploids by their total cell volumes, especially the cell cycle of the switch has to be highlighted: The double and triple addition strains divide mother and daughter cells at significantly smaller cell volumes compared to wild type, escaping into G1-phase faster. Here, the double additions all show a slightly but not significantly faster S/G2/M-phase, whereas the triple additions even show significantly lower lengths of this cell phase compared to wild type. Within the next cell cycle, these strains are approaching wild type size again. In contrast to these strains, the triple triple addition strain shows higher cell volumes while facing the switch in S/G2/M-phase. This can easily be explained by a generally slightly higher cell volume of this strain, as described before (Figure 28) and also visible already in G1-phase before the switch.

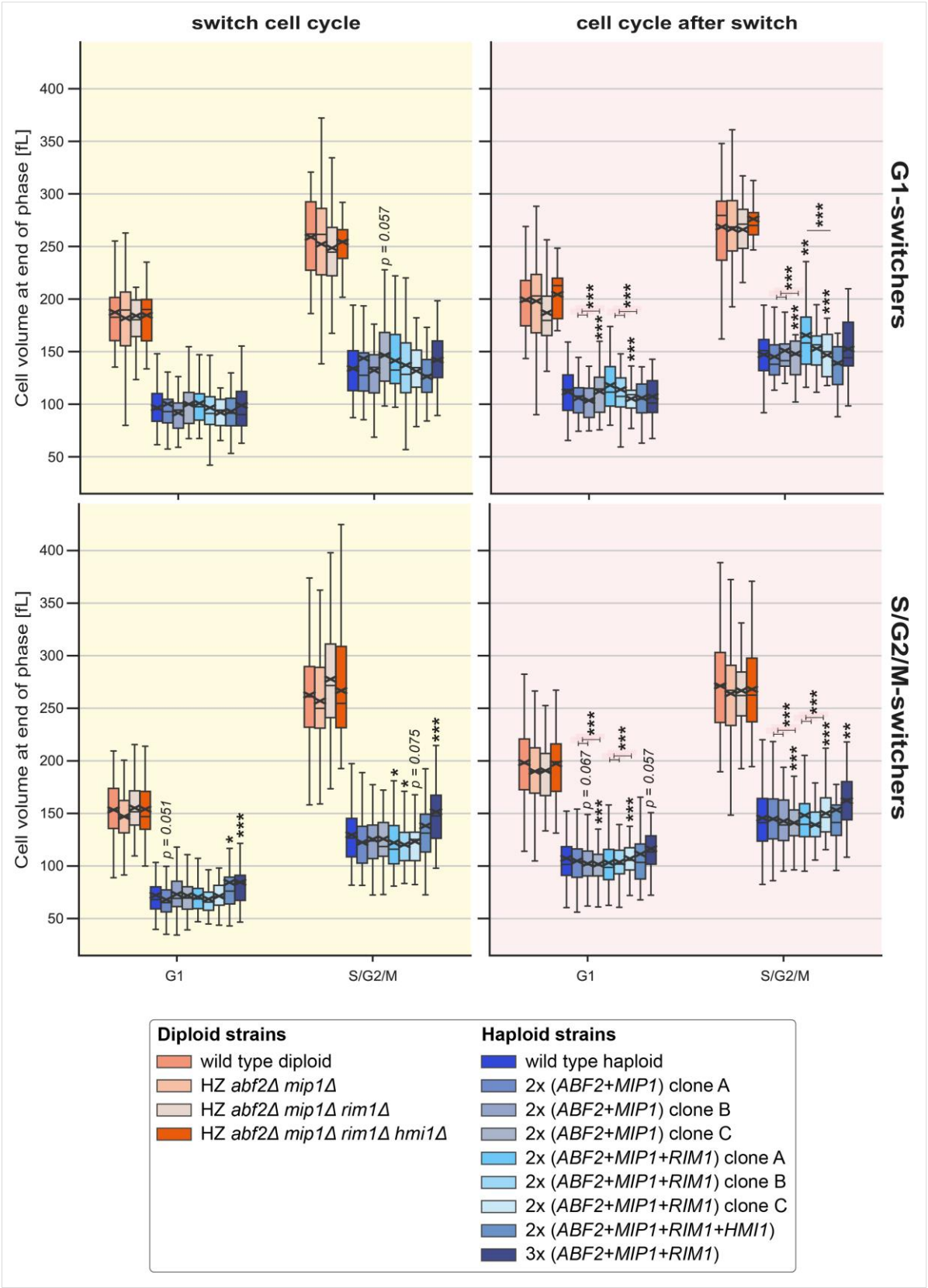

Figure 46: Cell volume at end of phase on single cell level while and after a nutrient switch from SCD into low-glucose SMMD media. Total cell volume of mother and bud at end of the cell cycle phase in fL measured by single-cell microscopy analysis. Boxplot including the interquartile range (box), total range of data (whisker), median (undashed line inside the box) and mean (cross inside the box). Statistical significances were calculated using a two-tailed two-handed t-tests. Statistical significances compared to the corresponding wild type are indicated as * for $p < 0.05$, ** for $p <$

0.01 and *** for p < 0.005. The chart is divided into four parts: G1-switchers at switch cell cycle (upper left; yellow) and cell cycle after the switch (upper right; red) as well as S/G2/M-switchers at switch cell cycle (bottom left; yellow) and cell cycle after the switch (bottom right; red). Number of G1-switchers included: Diploid strains (left; orange) including diploid wild type (32 analyzed cells), hemizygous double deletion of *abf2* and *mip1* (42 analyzed cells), hemizygous triple deletion of *abf2, mip1* and *rim1* (32 analyzed cells) and hemizygous quadruple deletion of *abf2, mip1, rim1* and *hmi1* (14 analyzed cells). Haploid strains (right; blue) including haploid wild type (83 analyzed cells), 3 individual clones A-C of double addition strains including one additional copy of *ABF2* and *MIP1* (clone A 81 analyzed cells, clone B 32 analyzed cells and C 30 analyzed cells), 3 individual clones A-C of triple addition strains with one additional copy of *ABF2, MIP1* and *RIM1* (clone A 65 analyzed cells, clone B 33 analyzed cells and C 24 analyzed cells), quadruple addition strain with one additional copy of *ABF2, MIP1, RIM1* and *HMI1* (44 analyzed cells), triple triple addition strain including two additional copies of *ABF2, MIP1* and *RIM1* (28 analyzed cells). Number S/G2/M-switchers included: Diploid strains (left; orange) including diploid wild type (87 analyzed cells), hemizygous double deletion of *abf2* and *mip1* (76 analyzed cells), hemizygous triple deletion of *abf2, mip1* and *rim1* (69 analyzed cells) and hemizygous quadruple deletion of *abf2, mip1, rim1* and *hmi1* (48 analyzed cells). Haploid strains (right; blue) including haploid wild type (155 analyzed cells), 3 individual clones A-C of double addition strains including one additional copy of *ABF2* and *MIP1* (clone A 152 analyzed cells, clone B 78 analyzed cells and C 69 analyzed cells), 3 individual clones A-C of triple addition strains with one additional copy of *ABF2, MIP1* and *RIM1* (clone A 107 analyzed cells, clone B 63 analyzed cells and C 62 analyzed cells), quadruple addition strain with one additional copy of *ABF2, MIP1, RIM1* and *HMI1* (75 analyzed cells), triple triple addition strain including two additional copies of *ABF2, MIP1* and *RIM1* (47 analyzed cells).

3.7.2.3. Increasing mtDNA concentrations as a disadvantage for overcoming low-glucose stress

Another quantified aspect was the phase length of each cell cycle stage of both kinds of switchers. Consistent with a previous study (Chadha *et al.*, 2024b), the length of the cell cycle stage in which the switch appears is increased, as the strains need to adapt to the new media. The phase length of the following cell cycle stages already reflects the strains' behavior in the new media. Here, the diploid G1-switchers did not show any significant differences between the strains, but it has to be noted that there is a tendency for shorter G1-phases with decreasing mtDNA concentrations (Figure 47). If the same strains face the switch during S/G2/M-phase, a similar and significant trend can be observed for the directly following G1-phase. In both the switch and after-switch S/G2/M-phases, there is no change in cell cycle length for the double and triple deletion strains compared to wild type. The quadruple deletion strain stays significantly longer in the switch-S/G2/M-phase when compared to wild type.

Comparing the haploid strains with increased mtDNA concentrations to wild type shows mild extensions of the switch cell cycle stage when facing the switch during G1-phase (Figure 47). With the following cell cycle phases, they overcome this disadvantage, leading to the slightly faster cell growth than wild type. By contrast, the haploid S/G2/M-switchers show various behaviors: While the double and triple addition strains behave similarly to wild type, the triple triple addition strain shows a longer S/G2/M-phase than wild type during the switch. The subsequently shorter G1-phase seems to help the strain to overcome the stress, resulting in a wild-type-like S/G2/M-phase afterwards.

When comparing the same genotypes of double or triple addition, a variation between the three clones is visible (Figure 47): for both cell volumes and phase lengths, clone C often shows significantly different results than clones A and B. As no changes on the genome level are known, further analysis of expression levels for RNA and proteins or genome sequencing needs to be done to understand their differences.

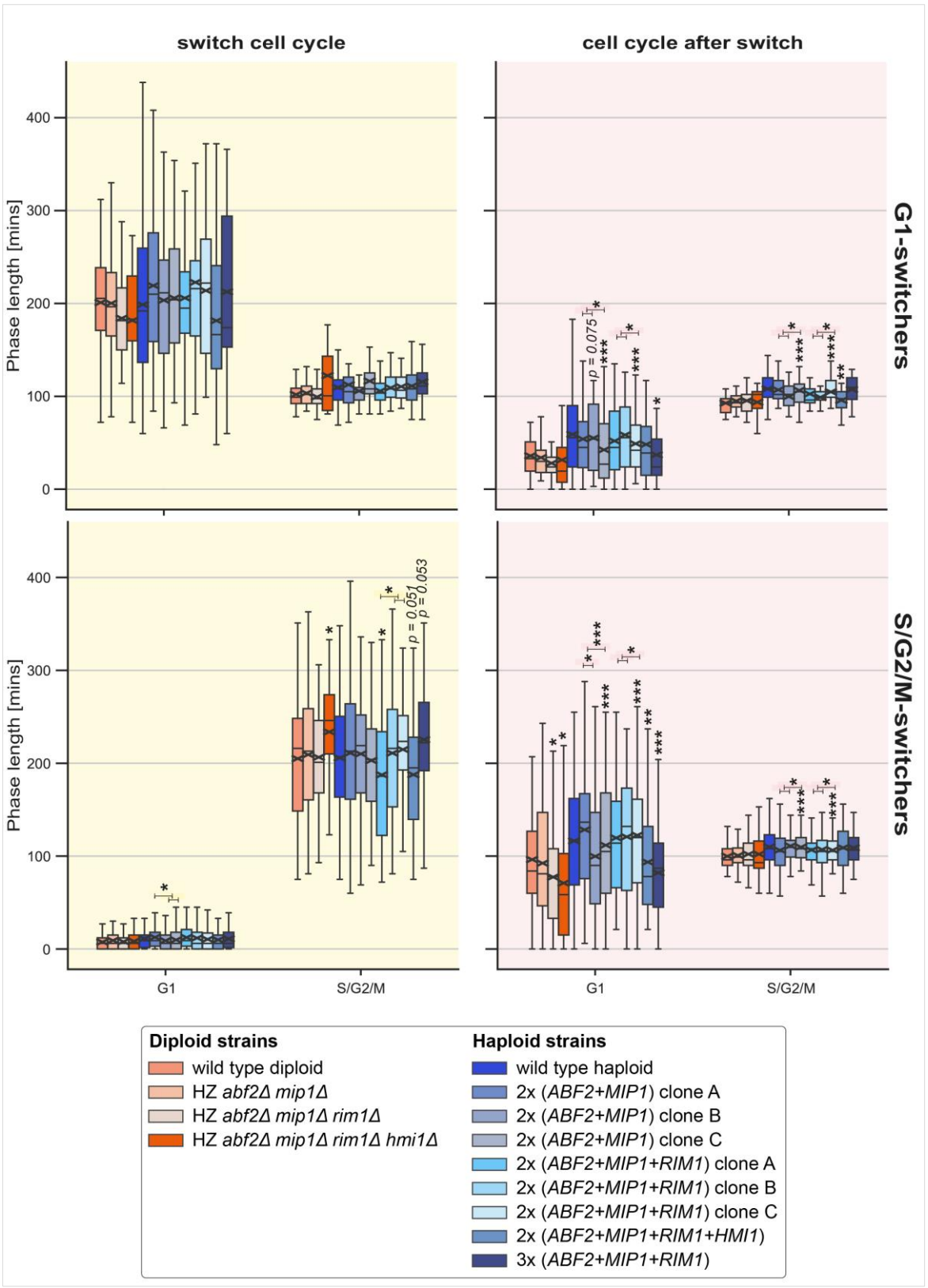

Figure 47: Cell cycle phase length on single cell level during and after a nutrient switch from SCD into low-glucose SMMD media. Length of cell cycle phase in minutes measured by single-cell microscopy analysis. Boxplot including the interquartile range (box), total range of data (whisker), median (undashed line inside the box) and mean (cross inside the box). Statistical significances were calculated using a two-tailed two-handed t-tests. Statistical significances compared to the corresponding wild type are indicated as * for $p < 0.05$, ** for $p < 0.01$ and *** for $p < 0.005$. The

chart is divided into four parts: G1-switchers at switch cell cycle (upper left; yellow) and cell cycle after the switch (upper right; red) as well as S/G2/M-switchers at switch cell cycle (bottom left; yellow) and cell cycle after the switch (bottom right; red). Number of G1-switchers included: Diploid strains (left; orange) including diploid wild type (32 analyzed cells), hemizygous double deletion of *abf2* and *mip1* (42 analyzed cells), hemizygous triple deletion of *abf2, mip1* and *rim1* (32 analyzed cells) and hemizygous quadruple deletion of *abf2, mip1, rim1* and *hmi1* (14 analyzed cells). Haploid strains (right; blue) including haploid wild type (83 analyzed cells), 3 individual clones A-C of double addition strains including one additional copy of *ABF2* and *MIP1* (clone A 81 analyzed cells, clone B 32 analyzed cells and C 30 analyzed cells), 3 individual clones A-C of triple addition strains with one additional copy of *ABF2, MIP1* and *RIM1* (clone A 65 analyzed cells, clone B 33 analyzed cells and C 24 analyzed cells), quadruple addition strain with one additional copy of *ABF2, MIP1, RIM1* and *HMI1* (44 analyzed cells), triple triple addition strain including two additional copies of *ABF2, MIP1* and *RIM1* (28 analyzed cells). Number S/G2/M-switchers included: Diploid strains (left; orange) including diploid wild type (87 analyzed cells), hemizygous double deletion of *abf2* and *mip1* (76 analyzed cells), hemizygous triple deletion of *abf2, mip1* and *rim1* (69 analyzed cells) and hemizygous quadruple deletion of *abf2, mip1, rim1* and *hmi1* (48 analyzed cells). Haploid strains (right; blue) including haploid wild type (155 analyzed cells), 3 individual clones A-C of double addition strains including one additional copy of *ABF2* and *MIP1* (clone A 152 analyzed cells, clone B 78 analyzed cells and C 69 analyzed cells), 3 individual clones A-C of triple addition strains with one additional copy of *ABF2, MIP1* and *RIM1* (clone A 107 analyzed cells, clone B 63 analyzed cells and C 62 analyzed cells), quadruple addition strain with one additional copy of *ABF2, MIP1, RIM1* and *HMI1* (75 analyzed cells), triple triple addition strain including two additional copies of *ABF2, MIP1* and *RIM1* (47 analyzed cells).

3.7.2.4. Higher amount of abnormal shaped buds when cells are facing the nutrient-switch with deviating mtDNA copy number

During the analysis of the time-lapse microscopy experiments, some special buds stood out as their shape appeared different from normal. After a closer look, it became clear that these buds all faced the switch as buds smaller than 26 fL and were therefore in early S/G2/M-phase together with their mothers. Generally, all buds that emerged shortly before the switch stop growing while adapting to the new media. However, it seems like some of them are unable to simply continue to grow afterwards. Those buds do not increase their cell volume by expansion as normally, but they seem to form a second bud on top of themselves. This ends up in different and abnormal shapes as shown in an exemplary picture in Figure 48a. The cells keep this shape throughout their entire life and can form normally shaped buds again.

It turned out that the frequency of those abnormally formed buds was increased in the strains with misregulated mtDNA concentration (Figure 48b). Both the haploid and diploid wild type also show this phenomenon in around 15 % of the small buds that face the switch. Misregulated mtDNA concentrations lead to an increase in abnormal bud formation, even higher than 20%. Curious about these abnormalities, the abnormal and normal buds that face the switch were compared regarding their cell volume as well as switch-cycle-length (Figure 48c). The cell volume of mother and bud did not result in any significant difference between normal and abnormal buds. This indicates that their shape is divergent, but their cell volume still stays constant, suggesting no bigger difficulties in cell size control. More interestingly, independent of the strain, the abnormal buds have all shown an increased length of their switch-S/G2/M-phase. This implies that those buds struggle more to adapt to the new media in order to continue to grow and are then missing the information about their previously formed shape. This observation needs to be studied more carefully to better understand the relationship between mtDNA copy number and bud formation, especially in low-glucose stress.

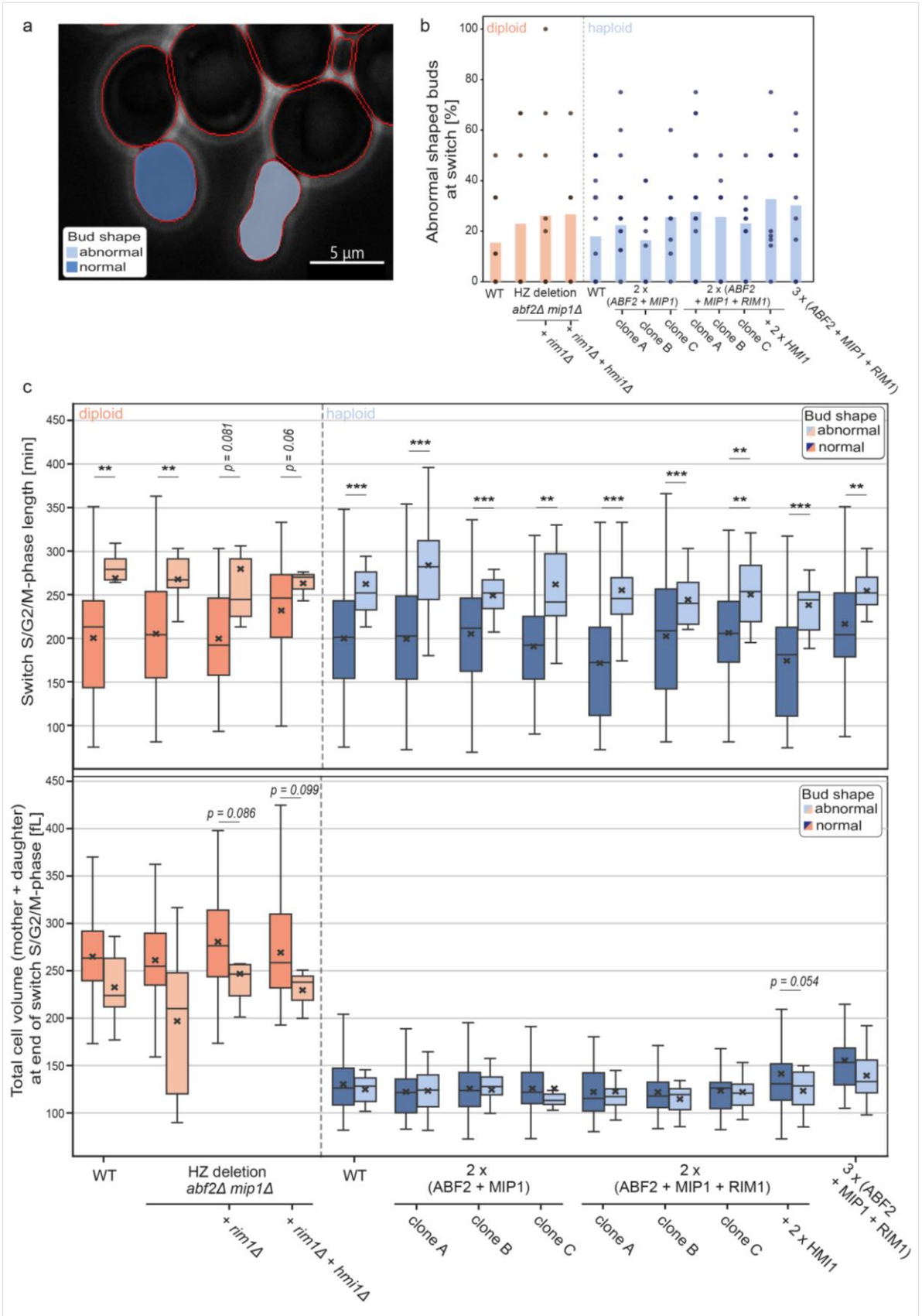
a
Bud shape
abnormal
normal
5 µm
b
diploid
haploid
Abnormal shaped buds at switch [%]
WT
HZ deletion abf2Δ mip1Δ
+ rim1Δ
+ rim1Δ + hmi1Δ
WT
2 x (ABF2 + MIP1)
clone A
clone B
clone C
2 x (ABF2 + MIP1 + RIM1)
clone A
clone B
clone C
+ 2 x HMI1
3 x (ABF2 + MIP1 + RIM1)
c
diploid
haploid
Bud shape
abnormal
normal
Switch S/G2/M-phase length [min]
p = 0.081
p = 0.06
Total cell volume (mother + daughter) at end of switch S/G2/M-phase [fL]
p = 0.099
p = 0.086
p = 0.054
WT
HZ deletion abf2Δ mip1Δ
+ rim1Δ
+ rim1Δ + hmi1Δ
WT
2 x (ABF2 + MIP1)
clone A
clone B
clone C
2 x (ABF2 + MIP1 + RIM1)
clone A
clone B
clone C
+ 2 x HMI1
3 x (ABF2 + MIP1 + RIM1)

Figure 48: Bud shape of S/G2/M-switchers with buds smaller than 26 fL while facing the switch from SCD into low-glucose SMMD media. a) Exemplary picture of a normal shaped bud (dark blue) and an abnormal bud formation (light blue) taken from the switch experiment of the double addition strain clone A. The scale bar represents 5 µm. **b-d)** Abnormal and normal bud shapes were identified for S/G2/M-switchers, whose buds are smaller than 26 fL at the time of the nutrient switch. Number of buds included: Diploid strains (left; orange) including diploid wild type (43 analyzed cells), hemizygous double deletion of *abf2* and *mip1* (29 analyzed cells), hemizygous triple deletion of *abf2, mip1* and *rim1* (28 analyzed cells) and hemizygous quadruple deletion of *abf2, mip1, rim1* and *hmi1* (17 analyzed cells). Haploid strains (right; blue) including haploid wild type (98 analyzed cells), 3 individual clones A-C of double addition strains including one additional copy of *ABF2* and *MIP1* (clone A 108 analyzed cells, clone B 57 analyzed cells and C 49 analyzed cells), 3 individual clones A-C of triple addition strains with one additional copy of *ABF2, MIP1* and *RIM1* (clone A 64 analyzed cells, clone B 47 analyzed cells and C 48 analyzed cells), quadruple addition strain with one additional copy of *ABF2, MIP1, RIM1* and *HMI1* (52 analyzed cells), triple triple addition strain including two additional copies of *ABF2, MIP1* and *RIM1* (30 analyzed cells). **b)** the percentage of abnormal shaped buds per buds at switch with bud volumes < 26 fL for diploid hemizygous deletions (orange) and haploid additional copy strains (blue). Bars indicate the mean frequency of abnormal bud shapes across all replicates and dots represent the frequency of abnormal bud shapes for each individual replicate. **c)** Length of S/G2/M-phase of the switch distinguishing between normal shaped buds (dark) and abnormal shaped buds (light). Boxplot including the interquartile range (box), total range of data (whisker), median (undashed line inside the box) and mean (cross inside the box). Statistical significances were calculated using a two-tailed two-handed t-tests. Statistical significances comparing the two different bud types of one strain are indicated as * for $p < 0.05$, ** for $p < 0.01$ and *** for $p < 0.005$. **d)** Total cell volume of the bud including its mother at the end of the switch distinguishing between normal shaped buds (dark) and abnormal shaped buds (light). Boxplot including the interquartile range (box), total range of data (whisker), median (undashed line inside the box) and mean (cross inside the box). Statistical significances were calculated using a two-tailed two-handed t-tests. Statistical significances comparing the two different bud types of one strain are indicated as * for $p < 0.05$, ** for $p < 0.01$ and *** for $p < 0.005$.

3.7.3. Aging experiments reveal clone variability

Mitochondrial function is also known to influence aging (Azbarova and Knorre, 2023), which motivated aging experiments to reveal a potential dependence on mtDNA concentrations. While replicative aging tracks the number of daughters one cell can form until it stops budding (Mortimer and Johnston, 1959), chronological aging reflects the survival rate of a cell population over time in stress conditions (Longo *et al.*, 1996; Longo and Fabrizio, 2012).

3.7.3.1. Chronological aging reveals the advantage of high mtDNA concentrations in some strains

To analyze the chronological aging with increasing mtDNA concentrations, the haploid strains were cultured in YPD until exponential growth and then transferred into water. Theoretically, after the residuals of glucose in the cells have been completely fermented into ethanol, the cells switch into respiration (Ephrussi and Slonimski, 1955; Ben Galeota-Sprung *et al.*, 2022). During respiration, the low amounts of ethanol are converted into acetic acid, which has a toxic impact on the cells (Guaragnella and Bettiga, 2021). When comparing the strains' viability, it becomes clear that there is no difference between wild type and the double addition strains (Figure 49a). The three clones of the double addition strains show only very small differences from each other. By contrast, the three clones of the triple addition strains show different behaviors, which makes it impossible to draw a final mtDNA concentration-dependent conclusion (Figure 49b). Nevertheless, it seems like the triple addition clone A and triple triple addition strain are advantageous for the strain's survival in the first 50 hours, but there is no difference anymore when culturing for longer times (Figure 49b). A potentially related observation in the proteomics data (see chapter 3.8.) of these strains cultured in SCGE has to be mentioned: These two strains with advantageous phenotypes show high levels of the kinase Sch9 (Figure 49c), which is reported to influence the G1/S-transition (Chadha *et al.*, 2024a) and is related to aging (Caligaris *et al.*, 2023). However, whether and how this explains the beneficial phenotype remains unclear and requires further analysis.

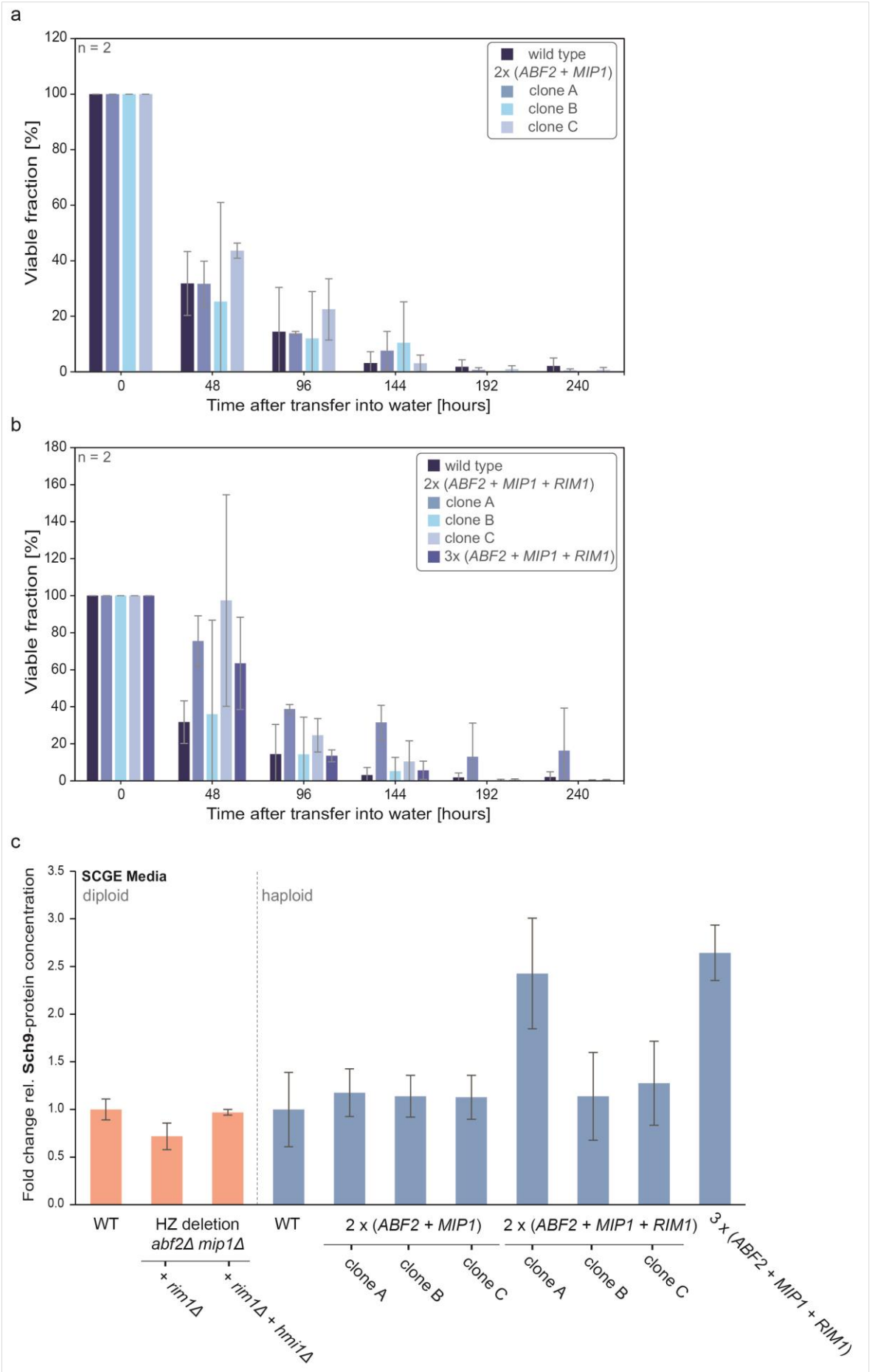
a
n = 2
wild type
2x (ABF2 + MIP1)
clone A
clone B
clone C
Viable fraction [%]
Time after transfer into water [hours]
b
n = 2
wild type
2x (ABF2 + MIP1 + RIM1)
clone A
clone B
clone C
3x (ABF2 + MIP1 + RIM1)
Viable fraction [%]
Time after transfer into water [hours]
c
SCGE Media
diploid
haploid
Fold change rel. Sch9-protein concentration
WT
HZ deletion
abf2Δ mip1Δ
+ rim1Δ
+ rim1Δ + hmi1Δ
WT
2 x (ABF2 + MIP1)
clone A
clone B
clone C
2 x (ABF2 + MIP1 + RIM1)
clone A
clone B
clone C
3 x (ABF2 + MIP1 + RIM1)

Figure 49: Chronological aging experiment showing viable fraction in water over time. a-b) Viable fraction of the culture (percentage) as a function of time after transfer into water (hours), indicating chronological aging/ survival in water over time. The bars indicate the mean values, calculated based on two replicates. Error bars indicate the standard deviation. Haploid strains measured simultaneously but plotted separately: **a)** haploid wild type, 3 individual clones A-C of double addition strain including one additional copy of *ABF2* and *MIP1*. **b)** haploid wild type, 3 individual clones A-C of triple addition strain with one additional copy of *ABF2, MIP1* and *RIM1*, triple triple addition strain with two additional copies of *ABF2, MIP1* and *RIM1.* **c)** Fold change of relative protein concentration of Sch9 measured by mass spectrometry. The bars indicate the mean values normalized on the corresponding wild type and error bars show the standard deviation. Diploid strains include wild type, hemizygous double deletion of *abf2* and *mip1* and hemizygous triple deletion of *abf2, mip1* and *rim1* (orange), Haploid strains include wild type, 3 individual clones A-C of double addition strains including one additional copy of *ABF2* and *MIP1*, 3 individual clones A-C of triple addition strains with one additional copy of *ABF2, MIP1* and *RIM1* and triple triple addition strain including two additional copies of *ABF2, MIP1* and *RIM1* (blue).

3.7.3.2. Increased mtDNA concentrations result in reduced replicative life span and increased frequency of misregulated cell formation

Replicative life span is reported to be reduced in *mip1Δ*-deletion strains (Caballero *et al.*, 2011) as well as increased in *rim1Δ*-deletion strains (McCormick *et al.*, 2015). This motivates the analysis of replicative life span in strains with increased mtDNA concentrations achieved by additional copies of the limiting machinery.

The analysis of replicative aging was done in cooperation with Jurgita Paukštytė from the Saarikangas Lab of the University of Helsinki in Finland. In this experiment, each cell is measured individually by counting and detaching the buds that are formed until the analyzed cell is dead (Paukštytė *et al.*, 2023). In the first replicate, the wild type, the double addition clone A, the triple addition clone A and a strain with a *mrx6Δ*-deletion were analyzed. When comparing the results (Figure 50a), it becomes clear that for the double and triple addition strain, the probability of survival is shorter as the median life span is reduced by approximately 25% compared to wild type. By contrast, the *mrx6Δ*-deletion shows a very similar time-dependent decrease of survival and median lifespan to wild type. This indicates that only a functional increase in mtDNA copy number leads to a reduced replicative aging phenotype. One of the most well-known proteins influencing replicative aging is Sir2 (Kaeberlein et al., 1999), a NAD+-dependent histone deacetylase (Imai et al., 2000), whose deletion leads to a 50% reduction in median lifespan in replicative aging (Kaeberlein *et al.*, 1999). As this is a commonly used reference strain, a second replicate including a *sir2Δ*-deletion strain was conducted. Additionally, a *sir2Δ*-deletion was introduced into the triple addition strain to test possible supplementary genetic interactions or changes in the replicative life span. In the second experiment, these two strains were tested together with the haploid wild type and the triple addition strain (clone A). As shown in Figure 50b, the 25 % reduced life span of the triple addition strain was confirmed. As expected, the *sir2Δ*-deletion strain resulted in a 50% reduced life span. The triple addition strain containing a *sir2Δ*-deletion shows the same time-dependent decrease in survival as the *sir2Δ*-deletion strain. This indicates that there is no additional effect of mtDNA concentration on replicative aging when cells are lacking *SIR2*.

While analyzing the strains' replicative life span, Jurgita Paukštytė noticed an interesting abnormality (Figure 50c): Some of the cells formed elongated buds, which in some strains occurred more often than in the wild type. While the wild type cells appear in an abnormal cell shape in approximately 25% of the cases, especially in older cells, the additional copy strains

showed abnormal cell formations in more than twice as many cases with approximately 60% probability. This indicates that there is a higher chance of misformation with increasing mtDNA concentrations. The *mrx6Δ*-deletion cells, which include increased mtDNA copy numbers (Figure 51) but no increase in mitochondrial RNA-levels (Schrott and Osman, 2023), showed a frequency of abnormal cell shapes similar to wild type (Figure 50c). This indicates that only an increase of functional mtDNA copy numbers, which have a transcriptional effect, enhances the probability of cell misformation. Surprisingly, the *sir2Δ*-deletion cells showed reduced levels of abnormal cell formations with about a fifth as many as wild type. When analyzing the mtDNA concentration of this strain, it showed similar values to wild type (Figure 51). The *sir2Δ*-deletion in the triple addition strain, which leads to an approximately 130% higher mtDNA concentration than wild type (Figure 51), also causes a higher chance for incorrect cell shapes (Figure 50c). For both background strains, the wild type and the triple addition strain, the *sir2Δ*-deletion decreases the probability of mis-shaped buds independently of the mtDNA copy number. All in all, this leads to the assumption that two factors are influencing the formation of elongated buds: With increasing functional mtDNA copy numbers, the frequency of abnormal cell shape increases, while the deletion of *SIR2* leads to a decreased frequency of this phenomenon.

The observation of abnormal bud shapes can be linked to the two different aging pathways in replicative aging leading to cell death (Jin *et al.*, 2019): Cells that face pathway A are described by a loss of chromatin silencing and show more or less constant cell cycle lengths. In particular, these cells give birth to elongated daughter cells within their last cell cycles (Azbarova and Knorre, 2023). By contrast, cells that face aging through pathway B form round daughter cells until the end, show increased cell cycle lengths, and are associated with mitochondrial dysfunction (Azbarova and Knorre, 2023) through a heme deficiency (Atamna *et al.*, 2002; Li *et al.*, 2020). Applying this knowledge to the results shown here (Figure 50c), it can be speculated that in cells with higher amounts of the mtDNA-limiting machinery, the frequency of cells aging through pathway A, including a loss of chromatin silencing, is increased. This might be explainable by a lower chance of mitochondrial deficiency in the cells (Pathway B) for cells with higher mtDNA concentrations. For a better understanding of the phenomenon, further analysis is needed.

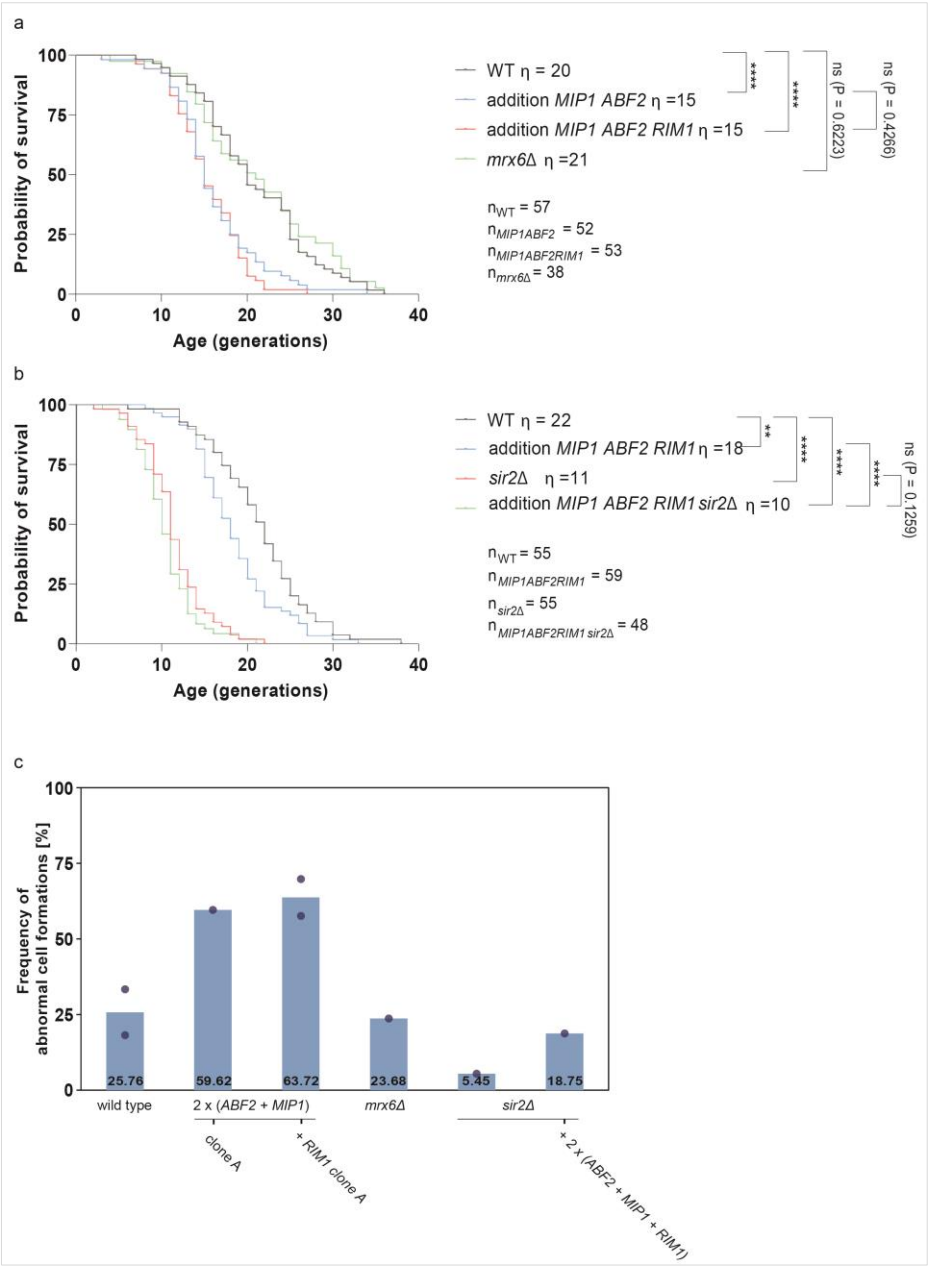

Figure 50: Replicative aging experiment showing the probability of survival and frequency of abnormal cell formation. Experiments performed by Jurgita Paukštytė (Saarikangas Lab, University of Helsinki, Finland) **a-b)** Probability of survival as a function of generations with η indicating the mean age of survival per strain and n indicating the number of analyzed cells. Statistical significances calculated by log-rank test. Statistical significances compared to wild type are indicated as * for $p < 0.05$, ** for $p < 0.01$, *** for $p < 0.005$ and **** for $p < 0.0001$. The different strains included in the two independent experiments are **a)** haploid wild type (black), double addition including one additional copy of *ABF2* and *MIP1* clone A (blue), triple addition including one additional copy of *ABF2*, *MIP1* and *RIM1* clone A (red) and a *mrx6Δ*-deletion strain (green) and **b)** haploid wild type (black), triple addition including one additional copy of *ABF2*, *MIP1* and *RIM1* clone A (blue), a *sir2Δ*-deletion strain (red) and triple addition strain with one additional copy of *ABF2, MIP1* and *RIM1* including *sir2Δ*-deletion (green). **c)** Frequency (percentage) with which abnormal shaped cells appeared during the replicative aging experiment. The bars indicate the mean values, calculated based on the two replicates (a&b). Individual replicates are shown as dots.

3.7.4. Analysis of *SIR2* downregulation as a cause of aging phenotypes reveals passenger mutations in some strains

To identify a potential mechanism for how increased mtDNA concentrations could lead to increased chronological life span (see 3.7.3.1.) as well as reduced replicative life span (see 3.7.3.2.), additional experiments were performed. Several mechanisms are known to influence yeast longevity (Beach *et al.*, 2015).

As mentioned before, one potential pathway is regulated by Sir2, which inhibits the synthesis of extrachromosomal rDNA circles (ERCs) (Gottlieb and Esposito, 1989). These ERCs are known to be one of the main drivers of replicative aging (Sinclair and Guarente, 1997). Deletion of *SIR2*, as also confirmed by the results in this study (Figure 50b), shortens the replicative life span (Kennedy *et al.*, 1994; Kaeberlein *et al.*, 1999). Sir2 is also contributing to a filtration of more beneficial mitochondria into the bud: Studies have reported an influence of Sir2 on the chaperonin CCT activity. This protein complex helps fold actin, a component of the actin cables, along which the mitochondria are transported into the bud (Liu *et al.*, 2010). A lower Sir2 concentration would therefore lead to lower amounts of native actin, which results in a lower cable flow from the bud into the mother (Higuchi *et al.*, 2013). Subsequently, due to the lower velocity at the actin cables, also the slow-transported oxidized mitochondria with lower quality have time to enter the bud, which leads to a reduced life span (Nyström, 2013).

RT-qPCR was performed to investigate whether *SIR2* is downregulated in the haploid strains with higher mtDNA concentrations. The results showed a downregulation in the double addition strain (clone A) to approximately 50% compared to wild type (Figure 51b). This matches perfectly with the replicative aging results, where it showed around 50% less reduction of life span than the *sir2Δ*-deletion strain (Figure 50b). Additionally, in the triple addition strain (clone A), a reduction of the *SIR2* RNA-concentration of around 40% compared to wild type was observed (Figure 50b). As *sir2Δ*-deletion strains are also reported to show an increased chronological life span (Casatta *et al.*, 2013), this could explain the shown aging phenotypes. The higher chronological aging in *sir2Δ*-deletion strains is explained by a faster extracellular ethanol consumption of the cells and a lower accumulation of acetate in the cells (Casatta *et al.*, 2013). Taking this into account, the clones A of the double and triple addition strains, which showed reduced *SIR2* RNA-concentrations, are expected to show a higher chronological life span. As shown before (Figure 49), clone A of the triple addition strain indeed resulted in an increased chronological life span.

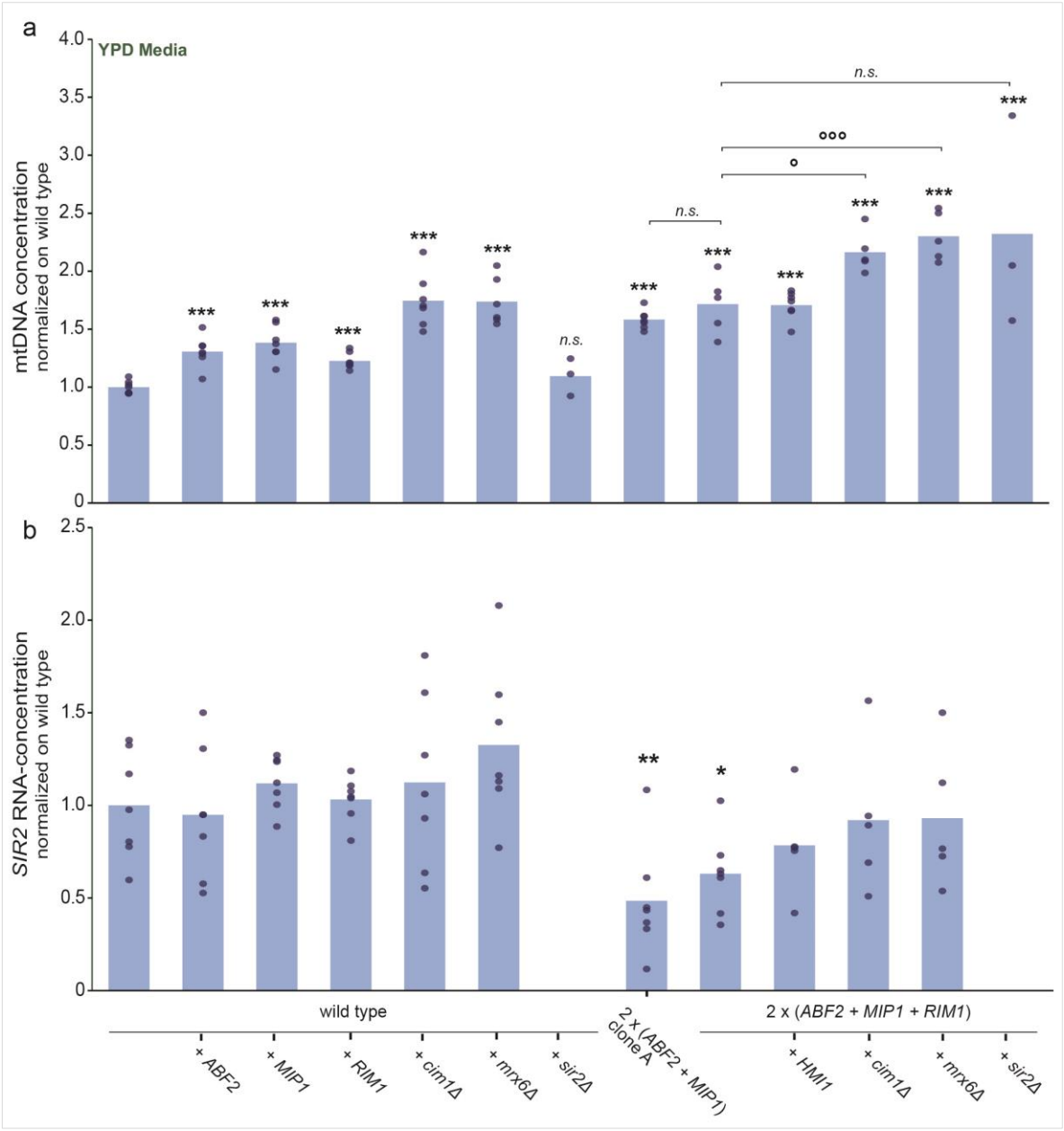

Figure 51: Mitochondrial DNA concentration and *SIR2* RNA-concentration normalized on wild type for selected strains to understand *SIR2*-regulation of haploid strains. Selected strains grown in YPD media were measured via qPCR to understand *SIR2*-regulation in the haploid additional copy strains. The bars indicate the mean values, calculated based on at least five replicates and individual replicates are shown as dots. Statistical significances were calculated using a two-tailed two-handed t-tests. Statistical significances comparing to wild type are indicated as * for $p < 0.05$, ** for $p < 0.01$ and *** for $p < 0.005$. Statistical significances comparing to the background strain are indicated as ° for $p < 0.05$, °° for $p < 0.01$ and °°° for $p < 0.005$. Strains included in the experiment (from left to right): haploid wild type, wild type with one additional copy of *ABF2*, wild type with one additional copy of MIP1, wild type with one additional copy of *RIM1,* wild type including *cim1Δ*-deletion, *mrx6Δ*-deletion or *sir2Δ*-deletion, double addition including one additional copy of *ABF2* and *MIP1* clone A, triple addition including one additional copy of *ABF2*, *MIP1* and *RIM1* clone A, quadruple addition strain with one additional copy of *ABF2, MIP1, RIM1* and *HMI1,* triple addition strain with one additional copy of *ABF2, MIP1* and *RIM1* including *cim1Δ*-deletion, *mrx6Δ*-deletion or *sir2Δ*-deletion. **a)** mtDNA concentration normalized on the haploid wild type and **b)** *SIR2* RNA-concentration normalized on the haploid wild type, measured by qPCR (*SIR2*- and *RDN18*-Primer).

To address whether one of the three genes of the limiting machinery or the mtDNA copy number itself is the reason for the *SIR2* downregulation, the single addition strains, as well as the *cim1Δ*- and *mrx6Δ*-deletion strains, were also included in the analysis. None of the three strains adding the single factors led to a decreased concentration of *SIR2* RNA, excluding each individual factor to be the reason (Figure 51b). Surprisingly, the *cim1Δ*- and *mrx6Δ*-deletion strains, which have mtDNA concentrations comparable to the triple addition strain, also did not show downregulation of *SIR2* RNA (Figure 51b).

After additional literature research, further experiments were planned: Smith describes a huge variability of rDNA copy number as a passenger mutation in lithium acetate transformations in yeast (Smith, 2022). These rDNA copy numbers are known to influence the Sir2 concentration (Kaeberlein *et al.*, 2004) and could therefore be the reason for the observed behavior. To exclude passenger mutations in the strains, the transformation of the double addition strain was repeated in two individual experiments. When measuring the *SIR2* RNA-concentration via RT-qPCR for the three resulting double addition clones when grown in YPD, the random mutation of *SIR2* was confirmed: both new clones B and C did not show the downregulation as measured in clone A (Figure 52). This leads to the conclusion that the identified aging phenotype might be based on a passenger mutation causing reduced *SIR2* RNA-concentrations. Afterwards, two individual triple addition strains were recreated, based on the double addition clones B and C. To rule out an effect on any other previously observed result, nearly all of the experiments were repeated with the new double and triple addition clones B and C, and summarized as described in the previous chapters. As shown, no influence on the major phenotypes (increasing mtDNA concentrations leads to slightly faster cell growth in SCGE (Figure 29) and reduced petite frequency (Figure 35)) was observed.

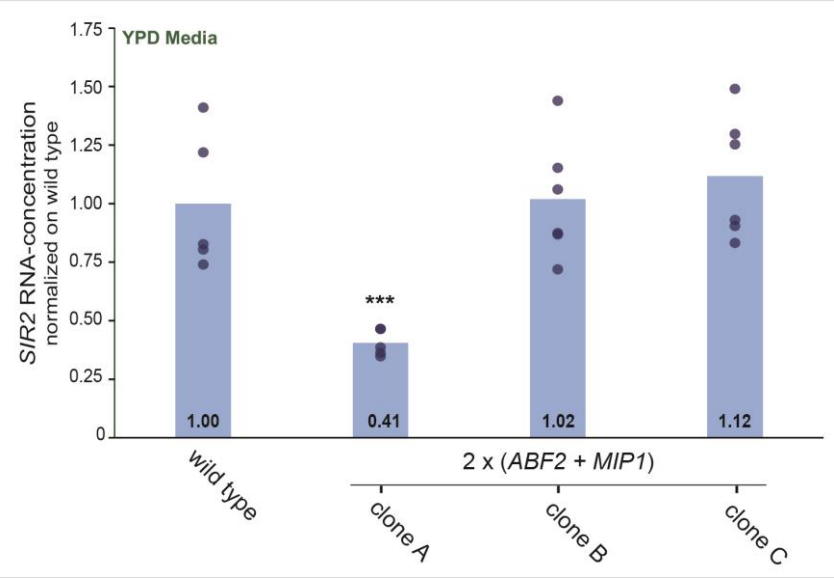

Figure 52: *SIR2* RNA-concentration normalized on wild type for three genomically identical clones created by independent yeast transformations to check for random passenger mutation leading to *SIR2* RNA-downregulation. *SIR2*-RNA-concentration for strains grown in YPD media measured via qPCR (*SIR2*- and *RDN18*-Primers). The bars indicate the mean values, calculated based the six replicates and individual replicates are shown as dots. Statistical significances were calculated using a two-tailed two-handed t-tests. Statistical significances compared to wild type are indicated as * for $p < 0.05$, ** for $p < 0.01$ and *** for $p < 0.005$. Strains included in the experiment (from left to right): haploid wild type and 3 individual clones A-C of double addition including one additional copy of *ABF2* and *MIP1*.

To also check the *SIR2*-RNA level, when culturing the strains in non-fermentable SCGE media, the results of an RNA-Seq analysis were analysed additionally. No differences were shown when comparing the hemizygous deletions, the triple triple addition, as well as clones B and C of the double and triple additions to the appropriate wild type (Figure 53). The double and triple addition clones A again showed a downregulated *SIR2* RNA-concentration, as also shown in YPD media before (Figure 52). Independent of the media, the double addition clone A shows a more drastic downregulation of *SIR2*-RNA than the triple addition clone A (Figures 51 and 53). This observation would suggest a lower replicative aging in the double addition compared to the triple addition of clones A. However, the curves of their replicative aging were exactly the same (Figure 50a). This might hint towards additional pathways influencing replicative aging with increasing mtDNA concentrations.

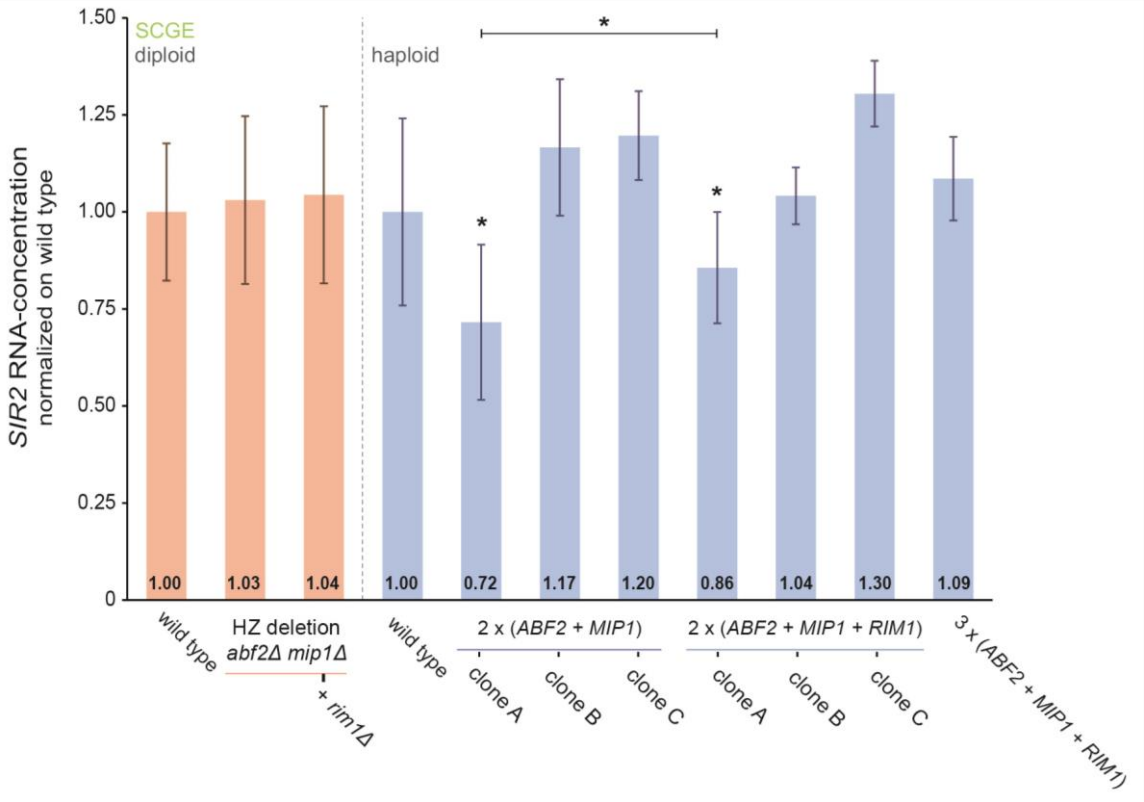

Figure 53: *SIR2* RNA-concentration normalized on wild type for relevant strains cultured in SCGE media. *SIR2* RNA-concentration of strains grown in non-fermentable SCGE media measured via RNA sequencing analysis with the help of Kim Job (Scaldione Lab, Helmholtz Munich, Germany). The bars indicate the mean values normalized on the corresponding wild type, calculated based on at least five replicates and error bars symbolizing the standard deviation. Statistical significances were calculated using a Wald test. Statistical significances are indicated as * for padj < 0.1. Strains included in the experiment (from left to right): Diploid strains (left; orange) including wild type, hemizygous double deletion of *abf2* and *mip1,* hemizygous triple deletion of *abf2, mip1* and *rim1.* Haploid strains (right; blue) including wild type, 3 individual clones A-C of double addition strains including one additional copy of *ABF2* and *MIP1*, 3 individual clones A-C of triple addition strains with one additional copy of *ABF2, MIP1* and *RIM1*, triple triple addition strain including two additional copies of *ABF2, MIP1* and *RIM1.*

A second possible mechanism influencing longevity in budding yeast is the mitochondrial retrograde signaling pathway (Bui and Labedzka-Dmoch, 2024). The two main drivers of this pathway, also known as the minimal binary switch of the retrograde response, are Mks1 and Rtg2 (Ferreira Júnior *et al.*, 2005). When those two proteins are bound to each other, the retrograde pathway is switched on and the two proteins Rtg1 and Rtg3 can bind to each other, then translocate to the nucleus passively and regulate transcription of effector genes (Sekito *et al.*, 2000; Dilova *et al.*, 2002). This way, the retrograde pathway is reported to extend replicative life span (Kirchman *et al.*, 1999; Liu and Butow, 1999). By contrast, if Mks1 is not bound by Rtg2, it gets hyperphosphorylated and binds to Bmh1 or Bmh2, inhibiting the retrograde pathway and reducing the replicative life span (Dilova *et al.*, 2004). Low mitochondrial membrane potential leads to increased Rtg2 levels and a positive retrograde response (Miceli *et al.*, 2011), whereas the binding of ATP to Rtg2 inhibits the Mks1-Rtg2 binding and results in a negative retrograde response (Zhang *et al.*, 2013). A previous study has speculated about a potential role of mtDNA in the retrograde response (Miceli *et al.*, 2011). This seems reasonable, as mtDNA concentrations are also reported to influence the mitochondrial membrane potential (Dilova *et al.*, 2004; Staneva *et al.*, 2023). Interestingly, the mass spectrometry data generated in this study (see chapter 3.8.) showed a mtDNA concentration-dependent downregulation of Rtg2 and upregulation of Bmh2 (Figure 54). Unfortunately, Mks1 could not be measured. When analyzing the relative protein concentrations in more detail, both proteins seem to be dependent on the amount of the nuclear-encoded machinery. With an increasing amount of the three factors, the relative protein concentration of Rtg2 decreases significantly, while the relative protein concentration of Bmh2 increases significantly. This hints towards a negative regulation of the retrograde pathway with increasing amounts of the limiting machinery of mtDNA. A consequently lower replicative aging with increasing mtDNA concentrations would be conceivable. As the differences of the protein levels for Rtg2 and Bmh2 between double and triple addition strains are small, this might be an explanation for the similar replicative aging result, independently of their *SIR2* RNA-concentration (Figure 50a).

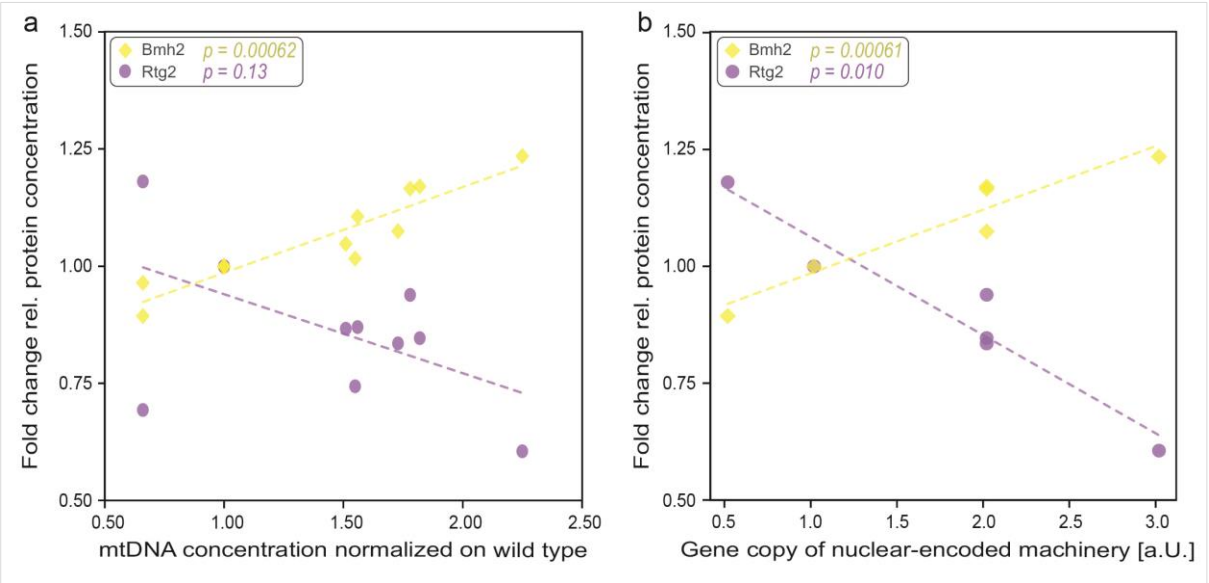

Figure 54: Fold change of relative protein concentration for Bmh2 and Rtg2 measured by mass spectrometry as a function of the mtDNA concentration normalized on wild type or gene copy number of nuclear-encoded machinery. Fold change of relative protein concentration measured by mass spectrometry with the help of Luisa Hernández Götz (Schmoller Lab, Helmholtz Munich,

Germany) and Michael Lanz (Skotheim Lab, Stanford University, USA). The fold change of the two retrograde pathway-proteins Bmh2 (diamond, yellow) and Rtg2 (dot, violet) is shown as function of the mtDNA concentration normalized on wild type **(a)** or gene copy of the complete nuclear-encoded machinery **(b).** Statistical significances shown p-values calculated by Spearman correlation analysis. **a-b)** Diploid strains include wild type and hemizygous triple deletion of *abf2, mip1* and *rim1.* Haploid strains include wild type, 3 individual clones A-C of triple addition strains with one additional copy of *ABF2, MIP1* and *RIM1*, triple triple addition strain including two additional copies of *ABF2, MIP1* and *RIM1.* **a)** additionally included only in plot (a) are the strains: hemizygous double deletion of *abf2* and *mip1* and 3 individual clones A-C of double addition strains including one additional copy of *ABF2* and *MIP1*.

To better understand the relationship between mtDNA copy number, replicative aging and the retrograde response, further experiments need to be done. The highest priority here should be a repetition of the replicative aging experiments with the newly constructed clones B and C, to get insights into the influence of mtDNA concentration on it independently of *SIR2*. If the reduced replicative life span could be confirmed in all clones, additional experiments to investigate the mitochondrial membrane potential and ATP levels depending on the mtDNA concentration should be performed. Additional experiments regarding the retrograde pathway should be performed to confirm its mtDNA copy number-dependent downregulation. Specifically, phosphate assays checking the phosphorylation of Mks1 in the strains of this study could give further insights into the state of the retrograde pathway with increasing mtDNA concentrations.

3.8. Analyzing the expression of nuclear and mitochondrial-encoded genes with altered mtDNA concentrations

Previous studies have shown that increased mtDNA copy numbers can result in increased transcription levels of mtDNA-encoded RNA, as for the *cim1Δ*-deletion strain, but can also show no different transcription levels compared to wild type, as for the *mrx6Δ*-deletion strain (Schrott and Osman, 2023). This highlights the importance of analyzing the dependence of transcription and translational regulations on mtDNA copy number using the diploid strains with hemizygous deletions or haploid additional copy strains of the limiting machinery, which could give further insights into the mtDNA-dependent mechanisms or regulations. For this, the misregulated mtDNA strains were compared to the corresponding wild type, performing two experiments in cooperation with other laboratories. To identify differentially expressed transcripts, RNA sequencing was performed as described in chapter 2.18.1. and the results were analyzed by Kim Job from the Scialdone Lab at Helmholtz Munich. Additionally, the translation was evaluated by mass spectrometry experiments with the help of Luisa Hernández Götz (Schmoller lab, Helmholtz Munich, Germany) and Michael Lanz (Skotheim lab, Stanford University, USA) as described in chapter 2.18.2. In the following chapters, four different aspects of the analysis of the expression rates will be highlighted: First of all, the relative RNA and protein concentrations of the nuclear-encoded limiting factors were checked. Next, additional nuclear-encoded factors, selected based on literature research, were looked at in more detail. Chapter 3.8.3. will analyze the mitochondrial-encoded RNAs and proteins in dependence on the mtDNA concentration. And the last sub-chapter will focus on the nuclear-encoded proteins, which are most likely mtDNA-concentration-dependently regulated.

3.8.1. RNA- and protein-levels of the mtDNA-limiting machinery confirm the performed genomic manipulation

First, the genomic manipulation of the strains was verified. As shown in Figure 55a, the hemizygous double deletion showed approximately 50% less RNA for *MIP1* and *ABF2*, while the *RIM1* RNA levels were comparable to wild type. The hemizygous triple deletion additionally shows the downregulation of *RIM1* on the RNA level. Also, the haploid strains with additional copies of *ABF2* and *MIP1* result in increased RNA levels of around 200% for these two genes in the double addition strains. While the double additions still show wild-type-like *RIM1* RNA-levels, the triple additions, as expected, result in around 200% for all three factors *ABF2*, *MIP1* and *RIM1*. The regulation on protein level shown in Figure 55b only included Abf2 and Rim1, as Mip1 could not be detected. The results confirm the decreased protein levels in the hemizygous deletion strains and the increased protein levels in the additional copy strains compared to the corresponding wild type, which matches their genotype. The mass spectrometry experiments also included the *cim1Δ*- and *mrx6Δ*-deletion strains to compare similar mtDNA concentrations achieved by alternative strategies. No changes on protein level for Abf2 or Rim1 could be observed in these two strains (Figure 55c). While the proteomics data do not include any information about the regulation of Cim1, the Mrx6-levels could be measured at least for the haploid strains. As shown in Figure 55d, none of the haploid addition strains resulted in a considerable difference in Mrx6 protein level compared to wild type.

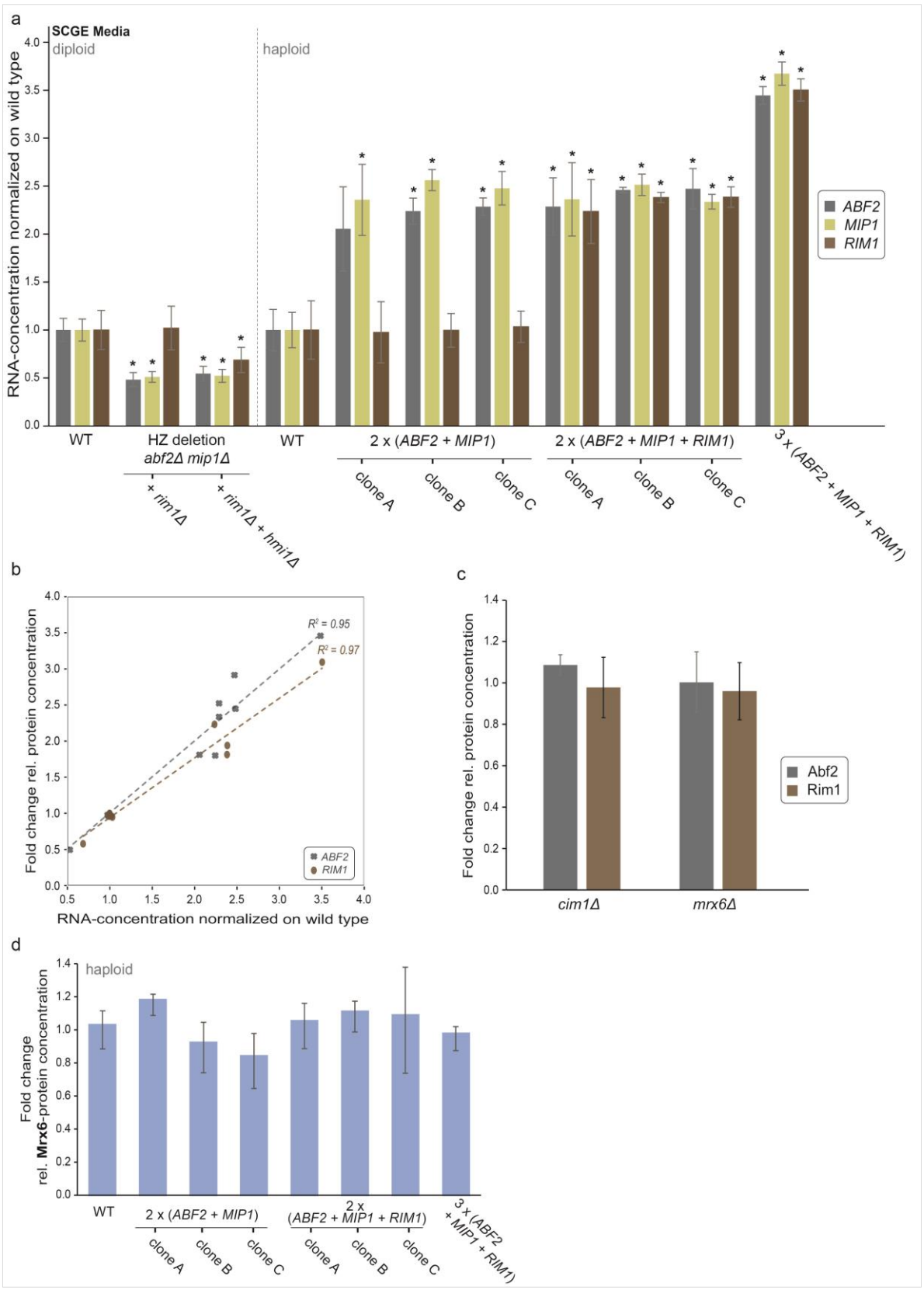

Figure 55: Analysis of the expression rate of the limiting machinery *ABF2, MIP1* and *RIM1* as well as *MRX6* in the most relevant strains of the study measured on RNA- and protein-level. a-d) Strains grown in non-fermentable SCGE media included in this figure: Diploid strains include wild type, hemizygous double deletion of *abf2* and *mip1*, hemizygous triple deletion of *abf2*, *mip1* and *rim1*. Haploid strains include wild type, 3 individual clones A-C of double addition strains including one additional copy of *ABF2* and *MIP1*, 3 individual clones A-C of triple addition strains with one additional copy of *ABF2*, *MIP1* and *RIM1*, triple

triple addition strain including two additional copies of *ABF2, MIP1* and *RIM1*, wild type including a *cim1Δ*-deletion or *mrx6Δ*-deletion. **a)** RNA-concentration normalized on the corresponding wild type measured via RNA sequencing with the help of Kim Job (Scaldione Lab, Helmholtz Munich, Germany). The bars indicate the mean values normalized on the corresponding wild type, calculated based on at least five replicates and error bars show the standard deviation. Statistical significances were calculated using a Wald test. Statistical significances are indicated as * for padj < 0.1. Analyzed RNA-levels of *ABF2* (dark grey), *MIP1* (yellow) and *RIM1* (brown). **b)** Fold change of relative protein concentration as a function of relative RNA-concentration normalized on the corresponding wild type for Abf2 (dark grey) and Rim1 (brown). Relative protein concentration measured by mass spectrometry with the help of Luisa Hernández Götz (Schmoller Lab, Helmholtz Munich, Germany) and Michael Lanz (Skotheim Lab, Stanford University, USA). R2 indicates the coefficient of determination for the shown linear regression. **c)** Fold change of relative protein concentration of Abf2 (dark grey) and Rim1 (brown) for the *cim1Δ*- and *mrx6Δ*-deletion strains. The bars indicate the mean values normalized on the corresponding wild type and error bars show the standard deviation. **d)** Fold change of relative protein concentration of Mrx6 for the haploid strains including additional copies of the limiting machinery. The bars indicate the mean values normalized on the corresponding wild type and error bars show the standard deviation.

3.8.2. Comparison of protein regulations in the various strategies of increasing mtDNA copy numbers

Recent studies have investigated mtDNA copy number in the context of *MRX6* dosage manipulations (Göke *et al.*, 2020; Schrott *et al.*, 2025). To test whether the effect is based on the *mrx6Δ*-deletion or the mtDNA increase, their results and the results of this study were compared. Increased protein levels of Rpo41 and Cha1 were found in the *mrx6Δ*-deletion strain (Schrott *et al.*, 2025). Analyzing these two proteins in the proteomics data of this study, the upregulation in the absence of *MRX6* can be confirmed (see Figure 56a and b). Analyzing the other strains, no strong misregulation of the two proteins was observed, except for a slight increase of Rpo41 and a slight decrease of Cha1 in the *cim1Δ*-deletion compared to wild type. This suggests that the Rpo41-upregulation on protein level is not a universal mtDNA-based phenomenon but instead due to the specific deletions. The exact mechanism of how *MRX6* influences mtDNA copy number is not known, but it is speculated to interact with Pim1 (Göke *et al.*, 2020). The Lon protease Pim1 is proposed to be involved in the degradation of proteins involved in mtDNA copy number regulation, such as Cim1 (Schrott and Osman, 2023). The speculated mechanistic connection between Mrx6 and Cim1 (Schrott *et al.*, 2025) could explain the upregulation of Rpo41 in both *mrx6Δ*- and *cim1Δ*-deletion strains to different extents. Another protein that has to be mentioned in the context of Mrx6 and Pim1 is Mam33, which binds and stabilizes Mrx6 (Schrott *et al.*, 2025). Schrott et al. also identified an *MRX6*-dependent interaction of Pim1 with Mnp1, Rim1, Mgm101 and Cha1 (Schrott *et al.*, 2025). By contrast to Rim1 and Cha1, the relative protein concentration of Pim1 shows a very small increase with increasing mtDNA concentrations (Figure 56c). When analyzing the statistical relationship of the relative protein concentration of Pim1 on the mtDNA concentration via Spearman correlation testing, this slight increase results in a significant p-value of 0.0015. Also, the relative protein concentrations of the proteins Mam33, Mgm101 and Mnp1 show a significant positive relation to the mtDNA concentrations (Figure 56d to 56f). However, for Mam33 it shows only increasing protein levels with increasing mtDNA concentrations for the haploid additional copy strains but nearly no change within the diploid strains (Figure 56d). Moreover, increasing mtDNA concentrations lead to increasing protein levels of Mgm101 and Mnp1 (Figure 56e and f). Both Mgm101 and Mnp1 seem to stay at wild type level in the *mrx6Δ*- and *cim1Δ*-deletion strain. The increase of those two proteins in the higher mtDNA concentrations achieved through overexpression of the limiting machinery is therefore specific to the three factors Abf2, Mip1 and Rim1. Mnp1, a protein of the large subunit of mitochondrial ribosome, is related to nucleoids, as part of mtDNA translation (Sato and Miyakawa, 2004). Additionally, studies have reported that Mgm101 is part of a potential mtDNA replisome that

consists of at least Mmm1, Mip1 and Mgm101, which is only present in some of the nucleoids (Meeusen and Nunnari, 2003). Also, recent studies in mammalian cells reported the presence of two different kinds of nucleoids, speculated to carry out different tasks (Isaac *et al.*, 2024). Taken together, this leads to the speculation that in budding yeast, also two types of nucleoids might be present: One type being active and serving for mtDNA replication and translation, and another type could provide a backup-like storage of mtDNA, supporting quality control.

This study showed that the *mrx6Δ*- and *cim1Δ*-dependent mtDNA copy number increase and the increase based on the nuclear-encoded machinery show different consequences on the transcriptome and proteome. These new proteomics results do not exclude an overlap of the two regulatory pathways. However, when speculating about the presence of two types of nucleoids containing mtDNA, another hypothesis can be put forward: it can be speculated that the different strategies to achieve increased mtDNA copy number affect different types of mtDNA. This could not only explain deviating regulations on protein level, but also the reason for the presence of transcriptional upregulation in these strains. Specifically, the *mrx6Δ*-deleted strains could show increased copy numbers of mtDNA, intended for “storage”-nucleoids, which is why their mitochondrial-encoded genes are not transcribed. While the *cim1Δ*-deletion strain, as well as the strains with increased mtDNA copy number due to the limiting machinery, are increasing mtDNA copies used for transcription. To further test the hypothesis, the RNA-levels of the mtDNA-encoded genes are also checked in the cells with misregulated amounts of the limiting machinery in the next chapter.

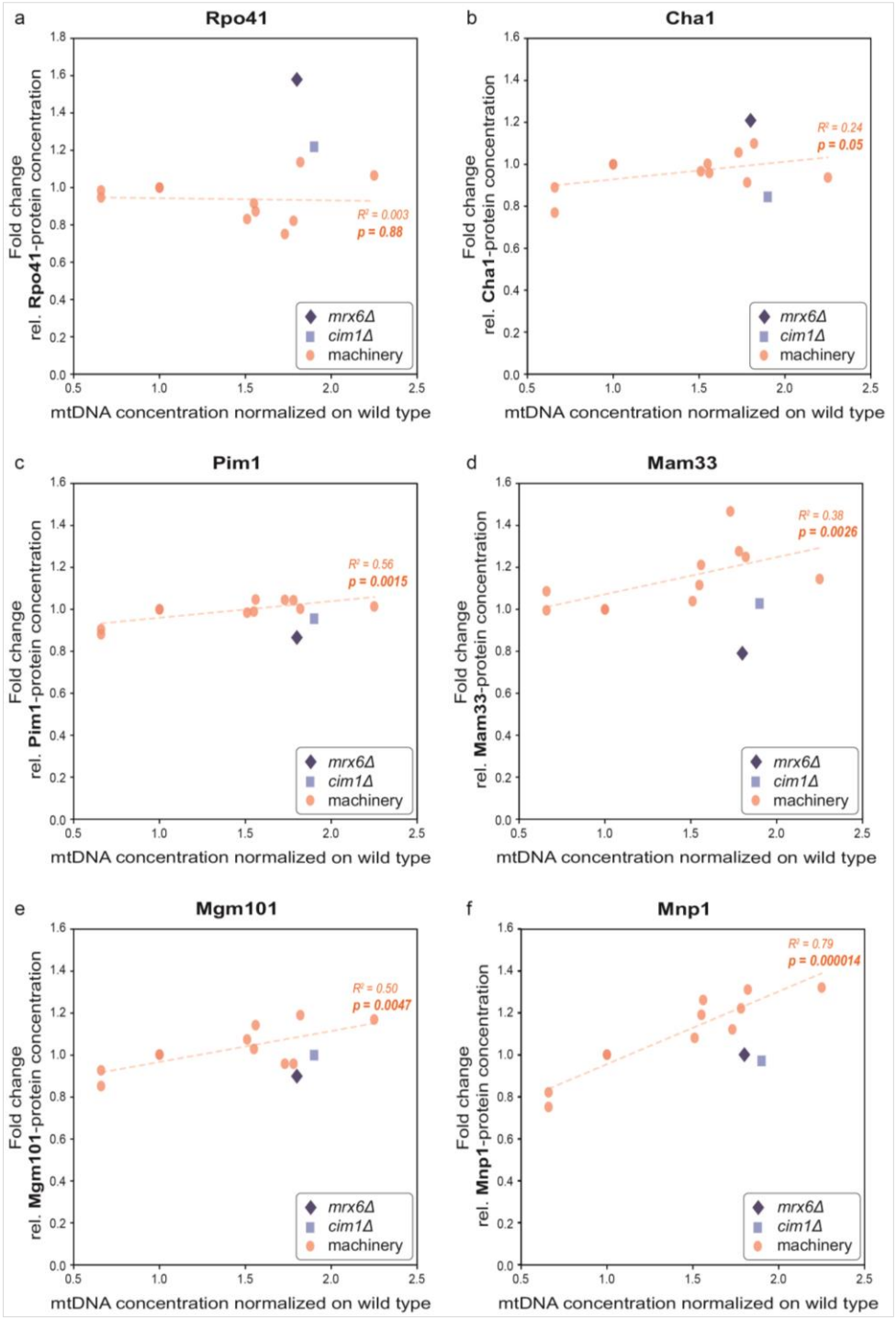

Figure 56: Fold change of relative protein concentration for Rpo41, Cha1, Pim1, Mam33, Mgm101 and Mnp1 as a function of the mtDNA concentration normalized on corresponding wild type. a-f) Strains grown in non-fermentable SCGE media and divided into three categories: "Machinery" symbolizing strains with genomic manipulations of the mtDNA-limiting machinery (dot; orange; Diploid strains include wild type, hemizygous double deletion of *abf2* and *mip1*, hemizygous triple deletion of *abf2*, *mip1* and *rim1*. Haploid strains include wild type, 3 individual clones A-C of double addition strains including one additional copy of *ABF2* and *MIP1*, 3 individual clones A-C of triple addition strains with one additional copy of *ABF2*, *MIP1* and *RIM1*, triple triple addition strain including two additional copies of *ABF2, MIP1* and *RIM1*), *cim1Δ*-deletion (diamond dark violet) or *mrx6Δ*-deletion (square; light blue).Linear regression and coefficient of determination (R^2) are considering the "machinery" values only. Statistical significances shown p-values calculated by Spearman correlation analysis of "machinery" values. Plot showing the fold change of relative protein concentration of **a)** Rpo41, **b)** Cha1, **c)** Pim1, **d)** Mam33, **e)** Mgm101 and **f)** Mnp1.

3.8.3. RNA-levels of mitochondrial-encoded genes depend on mtDNA concentration, while protein levels show varying results, potentially regulated by Aim23

Next, the behavior of the mitochondrial-encoded genes on RNA- and protein-level was analyzed. In budding yeast, the mtDNA encodes 8 proteins (Foury *et al.*, 1998), 8 origin-like elements (Tzagoloff and Myers, 1986) and 24 non-coding t-RNAs and ribosomal RNAs (Zamaroczy and Bernardi, 1986b). Figure 57 quantifies the dependency of all measured mitochondrial-encoded genes on RNA-level on the mtDNA concentration. Analyzing the RNA data in more detail, it seems like they are downregulated in the diploid hemizygous deletions and upregulated in the haploid additional copy strains compared to the corresponding wild type, according to the mtDNA copy number. However, the RNA levels of the double, triple and triple triple addition strain are similar between the strains. This might hint towards a potential limitation through the transcriptional machinery like the RNA-polymerase Rpo41 and/or its specificity factor Mtf1, whose relative protein concentrations stayed constant with increasing mtDNA concentrations (Figure 56). Further additions of the transcriptional machinery to the triple and triple triple addition strains could provide further information in the future. Nevertheless, the result confirms that the increased mtDNA copy number due to an increased amount of limiting machinery does result in increased relative RNA-concentrations of the mitochondrial encoding genes.

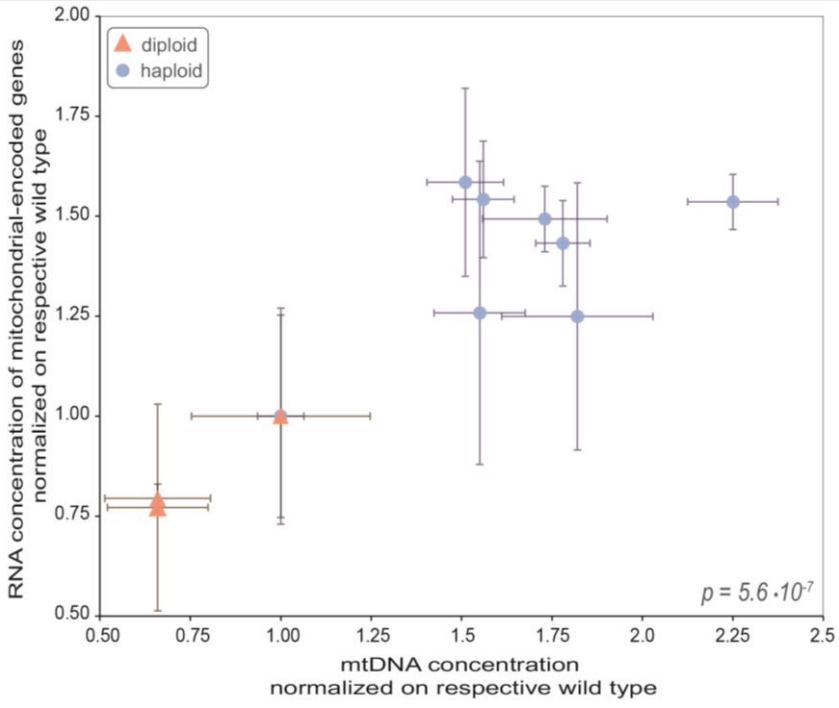

Figure 57: RNA concentration of mitochondrial-encoded genes normalized on respective wild type as a function of the normalized mtDNA concentration. RNA-concentration of mitochondrial-encoded genes normalized on the respective wild type (measured by RNA Seq) as a function of the mtDNA concentration normalized on the respective wild type. Symbols for diploid (triange; orange) and haploid (dot; blue) strains represent the mean and error bars showing the standard deviations. Statistical significance shown p-value calculated by Spearman correlation analysis. Diploid strains include wild type, hemizygous double deletion of *abf2* and *mip1*, hemizygous triple deletion of *abf2*, *mip1* and *rim1*. Haploid strains include wild type, 3 individual clones A-C of double addition strains including one additional copy of *ABF2* and *MIP1*, 3 individual clones A-C of triple addition strains with one additional copy of *ABF2*, *MIP1* and *RIM1*, triple triple addition strain including two additional copies of *ABF2, MIP1* and *RIM1.*

The 8 proteins encoded in the mtDNA of budding yeast are mainly part of the OXPHOS system (Foury *et al.*, 1998). Unfortunately, the mass spectrometry only detected half of the proteins encoded by mtDNA: Cox1, Cox2, Cob and Var1. As shown in Figure 58 and statistically proven via a Spearman correlation test, the RNA levels of *COX1*, *COB* and *VAR1* increase with increasing mtDNA concentrations, comparable to the general behavior of mitochondrial-encoded RNA (Figure 57). By contrast, the RNA levels of *COX2* stayed nearly constant. Analyzing relative concentrations of the four proteins in more detail, the levels of Cox2 as well as Cox1 increased significantly with increasing mtDNA concentration, while staying constant for Cob and Var1 (Figure 58). This suggests a variable regulation of the different mitochondrial-encoded proteins with increasing mtDNA copy number.

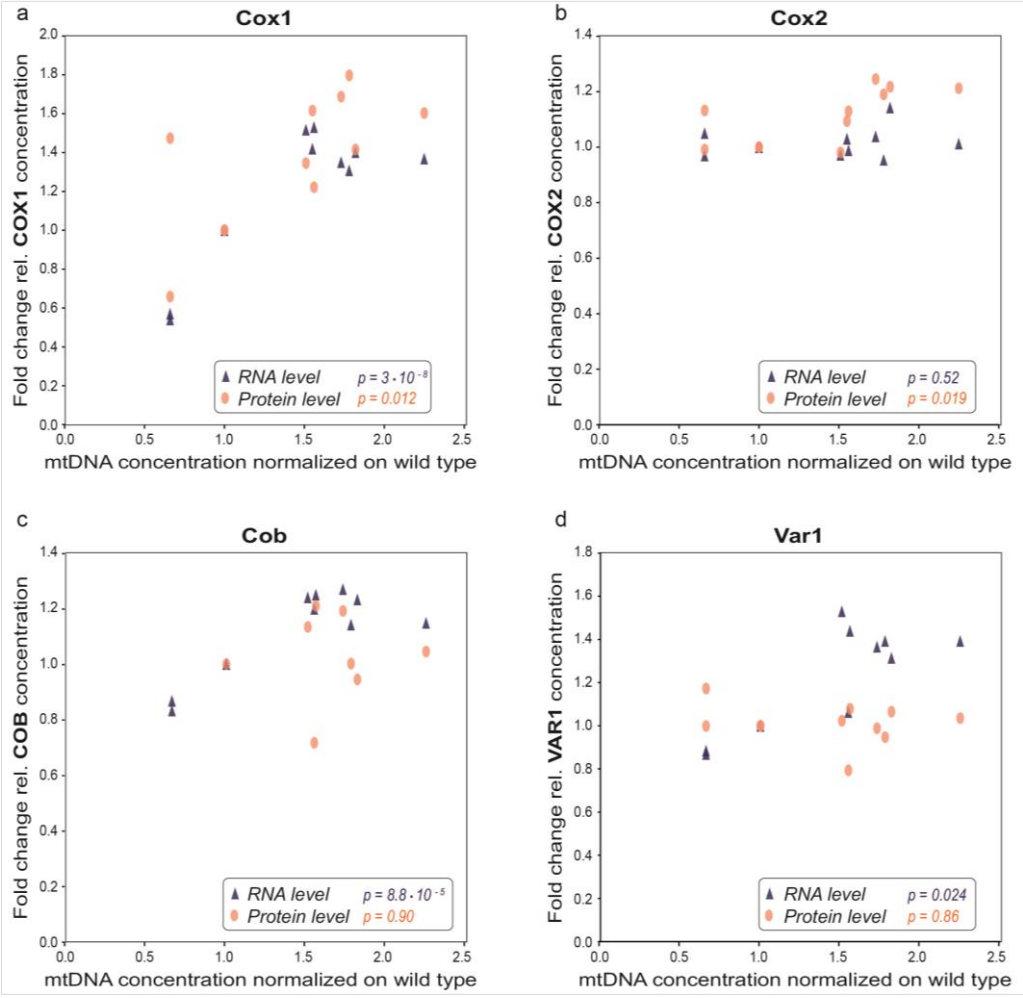

Figure 58: Relative concentration on RNA and Protein level as a function of the mtDNA concentration normalized on wild type for four mitochondrial-encoded proteins: Cox1, Cox2, Cob and Var1. Analysis of expression level dependent on the mtDNA concentration in the strains for the mitochondrial-encoded proteins **a)** Cox1, **b)** Cox2, **c)** Cob and **d)** Var1. Symbols distinguish between RNA- and protein-level. RNA-concentration of mitochondrial-encoded genes normalized on the respective wild type (measured by RNA Seq) as a function of the mtDNA concentration normalized on the respective wild type (triangle; dark violet). Fold change of relative protein concentration (measured by mass spectrometry) as a function of the mtDNA concentration normalized on the respective wild type (dot; orange). Statistical significance shown p-value calculated by Spearman correlation analysis. Diploid strains include wild type, hemizygous double deletion of *abf2* and *mip1*, hemizygous triple deletion of *abf2*, *mip1* and *rim1*. Haploid strains include wild type, 3 individual clones A-C of double addition strains including one additional copy of *ABF2* and *MIP1*, 3 individual clones A-C of triple addition strains with one additional copy of *ABF2*, *MIP1* and *RIM1*, triple triple addition strain including two additional copies of *ABF2, MIP1* and *RIM1.*

The different behavior of mitochondrial-encoded proteins with increasing mtDNA concentrations can not be explained easily, but two scenarios could be possible. Either the regulation of those proteins takes place on translational level, or alternatively, differentially regulated degradation rates of the different mitochondrial-encoded proteins lead to the observed differences. The exact mechanism is beyond the scope of this thesis and would be interesting to investigate in the future. Nevertheless, first indications regarding the first scenario can be suggested: It is known that most of the regulation of mitochondrial-encoded proteins in budding yeast is based on the activity of translational activators (Herrmann *et al.*, 2013). Most of those translational activators interact with the 5'-end of long untranslated regions (5'-UTRs) of mitochondrial mRNAs (Derbikova *et al.*, 2018). Thereby, multiple specialized translational activators coordinate the translation of one mitochondrial-encoded protein (Herrmann *et al.*, 2013). One example of the known translational activators for Cox1 is Mam33 (Roloff and Henry, 2015), which is mtDNA-dependently regulated, as this thesis has shown before (see Figure 56d). This could be one explanation, why the relative protein concentration of Cox1 is also increasing with increasing mtDNA concentration. Four of the nearly 20 known translational activators for the mitochondrial-encoded proteins (Derbikova *et al.*, 2018) were detected in the mass spectrometry measurements, but no other translational activator shows a major mtDNA-dependent change. Besides the individual factors, there are also speculations about "core components" that regulate the mitochondrial-encoded protein translation (Derbikova *et al.*, 2018). Two major proteins are considered to be potential "core components" in budding yeast (Derbikova *et al.*, 2018): The mitochondrial ribosome recycling factor Rrf1 (Kanai *et al.*, 1998) and the translation initiation factor Aim23 (Hess *et al.*, 2009). When plotting the relative concentrations of those two proteins, measured via mass spectrometry, as a function of the mtDNA concentration for the haploid strains, two different behaviors become visible (Figure 59). With increasing mtDNA concentrations, the relative concentration of Rrf1 shows only mild decreases (Figure 59a), whereas the relative concentration of Aim23 increases significantly (Figure 59b). A previous study that analyzed the expression of mitochondrial-encoded proteins in an *aim23*Δ-deletion strain observed different regulations of the proteins: While the protein biosynthesis of Var1 and Cob stayed on wild-type level, the protein-levels of Cox1, Cox2 and Cox3 decreased and the proteins Atp6, Atp8 and Atp9 showed increased protein concentrations, while the overall translation of mitochondrial-encoded genes showed comparable levels to wild type (Kuzmenko *et al.*, 2016). Interestingly, this describes exactly the opposite behavior as in the strains of this thesis (see Figure 58). This suggests that increasing mtDNA concentrations lead to increasing Aim23 protein concentrations (Figure 59b), therefore leading to increasing protein concentrations of Cox1 and Cox2 (Figure 58a and b) while the protein concentrations of Var1 and Cob remained unaltered (Figure 58c and d). The hypothesis of Aim23 regulating the mitochondrial-encoded proteins depending on the mtDNA concentration has to be analyzed in more detail in the future. One possible experiment could be the analysis of the proteins that are mitochondrial-encoded for a strain with an *aim23*Δ-deletion in the triple addition strain.

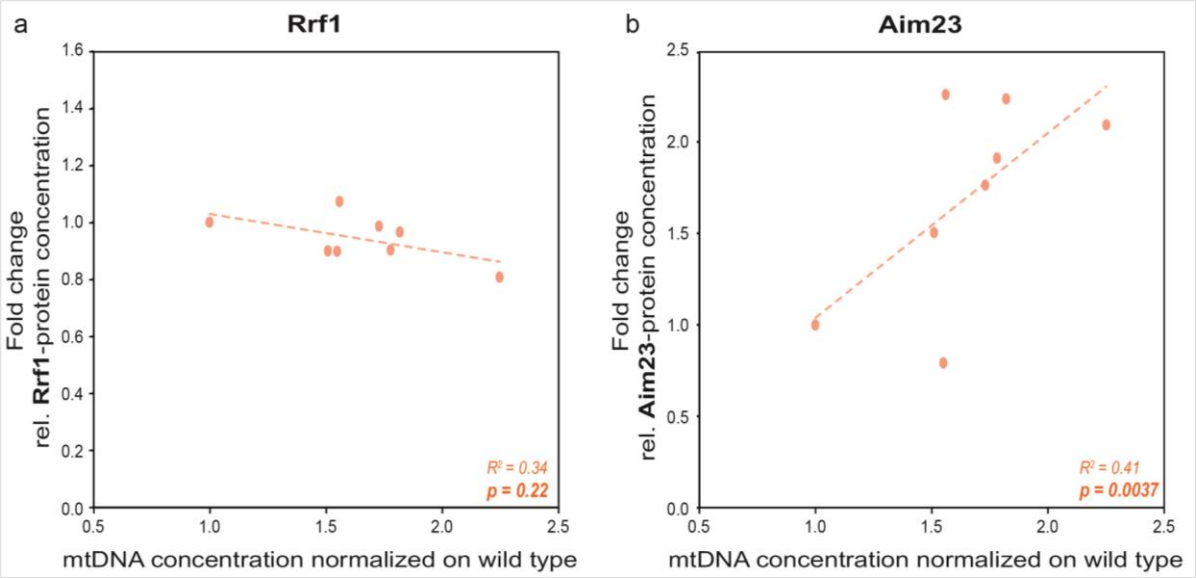

Figure 59: Fold change of relative protein concentration for Rrf1 and Aim23 as a function of the mtDNA concentration normalized on corresponding wild type. Strains grown in non-fermentable SCGE media and analyzed via mass spectrometry. Haploid strains include wild type, 3 individual clones A-C of double addition strains including one additional copy of *ABF2* and *MIP1*, 3 individual clones A-C of triple addition strains with one additional copy of *ABF2*, *MIP1* and *RIM1*, triple triple addition strain including two additional copies of *ABF2, MIP1* and *RIM1.* Statistical significances shown p-values calculated by Spearman correlation analysis of all values. Plot showing the fold change of relative protein concentration of **a)** Rrf1 and **b)** Aim23.

The shown results indicate a higher probability for a variable translational regulation of the mitochondrial-encoded proteins, but further experiemtns need to be done to also exclude potential degradation events. Nevertheless, the absence of an upregulation of all of the proteins encoded in the mtDNA, could be a possible explanation of the observed robustness of the cells to mtDNA changes.

3.8.4. Identification of the top 30 mtDNA-dependent proteins suggests a potential activation of mitophagy in increased mtDNA copy number strains

To better understand the mtDNA-dependent changes on protein level, a linear slope and coefficient of correlation for every protein were calculated as described in chapter 2.18.2. This was done including two different set of strains: The first set included all of the three diploid strains (wild type, hemizygous double deletion, hemizygous triple deletion) and the eight haploid strains (wild type, double addition clones A to C, triple addition clones A to C, triple triple addition). The second set included only those strains with manipulation of the complete nuclear-encoded machinery (diploid wild type, hemizygous triple deletion, haploid wild type, triple addition clones A to C, triple triple addition). So, the differences between the two sets of strains are the “double-strains”, which is why they are now called “with doubles” (strain set 1) and “without doubles” (strain set 2). The reason for this approach was to be able to distinguish between a mtDNA-dependent or three-factor-machinery-dependent regulation of a protein.

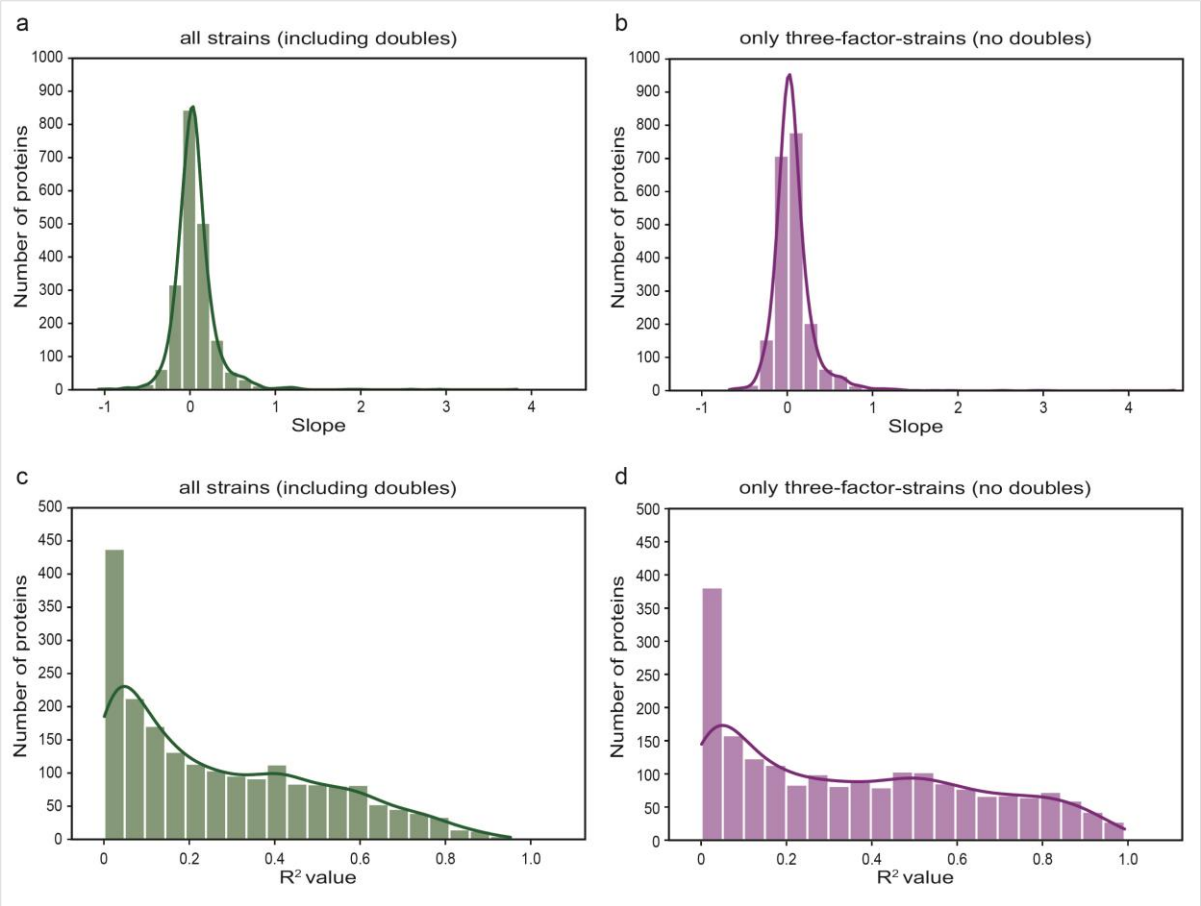

Figure 60: Analysis of mass spectrometry data searching for mtDNA concentration-dependent proteins. The dependency of single proteins on the mtDNA concentration was calculated as described in chapter 2.18.2.by creating a linear regression of the relative protein concentration as a function of the mtDNA concentration and calculating the corresponding coefficient of determination (R^2). Two rows showing the distribution of the resulting slopes (top; **a-b**) and the distribution of the resulting coefficient of determination (R^2-value; bottom; **c-d**). Strains included in both columns are: Diploid strains include wild type and hemizygous triple deletion of *abf2, mip1* and *rim1.* Haploid strains include wild type, 3 individual clones A-C of triple addition strains with one additional copy of *ABF2, MIP1* and *RIM1*, triple triple addition strain including two additional copies of *ABF2, MIP1* and *RIM1.* And the left columns (“all strains (including doubles)”; a+c; green) additionally included: hemizygous double deletion of *abf2* and *mip1* and 3 individual clones A-C of double addition strains including one additional copy of *ABF2* and *MIP1*.

When comparing the distribution of the slopes of all proteins, it becomes clear that more proteins are upregulated than downregulated in both strain sets (Figure 60a and b). Also, the distribution of the R^2-values within the two strain sets shows a slight difference: When the doubles are included in the analysis (Figure 60c), the frequency of R^2-values close to 0 is higher than in the dataset without the doubles. The amount of proteins with high R^2-values is visibly lower in the first dataset than in the second dataset without the doubles (Figure 60d). The second strain set (without doubles) includes 66 proteins with an R^2-value higher than 0.9, while the results for the strain set with doubles only include 6 proteins with this characteristic. When comparing the 66 proteins with the highest coefficient of correlation value of the strain set including the doubles, only 30 proteins agree with the 66 highest-R^2-proteins of the strain set without the doubles. One of those 30 proteins is Abf2, which can be explained by the manipulation of it in all strains. Also, the plasmid harboring Abf2 (ASE003-1) includes parts of the gene sequence for Tvp18, which is also included in the 30 proteins. After excluding those two proteins, the 28 remaining proteins are listed in Table 27 including their main function. With high confidence, they are regulated based on the mtDNA concentration. Interestingly, only 3 of those 28 Proteins are downregulated with increasing mtDNA concentration: Ald6, Gpi16 and Ybt1. When considering the 28 proteins, some observations can be documented. Around a third of the regulated proteins are involved in different stress response pathways. As previously mentioned (Figure 54), the results indicate that the retrograde pathway (Bui and Labedzka-Dmoch, 2024) is switched off upon increased mtDNA concentrations in budding yeast. Moreover, some proteins in the list are part of the cell wall integrity (CWI) pathway (Sanz *et al.*, 2022), the HOG-pathway (Nadal and Posas, 2022) and pathways related to endocytosis (Goode *et al.*, 2015), indicating that the cells are in a state of stress. These pathways have at least two things in common: their activity is dependent on the phosphorylation of defined proteins and they are reported to be related to mitophagy (Abeliovich, 2023). No final statement about a mtDNA-dependent pathway regulation can be made at this point and additional deeper evaluation of the data is needed. These results justify additional experiments in budding yeast with increased mtDNA concentrations regarding their rate of mitophagy. One possible experiment would be to inactivate mitophagy by deleting the gene of the mitochondrial membrane protein *ATG32,* which mainly initiates mitophagy (Innokentev and Kanki, 2021). Assuming that the mitophagy rate is increased in strains with increased mtDNA concentrations to keep the strains healthy, an inactivation of mitophagy might lead to more drastic negative phenotypes in the strains with increasing amounts of the mtDNA-limiting machinery. Additionally, phosphate assays to check the phosphorylation state in the mentioned pathways and specifically of Atg32, to check mitophagy, could give more insights. Is it possible that the yeast cells with high mtDNA concentrations try to get rid of the unnecessarily high mtDNA copy number? And if so, is there a connection to the recently documented (Roussou *et al.*, 2024) effort of budding yeast to maintain homoplasmy of mtDNA? The observation of a lower loss of mtDNA with increasing mtDNA copy number (Figure 35) might be a possible explanation for why the cell wants to maintain the wild-type amount of mtDNA. In case of a mutation, a higher mtDNA copy number might be a disadvantage, as it is harder to remove it and achieve a homoplasmic state. This can be supported by the fact that *mrx6Δ*-deletion strains with higher mtDNA copy numbers were reported to need more time to reach a homoplasmic state (Roussou *et al.*, 2024). Could it be that yeast cells with high mtDNA concentrations aim to reduce their mtDNA content to wild-type levels to more easily maintain homoplasmy and healthy mtDNA within the population? Of course, these ideas need multiple experiments to test them and open up a lot of new

questions. Possible experiments in the future would be to expose cells with different mtDNA concentrations to precise mtDNA stress. Previous studies in yeast used an inducible mitochondrial-targeted bacterial toxin, mtDarT, which creates adducts on ssDNA, to generate targeted mtDNA stress (Dua *et al.*, 2022). This would be one possible experimental design to study mtDNA stress response as a function of different mtDNA concentrations in budding yeast.

Table 27: Top 28 proteins showing dependency on mtDNA copy number

Protein	Description	Resource
Aim7	Protein interacting with Arp2/3, stimulating actin filament debranching and inhibiting actin nucleation	(Gandhi *et al.*, 2010; Koundinya *et al.*, 2025)
Ald6	Cytosolic aldehyde dehydrogenase, activated by Mg^{2+} and $NADP^{+}$-dependent, negative regulator of nonselective autophagy	(Meaden *et al.*, 1997; Delorme-Axford *et al.*, 2023)
Arc40	Subunit of Arp2/3 complex	(Winter *et al.*, 1999)
Bmh2	14-3-3 protein, involved in post-transcriptional control of the proteome and part of retrograde-pathway	(van Heusden *et al.*, 1995; Bui and Labedzka-Dmoch, 2024)
Cmk1	Calmodulin-dependent protein kinase with a potential role in stress response	(Cyert, 2001)
Cnb1	Calcineurin B involved in stress response	(Cyert and Thorner, 1992)
Dyn2	Microtubule motor protein for intracellular transport and cell division	(Stuchell-Brereton *et al.*, 2011)
Gpi16	Subunit of glycosylphosphatidylinositol transamidase complex	(Fraering *et al.*, 2001)
Gtt1	ER-associated glutathione S-transferase	(Choi *et al.*, 1998)
Hmf1	Complements transaminase of isoleucine in mitochondria, high-dosage growth inhibitor	(Deaconescu *et al.*, 2002)
Hsp12	Plasma-membrane protein involved in membrane maintenance, regulated by HOG and Ras-Pka pathways	(Praekelt and Meacock, 1990; Hirayama *et al.*, 1995)
Igo1	Protein involved in initiation of G0 program, regulated through Tor1 downstream of Rim15	(Talarek *et al.*, 2010; Foltman and Sanchez-Diaz, 2023)
Inh1	Protein inhibiting ATP hydrolysis (F1F0-synthase) with calmodulin-binding motif	(Ichikawa *et al.*, 1990; Contessi *et al.*, 2005)
Mcm4	Helicase as part of MCM2-7 complex, which binds pre-replication on DNA	(Tye, 1999)
Mix17	Mitochondrial intermembrane space protein involved in oxygen consumption	(Gabriel *et al.*, 2007)
Mrpl16	Mitochondrial ribosomal protein of the large subunit	(Kitakawa *et al.*, 1997)
Mrpl23	Mitochondrial ribosomal protein of the large subunit	(Kitakawa *et al.*, 1997)
Nhp2	Protein related to HMG-proteins	(Kolodrubetz and Burgum, 1991)
Pat1	Deadenylation-dependent mRNA-decapping factor, involved in rDNA locus stability maintenance	(Wang *et al.*, 1996; Wang *et al.*, 1999)
Pet10	Perilipin, involved in lipid droplet homeostasis, respiratory growth and ATP/ADP-exchange	(Athenstaedt *et al.*, 1999; Gao *et al.*, 2017)
Plp2	Protein interacting with CCT-complex to stimulate actin folding	(Flanary *et al.*, 2000; McCormack *et al.*, 2009)
Rho1	GTP-binding protein involved in cell polarity and part of the cell-wall-integrity pathway (CWI-pathway)	(Madaule *et al.*, 1987; Drgonová *et al.*, 1999; Sanz *et al.*, 2022)

Sec13	Structural component of three complexes: Nup84p nuclear pore subcomplex, subunit of COPII vesicle coat ER-to-Golgi-transport and subunit of SEACAT (activating Torc1-signalling)	(Novick *et al.*, 1980; Barlowe *et al.*, 1994; Siniossoglou *et al.*, 2000; Panchaud *et al.*, 2013)
Vma10	Subunit of V1 peripheral membrane domain of V-ATPase	(Supeková *et al.*, 1995)
Xpt1	Xanthine-guanine phosphoribosyl transferase	(Guetsova *et al.*, 1999)
Ybt1	Transporter of ATP-binding cassette family, regulates the release of luminal Ca^{2+} stores	(Ortiz *et al.*, 1997; Sasser *et al.*, 2012)
Yke2	Subunit of Gim/prefoldin protein complex, involved in folding alpha-, beta-tubulin and actin	(Shang *et al.*, 1994; Geissler *et al.*, 1998; Millán-Zambrano *et al.*, 2013)
Zeo1	Peripheral membrane protein that regulates the CWI pathway	(Green *et al.*, 2003)

3.9. Cell volume-dependent mtNetwork and nucleoids are regulated independently of mtDNA

Previous studies have shown that the mtNetwork volume (Rafelski *et al.*, 2012; Seel *et al.*, 2023), as well as the number of nucleoids, are dependent on cell volume (Osman *et al.*, 2015; Seel *et al.*, 2023). Independently, it was shown that mtDNA copy number is cell volume dependent (Seel *et al.*, 2023). Therefore, one concluding question arises: Is there a dependency of mtNetwork, nucleoids and mtDNA copy number on each other? The relationship between nucleoid number and mtDNA copy number is controversially discussed, as some papers report that one nucleoid contains only 1 to 2 copies of mtDNA (Chen and Butow, 2005; Kukat *et al.*, 2011), while other reviews report them to include up to 10 copies (Lipinski *et al.*, 2010). There are facts indicating a relation between nucleoids and mtDNA. For example, the mitochore, based on the three proteins Mmm1p, Mdm10p and Mdm12p, was found to mediate the nucleoid inheritance (Boldogh *et al.*, 2003). Boldogh et al. have reported a relation between mtDNA and these three genes, hinting also towards a relation of mtDNA to nucleoids beyond their simple localisation. Regarding the network of mitochondria and mtDNA copy number, there are already some indications of their independence. Firstly, petite cells lacking mtDNA still contain a mtNetwork and it has been shown that the network still scales with cell volume (Seel *et al.*, 2023). Moreover, a *mic60Δ*-deletion strain, which shows a reduced network phenotype (Jakubke *et al.*, 2021), was previously analyzed, showing reduced numbers of nucleoids but similar mtDNA concentrations compared to wild type (Seel *et al.*, 2023).

Most of the mentioned studies rely on a cell volume increase. By contrast, analyzing strains with variable mtDNA concentration but the same cell volume would open up new insights into the relationship of mtNetwork, nucleoids and mtDNA. By recreating the double and triple addition strain in a microscopy background with fluorescent reporters for visualization of the mitochondria, this was possible. To visualize the mtNetwork and nucleoids with microscopy, a previously published system was used (Figure 61a): The strain includes LacO repeats, which are integrated into the mtDNA (Osman *et al.*, 2015), as well as a two-times mNeon-tagged LacI repressor (Seel *et al.*, 2023). As the LacI proteins will bind the LacO repeats in the mtDNA, the nucleoids will therefore appear in green. Additionally, mKate2 was used in the strain to visualize the network of mitochondria. First, it was confirmed (Figure 61a) that the strains with additions of *ABF2* and *MIP1,* as well as the addition of *ABF2*, *MIP1* and *RIM1,* indeed result in comparable mtDNA concentrations as shown before in both SCGE and SCD (Figure 41). Both methods to track cell volume, Coulter counter (Figure 61b) and microscopy (Figure 61c), confirmed that there are no major differences in cell volumes between the strains. As before, the yeasts grow bigger when cultured in fermentable media. In line with a previous study (Seel *et al.*, 2023), the cells contain lower numbers of nucleoids when grown in SCD than in SCGE (Figure 61d). More interestingly, there is no major change in the number of nucleoids between the strains cultured in the same media (Figure 61h). This could be explained by a lack of resolution, especially in non-fermentable media. Also, no significant change in mtNetwork volume was measured with increasing mtDNA concentrations (Figure 61g). This answers parts of the question raised before: There is no dependency of the mitochondrial nucleoids and network length on mtDNA copy number. Combined with previously described published results, it can be concluded that mtNetwork volume, nucleoid numbers and mtDNA copy number are all regulated through different independent mechanisms, each of which leads to a proportional scaling with cell volume.

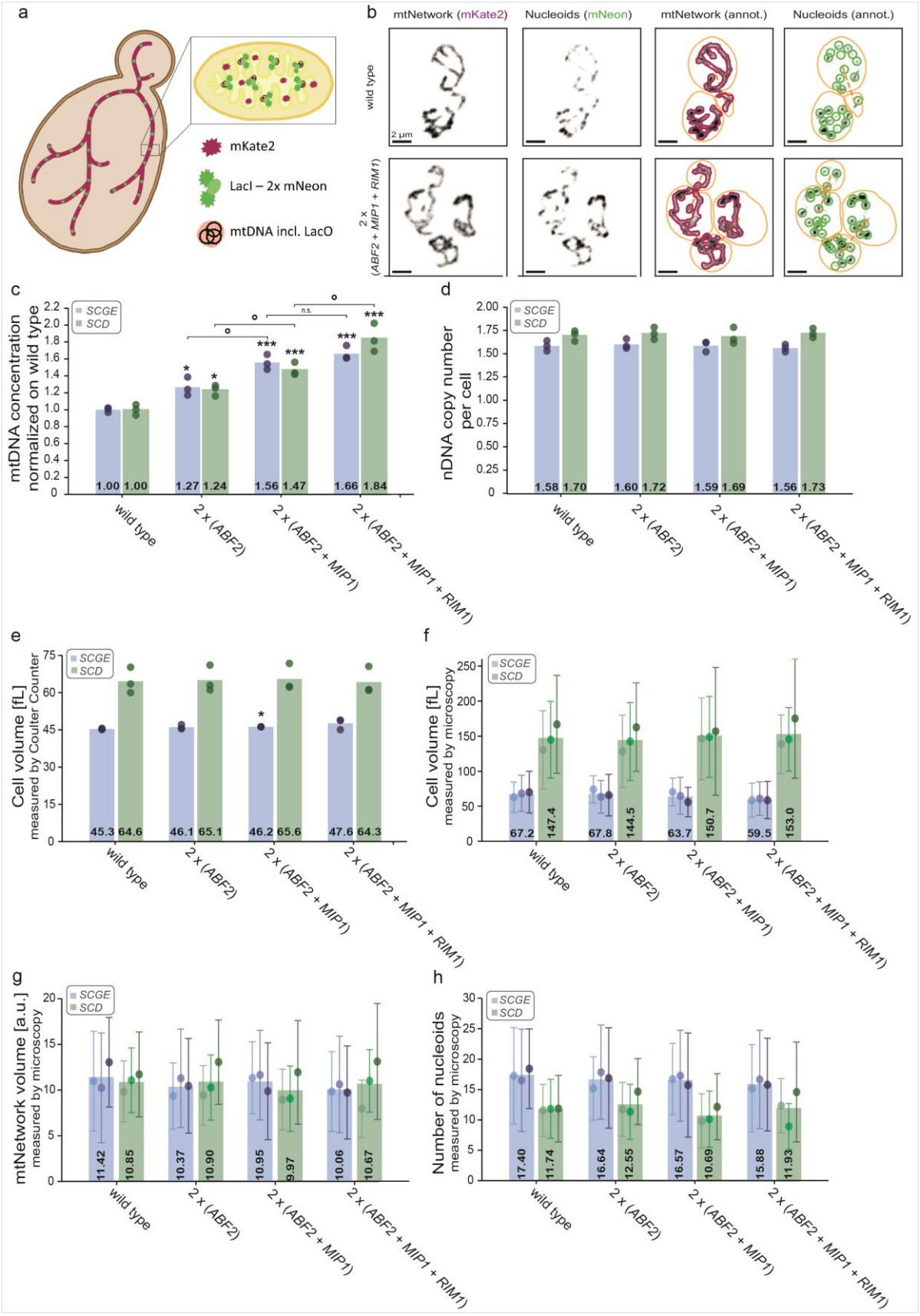
a
mKate2
LacI – 2x mNeon
mtDNA incl. LacO
b
mtNetwork (mKate2)
Nucleoids (mNeon)
mtNetwork (annot.)
Nucleoids (annot.)
wild type
2 x (ABF2 + MIP1 + RIM1)
2 µm
c
mtDNA concentration normalized on wild type
SCGE
SCD
1.00 1.00
1.27 1.24
1.56 1.47
1.66 1.84
d
nDNA copy number per cell
1.58 1.70
1.60 1.72
1.59 1.69
1.56 1.73
wild type
2 x (ABF2)
2 x (ABF2 + MIP1)
2 x (ABF2 + MIP1 + RIM1)
e
Cell volume [fL] measured by Coulter Counter
45.3 64.6
46.1 65.1
46.2 65.6
47.6 64.3
f
Cell volume [fL] measured by microscopy
67.2 147.4
67.8 144.5
63.7 150.7
59.5 153.0
g
mtNetwork volume [a.u.] measured by microscopy
11.42 10.85
10.37 10.90
10.95 9.97
10.06 10.67
h
Number of nucleoids measured by microscopy
17.40 11.74
16.64 12.55
16.57 10.69
15.88 11.93

Figure 61: Analysis of mtNetwork and number of nucleoids per cell with increasing mtDNA concentrations via microscopy. a) Schematic representation of LacI-LacO System used to visualize nucleoids. Multiple copies of LacO were integrated into the mtDNA (Osman *et al.*, 2015), which will be bound by LacI, which is fused to 2x mNeon (Seel *et al.*, 2023). This results in a green visualization of the nucleoids. Additionally, the mitochondrial network is visible in red, due to mKate2 targeted to the mitochondrial matrix. **b)** Exemplary confocal microscopy images of wild type (top) and triple addition strain (bottom), showing the mitochondrial network (first tile) and nucleoids (second tile) with automated network segmentation (third tile) and detected nucleoids (fourth tile). The scale bar represents 2 µm. **c-f)** Various measurements for microscopy strains with genomic manipulations (from left to right): haploid microscopy wild type, microscopy strain with one additional copy of *ABF2*, microscopy strain with one additional copy of *ABF2* and *MIP1*, microscopy strain with one additional copy of *ABF2, MIP1* and *RIM1*. Strains were grown and measured in two different conditions: non-fermentable SCGE media (blue) and fermentable SCD media (green). The bars indicate the mean values, calculated based on three replicates per media and individual replicates are shown as dots, with error bars for single cell analysis, showing the standard deviation. Statistical significances were calculated using a two-tailed two-handed t-tests. Statistical significances compared to wild type are indicated as * for $p < 0.05$, ** for $p < 0.01$ and *** for $p < 0.005$. Statistical significances compared to the background strain are indicated as ° for $p < 0.05$, °° for $p < 0.01$ and °°° for $p < 0.005$. **c)** mtDNA concentration normalized on wild type, **d)** nDNA copy number per cell measured by visual inspection under the microscopy (“bud counts”), **e)** Cell volume in fL measured by Coulter counter, **f)** cell volume in fL measured by microscopy generated by automated segmentation based on bright field, which is prone to overestimate cell volume. Absolute values are therefore not directly comparable to Coulter counter data. **g)** Mitochondrial network volume in arb. units measured by microscopy and **h)** Number of nucleoids per cell measured by microscopy. **f-h)** Number of cells included for culturing in SCGE: wild type replicate 1 (rep1) 71 cells, rep2 57 cells, rep3 62 cells, additional *ABF2* rep1 51 cells, rep2 63 cells, rep3 56 cells, additional *ABF2 MIP1* rep1 58 cells, rep2 56 cells, rep3 59 cells, additional *ABF2 MIP1 RIM1* rep1 56 cells, rep2 57 cells rep3 69 cells. Number of cells included for culturing in SCD: wild type rep1 57 cells, rep2 59 cells, rep3 60 cells, additional *ABF2* rep1 60 cells, rep2 56 cells, rep3 56 cells, additional *ABF2 MIP1* rep1 57 cells, rep2 60 cells, rep3 61 cells, additional *ABF2 MIP1 RIM1* rep1 52 cells, rep2 56 cells rep3 55 cells.

4. Discussion

Although mitochondria and mtDNA are affected in various human diseases (Niyazov *et al.*, 2016; Bernardino Gomes *et al.*, 2024), their regulation is still not completely understood. A previous study in *S. cerevisiae* has linked the regulation of mtDNA copy number to cell size and identified two major regulatory factors to be the mtDNA polymerase Mip1 and the packaging factor Abf2 (Seel *et al.*, 2023). The amount of this nuclear-encoded machinery increases with increasing cell volume, therefore leading to increased mtDNA copy numbers (Seel *et al.*, 2023). While Abf2 and Mip1 were sufficient to largely explain the mtDNA regulation in hemizygous diploid deletions, an overexpression of the two genes did not result in a proportional increase of mtDNA copy number as expected (Seel *et al.*, 2023). This indicates that besides Abf2 and Mip1, one or several additional proteins are part of the nuclear encoding machinery limiting mtDNA copy number. This study identified the third factor responsible for the cell volume dependency of mtDNA copy number to be the ssDNA-binding protein Rim1. Also, a strategy was established to uncouple the cell volume-dependency of the mtDNA-limiting factors. This could provide information about the influence of cell volume on the mtDNA copy number independently of the factors. In addition, this thesis identified a surprising robustness of budding yeast against mtDNA changes, suggesting the presence of control mechanisms to maintain a healthy state of the cell. Initial evidence described in this thesis hints towards a translational dosage compensation of mitochondrial-encoded proteins and/or an involvement of mitophagy through nuclear-encoded proteins as control mechanisms. Additionally, this study shows the mtDNA copy number independence of the mitochondrial network length and the number of nucleoids.

4.1. The nuclear-encoded machinery limiting mtDNA copy number consists of Abf2, Mip1 and Rim1

The regulation of mtDNA copy number has been shown to be cell volume-dependently regulated by two major factors: the mtDNA packaging factor Abf2 and the mitochondrial polymerase Mip1 (Seel *et al.*, 2023). As an overexpression of those two proteins was not sufficient to fully explain the mtDNA regulation (Seel *et al.*, 2023), the assumption of potential additional factors limiting mtDNA copy number arose. To identify those additional factors of the nuclear-encoded machinery limiting mtDNA copy number, hemizygous deletions as well as additional copy strains were created and their mtDNA concentration was measured (see chapter 3.2.). The results identified the ssDNA-binding protein Rim1 as the third factor limiting mtDNA copy number, together with Abf2 and Mip1 (see Figures 15 and 16). The minor contribution of a fourth factor in the identified machinery cannot be ruled out, but in the tested conditions, it has been shown that Hmi1 and Mgm101, which were the most likely candidates, are not among them (see Figure 17). Overexpression of the three factors separately resulted in increasing mtDNA concentrations with individual upper limits (see Figure 19). A simultaneous overexpression of all three factors to threefold could exceed these individual mtDNA concentration limits, but does not show a perfect proportional scaling of the mtDNA concentration with the gene copy number of the limiting machinery (see Figure 20). This hints towards an mtDNA copy number close to saturation. Analyzing strains with higher overexpression of all three factors could give more insights. All in all, this thesis has confirmed that in budding yeast, an increase of cell volume leads to an increase of the limiting factors Abf2, Mip1 and Rim1 and therefore results in an increased mtDNA copy number (Figure 62).

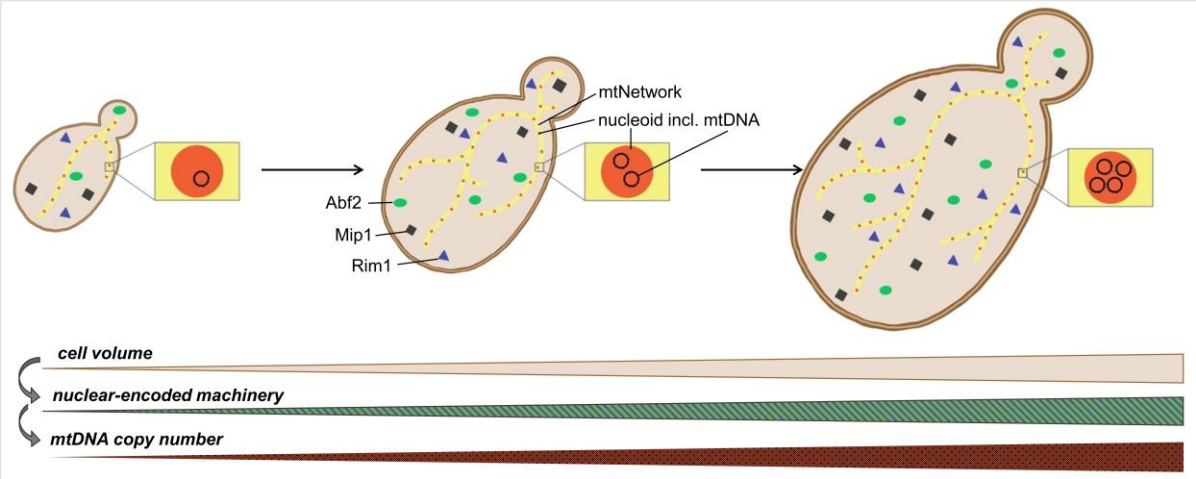

Figure 62: Cell volume-dependent regulation of mtDNA copy number through the limiting machinery (Abf2, Mip1 and Rim1). With increasing cell volume, the amount of the limiting machinery increases and therefore leads to increased mtDNA copy numbers. This study has identified the third factor of the mtDNA limiting machinery beside Abf2 and Mip1 to be Rim1. The actual location of the nuclear-encoded factors (Mip1, Abf2 and Rim1) is the mitochondria, but they are visualized in the cytoplasm for simplification of the scheme.

A study in higher eukaryotes has also shown a dependency of mitochondria on cell volume (Miettinen and Björklund, 2016), as reported in budding yeast (Rafelski *et al.*, 2012; Osman *et al.*, 2015; Seel *et al.*, 2023). Most proteins involved in mitochondrial replication in yeast are conserved to higher eukaryotes (Shadel, 1999). All three factors identified to limit mtDNA copy number in this study are known to have a human homolog: The mtDNA polymerase Mip1 in budding yeast is known as PolG in mammals (Lodi *et al.*, 2015). Also, the packaging factor of mtDNA Abf2 has a homolog in mammals called TFAM (Ekstrand *et al.*, 2004). Moreover, the ssDNA-binding protein known as Rim1 in yeast is known as SSBP1 in human cells (Spelbrink, 2010). A study in human epithelial cells has also shown that those mammalian homologues are expressed in a cell volume-dependent manner (Lanz *et al.*, 2022). More interestingly, some studies have also shown a dependency of mtDNA copy number in mammalian cells on TFAM (Larsson *et al.*, 1998; Ekstrand *et al.*, 2004; Kang *et al.*, 2007), PolG (Korhonen *et al.*, 2004; Graziewicz *et al.*, 2006) and SSBP1 (Jiang *et al.*, 2021; Riccio *et al.*, 2024). As in budding yeast, the three individual proteins limit the mtDNA copy number in mammals but they could not fully explain the mtDNA copy number regulation as a single factor. Moreover, another protein is known to show dosage-dependent effects on the mtDNA copy number in eukaryotes: the helicase TWINKLE (Tyynismaa *et al.*, 2004; Matsushima and Kaguni, 2007). This is also the reason why PolG, SSBP1 and TWINKLE are speculated to be the core mitochondrial replisome in mammalian cells (Korhonen *et al.*, 2004). Even though there is no known homolog of TWINKLE in *S. cerevisiae*, there are mitochondrial helicases known in budding yeast: Pif1 and Hmi1 (Lahaye *et al.*, 1991; Sedman *et al.*, 2000). Both were included in the analysis of this thesis, but did not show a relevant dosage-dependent effect on the mtDNA copy number (see Figures 15 and 16). This suggests that mtDNA copy number is cell volume-dependently regulated through the amount of a nuclear-encoded machinery in budding yeast and mammalian cells. But even though there are many similarities in the mtDNA homeostasis, the composition of this limiting machinery may vary between organisms or even cell types. Focused studies in mammalian cells to identify the actual mtDNA-limiting machinery are necessary in the future.

4.2. First evidence towards excluding a limiting-machinery-independent influence of cell volume on mtDNA copy number

The current hypothesis of mtDNA copy number regulation is as follows: With increasing cell volume, the amount of the nuclear-encoded machinery – now identified to consist of Abf2, Mip1 and Rim1 – increases, and therefore the mtDNA copy number is increasing, too. Previous studies have shown the dependency of Abf2, Mip1 and Rim1 on cell volume (Lanz *et al.*, 2022; Seel *et al.*, 2023). In addition, the dependency of the mtDNA copy number on these three proteins has been shown in this study (see chapter 3.2.). This leaves the open question of whether the cell volume is influencing mtDNA copy numbers only through the nuclear-encoded machinery or if it also has an independent additional effect on it. To uncouple the amount of the limiting machinery from cell volume, this study made use of histone promoters. It has been shown that the use of histone promoters driving the expression of a fluorescent protein leads to decreasing mRNA-concentrations of the protein with increasing cell size (Claude *et al.*, 2021). As this behavior would represent a constant amount of the protein with increasing cell size, the aim of this part of the study was to express the three mtDNA-limiting genes under control of a histone promoter. Integrating these manipulations into a Whi5-inducable strain would open up the possibility to study mtDNA copy numbers in increasing cell volumes while the nuclear-encoded machinery stays at constant mRNA-amounts. Theoretically, if the mtDNA copy number in this strain would also stay constant, it suggests that cell volume has no additional effect on mtDNA copy number independently of the limiting machinery.

After a number of optimizations, a strain with almost constant and wild-type comparable mRNA-amounts of *ABF2* was created and measured. Since *MIP1* and *RIM1* are still scaling with cell volume, only first estimations can be made. These first results indicate a cell volume-independent behavior of mtDNA copy number (see Figure 25) and prove the possibility of the concept. However, further research is needed to answer the posed question definitively. For this, a strain optimization towards constant amounts of *MIP1* and *RIM1* has to be carried out in the future.

4.3. The robustness of budding yeast to variable mtDNA concentrations leads to mild phenotypes

The strains created in this study harbor increasing or decreasing mtDNA concentrations depending on the gene copy amount of the limiting machinery. The analysis of some selected strains provided a great potential to study the cells' characteristics with changing mtDNA concentrations. This could answer the question of whether mtDNA changes have an impact on the cell physiology.

In both fermentable and non-fermentable media, there were no notable differences in cell volume with increasing mtDNA concentrations (see Figure 28a, Figure 38, Figure 39 and Figure 43a). Moreover, no changes in the copy number of nDNA per cell with increasing mtDNA concentrations were found in both media (see Figure 28b and Figure 40). This suggests that changes in mtDNA copy number do not lead to any feedback mechanism regulating nDNA copy number or cell volume in budding yeast.

Moreover, increasing mtDNA concentrations in budding yeast led to a slightly faster growth rate in non-fermentable SCGE media (see Figure 29 and Figure 43b). Surprisingly, when repeating the growth experiments in fermentable SCD media, the faster growth rate with increasing mtDNA concentrations was not observable (see Figure 42 and Figure 45). In conclusion, higher mtDNA concentrations are only beneficial when mitochondria and their DNA are needed, as in non-fermentable media. How the faster cell growth in SCGE media is achieved remains unknown, but it could be speculated that higher mtDNA copy numbers lead to higher ATP production at the ETC in mitochondria when cultured in non-fermentable media. This could be beneficial for the cells in respiring media (as SCGE) and unnecessary in fermentable media (as SCD). Also, a study in colorectal cancer cells has shown faster cell proliferation for cells with increased mtDNA copy number (Sun *et al.*, 2018). It is assumed that the main reason is an increased oxidative phosphorylation with increasing mtDNA copy number (Sun *et al.*, 2018). To verify this hypothesis in the strains of this study, a first approach could be to compare the ATP production rates between the strains with various mtDNA concentrations by Seahorse assays. It would also be interesting to test the mitochondrial membrane potential in the different strains, to check for abnormalities.

The observed faster growth in non-fermentable media (see Figure 29 and Figure 43b) might also be related to an enhanced respiratory capacity. That is why the frequency of petite colonies was investigated in the strains, too. With increasing mtDNA concentration, the frequency of petite colonies decreased significantly (see Figure 35), which is in agreement with results of recent studies (Stuart *et al.*, 2006; Schrott and Osman, 2023; Ray *et al.*, 2025). This can easily be explained by the stochastic loss of mtDNA at cell division: A higher mtDNA copy number per cell decreases the chance for individual cells to lose their complete mtDNA. Also, a study that intended to deplete mtDNA in different mammalian cell types by an enzymatic approach revealed different timings until mtDNA was depleted completely, dependent on the initial mtDNA content (Schubert *et al.*, 2015), supporting the observed mtDNA-dependent loss of respiratory capacity.

A calorie restriction by switching from fermentable SCD media to low-glucose minimal media revealed that high mtDNA concentrations can even be a disadvantage to the cells: The calorie restriction-based cell cycle arrest of cells facing the switch during G1-phase prolonged with increasing mtDNA concentrations (see Figure 47). Additionally, an increased frequency of abnormally shaped buds of cells facing the switch in S/G2/M-phase was observed in strains with misregulated mtDNA concentrations (see Figure 48b). Cells with this phenotype stayed significantly longer in their cell cycle arrest than cells that formed normally shaped buds (see Figure 48c). Independent of its shape, the bud divided from the mother with the same total cell volume (see Figure 48d), providing evidence of a shape-independent but cell volume-dependent regulation for the cells to undergo cytokinesis. The described aberrant phenomenon only occurred in buds that faced the media switch smaller than 26 fL, which equals around half of their final size at division. Previous studies have observed that the transport of mitochondria from the mother into the bud takes place until the bud reaches approximately half of its final size (Rafelski *et al.*, 2012). This suggests a more challenging cell cycle progression for budding cells, which face stresses such as calorie restriction with incomplete mitochondrial transmission. A deviant mtDNA concentration seems to enhance this handicap.

A similar but distinct observation was made during replicative aging experiments, where the occurrence of elongated buds in older cells showed a relation to the amount of the three factors limiting mtDNA (see Figure 50c). Regardless of this observation, it has been shown that the replicative aging is reduced with increasing mtDNA concentrations (see Figure 50). It has to be noted that an accidental passenger mutation led to a down-regulation of Sir2, a commonly known protein influencing aging (Kaeberlein *et al.*, 1999), in the tested strains (see Figures 51 to 53). Whether this down-regulation of Sir2 is the only reason for the observed reduced replicative life span remains unknown. Additionally, there is evidence for a mtDNA-dependent inactivation of the retrograde pathway on protein level (see Figure 54), which could also explain a Sir2-independent replicative aging phenotype. Future experiments with high mtDNA copy number strains without this downregulation of the aging-influencing protein Sir2 are therefore needed.

All in all, the major mtDNA-dependent phenotypes were surprisingly mild (Figure 63). An increase of mtDNA concentration in budding yeast leads to a:

1. slightly faster cell growth in non-fermentable media.
2. reduced frequency of petite cells.
3. delayed response to low-glucose stress.

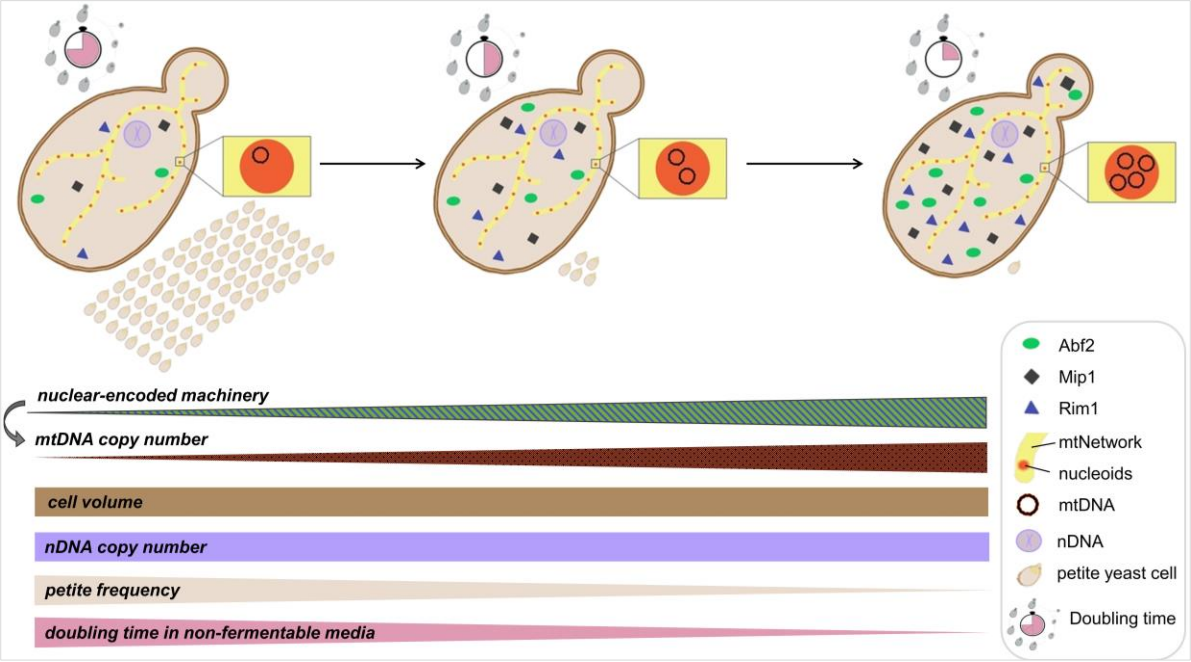

Figure 63: The phenotypes of budding yeast with different mtDNA concentrations are surprisingly mild. When changing the mtDNA copy number by increasing the gene copy number of the mtDNA limiting machinery (Abf2, Mip1 and Rim1), surprisingly mild phenotypes were observed. Firstly, no changes in cell volume or average nDNA copy number per cell were measured. Secondly, a decreased frequency of petite cells with increasing mtDNA concentrations was found. And thirdly, a reduced doubling time with increasing mtDNA concentrations was shown when culturing the cells in non-fermentable media. The actual location of the nuclear-encoded factors (Mip1, Abf2 and Rim1) is the mitochondria, but they are visualized in the cytoplasm for simplification of the scheme.

Alternative ways to achieve increased mtDNA concentrations were performed to test whether the results are based on the mtDNA copy number or the manipulated factors themselves. For this, the Abf2-antagonist *CIM1* and the mitochondrial ribosome-associated *MRX6* were

knocked out individually. The missing upregulation of mitochondrial-encoded RNA in the *mrx6Δ*-deletion strain (Schrott and Osman, 2023) disqualified it from the intended verification. However, the *cim1Δ*-deletion strain could confirm the slightly faster cell growth (see Figure 36d). Previous studies have also shown reduced frequencies of petite cells in this strain (Schrott and Osman, 2023). To also test the combinability of the two strategies to increase the mtDNA copy number by either the addition of the mtDNA-limiting factors (Abf2, Mip1, Rim1) or alternatively deleting mtDNA-specific genes (*CIM1* or *MRX6*), the deletions were also introduced into the strain including two copies of the mtDNA-limting machinery genes. An additional *cim1Δ*-deletion in this triple addition strain showed additive effects regarding the mtDNA concentration. This strain resulted in similar mtDNA concentrations and cell physiologies as the strain with three copies of all limiting factors (see Figure 36).

All in all, this thesis observed budding yeast to be a robust system against mtDNA copy number changes, leading to only mild phenotypes even upon changes up to 3-fold. A study in transgenic mice overexpressing TFAM and therefore leading to increased mtDNA copy numbers has also documented the robustness of the cells, as no increased activity of the enzymes of the respiratory chain could be observed (Ekstrand *et al.*, 2004). Also, a decrease in TFAM levels leading to decreased mtDNA copy numbers only mildly affects the cell characteristics (Kremer *et al.*, 2025). This hints towards a robustness to mtDNA changes in mammalian cells as well.

4.4. Protein-level dosage compensation of mitochondrial genes with increasing mtDNA concentrations could potentially explain the robustness of the cells

The observed robustness of the cells to mtDNA copy number changes leads to the question of whether the expression rate of the mitochondrial-encoded genes is changed. Interestingly, a *cim1Δ*-deletion strain results in increased mitochondrial-encoded transcript amounts, while a *mrx6Δ*-deletion strain showed mitochondrial-encoded transcript levels as the wild type, even though both strains increase the mtDNA copy number (Schrott and Osman, 2023). This suggests that an mtDNA copy number increase does not necessarily result in increased expression rates of the mitochondrial-encoded genes.

When testing the strains with increasing mtDNA copy numbers due to increasing amounts of the mtDNA-limiting machinery (Abf2, Mip1 and Rim1), this thesis has shown that the RNA level of the mitochondrial-encoded genes is regulated based on the mtDNA concentrations until a certain threshold (see Figure 57). At this point, the RNA levels remain constant, which could hint towards a limitation by the transcriptional machinery. A possible approach to test this statement could be an overexpression of the mtRNA-polymerase Rpo41 and its specificity factor Mtf1 in the affected strains. The four detected mitochondrial-encoded proteins showed variable behavior with increasing mtDNA concentrations: While Cob1 and Var1 stayed nearly constant in their relative concentration, the proteins Cox1 and Cox2 increased in their relative concentration with increasing mtDNA concentrations (see Figure 58). Whether this regulation on protein level is achieved through translational dosage compensation or targeted degradation remains unclear. First observations hint toward an individual translational regulation, as the relative protein concentration of the mitochondrial translational initiation factor Aim23, which is speculated to act as a “core component” of translational activators (Kuzmenko *et al.*, 2016), is increasing with increasing mtDNA concentration (see Figure 59).

As experiments with an *aim23Δ*-deletion showed exactly the opposite regulations of the mitochondrial-encoded proteins (Kuzmenko *et al.*, 2016) than described in this thesis, the mtDNA-dependent Aim23 protein concentration could explain the observed variable translation of mtDNA-encoded proteins (see Figure 58). Taken together, increasing amounts of the limiting machinery (Abf2, Mip1 and Rim1) result in increasing mtDNA copy numbers, leading to increased mitochondrial-encoded transcripts but not a proportional increase of all corresponding proteins. Overall, the absence of a total upregulation of the mitochondrial-encoded proteins with increasing mtDNA concentrations could explain the observed robustness of the cells.

But why do increasing mtDNA copy numbers not necessarily lead to increased mitochondrial-encoded transcript concentrations? While increasing the mtDNA copy number by the amount of the limiting machinery (see Figure 57) or by deleting *CIM1* does increase the transcript concentrations of mitochondrial-encoded genes, the *mrx6Δ*-deletion strain shows no increase (Schrott and Osman, 2023). In mammalian cells, there are observations about two types of nucleoids: The tightly packaged “inactive nucleoids” and the less packaged “active nucleoids” (Isaac *et al.*, 2024). Dependent on the TFAM-levels present in the nucleoids, the mtDNA is more or less accessible for replication and transcription (Isaac *et al.*, 2024). That is why “inactive nucleoids” are speculated to function as a genetic reservoir, while “active nucleoids” are used for replication and transcription (Isaac *et al.*, 2024). Applying this idea to the observed differences in transcriptomic regulation, a hypothesis arises: Maybe the deletion of *MRX6* leads to an increase in the mtDNA copy number of mtDNA intended for storage-nucleoids, which is why the mtDNA is not used for transcription. This would also imply that the other two described strategies to increase mtDNA copy number affect the mtDNA of active nucleoids, allowing transcription. This would also support the suggestion that Mrx6 mainly affects the quality control system of mtDNA, while the mtDNA-limiting machinery (Abf2, Mip1 and Rim1), as well as Cim1, are used for the quantitative regulation of mtDNA copy number. Future experiments testing the nucleoid-hypothesis could help to better understand the differences of the described strategies to increase mtDNA copy number. A potential experiment could be the visualization of mtDNA replication via 5’-ethynyl-2’-deoxyuridine (EdU) labeling.

4.5. An excess of mtDNA copy numbers might lead to mitophagy to achieve a homoplasmic mtDNA state

Besides the mitochondrial-encoded protein, this thesis also analyzed the regulation of nuclear-encoded proteins in dependence of the mtDNA concentration (see Table 27). As some of those mtDNA-dependent nuclear proteins are involved in stress responses resulting in mitophagy, it can be speculated that the rate of mitophagy is increased with increasing mtDNA concentrations. Roussou et al. have recently documented that budding yeast aim to achieve a homoplasmic mtDNA state (Roussou *et al.*, 2024). A strain with higher mtDNA copy numbers, obtained by a *mrx6Δ*-deletion, was reported to need longer to achieve this homogeneous state (Roussou *et al.*, 2024). Taking all of this into account, a potential answer to the question arises: high mtDNA copy numbers might be a disadvantage in coping with potential mutations in the mtDNA. And too high mtDNA copy numbers could therefore aim to be reduced by mitophagy to protect the cells. To analyze this hypothesis, besides measuring the ATP-levels and mitochondrial membrane potential in strains with higher mtDNA concentrations, radioactive phosphate labelling or kinase activity assays could be helpful. This could analyze the phosphorylation of stress response pathways, for example the RTG-

pathway, which is speculated to be related to mtDNA in this thesis (see Figure 54 and Table 27). The involvement of mtDNA copy number in mitophagy should be tested in the future.

4.6. Mitochondrial network and nucleoids are regulated independently of mtDNA copy number

Previous studies have shown a cell volume-dependency of mtDNA copy number (Seel *et al.*, 2023), the number of nucleoids (Osman *et al.*, 2015; Seel *et al.*, 2023) and the mitochondrial network (Rafelski *et al.*, 2012; Seel *et al.*, 2023). Also, the independence of mtDNA copy number on the length of the mitochondrial network has been reported (Seel *et al.*, 2023). Still, the question remained whether increasing mtDNA copy numbers are influencing the mtNetwork length or number of nucleoids. A lower number of nucleoids when culturing the cells in fermentable media than in non-fermentable media was shown in this study (see Figure 61h), which is in agreement with recent data (Seel *et al.*, 2023). Also, the results confirmed the independence of mtNetwork and nucleoids on mtDNA copy number (see Figure 61). This leads to the conclusion of a cell volume-dependent but mtDNA copy number-independent regulation of the mitochondrial network and the number of nucleoids in budding yeast (Figure 64).

Interestingly, when overexpressing TFAM in mouse embryonic fibroblasts, which leads to an increase of mtDNA copy number of around 2.5-fold, differences in the number of nucleoids were found (Kukat *et al.*, 2015). The TFAM-overexpression cells showed more nucleoids per cell than the wild type mouse embryonic fibroblasts, resulting in approximately 1.1 mtDNA copies per nucleoid in both cases (Kukat *et al.*, 2015). No information about the mitochondrial mass or mtNetwork length was given in this study. However, other researchers have increased the mtDNA copy number by increasing TFAM expression in transformed mice, reporting that there is no change in mitochondrial mass (Ekstrand *et al.*, 2004). Those results do not directly contradict the results shown in this study in budding yeast. Both mentioned studies increased the mtDNA copy number by overexpression of TFAM, but this thesis increased all three known factors limiting the mtDNA copy number (Abf2, Mip1 and Rim1). It would be interesting to also test all of the factors included in the limiting machinery in a mammalian cell line to see if the independence of mtNetwork length and nucleoid number shown in this thesis is only true in budding yeast or conserved from yeast to mammals. As mentioned previously, the mtDNA-limiting machinery might not be exactly the same, which is why an identification of all of the factors involved in mammalian cells should be prioritized first.

The results of this thesis were obtained based on the well-established LacI-LacO system (Osman *et al.*, 2015) to visualize mtDNA. To confirm these results, alternative systems such as the mt-HI-NESS-System could be consulted (Deng *et al.*, 2023). However, this study only considered increases of mtDNA copy number due to additional gene copies of the limiting machinery. Independent of the visualization strategy, the reverse view into strains with reduced mtDNA copy numbers could be interesting in the future. For this, haploid microscopy strains with a hemizygous deletion of *ABF2*, *MIP1* and *RIM1* could be used.

Overall, the absence of any change in mtNetwork length or nucleoid number with increasing mtDNA copy numbers could also be another possible reason for the robustness of the cells against the mtDNA changes.

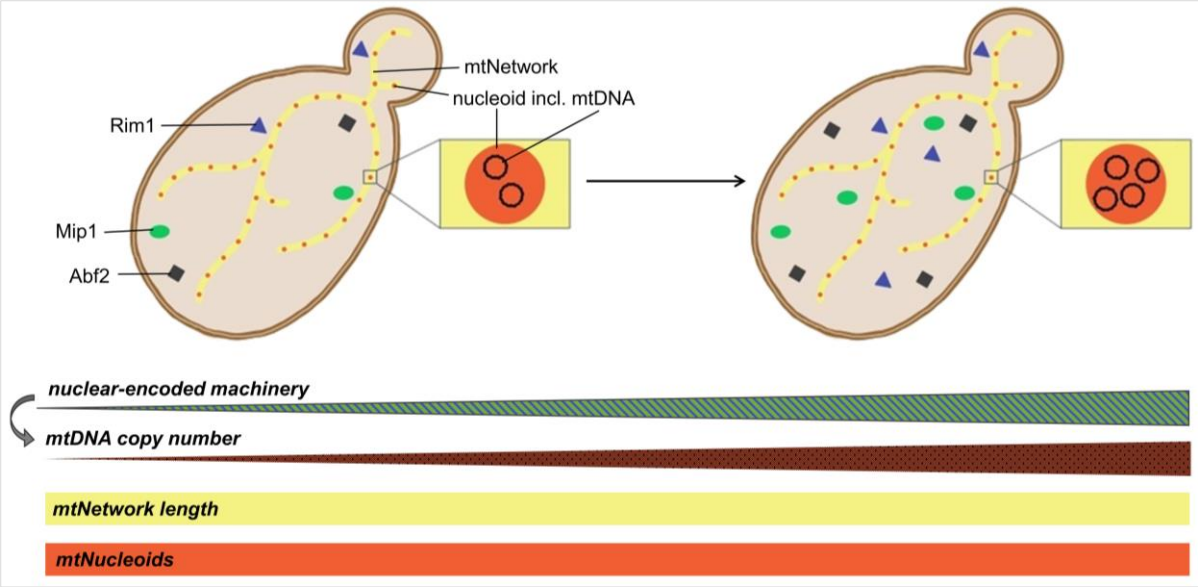

Figure 64: An increased mtDNA concentration does not lead to any changes in the mtNetwork length or number of nucleoids. Manipulating the mtDNA copy number by increasing the gene copy number of the mtDNA limiting machinery (Abf2, Mip1 and Rim1) in a strain including a LacI-LacO System to visualize mtDNA, reveals that mtNetwork length (yellow) and the number of nucleoids (orange) do not change. The actual location of the nuclear-encoded factors (Mip1, Abf2 and Rim1) is the mitochondria, but they are visualized in the cytoplasm for simplification of the scheme.

4.7. Concluding remarks

The primary goal of this thesis was to gain a better understanding of the mtDNA copy number regulation in budding yeast. With increasing cell volume, the amount of a nuclear-encoded machinery increases, which leads to increasing mtDNA copy numbers (Seel *et al.*, 2023). This work has provided new insights into identifying the nuclear-encoded mtDNA-limiting factors: The mitochondrial packaging factor Abf2, the mitochondrial polymerase Mip1 and the ssDNA-binding protein Rim1. Additionally, first evidences in this work hint towards no cell volume-dependent influence on the mtDNA copy number when lacking the increase of the limiting-machinery in its amount. The deletion or addition of the mtDNA-limiting factor genes provided a great opportunity to study mtDNA-dependent cell characteristics. The analysis included the cell volume, nDNA copy number per cell, cell growth, cell stress response as well as aging experiments. Surprisingly, the cells turned out to be very robust against mtDNA copy number changes up to 3-fold. The observed mild phenotypes included a slightly faster cell growth in non-fermentable media and a smaller chance of losing their mtDNA completely with increasing mtDNA concentrations. Besides those two beneficial phenotypes, a disadvantage was also identified for cells facing a calorie restriction: Increasing mtDNA concentrations lead to a longer cell cycle arrest in order to adapt to the new conditions. Nevertheless, the documented differences were comparatively small considering the extent of mtDNA changes. This thesis has documented two findings that could explain the absence of a clear phenotype. Whether only one or both of those findings are the reason or if they might be linked to each other is beyond the scope of this thesis. First, the increasing mtDNA concentration leads to an increase of mitochondrial-encoded transcripts but not an increase of the concentration of all mitochondrial-encoded proteins. This implies that the concentration of the mitochondrial complexes of the ETC might also be the same as in the wild type. Subsequently, it could be that the increased mtDNA copy number does not have any impact on the metabolic state of

the cell, such as no change in the ATP-level. The second explanation of the observed mild phenotypes could be the constant length of the mtNetwork and number of nucleoids with increasing mtDNA copy number. The lack of a change in the network length limits the space for the formation of additional ETCs at the mitochondrial inner membrane. Also, it might be possible that higher mtDNA copy numbers distributed into the same number of nucleoids lead to a more tightly packaged mtDNA. This could provide problems for the accessibility of the mtDNA during replication.

As mtDNA misregulations are commonly observed in a variety of human diseases (Niyazov *et al.*, 2016; Bernardino Gomes *et al.*, 2024), the findings of this thesis could be beneficial for a better understanding and control of these diseases. The results obtained in budding yeast can be partially conserved in higher eukaryotes. First evidences point towards the same mechanism of a cell volume-dependent regulation of nuclear-encoded factors, which limit mtDNA copy number also in mammalian cells. However, it is most likely that the factors might vary between species or cell types. More detailed analyses in mammalian cells, also distinguishing between cell types, are needed in the future. An interesting aspect would also be to find out whether there are indeed two different types of nucleoids – one for storage and one for usage – as speculated in this thesis. Moreover, future experiments need to investigate the speculated induced mitophagy in cells with too high mtDNA concentrations as a potential control mechanism to maintain appropriate mtDNA copy numbers.

Taken together, the large number of experiments performed for this work have helped answer a number of open questions about the regulation of mtDNA copy number in budding yeast, enabling targeted follow-up studies in the future. All of the findings presented in this work contribute to a better understanding of the mtDNA homeostasis and the influence of the mtDNA copy number on the cell characteristics.

REFERENCES

Abeliovich, H. (2023) Mitophagy in yeast: known unknowns and unknown unknowns. *Biochem J* **480** (20): 1639–1657.

Ahuja, P., Wanagat, J., Wang, Z., Wang, Y., Liem, D.A., Ping, P., *et al.* (2013) Divergent mitochondrial biogenesis responses in human cardiomyopathy. *Circulation* **127** (19): 1957–1967.

Alberts, B., Heald, R., Johnson, A., Morgan, D., Raff, M., Roberts, K., and Walter, P. (2025) *Molekularbiologie der Zelle.* Weinheim, Germany: Wiley VCH.

Altmann, K., Frank, M., Neumann, D., Jakobs, S., and Westermann, B. (2008) The class V myosin motor protein, Myo2, plays a major role in mitochondrial motility in Saccharomyces cerevisiae. *J Cell Biol* **181** (1): 119–130.

Anderson, S., Bankier, A.T., Barrell, B.G., Bruijn, M.H. de, Coulson, A.R., Drouin, J., *et al.* (1981) Sequence and organization of the human mitochondrial genome. *Nature* **290** (5806): 457–465.

Aretz, I., Jakubke, C., and Osman, C. (2020) Power to the daughters - mitochondrial and mtDNA transmission during cell division. *Biol Chem* **401** (5): 533–546.

Atamna, H., Killilea, D.W., Killilea, A.N., and Ames, B.N. (2002) Heme deficiency may be a factor in the mitochondrial and neuronal decay of aging. *Proc Natl Acad Sci U S A* **99** (23): 14807–14812.

Athenstaedt, K., Zweytick, D., Jandrositz, A., Kohlwein, S.D., and Daum, G. (1999) Identification and characterization of major lipid particle proteins of the yeast Saccharomyces cerevisiae. *J Bacteriol* **181** (20): 6441–6448.

Atkins, J.F., Wills, N.M., Loughran, G., Wu, C.-Y., Parsawar, K., Ryan, M.D., *et al.* (2007) A case for "StopGo": reprogramming translation to augment codon meaning of GGN by promoting unconventional termination (Stop) after addition of glycine and then allowing continued translation (Go). *RNA* **13** (6): 803–810.

Azbarova, A.V., and Knorre, D.A. (2023) Role of Mitochondrial DNA in Yeast Replicative Aging. *Biochemistry (Mosc)* **88** (12): 1997–2006.

Backert, S., Dörfel, P., Lurz, R., and Börner, T. (1996) Rolling-circle replication of mitochondrial DNA in the higher plant Chenopodium album (L.). *Mol Cell Biol* **16** (11): 6285–6294.

Barlowe, C., Orci, L., Yeung, T., Hosobuchi, M., Hamamoto, S., Salama, N., *et al.* (1994) COPII: a membrane coat formed by Sec proteins that drive vesicle budding from the endoplasmic reticulum. *Cell* **77** (6): 895–907.

Bastajian, N., Friesen, H., and Andrews, B.J. (2013) Bck2 acts through the MADS box protein Mcm1 to activate cell-cycle-regulated genes in budding yeast. *PLoS Genet* **9** (5): e1003507.

Beach, A., Leonov, A., Arlia-Ciommo, A., Svistkova, V., Lutchman, V., and Titorenko, V.I. (2015) Mechanisms by which different functional states of mitochondria define yeast longevity. *Int J Mol Sci* **16** (3): 5528–5554.

Ben Galeota-Sprung, Amy Fernandez, and Paul Sniegowski (2022) *Supplementary material from "Changes to the mtDNA copy number during yeast culture growth"*.

Bendich, A.J. (1996) Structural analysis of mitochondrial DNA molecules from fungi and plants using moving pictures and pulsed-field gel electrophoresis. *J Mol Biol* **255** (4): 564–588.

Benjamini, Y., and Hochberg, Y. (1995) Controlling the False Discovery Rate: A Practical and Powerful Approach to Multiple Testing. *Journal of the Royal Statistical Society Series B: Statistical Methodology* **57** (1): 289–300.

Bernardino Gomes, T.M., Vincent, A.E., Menger, K.E., Stewart, J.B., and Nicholls, T.J. (2024) Mechanisms and pathologies of human mitochondrial DNA replication and deletion formation. *Biochem J* **481** (11): 683–715.

Bleeg, H.S., Bak, A.L., Christiansen, C., Smith, K.E., and Stenderup, A. (1972) Mitochondrial DNA and glucose repression in yeast. *Biochem Biophys Res Commun* **47** (2): 524–530.

Boldogh, I.R., Nowakowski, D.W., Yang, H.-C., Chung, H., Karmon, S., Royes, P., and Pon, L.A. (2003) A protein complex containing Mdm10p, Mdm12p, and Mmm1p links mitochondrial membranes and DNA to the cytoskeleton-based segregation machinery. *Mol Biol Cell* **14** (11): 4618–4627.

Boldogh, I.R., Yang, H.C., and Pon, L.A. (2001) Mitochondrial inheritance in budding yeast. *Traffic* **2** (6): 368–374.

Braymer, J.J., and Lill, R. (2017) Iron-sulfur cluster biogenesis and trafficking in mitochondria. *J Biol Chem* **292** (31): 12754–12763.

Brewer, L.R., Friddle, R., Noy, A., Baldwin, E., Martin, S.S., Corzett, M., *et al.* (2003) Packaging of single DNA molecules by the yeast mitochondrial protein Abf2p. *Biophys J* **85** (4): 2519–2524.

Broach, J.R. (2012) Nutritional control of growth and development in yeast. *Genetics* **192** (1): 73–105.

Bui, T.H.D., and Labedzka-Dmoch, K. (2024) RetroGREAT signaling: The lessons we learn from yeast. *IUBMB Life* **76** (1): 26–37.

Caballero, A., Ugidos, A., Liu, B., Öling, D., Kvint, K., Hao, X., *et al.* (2011) Absence of mitochondrial translation control proteins extends life span by activating sirtuin-dependent silencing. *Mol Cell* **42** (3): 390–400.

Caligaris, M., Sampaio-Marques, B., Hatakeyama, R., Pillet, B., Ludovico, P., Virgilio, C. de, *et al.* (2023) The Yeast Protein Kinase Sch9 Functions as a Central Nutrient-Responsive Hub That Calibrates Metabolic and Stress-Related Responses. *J Fungi (Basel)* **9** (8).

Casatta, N., Porro, A., Orlandi, I., Brambilla, L., and Vai, M. (2013) Lack of Sir2 increases acetate consumption and decreases extracellular pro-aging factors. *Biochim Biophys Acta* **1833** (3): 593–601.

Ceccatelli Berti, C., Di Punzio, G., Dallabona, C., Baruffini, E., Goffrini, P., Lodi, T., and Donnini, C. (2021) The Power of Yeast in Modelling Human Nuclear Mutations Associated with Mitochondrial Diseases. *Genes (Basel)* **12** (2).

Chadha, Y., Khurana, A., and Schmoller, K.M. (2024a) Eukaryotic cell size regulation and its implications for cellular function and dysfunction. *Physiol Rev* **104** (4): 1679–1717.

Chadha, Y., Kukhtevich, I.V., Padovani, F., Schneider, R., and Schmoller, K.M. (2024b) *Single-cell imaging reveals a key role of Bck2 in budding yeast cell size adaptation to nutrient challenges*.

Chen, T., He, J., Huang, Y., and Zhao, W. (2011) The generation of mitochondrial DNA large-scale deletions in human cells. *J Hum Genet* **56** (10): 689–694.

Chen, X.J., and Butow, R.A. (2005) The organization and inheritance of the mitochondrial genome. *Nat Rev Genet* **6** (11): 815–825.

Chen, X.J., Guan, M.X., and Clark-Walker, G.D. (1993) MGM101, a nuclear gene involved in maintenance of the mitochondrial genome in Saccharomyces cerevisiae. *Nucleic Acids Res* **21** (15): 3473–3477.

Chen, Y., Zhao, G., Zahumensky, J., Honey, S., and Futcher, B. (2020) Differential Scaling of Gene Expression with Cell Size May Explain Size Control in Budding Yeast. *Mol Cell* **78** (2): 359-370.e6.

Cho, J.H., Ha, S.J., Kao, L.R., Megraw, T.L., and Chae, C.B. (1998) A novel DNA-binding protein bound to the mitochondrial inner membrane restores the null mutation of mitochondrial histone Abf2p in Saccharomyces cerevisiae. *Mol Cell Biol* **18** (10): 5712–5723.

Choi, J.H., Lou, W., and Vancura, A. (1998) A novel membrane-bound glutathione S-transferase functions in the stationary phase of the yeast Saccharomyces cerevisiae. *Journal of Biological Chemistry* **273** (45): 29915–29922.

Claude, K.-L., Bureik, D., Chatzitheodoridou, D., Adarska, P., Singh, A., and Schmoller, K.M. (2021) Transcription coordinates histone amounts and genome content. *Nat Commun* **12** (1): 4202.

Clay Montier, L.L., Deng, J.J., and Bai, Y. (2009) Number matters: control of mammalian mitochondrial DNA copy number. *J Genet Genomics* **36** (3): 125–131.

Conrad, M.N., and Newlon, C.S. (1982) The regulation of mitochondrial DNA levels in Saccharomyces cerevisiae. *Curr Genet* **6** (2): 147–152.

Contamine, V., and Picard, M. (2000) Maintenance and integrity of the mitochondrial genome: a plethora of nuclear genes in the budding yeast. *Microbiol Mol Biol Rev* **64** (2): 281–315.

Contessi, S., Haraux, F., Mavelli, I., and Lippe, G. (2005) Identification of a conserved calmodulin-binding motif in the sequence of F0F1 ATPsynthase inhibitor protein. *J Bioenerg Biomembr* **37** (5): 317–326.

Costanzo, M., Nishikawa, J.L., Tang, X., Millman, J.S., Schub, O., Breitkreuz, K., *et al.* (2004) CDK activity antagonizes Whi5, an inhibitor of G1/S transcription in yeast. *Cell* **117** (7): 899–913.

Crabtree, H.G. (1929) Observations on the carbohydrate metabolism of tumours. *Biochem J* **23** (3): 536–545.

Cyert, M.S. (2001) Genetic analysis of calmodulin and its targets in Saccharomyces cerevisiae. *Annu Rev Genet* **35:** 647–672.

Cyert, M.S., and Thorner, J. (1992) Regulatory subunit (CNB1 gene product) of yeast Ca2+/calmodulin-dependent phosphoprotein phosphatases is required for adaptation to pheromone. *Mol Cell Biol* **12** (8): 3460–3469.

Deaconescu, A.M., Roll-Mecak, A., Bonanno, J.B., Gerchman, S.E., Kycia, H., Studier, F.W., and Burley, S.K. (2002) X-ray structure of Saccharomyces cerevisiae homologous mitochondrial matrix factor 1 (Hmf1). *Proteins* **48** (2): 431–436.

Decker, M., Jaensch, S., Pozniakovsky, A., Zinke, A., O'Connell, K.F., Zachariae, W., *et al.* (2011) Limiting amounts of centrosome material set centrosome size in C. elegans embryos. *Curr Biol* **21** (15): 1259–1267.

Delorme-Axford, E., Wen, X., and Klionsky, D.J. (2023) The yeast transcription factor Stb5 acts as a negative regulator of autophagy by modulating cellular metabolism. *Autophagy* **19** (10): 2719–2732.

Deng, J., Swift, L., Zaman, M., Shahhosseini, F., Sharma, A., Bureik, D., *et al.* (2023) *A novel genetic fluorescent reporter to visualize mitochondrial nucleoids*.

Derbikova, K.S., Levitsky, S.A., Chicherin, I.V., Vinogradova, E.N., and Kamenski, P.A. (2018) Activation of Yeast Mitochondrial Translation: Who Is in Charge? *Biochemistry (Mosc)* **83** (2): 87–97.

Di Talia, S., Skotheim, J.M., Bean, J.M., Siggia, E.D., and Cross, F.R. (2007) Erratum: The effects of molecular noise and size control on variability in the budding yeast cell cycle. *Nature* **450** (7173): 1272.

Di Talia, S., Wang, H., Skotheim, J.M., Rosebrock, A.P., Futcher, B., and Cross, F.R. (2009) Daughter-specific transcription factors regulate cell size control in budding yeast. *PLoS Biol* **7** (10): e1000221.

Dietler, N., Minder, M., Gligorovski, V., Economou, A.M., Joly, D.A.H.L., Sadeghi, A., *et al.* (2020) A convolutional neural network segments yeast microscopy images with high accuracy. *Nat Commun* **11** (1): 5723.

Diffley, J.F., and Stillman, B. (1991) A close relative of the nuclear, chromosomal high-mobility group protein HMG1 in yeast mitochondria. *Proc Natl Acad Sci U S A* **88** (17): 7864–7868.

Diffley, J.F., and Stillman, B. (1992) DNA binding properties of an HMG1-related protein from yeast mitochondria. *Journal of Biological Chemistry* **267** (5): 3368–3374.

Dilova, I., Aronova, S., Chen, J.C.-Y., and Powers, T. (2004) Tor signaling and nutrient-based signals converge on Mks1p phosphorylation to regulate expression of Rtg1.Rtg3p-dependent target genes. *Journal of Biological Chemistry* **279** (45): 46527–46535.

Dilova, I., Chen, C.-Y., and Powers, T. (2002) Mks1 in concert with TOR signaling negatively regulates RTG target gene expression in S. cerevisiae. *Curr Biol* **12** (5): 389–395.

Ding, W.-X., Li, M., Biazik, J.M., Morgan, D.G., Guo, F., Ni, H.-M., *et al.* (2012) Electron microscopic analysis of a spherical mitochondrial structure. *J Biol Chem* **287** (50): 42373–42378.

Donnelly, M.L.L., Luke, G., Mehrotra, A., Li, X., Hughes, L.E., Gani, D., and Ryan, M.D. (2001) Analysis of the aphthovirus 2A/2B polyprotein 'cleavage' mechanism indicates not a proteolytic reaction, but a novel translational effect: a putative ribosomal 'skip'. *J Gen Virol* **82** (Pt 5): 1013–1025.

Doudican, N.A., Song, B., Shadel, G.S., and Doetsch, P.W. (2005) Oxidative DNA damage causes mitochondrial genomic instability in Saccharomyces cerevisiae. *Mol Cell Biol* **25** (12): 5196–5204.

Drgonová, J., Drgon, T., Roh, D.H., and Cabib, E. (1999) The GTP-binding protein Rho1p is required for cell cycle progression and polarization of the yeast cell. *J Cell Biol* **146** (2): 373–387.

Dua, N., Seshadri, A., and Badrinarayanan, A. (2022) DarT-mediated mtDNA damage induces dynamic reorganization and selective segregation of mitochondria. *J Cell Biol* **221** (10).

Duina, A.A., Miller, M.E., and Keeney, J.B. (2014) Budding yeast for budding geneticists: a primer on the Saccharomyces cerevisiae model system. *Genetics* **197** (1): 33–48.

Dunbar, D.R., Moonie, P.A., Swingler, R.J., Davidson, D., Roberts, R., and Holt, I.J. (1993) Maternally transmitted partial direct tandem duplication of mitochondrial DNA associated with diabetes mellitus. *Hum Mol Genet* **2** (10): 1619–1624.

Ekstrand, M.I., Falkenberg, M., Rantanen, A., Park, C.B., Gaspari, M., Hultenby, K., *et al.* (2004) Mitochondrial transcription factor A regulates mtDNA copy number in mammals. *Hum Mol Genet* **13** (9): 935–944.

Ephrussi, B., and Slonimski, P.P. (1955) Subcellular units involved in the synthesis of respiratory enzymes in yeast. *Nature* **176** (4495): 1207–1208.

Ephrussi B, Hottinguer H, Tavlitzki J. (1949) Action de l'acriflavine sur les levures. I. La mutation 'petite colonie'. *Ann Inst Pasteur* **1949** (76): 351–367.

Ewald, J.C., Kuehne, A., Zamboni, N., and Skotheim, J.M. (2016) The Yeast Cyclin-Dependent Kinase Routes Carbon Fluxes to Fuel Cell Cycle Progression. *Mol Cell* **62** (4): 532–545.

Fangman, W.L., Henly, J.W., and Brewer, B.J. (1990a) RPO41-independent maintenance of [rho-] mitochondrial DNA in Saccharomyces cerevisiae. *Mol Cell Biol* **10** (1): 10–15.

Fangman, W.L., Henly, J.W., and Brewer, B.J. (1990b) RPO41-independent maintenance of rho- mitochondrial DNA in Saccharomyces cerevisiae. *Mol Cell Biol* **10** (1): 10–15.

Faye, G., Fukuhara, H., Grandchamp, C., Lazowska, J., Michel, F., Casey, J., *et al.* (1973) Mitochondrial nucleic acids in the petite colonie mutants: deletions and repetition of genes. *Biochimie* **55** (6): 779–792.

Feldmann, H. (2012) *Yeast:* Wiley.

Ferreira Júnior, J.R., Spírek, M., Liu, Z., and Butow, R.A. (2005) Interaction between Rtg2p and Mks1p in the regulation of the RTG pathway of Saccharomyces cerevisiae. *Gene* **354:** 2–8.

Flanary, P.L., DiBello, P.R., Estrada, P., and Dohlman, H.G. (2000) Functional analysis of Plp1 and Plp2, two homologues of phosducin in yeast. *Journal of Biological Chemistry* **275** (24): 18462–18469.

Foltman, M., and Sanchez-Diaz, A. (2023) TOR Complex 1: Orchestrating Nutrient Signaling and Cell Cycle Progression. *Int J Mol Sci* **24** (21).

Förtsch, J., Hummel, E., Krist, M., and Westermann, B. (2011) The myosin-related motor protein Myo2 is an essential mediator of bud-directed mitochondrial movement in yeast. *J Cell Biol* **194** (3): 473–488.

Foury, F. (1989) Cloning and sequencing of the nuclear gene MIP1 encoding the catalytic subunit of the yeast mitochondrial DNA polymerase. *Journal of Biological Chemistry* **264** (34): 20552–20560.

Foury, F., and Kolodynski, J. (1983) pif mutation blocks recombination between mitochondrial rho+ and rho- genomes having tandemly arrayed repeat units in Saccharomyces cerevisiae. *Proc Natl Acad Sci U S A* **80** (17): 5345–5349.

Foury, F., Roganti, T., Lecrenier, N., and Purnelle, B. (1998) The complete sequence of the mitochondrial genome of Saccharomyces cerevisiae. *FEBS Lett* **440** (3): 325–331.

Foury, F., and Vanderstraeten, S. (1992) Yeast mitochondrial DNA mutators with deficient proofreading exonucleolytic activity. *EMBO J* **11** (7): 2717–2726.

Fox, T.D., Folley, L.S., Mulero, J.J., McMullin, T.W., Thorsness, P.E., Hedin, L.O., and Costanzo, M.C. (1991) Analysis and manipulation of yeast mitochondrial genes. *Methods Enzymol* **194:** 149–165.

Fraering, P., Imhof, I., Meyer, U., Strub, J.M., van Dorsselaer, A., Vionnet, C., and Conzelmann, A. (2001) The GPI transamidase complex of Saccharomyces cerevisiae contains Gaa1p, Gpi8p, and Gpi16p. *Mol Biol Cell* **12** (10): 3295–3306.

Gabriel, K., Milenkovic, D., Chacinska, A., Müller, J., Guiard, B., Pfanner, N., and Meisinger, C. (2007) Novel mitochondrial intermembrane space proteins as substrates of the MIA import pathway. *J Mol Biol* **365** (3): 612–620.

Gameiro, P.A., and Struhl, K. (2018) Nutrient Deprivation Elicits a Transcriptional and Translational Inflammatory Response Coupled to Decreased Protein Synthesis. *Cell Rep* **24** (6): 1415–1424.

Gancedo, J.M. (1998) Yeast carbon catabolite repression. *Microbiol Mol Biol Rev* **62** (2): 334–361.

Gandhi, M., Smith, B.A., Bovellan, M., Paavilainen, V., Daugherty-Clarke, K., Gelles, J., *et al.* (2010) GMF is a cofilin homolog that binds Arp2/3 complex to stimulate filament debranching and inhibit actin nucleation. *Curr Biol* **20** (9): 861–867.

Gao, Q., Binns, D.D., Kinch, L.N., Grishin, N.V., Ortiz, N., Chen, X., and Goodman, J.M. (2017) Pet10p is a yeast perilipin that stabilizes lipid droplets and promotes their assembly. *J Cell Biol* **216** (10): 3199–3217.

Geissler, S., Siegers, K., and Schiebel, E. (1998) A novel protein complex promoting formation of functional alpha- and gamma-tubulin. *EMBO J* **17** (4): 952–966.

Genga, A., Bianchi, L., and Foury, F. (1986) A nuclear mutant of Saccharomyces cerevisiae deficient in mitochondrial DNA replication and polymerase activity. *Journal of Biological Chemistry* **261** (20): 9328–9332.

Gichner, T. (1982) The molecular biology of the yeast saccharomyces. *Biol Plant* **24** (5): 340.

Glastad, R.C., and Johnston, I.G. (2023) Mitochondrial network structure controls cell-to-cell mtDNA variability generated by cell divisions. *PLoS Comput Biol* **19** (3): e1010953.

Göke, A., Schrott, S., Mizrak, A., Belyy, V., Osman, C., and Walter, P. (2020) Mrx6 regulates mitochondrial DNA copy number in Saccharomyces cerevisiae by engaging the evolutionarily conserved Lon protease Pim1. *Mol Biol Cell* **31** (7): 527–545.

Goode, B.L., Eskin, J.A., and Wendland, B. (2015) Actin and endocytosis in budding yeast. *Genetics* **199** (2): 315–358.

Gottlieb, S., and Esposito, R.E. (1989) A new role for a yeast transcriptional silencer gene, SIR2, in regulation of recombination in ribosomal DNA. *Cell* **56** (5): 771–776.

Graziewicz, M.A., Longley, M.J., and Copeland, W.C. (2006) DNA polymerase gamma in mitochondrial DNA replication and repair. *Chem Rev* **106** (2): 383–405.

Green, R., Lesage, G., Sdicu, A.-M., Ménard, P., and Bussey, H. (2003) A synthetic analysis of the Saccharomyces cerevisiae stress sensor Mid2p, and identification of a Mid2p-interacting protein, Zeo1p, that modulates the PKC1-MPK1 cell integrity pathway. *Microbiology (Reading)* **149** (Pt 9): 2487–2499.

Greenleaf, A.L., Kelly, J.L., and Lehman, I.R. (1986) Yeast RPO41 gene product is required for transcription and maintenance of the mitochondrial genome. *Proc Natl Acad Sci U S A* **83** (10): 3391–3394.

Groot, G.S., Flavell, R.A., van Ommen, G.J., and Grivell, L.A. (1974) Yeast mitochondrial RNA does not contain poly(A). *Nature* **252** (5479): 167–169.

Guaragnella, N., and Bettiga, M. (2021) Acetic acid stress in budding yeast: From molecular mechanisms to applications. *Yeast* **38** (7): 391–400.

Guetsova, M.L., Crother, T.R., Taylor, M.W., and Daignan-Fornier, B. (1999) Isolation and characterization of the Saccharomyces cerevisiae XPT1 gene encoding xanthine phosphoribosyl transferase. *J Bacteriol* **181** (9): 2984–2986.

Guthrie, C., and Fink, G.R. (ed.) (1991) *Guide to yeast genetics and molecular biology.* San Diego, California: Harcourt Brace Jovanovich Publishers.

Haag-Liautard, C., Coffey, N., Houle, D., Lynch, M., Charlesworth, B., and Keightley, P.D. (2008) Direct estimation of the mitochondrial DNA mutation rate in Drosophila melanogaster. *PLoS Biol* **6** (8): e204.

Hara, Y., and Kimura, A. (2009) Cell-size-dependent spindle elongation in the Caenorhabditis elegans early embryo. *Curr Biol* **19** (18): 1549–1554.

Harbauer, A.B., Opalińska, M., Gerbeth, C., Herman, J.S., Rao, S., Schönfisch, B., *et al.* (2014) Mitochondria. Cell cycle-dependent regulation of mitochondrial preprotein translocase. *Science* **346** (6213): 1109–1113.

Harner, M., Körner, C., Walther, D., Mokranjac, D., Kaesmacher, J., Welsch, U., *et al.* (2011) The mitochondrial contact site complex, a determinant of mitochondrial architecture. *EMBO J* **30** (21): 4356–4370.

Hartwell, L.H., and Unger, M.W. (1977) Unequal division in Saccharomyces cerevisiae and its implications for the control of cell division. *J Cell Biol* **75** (2 Pt 1): 422–435.

Hayward, D.C., Dosztányi, Z., and Clark-Walker, G.D. (2013) The N-terminal intrinsically disordered domain of Mgm101p is localized to the mitochondrial nucleoid. *PLoS One* **8** (2): e56465.

Hermann, G.J., Thatcher, J.W., Mills, J.P., Hales, K.G., Fuller, M.T., Nunnari, J., and Shaw, J.M. (1998) Mitochondrial fusion in yeast requires the transmembrane GTPase Fzo1p. *J Cell Biol* **143** (2): 359–373.

Herrmann, J.M., Woellhaf, M.W., and Bonnefoy, N. (2013) Control of protein synthesis in yeast mitochondria: the concept of translational activators. *Biochim Biophys Acta* **1833** (2): 286–294.

Hess, D.C., Myers, C.L., Huttenhower, C., Hibbs, M.A., Hayes, A.P., Paw, J., *et al.* (2009) Computationally driven, quantitative experiments discover genes required for mitochondrial biogenesis. *PLoS Genet* **5** (3): e1000407.

Higuchi, R., Vevea, J.D., Swayne, T.C., Chojnowski, R., Hill, V., Boldogh, I.R., and Pon, L.A. (2013) Actin dynamics affect mitochondrial quality control and aging in budding yeast. *Curr Biol* **23** (23): 2417–2422.

Hirayama, T., Maeda, T., Saito, H., and Shinozaki, K. (1995) Cloning and characterization of seven cDNAs for hyperosmolarity-responsive (HOR) genes of Saccharomyces cerevisiae. *Mol Gen Genet* **249** (2): 127–138.

Hoffman, M., Góra, M., and Rytka, J. (2003) Identification of rate-limiting steps in yeast heme biosynthesis. *Biochem Biophys Res Commun* **310** (4): 1247–1253.

Hori, A., Yoshida, M., Shibata, T., and Ling, F. (2009) Reactive oxygen species regulate DNA copy number in isolated yeast mitochondria by triggering recombination-mediated replication. *Nucleic Acids Res* **37** (3): 749–761.

Hu, J.P., Vanderstraeten, S., and Foury, F. (1995) Isolation and characterization of ten mutator alleles of the mitochondrial DNA polymerase-encoding MIP1 gene from Saccharomyces cerevisiae. *Gene* **160** (1): 105–110.

Ichikawa, N., Yoshida, Y., Hashimoto, T., Ogasawara, N., Yoshikawa, H., Imamoto, F., and Tagawa, K. (1990) Activation of ATP hydrolysis by an uncoupler in mutant mitochondria lacking an intrinsic ATPase inhibitor in yeast. *Journal of Biological Chemistry* **265** (11): 6274–6278.

Innokentev, A., and Kanki, T. (2021) Mitophagy in Yeast: Molecular Mechanism and Regulation. *Cells* **10** (12).

Inoue, H., Nojima, H., and Okayama, H. (1990) High efficiency transformation of Escherichia coli with plasmids. *Gene* **96** (1): 23–28.

Isaac, R.S., Tullius, T.W., Hansen, K.G., Dubocanin, D., Couvillion, M., Stergachis, A.B., and Churchman, L.S. (2024) Single-nucleoid architecture reveals heterogeneous packaging of mitochondrial DNA. *Nat Struct Mol Biol* **31** (3): 568–577.

Itoh, T., Watabe, A., Toh-E, A., and Matsui, Y. (2002) Complex formation with Ypt11p, a rab-type small GTPase, is essential to facilitate the function of Myo2p, a class V myosin, in mitochondrial distribution in Saccharomyces cerevisiae. *Mol Cell Biol* **22** (22): 7744–7757.

Jajoo, R., Jung, Y., Huh, D., Viana, M.P., Rafelski, S.M., Springer, M., and Paulsson, J. (2016) Accurate concentration control of mitochondria and nucleoids. *Science* **351** (6269): 169–172.

Jakubke, C., Roussou, R., Maiser, A., Schug, C., Thoma, F., Bunk, D., *et al.* (2021) Cristae-dependent quality control of the mitochondrial genome. *Sci Adv* **7** (36): eabi8886.

Jenkins, B.C., Neikirk, K., Katti, P., Claypool, S.M., Kirabo, A., McReynolds, M.R., and Hinton, A. (2024) Mitochondria in disease: changes in shapes and dynamics. *Trends Biochem Sci* **49** (4): 346–360.

Jiang, M., Xie, X., Zhu, X., Jiang, S., Milenkovic, D., Misic, J., *et al.* (2021) The mitochondrial single-stranded DNA binding protein is essential for initiation of mtDNA replication. *Sci Adv* **7** (27).

Jin, M., Li, Y., O'Laughlin, R., Bittihn, P., Pillus, L., Tsimring, L.S., *et al.* (2019) Divergent Aging of Isogenic Yeast Cells Revealed through Single-Cell Phenotypic Dynamics. *Cell Syst* **8** (3): 242-253.e3.

Johnston, G.C., Pringle, J.R., and Hartwell, L.H. (1977) Coordination of growth with cell division in the yeast Saccharomyces cerevisiae. *Exp Cell Res* **105** (1): 79–98.

Johnston, I.G. (2019) Varied Mechanisms and Models for the Varying Mitochondrial Bottleneck. *Front Cell Dev Biol* **7:** 294.

Johnston, I.G., Burgstaller, J.P., Havlicek, V., Kolbe, T., Rülicke, T., Brem, G., *et al.* (2015) Stochastic modelling, Bayesian inference, and new in vivo measurements elucidate the debated mtDNA bottleneck mechanism. *Elife* **4:** e07464.

Jorgensen, P., Edgington, N.P., Schneider, B.L., Rupes, I., Tyers, M., and Futcher, B. (2007) The size of the nucleus increases as yeast cells grow. *Mol Biol Cell* **18** (9): 3523–3532.

Jorgensen, P., Nishikawa, J.L., Breitkreutz, B.-J., and Tyers, M. (2002) Systematic identification of pathways that couple cell growth and division in yeast. *Science* **297** (5580): 395–400.

Kaeberlein, M., Kirkland, K.T., Fields, S., and Kennedy, B.K. (2004) Sir2-independent life span extension by calorie restriction in yeast. *PLoS Biol* **2** (9): E296.

Kaeberlein, M., McVey, M., and Guarente, L. (1999) The SIR2/3/4 complex and SIR2 alone promote longevity in Saccharomyces cerevisiae by two different mechanisms. *Genes Dev* **13** (19): 2570–2580.

Kanai, T., Takeshita, S., Atomi, H., Umemura, K., Ueda, M., and Tanaka, A. (1998) A regulatory factor, Fil1p, involved in derepression of the isocitrate lyase gene in Saccharomyces cerevisiae--a possible mitochondrial protein necessary for protein synthesis in mitochondria. *Eur J Biochem* **256** (1): 212–220.

Kang, D., Kim, S.H., and Hamasaki, N. (2007) Mitochondrial transcription factor A (TFAM): roles in maintenance of mtDNA and cellular functions. *Mitochondrion* **7** (1-2): 39–44.

Kauppila, T.E.S., Kauppila, J.H.K., and Larsson, N.-G. (2017) Mammalian Mitochondria and Aging: An Update. *Cell Metab* **25** (1): 57–71.

Kennedy, B.K., Austriaco, N.R., and Guarente, L. (1994) Daughter cells of Saccharomyces cerevisiae from old mothers display a reduced life span. *J Cell Biol* **127** (6 Pt 2): 1985–1993.

Keogh, M.J., and Chinnery, P.F. (2015) Mitochondrial DNA mutations in neurodegeneration. *Biochim Biophys Acta* **1847** (11): 1401–1411.

Kilberg, M.S., Pan, Y.-X., Chen, H., and Leung-Pineda, V. (2005) Nutritional control of gene expression: how mammalian cells respond to amino acid limitation. *Annu Rev Nutr* **25:** 59–85.

Kirchman, P.A., Kim, S., Lai, C.Y., and Jazwinski, S.M. (1999) Interorganelle signaling is a determinant of longevity in Saccharomyces cerevisiae. *Genetics* **152** (1): 179–190.
Kitakawa, M., Graack, H.R., Grohmann, L., Goldschmidt-Reisin, S., Herfurth, E., Wittmann-Liebold, B., *et al.* (1997) Identification and characterization of the genes for mitochondrial ribosomal proteins of Saccharomyces cerevisiae. *Eur J Biochem* **245** (2): 449–456.
Klecker, T., Scholz, D., Förtsch, J., and Westermann, B. (2013) The yeast cell cortical protein Num1 integrates mitochondrial dynamics into cellular architecture. *J Cell Sci* **126** (Pt 13): 2924–2930.
Kohlhaw, G.B. (2003) Leucine biosynthesis in fungi: entering metabolism through the back door. *Microbiol Mol Biol Rev* **67** (1): 1-15, table of contents.
Kolodrubetz, D., and Burgum, A. (1991) Sequence and genetic analysis of NHP2: a moderately abundant high mobility group-like nuclear protein with an essential function in Saccharomyces cerevisiae. *Yeast* **7** (2): 79–90.
Korhonen, J.A., Pham, X.H., Pellegrini, M., and Falkenberg, M. (2004) Reconstitution of a minimal mtDNA replisome in vitro. *EMBO J* **23** (12): 2423–2429.
Kornmann, B., Currie, E., Collins, S.R., Schuldiner, M., Nunnari, J., Weissman, J.S., and Walter, P. (2009) An ER-mitochondria tethering complex revealed by a synthetic biology screen. *Science* **325** (5939): 477–481.
Kotrys, A.V., Durham, T.J., Guo, X.A., Vantaku, V.R., Parangi, S., and Mootha, V.K. (2024) Single-cell analysis reveals context-dependent, cell-level selection of mtDNA. *Nature* **629** (8011): 458–466.
Koundinya, N., Aguilar, R.M., Wetzel, K., Tomasso, M.R., Nagarajan, P., McGuirk, E.R., *et al.* (2025) Two ligands of Arp2/3 complex, yeast coronin and GMF, interact and synergize in pruning branched actin networks. *J Biol Chem* **301** (3): 108191.
Kowald, A., and Kirkwood, T.B.L. (2011) Evolution of the mitochondrial fusion-fission cycle and its role in aging. *Proc Natl Acad Sci U S A* **108** (25): 10237–10242.
Kremer, L.S., Gao, G., Rigoni, G., Filograna, R., Mennuni, M., Wibom, R., *et al.* (2025) *Tissue-specific responses to TFAM and mtDNA copy number manipulation in prematurely ageing mice*.
Kukat, C., Davies, K.M., Wurm, C.A., Spåhr, H., Bonekamp, N.A., Kühl, I., *et al.* (2015) Cross-strand binding of TFAM to a single mtDNA molecule forms the mitochondrial nucleoid. *Proc Natl Acad Sci U S A* **112** (36): 11288–11293.
Kukat, C., Wurm, C.A., Spåhr, H., Falkenberg, M., Larsson, N.-G., and Jakobs, S. (2011) Super-resolution microscopy reveals that mammalian mitochondrial nucleoids have a uniform size and frequently contain a single copy of mtDNA. *Proc Natl Acad Sci U S A* **108** (33): 13534–13539.
Kukhtevich, I.V., Rivero-Romano, M., Rakesh, N., Bheda, P., Chadha, Y., Rosales-Becerra, P., *et al.* (2022) Quantitative RNA imaging in single live cells reveals age-dependent asymmetric inheritance. *Cell Rep* **41** (7): 111656.
Kuzmenko, A., Derbikova, K., Salvatori, R., Tankov, S., Atkinson, G.C., Tenson, T., *et al.* (2016) Aim-less translation: loss of Saccharomyces cerevisiae mitochondrial translation initiation factor mIF3/Aim23 leads to unbalanced protein synthesis. *Sci Rep* **6:** 18749.
Lackner, L.L., Ping, H., Graef, M., Murley, A., and Nunnari, J. (2013) Endoplasmic reticulum-associated mitochondria-cortex tether functions in the distribution and inheritance of mitochondria. *Proc Natl Acad Sci U S A* **110** (6): E458-67.
Lahaye, A., Stahl, H., Thines-Sempoux, D., and Foury, F. (1991) PIF1: a DNA helicase in yeast mitochondria. *EMBO J* **10** (4): 997–1007.

Lanz, M.C., Zatulovskiy, E., Swaffer, M.P., Zhang, L., Ilerten, I., Zhang, S., *et al.* (2022) Increasing cell size remodels the proteome and promotes senescence. *Mol Cell* **82** (17): 3255-3269.e8.

Lanz, M.C., Zhang, S., Swaffer, M.P., Hernández Götz, L., McCarty, F., Ziv, I., *et al.* (2023) Genome dilution by cell growth drives starvation-like proteome remodeling in mammalian and yeast cells. *bioRxiv*.

Larsson, N.G., Wang, J., Wilhelmsson, H., Oldfors, A., Rustin, P., Lewandoski, M., *et al.* (1998) Mitochondrial transcription factor A is necessary for mtDNA maintenance and embryogenesis in mice. *Nat Genet* **18** (3): 231–236.

Lecrenier, N., and Foury, F. (1995) Overexpression of the RNR1 gene rescues Saccharomyces cerevisiae mutants in the mitochondrial DNA polymerase-encoding MIP1 gene. *Mol Gen Genet* **249** (1): 1–7.

Lecrenier, N., and Foury, F. (2000) New features of mitochondrial DNA replication system in yeast and man. *Gene* **246** (1-2): 37–48.

Lemasters, J.J. (2007) Modulation of mitochondrial membrane permeability in pathogenesis, autophagy and control of metabolism. *J Gastroenterol Hepatol* **22 Suppl 1:** S31-7.

Lew, D.J., and Reed, S.I. (1995) A cell cycle checkpoint monitors cell morphogenesis in budding yeast. *J Cell Biol* **129** (3): 739–749.

Lewis, S.C., Joers, P., Willcox, S., Griffith, J.D., Jacobs, H.T., and Hyman, B.C. (2015) A rolling circle replication mechanism produces multimeric lariats of mitochondrial DNA in Caenorhabditis elegans. *PLoS Genet* **11** (2): e1004985.

Lewis, S.C., Uchiyama, L.F., and Nunnari, J. (2016) ER-mitochondria contacts couple mtDNA synthesis with mitochondrial division in human cells. *Science* **353** (6296): aaf5549.

Li, Y., Jiang, Y., Paxman, J., O'Laughlin, R., Klepin, S., Zhu, Y., *et al.* (2020) A programmable fate decision landscape underlies single-cell aging in yeast. *Science* **369** (6501): 325–329.

Ling, F., Hori, A., and Shibata, T. (2007) DNA recombination-initiation plays a role in the extremely biased inheritance of yeast rho- mitochondrial DNA that contains the replication origin ori5. *Mol Cell Biol* **27** (3): 1133–1145.

Ling, F., Hori, A., Yoshitani, A., Niu, R., Yoshida, M., and Shibata, T. (2013) Din7 and Mhr1 expression levels regulate double-strand-break-induced replication and recombination of mtDNA at ori5 in yeast. *Nucleic Acids Res* **41** (11): 5799–5816.

Ling, F., Makishima, F., Morishima, N., and Shibata, T. (1995) A nuclear mutation defective in mitochondrial recombination in yeast. *EMBO J* **14** (16): 4090–4101.

Ling, F., and Shibata, T. (2002) Recombination-dependent mtDNA partitioning: in vivo role of Mhr1p to promote pairing of homologous DNA. *EMBO J* **21** (17): 4730–4740.

Lipinski, K.A., Kaniak-Golik, A., and Golik, P. (2010) Maintenance and expression of the S. cerevisiae mitochondrial genome--from genetics to evolution and systems biology. *Biochim Biophys Acta* **1797** (6-7): 1086–1098.

Lisowsky, T., and Michaelis, G. (1988) A nuclear gene essential for mitochondrial replication suppresses a defect of mitochondrial transcription in Saccharomyces cerevisiae. *Mol Gen Genet* **214** (2): 218–223.

Lisowsky, T., and Michaelis, G. (1989) Mutations in the genes for mitochondrial RNA polymerase and a second mitochondrial transcription factor of Saccharomyces cerevisiae. *Mol Gen Genet* **219** (1-2): 125–128.

Liu, B., Larsson, L., Caballero, A., Hao, X., Oling, D., Grantham, J., and Nyström, T. (2010) The polarisome is required for segregation and retrograde transport of protein aggregates. *Cell* **140** (2): 257–267.
Liu, Z., and Butow, R.A. (1999) A transcriptional switch in the expression of yeast tricarboxylic acid cycle genes in response to a reduction or loss of respiratory function. *Mol Cell Biol* **19** (10): 6720–6728.
Lodi, T., Dallabona, C., Nolli, C., Goffrini, P., Donnini, C., and Baruffini, E. (2015) DNA polymerase γ and disease: what we have learned from yeast. *Front Genet* **6:** 106.
Logothetis, S., Walker, G., and Nerantzis, E. (2007) Effect of salt hyperosmotic stress on yeast cell viability. *Zb Mat srp prir nauk* (113): 271–284.
Longo, V.D., and Fabrizio, P. (2012) Chronological aging in Saccharomyces cerevisiae. *Subcell Biochem* **57:** 101–121.
Longo, V.D., Gralla, E.B., and Valentine, J.S. (1996) Superoxide dismutase activity is essential for stationary phase survival in Saccharomyces cerevisiae. Mitochondrial production of toxic oxygen species in vivo. *Journal of Biological Chemistry* **271** (21): 12275–12280.
Lynch, M., Sung, W., Morris, K., Coffey, N., Landry, C.R., Dopman, E.B., *et al.* (2008) A genome-wide view of the spectrum of spontaneous mutations in yeast. *Proc Natl Acad Sci U S A* **105** (27): 9272–9277.
Madaule, P., Axel, R., and Myers, A.M. (1987) Characterization of two members of the rho gene family from the yeast Saccharomyces cerevisiae. *Proc Natl Acad Sci U S A* **84** (3): 779–783.
Maleszka, R., Skelly, P.J., and Clark-Walker, G.D. (1991) Rolling circle replication of DNA in yeast mitochondria. *EMBO J* **10** (12): 3923–3929.
Margulis, L. (1970) *Origin of eukaryotic cells: Evidence and research implications for a theory of the origin and evolution of microbial, plant, and animal cells on the Precambrian earth.* New Haven usw.: Yale Univ. Pr.
Matsushima, Y., and Kaguni, L.S. (2007) Differential phenotypes of active site and human autosomal dominant progressive external ophthalmoplegia mutations in Drosophila mitochondrial DNA helicase expressed in Schneider cells. *Journal of Biological Chemistry* **282** (13): 9436–9444.
Mbantenkhu, M., Wang, X., Nardozzi, J.D., Wilkens, S., Hoffman, E., Patel, A., *et al.* (2011) Mgm101 is a Rad52-related protein required for mitochondrial DNA recombination. *J Biol Chem* **286** (49): 42360–42370.
McCormack, E.A., Altschuler, G.M., Dekker, C., Filmore, H., and Willison, K.R. (2009) Yeast phosducin-like protein 2 acts as a stimulatory co-factor for the folding of actin by the chaperonin CCT via a ternary complex. *J Mol Biol* **391** (1): 192–206.
McCormick, M.A., Delaney, J.R., Tsuchiya, M., Tsuchiyama, S., Shemorry, A., Sim, S., *et al.* (2015) A Comprehensive Analysis of Replicative Lifespan in 4,698 Single-Gene Deletion Strains Uncovers Conserved Mechanisms of Aging. *Cell Metab* **22** (5): 895–906.
McFaline-Figueroa, J.R., Vevea, J., Swayne, T.C., Zhou, C., Liu, C., Leung, G., *et al.* (2011) Mitochondrial quality control during inheritance is associated with lifespan and mother-daughter age asymmetry in budding yeast. *Aging Cell* **10** (5): 885–895.
McMillan, J.N., Sia, R.A., and Lew, D.J. (1998) A morphogenesis checkpoint monitors the actin cytoskeleton in yeast. *J Cell Biol* **142** (6): 1487–1499.

Meaden, P.G., Dickinson, F.M., Mifsud, A., Tessier, W., Westwater, J., Bussey, H., and Midgley, M. (1997) The ALD6 gene of Saccharomyces cerevisiae encodes a cytosolic, Mg(2+)-activated acetaldehyde dehydrogenase. *Yeast* **13** (14): 1319–1327.

Mears, J.A., Lackner, L.L., Fang, S., Ingerman, E., Nunnari, J., and Hinshaw, J.E. (2011) Conformational changes in Dnm1 support a contractile mechanism for mitochondrial fission. *Nat Struct Mol Biol* **18** (1): 20–26.

Meeusen, S., and Nunnari, J. (2003) Evidence for a two membrane-spanning autonomous mitochondrial DNA replisome. *J Cell Biol* **163** (3): 503–510.

Miceli, M.V., Jiang, J.C., Tiwari, A., Rodriguez-Quiñones, J.F., and Jazwinski, S.M. (2011) Loss of mitochondrial membrane potential triggers the retrograde response extending yeast replicative lifespan. *Front Genet* **2:** 102.

Miettinen, T.P., and Björklund, M. (2016) Cellular Allometry of Mitochondrial Functionality Establishes the Optimal Cell Size. *Dev Cell* **39** (3): 370–382.

Millán-Zambrano, G., Rodríguez-Gil, A., Peñate, X., Miguel-Jiménez, L. de, Morillo-Huesca, M., Krogan, N., and Chávez, S. (2013) The prefoldin complex regulates chromatin dynamics during transcription elongation. *PLoS Genet* **9** (9): e1003776.

Miyakawa, I., Miyamoto, M., Kuroiwa, T., and Sando, N. (2004) DNA Content of Individual Mitochondrial Nucleoids Varies Depending on the Culture Conditions of the Yeast Saccharomyces cerevisiae. *cytologia* **69** (1): 101–107.

Monroe, D.S., Leitzel, A.K., Klein, H.L., and Matson, S.W. (2005) Biochemical and genetic characterization of Hmi1p, a yeast DNA helicase involved in the maintenance of mitochondrial DNA. *Yeast* **22** (16): 1269–1286.

Morgan, D. (2007) *The cell cycle: Principles of control.* Corby, Oxford, Sunderland, MA: Oxford University Press; Sinauer.

Morgenstern, M., Stiller, S.B., Lübbert, P., Peikert, C.D., Dannenmaier, S., Drepper, F., *et al.* (2017) Definition of a High-Confidence Mitochondrial Proteome at Quantitative Scale. *Cell Rep* **19** (13): 2836–2852.

Mortimer, R.K., Contopoulou, C.R., and King, J.S. (1992) Genetic and physical maps of Saccharomyces cerevisiae, Edition 11. *Yeast* **8** (10): 817–902.

Mortimer, R.K., and Johnston, J.R. (1959) Life span of individual yeast cells. *Nature* **183** (4677): 1751–1752.

Murley, A., Lackner, L.L., Osman, C., West, M., Voeltz, G.K., Walter, P., and Nunnari, J. (2013) ER-associated mitochondrial division links the distribution of mitochondria and mitochondrial DNA in yeast. *Elife* **2:** e00422.

Murphy, J.P., Stepanova, E., Everley, R.A., Paulo, J.A., and Gygi, S.P. (2015) Comprehensive Temporal Protein Dynamics during the Diauxic Shift in Saccharomyces cerevisiae. *Mol Cell Proteomics* **14** (9): 2454–2465.

Nadal, E. de, and Posas, F. (2022) The HOG pathway and the regulation of osmoadaptive responses in yeast. *FEMS Yeast Res* **22** (1).

Nass, M.M., and Nass, S. (1963) INTRAMITOCHONDRIAL FIBERS WITH DNA CHARACTERISTICS. I. FIXATION AND ELECTRON STAINING REACTIONS. *J Cell Biol* **19** (3): 593–611.

Newlon, C.S., and Fangman, W.L. (1975) Mitochondrial DNA synthesis in cell cycle mutants of Saccharomyces cerevisiae. *Cell* **5** (4): 423–428.

Newman, J.R.S., Ghaemmaghami, S., Ihmels, J., Breslow, D.K., Noble, M., DeRisi, J.L., and Weissman, J.S. (2006) Single-cell proteomic analysis of S. cerevisiae reveals the architecture of biological noise. *Nature* **441** (7095): 840–846.

Niyazov, D.M., Kahler, S.G., and Frye, R.E. (2016) Primary Mitochondrial Disease and Secondary Mitochondrial Dysfunction: Importance of Distinction for Diagnosis and Treatment. *Mol Syndromol* **7** (3): 122–137.

Nolfi-Donegan, D., Braganza, A., and Shiva, S. (2020) Mitochondrial electron transport chain: Oxidative phosphorylation, oxidant production, and methods of measurement. *Redox Biol* **37:** 101674.

Novick, P., Field, C., and Schekman, R. (1980) Identification of 23 complementation groups required for post-translational events in the yeast secretory pathway. *Cell* **21** (1): 205–215.

Nunnari, J., Marshall, W.F., Straight, A., Murray, A., Sedat, J.W., and Walter, P. (1997) Mitochondrial transmission during mating in Saccharomyces cerevisiae is determined by mitochondrial fusion and fission and the intramitochondrial segregation of mitochondrial DNA. *Mol Biol Cell* **8** (7): 1233–1242.

Nyström, T. (2013) Aging: Filtering Out Bad Mitochondria. *Current Biology* **23** (23): R1037-R1039.

Okamoto, K., Perlman, P.S., and Butow, R.A. (1998) The sorting of mitochondrial DNA and mitochondrial proteins in zygotes: preferential transmission of mitochondrial DNA to the medial bud. *J Cell Biol* **142** (3): 613–623.

Ortiz, D.F., St Pierre, M.V., Abdulmessih, A., and Arias, I.M. (1997) A yeast ATP-binding cassette-type protein mediating ATP-dependent bile acid transport. *Journal of Biological Chemistry* **272** (24): 15358–15365.

Osman, C., Noriega, T.R., Okreglak, V., Fung, J.C., and Walter, P. (2015) Integrity of the yeast mitochondrial genome, but not its distribution and inheritance, relies on mitochondrial fission and fusion. *Proc Natl Acad Sci U S A* **112** (9): E947-56.

Padovani, F., Čavka, I., Neves, A.R.R., López, C.P., Al-Refaie, N., Bolcato, L., *et al.* (2024) *SpotMAX: a generalist framework for multi-dimensional automatic spot detection and quantification*.

Padovani, F., Mairhörmann, B., Falter-Braun, P., Lengefeld, J., and Schmoller, K.M. (2022) Segmentation, tracking and cell cycle analysis of live-cell imaging data with Cell-ACDC. *BMC Biol* **20** (1): 174.

Padovan-Merhar, O., Nair, G.P., Biaesch, A.G., Mayer, A., Scarfone, S., Foley, S.W., *et al.* (2015) Single mammalian cells compensate for differences in cellular volume and DNA copy number through independent global transcriptional mechanisms. *Mol Cell* **58** (2): 339–352.

Pagliarini, D.J., Calvo, S.E., Chang, B., Sheth, S.A., Vafai, S.B., Ong, S.-E., *et al.* (2008) A mitochondrial protein compendium elucidates complex I disease biology. *Cell* **134** (1): 112–123.

Panchaud, N., Péli-Gulli, M.-P., and Virgilio, C. de (2013) SEACing the GAP that nEGOCiates TORC1 activation: evolutionary conservation of Rag GTPase regulation. *Cell Cycle* **12** (18): 2948–2952.

Park, C.B., and Larsson, N.-G. (2011) Mitochondrial DNA mutations in disease and aging. *J Cell Biol* **193** (5): 809–818.

Parts, L., Liu, Y.-C., Tekkedil, M.M., Steinmetz, L.M., Caudy, A.A., Fraser, A.G., *et al.* (2014) Heritability and genetic basis of protein level variation in an outbred population. *Genome Res* **24** (8): 1363–1370.

Paukštytė, J., López Cabezas, R.M., Feng, Y., Tong, K., Schnyder, D., Elomaa, E., *et al.* (2023) Global analysis of aging-related protein structural changes uncovers enzyme-polymerization-based control of longevity. *Mol Cell* **83** (18): 3360-3376.e11.

Pérez-Hidalgo, L., and Moreno, S. (2016) Nutrients control cell size. *Cell Cycle* **15** (13): 1655–1656.

Pernice, W.M., Vevea, J.D., and Pon, L.A. (2016) A role for Mfb1p in region-specific anchorage of high-functioning mitochondria and lifespan in Saccharomyces cerevisiae. *Nat Commun* **7:** 10595.

Pitceathly, R.D.S., Rahman, S., and Hanna, M.G. (2012) Single deletions in mitochondrial DNA--molecular mechanisms and disease phenotypes in clinical practice. *Neuromuscul Disord* **22** (7): 577–586.

Poulton, J., Deadman, M.E., and Gardiner, R.M. (1989) Duplications of mitochondrial DNA in mitochondrial myopathy. *Lancet* **1** (8632): 236–240.

Praekelt, U.M., and Meacock, P.A. (1990) HSP12, a new small heat shock gene of Saccharomyces cerevisiae: analysis of structure, regulation and function. *Mol Gen Genet* **223** (1): 97–106.

Prokisch, H., Scharfe, C., Camp, D.G., Xiao, W., David, L., Andreoli, C., *et al.* (2004) Integrative analysis of the mitochondrial proteome in yeast. *PLoS Biol* **2** (6): e160.

Rafelski, S.M., Viana, M.P., Zhang, Y., Chan, Y.-H.M., Thorn, K.S., Yam, P., *et al.* (2012) Mitochondrial network size scaling in budding yeast. *Science* **338** (6108): 822–824.

Ralser, M., Kuhl, H., Ralser, M., Werber, M., Lehrach, H., Breitenbach, M., and Timmermann, B. (2012) The Saccharomyces cerevisiae W303-K6001 cross-platform genome sequence: insights into ancestry and physiology of a laboratory mutt. *Open Biol* **2** (8): 120093.

Ramanagoudr-Bhojappa, R., Blair, L.P., Tackett, A.J., and Raney, K.D. (2013) Physical and functional interaction between yeast Pif1 helicase and Rim1 single-stranded DNA binding protein. *Nucleic Acids Res* **41** (2): 1029–1046.

Ray, M.W., Chen, W., Duan, C., Bravo, G., Krueger, K., Rosario, E.M., *et al.* (2025) The Volume of Mitochondria Inherited Impacts mtDNA Homeostasis in Budding Yeast. *bioRxiv*.

Reinders, J., Zahedi, R.P., Pfanner, N., Meisinger, C., and Sickmann, A. (2006) Toward the complete yeast mitochondrial proteome: multidimensional separation techniques for mitochondrial proteomics. *J Proteome Res* **5** (7): 1543–1554.

Riccio, A.A., Bouvette, J., Pedersen, L.C., Somai, S., Dutcher, R.C., Borgnia, M.J., and Copeland, W.C. (2024) Structures of the mitochondrial single-stranded DNA binding protein with DNA and DNA polymerase γ. *Nucleic Acids Res* **52** (17): 10329–10340.

Richardson, H.E., Wittenberg, C., Cross, F., and Reed, S.I. (1989) An essential G1 function for cyclin-like proteins in yeast. *Cell* **59** (6): 1127–1133.

Roloff, G.A., and Henry, M.F. (2015) Mam33 promotes cytochrome c oxidase subunit I translation in Saccharomyces cerevisiae mitochondria. *Mol Biol Cell* **26** (16): 2885–2894.

Rossignol, R., Faustin, B., Rocher, C., Malgat, M., Mazat, J.-P., and Letellier, T. (2003) Mitochondrial threshold effects. *Biochem J* **370** (Pt 3): 751–762.

Rötig, A., Bessis, J.L., Romero, N., Cormier, V., Saudubray, J.M., Narcy, P., *et al.* (1992) Maternally inherited duplication of the mitochondrial genome in a syndrome of proximal tubulopathy, diabetes mellitus, and cerebellar ataxia. *Am J Hum Genet* **50** (2): 364–370.

Roussou, R., Metzler, D., Padovani, F., Thoma, F., Schwarz, R., Shraiman, B., *et al.* (2024) Real-time assessment of mitochondrial DNA heteroplasmy dynamics at the single-cell level. *EMBO J* **43** (22): 5340–5359.

Ryan, M.D., Donnelly, M., Lewis, A., Mehrotra, A.P., Wilkie, J., and Gani, D. (1999) A Model for Nonstoichiometric, Cotranslational Protein Scission in Eukaryotic Ribosomes. *Bioorganic Chemistry* **27** (1): 55–79.

Ryan, M.D., and Drew, J. (1994) Foot-and-mouth disease virus 2A oligopeptide mediated cleavage of an artificial polyprotein. *EMBO J* **13** (4): 928–933.

Ryan, M.D., King, A.M., and Thomas, G.P. (1991) Cleavage of foot-and-mouth disease virus polyprotein is mediated by residues located within a 19 amino acid sequence. *J Gen Virol* **72 (Pt 11):** 2727–2732.

Sanchez-Sandoval, E., Diaz-Quezada, C., Velazquez, G., Arroyo-Navarro, L.F., Almanza-Martinez, N., Trasviña-Arenas, C.H., and Brieba, L.G. (2015) Yeast mitochondrial RNA polymerase primes mitochondrial DNA polymerase at origins of replication and promoter sequences. *Mitochondrion* **24:** 22–31.

Sanz, A.B., García, R., Pavón-Vergés, M., Rodríguez-Peña, J.M., and Arroyo, J. (2022) Control of Gene Expression via the Yeast CWI Pathway. *Int J Mol Sci* **23** (3).

Sasser, T.L., Padolina, M., and Fratti, R.A. (2012) The yeast vacuolar ABC transporter Ybt1p regulates membrane fusion through Ca2+ transport modulation. *Biochem J* **448** (3): 365–372.

Sato, H., and Miyakawa, I. (2004) A 22 kDa protein specific for yeast mitochondrial nucleoids is an unidentified putative ribosomal protein encoded in open reading frame YGL068W. *Protoplasma* **223** (2-4): 175–182.

Sauer, H., Wartenberg, M., and Hescheler, J. (2001) Reactive oxygen species as intracellular messengers during cell growth and differentiation. *Cell Physiol Biochem* **11** (4): 173–186.

Schatz, G., Haslbrunner, E., and Tuppy, H. (1964) DEOXYRIBONUCLEIC ACID ASSOCIATED WITH YEAST MITOCHONDRIA. *Biochem Biophys Res Commun* **15** (2): 127–132.

Schmoller, K.M., Turner, J.J., Kõivomägi, M., and Skotheim, J.M. (2015) Dilution of the cell cycle inhibitor Whi5 controls budding-yeast cell size. *Nature* **526** (7572): 268–272.

Schrott, S., Gerle, C., Bibinger, S., Bertgen, L., Marino, G., Schwenkert, S., *et al.* (2025) *Mrx6 binds the Lon protease Pim1 N-terminal domain to confer selective substrate specificity and regulate mtDNA copy number*.

Schrott, S., and Osman, C. (2023) Two mitochondrial HMG-box proteins, Cim1 and Abf2, antagonistically regulate mtDNA copy number in Saccharomyces cerevisiae. *Nucleic Acids Res* **51** (21): 11813–11835.

Schubert, S., Heller, S., Löffler, B., Schäfer, I., Seibel, M., Villani, G., and Seibel, P. (2015) Generation of Rho Zero Cells: Visualization and Quantification of the mtDNA Depletion Process. *Int J Mol Sci* **16** (5): 9850–9865.

Sedman, T., Jõers, P., Kuusk, S., and Sedman, J. (2005) Helicase Hmi1 stimulates the synthesis of concatemeric mitochondrial DNA molecules in yeast Saccharomyces cerevisiae. *Curr Genet* **47** (4): 213–222.

Sedman, T., Kuusk, S., Kivi, S., and Sedman, J. (2000) A DNA helicase required for maintenance of the functional mitochondrial genome in Saccharomyces cerevisiae. *Mol Cell Biol* **20** (5): 1816–1824.

Seel, A., Padovani, F., Mayer, M., Finster, A., Bureik, D., Thoma, F., *et al.* (2023) Regulation with cell size ensures mitochondrial DNA homeostasis during cell growth. *Nat Struct Mol Biol* **30** (10): 1549–1560.

Seel, A.V. (2022) *Coordination of mitochondrial DNA homeostasis with cell growth.* München: Universitätsbibliothek der Ludwig-Maximilians-Universität.

Sekito, T., Thornton, J., and Butow, R.A. (2000) Mitochondria-to-nuclear signaling is regulated by the subcellular localization of the transcription factors Rtg1p and Rtg3p. *Mol Biol Cell* **11** (6): 2103–2115.

Shadel, G.S. (1999) Yeast as a model for human mtDNA replication. *Am J Hum Genet* **65** (5): 1230–1237.

Shang, H.S., Wong, S.M., Tan, H.M., and Wu, M. (1994) YKE2, a yeast nuclear gene encoding a protein showing homology to mouse KE2 and containing a putative leucine-zipper motif. *Gene* **151** (1-2): 197–201.

Shapiro, L., Grossman, L.I., Marmur, J., and Kleinschmidt, A.K. (1968) Physical studies on the structure of yeast mitochondrial DNA. *J Mol Biol* **33** (3): 907–922.

Shaw, A.E., Mihelich, M.N., Whitted, J.E., Reitman, H.J., Timmerman, A.J., Tehseen, M., *et al.* (2024) Revised mechanism of hydroxyurea-induced cell cycle arrest and an improved alternative. *Proc Natl Acad Sci U S A* **121** (42): e2404470121.

Simon, V.R., Karmon, S.L., and Pon, L.A. (1997) Mitochondrial inheritance: Cell cycle and actin cable dependence of polarized mitochondrial movements inSaccharomyces cerevisiae. *Cell Motil. Cytoskeleton* **37** (3): 199–210.

Sinclair, D.A., and Guarente, L. (1997) Extrachromosomal rDNA circles--a cause of aging in yeast. *Cell* **91** (7): 1033–1042.

Siniossoglou, S., Lutzmann, M., Santos-Rosa, H., Leonard, K., Mueller, S., Aebi, U., and Hurt, E. (2000) Structure and assembly of the Nup84p complex. *J Cell Biol* **149** (1): 41–54.

Smith, J.S. (2022) The long and short of rDNA and yeast replicative aging. *Proc Natl Acad Sci U S A* **119** (23): e2205124119.

Spelbrink, J.N. (2010) Functional organization of mammalian mitochondrial DNA in nucleoids: history, recent developments, and future challenges. *IUBMB Life* **62** (1): 19–32.

Staneva, D., Vasileva, B., Podlesniy, P., Miloshev, G., and Georgieva, M. (2023) Yeast Chromatin Mutants Reveal Altered mtDNA Copy Number and Impaired Mitochondrial Membrane Potential. *J Fungi (Basel)* **9** (3).

Stewart, J.B., and Chinnery, P.F. (2021) Extreme heterogeneity of human mitochondrial DNA from organelles to populations. *Nat Rev Genet* **22** (2): 106–118.

Stuart, G.R., Santos, J.H., Strand, M.K., van Houten, B., and Copeland, W.C. (2006) Mitochondrial and nuclear DNA defects in Saccharomyces cerevisiae with mutations in DNA polymerase gamma associated with progressive external ophthalmoplegia. *Hum Mol Genet* **15** (2): 363–374.

Stuchell-Brereton, M.D., Siglin, A., Li, J., Moore, J.K., Ahmed, S., Williams, J.C., and Cooper, J.A. (2011) Functional interaction between dynein light chain and intermediate chain is required for mitotic spindle positioning. *Mol Biol Cell* **22** (15): 2690–2701.

Stumpf, J.D., Bailey, C.M., Spell, D., Stillwagon, M., Anderson, K.S., and Copeland, W.C. (2010) mip1 containing mutations associated with mitochondrial disease causes mutagenesis and depletion of mtDNA in Saccharomyces cerevisiae. *Hum Mol Genet* **19** (11): 2123–2133.

Sultana, S., Solotchi, M., Ramachandran, A., and Patel, S.S. (2017) Transcriptional fidelities of human mitochondrial POLRMT, yeast mitochondrial Rpo41, and phage T7 single-subunit RNA polymerases. *J Biol Chem* **292** (44): 18145–18160.

Sun, X., Zhan, L., Chen, Y., Wang, G., He, L., Wang, Q., *et al.* (2018) Increased mtDNA copy number promotes cancer progression by enhancing mitochondrial oxidative phosphorylation in microsatellite-stable colorectal cancer. *Signal Transduct Target Ther* **3:** 8.

Supeková, L., Supek, F., and Nelson, N. (1995) The Saccharomyces cerevisiae VMA10 is an intron-containing gene encoding a novel 13-kDa subunit of vacuolar H(+)-ATPase. *Journal of Biological Chemistry* **270** (23): 13726–13732.

Swaffer, M.P., Kim, J., Chandler-Brown, D., Langhinrichs, M., Marinov, G.K., Greenleaf, W.J., *et al.* (2021) Transcriptional and chromatin-based partitioning mechanisms uncouple protein scaling from cell size. *Mol Cell* **81** (23): 4861-4875.e7.

Swaffer, M.P., Marinov, G.K., Zheng, H., Fuentes Valenzuela, L., Tsui, C.Y., Jones, A.W., *et al.* (2023) RNA polymerase II dynamics and mRNA stability feedback scale mRNA amounts with cell size. *Cell* **186** (24): 5254-5268.e26.

Swayne, T.C., Zhou, C., Boldogh, I.R., Charalel, J.K., McFaline-Figueroa, J.R., Thoms, S., *et al.* (2011) Role for cER and Mmr1p in anchorage of mitochondria at sites of polarized surface growth in budding yeast. *Curr Biol* **21** (23): 1994–1999.

Talarek, N., Cameroni, E., Jaquenoud, M., Luo, X., Bontron, S., Lippman, S., *et al.* (2010) Initiation of the TORC1-regulated G0 program requires Igo1/2, which license specific mRNAs to evade degradation via the 5'-3' mRNA decay pathway. *Mol Cell* **38** (3): 345–355.

Tam, Z.Y., Gruber, J., Halliwell, B., and Gunawan, R. (2013) Mathematical modeling of the role of mitochondrial fusion and fission in mitochondrial DNA maintenance. *PLoS One* **8** (10): e76230.

Tilokani, L., Nagashima, S., Paupe, V., and Prudent, J. (2018) Mitochondrial dynamics: overview of molecular mechanisms. *Essays Biochem* **62** (3): 341–360.

Turcotte, B., Liang, X.B., Robert, F., and Soontorngun, N. (2010) Transcriptional regulation of nonfermentable carbon utilization in budding yeast. *FEMS Yeast Res* **10** (1): 2–13.

Tye, B.K. (1999) MCM proteins in DNA replication. *Annu Rev Biochem* **68:** 649–686.

Tyynismaa, H., Sembongi, H., Bokori-Brown, M., Granycome, C., Ashley, N., Poulton, J., *et al.* (2004) Twinkle helicase is essential for mtDNA maintenance and regulates mtDNA copy number. *Hum Mol Genet* **13** (24): 3219–3227.

Tzagoloff, A., and Myers, A.M. (1986) Genetics of mitochondrial biogenesis. *Annu Rev Biochem* **55:** 249–285.

Ulery, T.L., Jang, S.H., and Jaehning, J.A. (1994) Glucose repression of yeast mitochondrial transcription: kinetics of derepression and role of nuclear genes. *Mol Cell Biol* **14** (2): 1160–1170.

van Dyck, E., Foury, F., Stillman, B., and Brill, S.J. (1992) A single-stranded DNA binding protein required for mitochondrial DNA replication in S. cerevisiae is homologous to E. coli SSB. *EMBO J* **11** (9): 3421–3430.

van Heusden, G.P., Griffiths, D.J., Ford, J.C., Chin-A-Woeng, T.F., Schrader, P.A., Carr, A.M., and Steensma, H.Y. (1995) The 14-3-3 proteins encoded by the BMH1 and BMH2 genes are essential in the yeast Saccharomyces cerevisiae and can be replaced by a plant homologue. *Eur J Biochem* **229** (1): 45–53.

Vries, S. de, and Marres, C.A. (1987) The mitochondrial respiratory chain of yeast. Structure and biosynthesis and the role in cellular metabolism. *Biochim Biophys Acta* **895** (3): 205–239.

Wang, X., Watt, P.M., Borts, R.H., Louis, E.J., and Hickson, I.D. (1999) The topoisomerase II-associated protein, Pat1p, is required for maintenance of rDNA locus stability in Saccharomyces cerevisiae. *Mol Gen Genet* **261** (4-5): 831–840.

Wang, X., Watt, P.M., Louis, E.J., Borts, R.H., and Hickson, I.D. (1996) Pat1: a topoisomerase II-associated protein required for faithful chromosome transmission in Saccharomyces cerevisiae. *Nucleic Acids Res* **24** (23): 4791–4797.

Wang, Z., and Wu, M. (2015) An integrated phylogenomic approach toward pinpointing the origin of mitochondria. *Sci Rep* **5:** 7949.

Weber, S.C., and Brangwynne, C.P. (2015) Inverse size scaling of the nucleolus by a concentration-dependent phase transition. *Curr Biol* **25** (5): 641–646.

Wen, H., Deng, H., Li, B., Chen, J., Zhu, J., Zhang, X., *et al.* (2025) Mitochondrial diseases: from molecular mechanisms to therapeutic advances. *Signal Transduct Target Ther* **10** (1): 9.

Wengert, S., Giannoulis, X., Kreitmaier, P., Kautz, P., Ludwig, L.S., Prokisch, H., *et al.* (2024) *Tissue-specific apparent mtDNA heteroplasmy and its relationship with ageing and mtDNA gene expression*.

Williamson, D.H., and Fennell, D.J. (1975) The use of fluorescent DNA-binding agent for detecting and separating yeast mitochondrial DNA. *Methods Cell Biol* **12:** 335–351.

Winter, D.C., Choe, E.Y., and Li, R. (1999) Genetic dissection of the budding yeast Arp2/3 complex: a comparison of the in vivo and structural roles of individual subunits. *Proc Natl Acad Sci U S A* **96** (13): 7288–7293.

Wu, C.-Y., Rolfe, P.A., Gifford, D.K., and Fink, G.R. (2010) Control of transcription by cell size. *PLoS Biol* **8** (11): e1000523.

Xu, H., Andi, B., Qian, J., West, A.H., and Cook, P.F. (2006) The alpha-aminoadipate pathway for lysine biosynthesis in fungi. *Cell Biochem Biophys* **46** (1): 43–64.

Yamanishi, M., Ito, Y., Kintaka, R., Imamura, C., Katahira, S., Ikeuchi, A., *et al.* (2013) A genome-wide activity assessment of terminator regions in Saccharomyces cerevisiae provides a ″terminatome″ toolbox. *ACS Synth Biol* **2** (6): 337–347.

Yang, S.S., Yeh, E., Salmon, E.D., and Bloom, K. (1997) Identification of a mid-anaphase checkpoint in budding yeast. *J Cell Biol* **136** (2): 345–354.

Youle, R.J., and van der Bliek, A.M. (2012) Mitochondrial fission, fusion, and stress. *Science* **337** (6098): 1062–1065.

Young, C.W., and Hodas, S. (1964) HYDROXYUREA: INHIBITORY EFFECT ON DNA METABOLISM. *Science* **146** (3648): 1172–1174.

Zamaroczy, M. de, and Bernardi, G. (1986a) The GC clusters of the mitochondrial genome of yeast and their evolutionary origin. *Gene* **41** (1): 1–22.

Zamaroczy, M. de, and Bernardi, G. (1986b) The primary structure of the mitochondrial genome of Saccharomyces cerevisiae--a review. *Gene* **47** (2-3): 155–177.

Zelenaya-Troitskaya, O., Newman, S.M., Okamoto, K., Perlman, P.S., and Butow, R.A. (1998) Functions of the high mobility group protein, Abf2p, in mitochondrial DNA segregation, recombination and copy number in Saccharomyces cerevisiae. *Genetics* **148** (4): 1763–1776.

Zelenaya-Troitskaya, O., Perlman, P.S., and Butow, R.A. (1995) An enzyme in yeast mitochondria that catalyzes a step in branched-chain amino acid biosynthesis also functions in mitochondrial DNA stability. *EMBO J* **14** (13): 3268–3276.

Zhang, F., Pracheil, T., Thornton, J., and Liu, Z. (2013) Adenosine Triphosphate (ATP) Is a Candidate Signaling Molecule in the Mitochondria-to-Nucleus Retrograde Response Pathway. *Genes (Basel)* **4** (1): 86–100.

Zhang, R., Wang, Y., Ye, K., Picard, M., and Gu, Z. (2017) Independent impacts of aging on mitochondrial DNA quantity and quality in humans. *BMC Genomics* **18** (1): 890.

Zhurinsky, J., Leonhard, K., Watt, S., Marguerat, S., Bähler, J., and Nurse, P. (2010) A coordinated global control over cellular transcription. *Curr Biol* **20** (22): 2010–2015.

Acknowledgements

I want to thank all of the people who supported me during the research and writing of my doctoral thesis over the last years. First and foremost, I would like to express my deepest gratitude to Dr. Kurt Schmoller, who gave me the opportunity to conduct research in his group at Helmholtz Munich. Thank you for trusting me to work on this exciting research question, for supporting me with a lot of helpful discussions and for always motivating me with your great optimism!

I would also like to thank the members of my Thesis Advisory Committee: Prof. Dr. Christof Osman and Dr. Dejana Mokranjac, for their support of my doctoral thesis. Thanks for your time, support and productive input during our meetings. Special thanks to my university supervisor, Prof. Dr. Christof Osman, for sharing valuable scientific resources and insights that helped strengthen this project. I would also like to extend a big thank you to Dr. Anika Seel for handing over this exciting research topic to me. Additionally, this endeavor would not have been possible without our collaborators. Thank you, Jurgita Paukštytė, for performing the replicative aging experiments for us. A big thank you to Kim Job for helping me analyze the RNA sequencing data. I would also like to thank Michael Lanz and Luisa Hernández Götz for their support in the mass spectrometry experiments. Thank you, Igor Kukhtevich and Yagya Chadha, for your help in performing and analyzing the microfluidic single-cell microscopy experiments. A big thank you also to Francesco Padovani and Daniela Bureik for your support in the lab.

I would also like to sincerely thank all current and former members of the Institute and the working groups for your critical questions and helpful input. In particular, I would like to thank all of the members of the Schmoller lab. Thank you for all the scientific and non-scientific conversations and discussions, as well as the great atmosphere in the group. I want to highlight my gratitude to those with whom I spent most of my time during this journey. Thanks to Dr. Anika Seel and Dr. Dimitra Chatzitheodoridou for your support and for including me in the group so well. Thanks to Arohi Khurana and Timon Stegmaier for always listening carefully and asking critical questions. And of course, a big thank you to Daniela Bureik, Yagya Chadha and Luisa Hernández Götz, for being a great support in the lab and for sharing every joy and sorrow with me. You always stood by my side with helpful advice and this experience would have been way less enjoyable without you.

Finally, I would like to thank my friends and family, especially my parents, Corinna and Lothar Finster and my brother Cedric Finster, who have supported me unconditionally and have always had my back. Thank you to my longest and dearest friend, Jana Hubel, for always being there for me. All of you are the greatest gift and the best support system I could have wished for. Thank you so much! Last but not least, a big thank you also goes to my husband, Maximilian Benedikt. Thank you for listening patiently to each of my challenges, for motivating me and for always making me laugh, even in stressful phases. I couldn’t have done it without you!